

# NASA Contract Report 165406

## Final Report

(NASA-CK-165406) TURBOJET ENGINE BLADE  
DAMPING Final Report (United Technologies  
Research Center) 182 p HC A05/RF A01

N81-29130

CSCI 21E

Unclass

63/07 33519

# Turbojet Engine Blade Damping

**A.V. Srinivasan**  
**D.G. Cutts**  
**S. Sridhar**

**UNITED TECHNOLOGIES RESEARCH CENTER**  
East Hartford, CT 06108

**Contract NAS3-21708**

**July 1981**

REPRODUCED BY  
**NATIONAL TECHNICAL  
INFORMATION SERVICE**  
U.S. DEPARTMENT OF COMMERCE  
SPRINGFIELD, VA. 22161

**NASA**

National Aeronautics and  
Space Administration

**Lewis Research Center**  
Cleveland, Ohio 44135



**U.S. DEPARTMENT OF COMMERCE**  
**National Technical Information Service**

N81 29130

TURBOJET ENGINE BLADE DAMPING

United Technologies Research Center  
East Hartford, Connecticut

Jul 81



Turbojet Engine Blade Damping

TABLE OF CONTENTS

	<u>Page</u>
FOREWORD . . . . .	i
LIST OF FIGURES . . . . .	ii
LIST OF TABLES . . . . .	v
NOMENCLATURE . . . . .	vi
SUMMARY . . . . .	ix
1. INTRODUCTION . . . . .	1
2. TECHNICAL APPROACH . . . . .	3
2.1 Analytical Approaches . . . . .	3
2.2 Experimental Procedures . . . . .	6
3. MATERIAL DAMPING . . . . .	10
3.1 Determination of Material Damping in a Vibrating Blade . . . . .	10
3.2 Determination of Damping Constants J and n . . . . .	12
3.3 Material Damping Tests . . . . .	17
3.4 Numerical Results and Discussion . . . . .	26
4. DAMPING DUE TO SLIPPING AT ROOT . . . . .	30
4.1 Forced Response of a Fan Blade with Slip at the Root . . . . .	30
4.2 Experimental Investigation of Damping at Blade Root . . . . .	35
4.3 Discussion of Results . . . . .	36
5. DAMPING DUE TO RUBBING AT SHROUD INTERFACES . . . . .	38
5.1 Forced Response of a Fan Blade with Rubbing at Shrouds . . . . .	38
5.2 Experimental Investigation of Damping at Shrouds . . . . .	42
5.3 Discussion of Results . . . . .	45
5.4 Characteristics of Sliding Friction . . . . .	47

TABLE OF CONTENTS (Cont'd)

	<u>Page</u>
6. DAMPING DUE TO PLATFORM-DAMPERS . . . . .	50
6.1 Forced Response of a Turbine Blade with a Platform Damper . . . . .	50
6.2 Platform Damping Tests . . . . .	55
6.3 Discussion of Results . . . . .	57
7. GENERAL CONCLUSIONS AND RECOMMENDATIONS . . . . .	60
8. REFERENCES . . . . .	63
APPENDIX A - COMPUTER PROGRAMS . . . . .	67
APPENDIX B - TEST ASSEMBLIES, INSTRUMENTATION AND DATA REDUCTION . . . . .	86
APPENDIX C - DAMPING IN AN ASSEMBLY OF BLADES . . . . .	92
TABLES . . . . .	96-106
FIGURES . . . . .	107-168

## FOREWORD

The development of the analytical and test programs presented herein was sponsored by the National Aeronautics and Space Administration, Lewis Research Center, under Contract NAS3-21708. The NASA Project Manager was Mr. L. J. Kiraly.

Principal United Technologies Research Center (UTRC) participants in the contract activity were Dr. A. V. Srinivasan, Mr. D. G. Cutts, Dr. S. Sridhar and Mr. J. Zucker. Dr. Srinivasan was the Principal Investigator and Program Manager with primary overall responsibility for the development and application of the analyses and coordinating the test phases of the program. Dr. Sridhar provided the bulk of the support in the analytical aspects of the program and was primarily responsible in formulating the mathematical models and obtaining numerical solution through a series of computer programs he developed. Mr. Cutts provided the bulk of the support in the test programs and was primarily responsible for outlining the tests, designing the fixtures and instrumentation, directing the tests and data reduction. Mr. Cutts was assisted by Mr. John Zucker throughout the test programs.

This report is the final documentation of (a) analytical modeling of nonaerodynamic sources of damping in engine blades, and (b) testing performed on blades and blade-like components to measure the levels of damping available in these components.

LIST OF FIGURES

<u>Figure</u>	<u>Title</u>	<u>Page</u>
1	Blades and Other Test Components Used in the Program . . .	.107
2	Twisted Plate Mounted on Centrifuge Arm. . . . .	.108
3	Twisted Plate Installation for Centrifugal Test . . . . .	.109
4	Turbine Blade/Platform Damper Vibration Test Set Up . . .	.110
5	Hysteresis Loop for Material Damping . . . . .	.111
6a	Typical Blade Element . . . . .	.111
6b	Stress Distribution Across Element Thickness . . . . .	.111
7	Material Damping Constant Measurement Test Hardware . . .	.112
8	Assembly of Centrifugal Test Rig for the Twisted Plate . .	.113
9	Twisted Plate Mounted in Bench Test Fixture . . . . .	.114
10	NASTRAN Finite Element Model for the Twisted Plate . . . .	.115
11	Block Diagram of the Driving and Recording Systems Used to Obtain Vibration Decay Data for the Twisted Plate on the Centrifuge . . . . .	.116
12	Variation of Modal Damping (Loss Factor) with Rotational Speed for Titanium Twisted Plate in Partial Vacuum (5 torr) . . . . .	.117
13	Decay Characteristics of Twisted Plate Vibrating in Its First Three Modes at Zero Speed in Vacuum . . . . .	.118
14	Decay Characteristics of Twisted Plate Vibrating in Its First Mode at Speed in Vacuum (Two Samples). . . . .	.119
15	Decay Characteristics of Twisted Plate Vibrating in Its Second and Third Modes at Speed in Vacuum (5 torr) . .	.120
16	Instrumented Fan Blade Showing "Root" Strain Gage . . . . .	.121
17	Instrumented Fan Blade Showing A.S.M.T. Strain Gage . . . .	.122
18	Test Set-Up For Fan Blade Material Damping Investigation at Elevated Temperatures . . . . .	.123
19	Variation of Measured Modal Damping with Air Pressure for Fan Blade . . . . .	.124
20	Variation of Measured First Mode Frequency Ratio with Air Pressure for Fan Blade . . . . .	.125
21	Material Damping in a Typical Fan Blade . . . . .	.126
22	Variation of Loss Factor with Root Stress and Soak Temperature . . . . .	.127
23	Stress Amplitude Decay Curves for a Fan Blade Vibrating in Air In Its Second Bending Mode for Two Temperature Conditions . . . . .	.128
24	Stress Amplitude Decay Curves for a Fan Blade Vibrating in Air In Its First Torsion Mode for Two Temperature Conditions . . . . .	.129
25	Typical Composite Material Test Piece . . . . .	.130

LIST OF FIGURES (Cont'd)

<u>Figure</u>	<u>Title</u>	<u>Page</u>
26	Composite Material Cantilevered Beam Vibration Test Set Up. . . . .	131
27	Composite Material Damping . . . . .	132
28	Spanwise Distributions of Outer Fiber Major Principal Stresses for Twisted Plate . . . . .	133
29	Twisted Plate Forced Response in Partial Vacuum (10 Torr). . . . .	134
30a	Motions of Blade with Slip at Root . . . . .	135
30b	Analytical Model of Blade with Slip at Root . . . . .	135
31	Test Fixture and Root Loading Device for Fan Blade Root Damping Tests . . . . .	136
32	Fan Blade/Fixture Test Assembly for Root Damping Investigation . . . . .	137
33	Circuit and Switching Arrangement for Strain Gage Load Bolts . . . . .	138
34	Decays of Blade Response with an Applied Root Loading of 576N . . . . .	139
35	Decays of Blade Response with an Applied Root Loading of 2879N . . . . .	140
36	Damping at Fan Blade Root . . . . .	141
37	Variation of Root Vibratory Stress with Root Loading . . . . .	142
38	Variation of Blade Response Frequency with Root Normal Load for Various Excitation Levels . . . . .	143
39a,b	Schematic of Shroud Rubbing . . . . .	144
40	Analytical Model for Shroud Rubbing . . . . .	144
41	Shroud Loading Device for Investigation of Fan Blade Shroud Damping Mechanism . . . . .	145
42	Shroud Loading Mechanism . . . . .	146
43	Block Diagram of Basic Excitation and Recording Systems Used to Obtain Strain and Acceleration Response Data From Test Items Excited by the Electro-dynamic Shaker . . . . .	147
44	Test Set-Up for Shroud Damping Investigation . . . . .	148
45	Fan Blade Response Characteristics from a 2g Level Exploratory Sweep - Shrouds Loaded with 102N . . . . .	149
46	Fan Blade Response Characteristics from a 2g Level Exploratory Sweep - Shrouds Loaded with 150N . . . . .	150
47	First Flap Mode Response to a Slow Frequency Sweep at Constant Input Acceleration Levels . . . . .	151
48	Damping Due to Rubbing at Shroud for a Typical Fan Blade - Variation of Response Decay with Initial Stress. . . . .	152
49	Damping Due to Rubbing at Shroud for a Typical Fan Blade - Variation of Response Decay with Shroud Load and Initial Stress . . . . .	153
50	Shroud Damping Effects on Blade Response (First Flap Mode $\sim$ 280 Hz) . . . . .	154

LIST OF FIGURES (Cont'd)

<u>Figure</u>	<u>Title</u>	<u>Page</u>
51	Blade Response in the Above-Shroud Torsion Mode . . . . .	.155
52	Wear Areas on Shroud Load Platens . . . . .	.156
53	Friction Test Assembly (Upper Arm Raised) . . . . .	.157
54	Friction Test Assembly . . . . .	.158
55a	Typical Signals from Acceleration and Force Transducers .	.159
55b	Typical Measured Friction Force - Slip Loops . . . . .	.159
56	Variation of Equivalent Friction Coefficient During Sinusoidal Motion With Normal Load, Frequency and Maximum Relative Velocity . . . . .	.160
57a	Schematic of Turbine Blade and Platform Damper . . . . .	.161
57b	Analytical Model for Platform Damping . . . . .	.161
58a	Dampèr Force vs Blade Displacement at Platform . . . . .	.162
58b	Blade and Damper Spring Displacements Over One Cycle of Vibration . . . . .	.162
59	Turbine Blade Test Piece Geometry . . . . .	.163
60	Damper Stress Response Signals for Varying Input Acceleration Levels . . . . .	.164
61	Baseline Conditions for Turbine Blade . . . . .	.164
62	Platform Damping Test Results (Large Damper) . . . . .	.165
63	Platform Damping Test Results (Small Damper) . . . . .	.166
64	Turbine Blade Platform Damping Characteristics (Small Damper) . . . . .	.167
65	Influence of Damper Stiffness on Platform Damping . . . . .	.168

LIST OF TABLES

<u>Table</u>	<u>Title</u>	<u>Page</u>
I	Titanium Cantilever Beam Test Results . . . . .	96
II	Summary of Twisted Plate Test Results . . . . .	97
III	Summary of Data for Fan Blade Material Damping Tests. . . . .	98
IV	Summary of Root Damping Test Data . . . . .	99
V	Summary of Shrouded Blade Response Test Data. . . . .	100
VI	Summary of Friction Test Results. . . . .	101
VII	Summary of Turbine Blade Response Test Results. . . . .	102
VIII	Summary of Turbine Blade Platform Damping Test Results ("Small Damper"). . . . .	103
IX	Summary of Turbine Blade Platform Damping Test Results ("Large Damper"). . . . .	104
B-1	Test Components and Other Hardware Designed and Fabricated for the Test Program. . . . .	105
B-2	Equipment Used in Test Program. . . . .	106

## NOMENCLATURE

A	area of beam cross-section; surface area of element
a	amplitude, nondimensional, of forced response
b	measure of slip amplitude for platform damper
$C_i$	constants, in Section 3.2
c	linear viscous damping coefficient
D	energy dissipated during one cycle of vibration
d	as a subscript denotes damper location for platform damper
E	modulus of elasticity of material
F	frictional force, nondimensional, at an interface
f	as a subscript, denotes friction
G	slip amplitude, nondimensional
g	acceleration due to gravity
H	as a subscript, denotes hysteresis
h	thickness of uniform cantilever beam
$I_o$	mass moment of inertia of fan blade about root
I	cross-sectional area moment of inertia of beam
i	as a subscript, denotes element number
J	damping constant, for material damping
K	modal stiffness; also used as cantilever beam frequency parameter in Section 3.1
L	length of beam, and fan blade
$\ell$	as a subscript, denotes lower surface for material damping calculations

## NOMENCLATURE (Cont'd)

M	moments; bending, frictional, and vibratory
m	modal mass
N	normal load at an interface
n	damping constant for material damping calculations; also used as subscript to denotes mode number in Section 3.2
P	amplitude of external excitation
p	amplitude, nondimensional, of external excitation
Q	ratio of response amplitude to external excitation amplitude, "magnification factor"
$q_i$	constants in Section 3.2
R	effective radius to the rubbing surface for a dovetail root
t	time
U	strain energy stored during one cycle of vibration
x	forced response; also tip deflection of blade
$\alpha$	sine and cosine components of the amplitude magnification factor
$\beta$	stiffness ratio for shroud damping and mass ratio for root damping
$\gamma, \delta, \theta$	phase angles
$\epsilon$	small dimensionless parameter; also used to denote strain in Section 3.2
$\zeta$	linear viscous damping constant, non-dimensional
$\kappa$	correction factor for dovetail geometry
$\mu$	coefficient of dry friction
$\rho$	mass density

NOMENCLATURE (Cont'd)

$\sigma$	blade stress
$\tau$	time parameter, nondimensional, for platform damping
$\phi$	modeshape; also used as phase angle
$\omega$	circular frequency

## SUMMARY

The potentials of various sources of nonaerodynamic damping in engine blading are evaluated through a combination of advanced analysis and testing. The sources studied include material hysteresis, dry friction at shroud and root-disk interfaces as well as at platform type external dampers. A limited series of tests were conducted to evaluate damping capacities of composite materials (B/AL, B/AL/Ti) and thermal barrier coatings. Further, certain basic experiments were performed on titanium specimens to establish the characteristics of sliding friction and to determine material damping constants  $J$  and  $n$ .

The test components used in this program included part span shrouded fan blades, turbine blades, a twisted plate and uniform beams. Fixtures, loading devices, excitation and instrumentation systems were designed for use in each series of tests taking special care to highlight the mechanism under study and to minimize fixture participation. Measurement methods adopted for use in this program varied over a wide range requiring modifications to conventional procedures.

The series of tests indicated that contributions to damping from material hysteresis is negligible for the titanium alloy used in this program. Further, the effect of root damping diminishes rapidly to negligible levels at projected operating speeds of a typical advanced fan with a dovetail type of root structure. A simulated thermal environment typical of a fan blade application showed essentially no changes in material damping characteristics. Similarly, the series of tests in which a twisted titanium plate was spun indicated essentially no changes in material damping levels.

Damping at shroud interfaces is most likely to be the only nonaerodynamic source available at all speeds to limit vibration of shrouded fan blades. The nature of this damping has been found to be a complicated mechanism involving both micro- and macroslip conditions. The stress amplitude at slip resonance has been found to be proportional to shroud load and excitation levels whereas off resonance it is proportional to excitation levels only. The boundary conditions at the interfaces appear to change during vibration resulting in a very narrow region of contact.

The mechanism of damping due to external dampers such as platform type dampers is, like shroud damping, inherently nonlinear. Depending upon the loading on the platform, the response characteristics change from a nearly sinusoidal signal to a stick-slip signal to a response emitting audible noise. Contributions to stress attenuation can come from damping due to rubbing as well as due to a change in mode shape brought about by the extent of stiffness of the damper. Test data showed changes in mode shapes occurring as the principal test parameters (excitation level, normal load) varied.

Thermal barrier coatings appear to have no influence on damping of turbine blade vibrations. Tests on composite material specimens indicate the problem of repeatability and suggest a broader program of tests involving a larger number of specimens and tests.

A unique fixture design has been developed from which fundamental sliding friction characteristics of rubbing surfaces can be measured. The laboratory set-up is such that friction-displacement loops can be obtained from which work done/cycle of motion as well as coefficient of friction can be measured. For the titanium pieces with tungsten carbide surface treatment used in this program, the coefficient of friction was found to be between .3 and .5 depending upon the normal load and independent of velocity.

Although all the tests were conducted on single blades and appropriate mathematical models were developed to represent the several mechanisms of damping, procedures to apply this data to predict damping levels in an assembly of blades have been developed and discussed.

## 1. INTRODUCTION

Vibration induced fatigue failure of blades is of continuing concern to the designer of aircraft engines. The emphasis on improved engine performance under the necessary constraints of minimum weight and satisfactory life requires that vibration levels be kept low. Further, certain important design considerations require a thorough understanding of the structural dynamic characteristics of blades. These design considerations include (1) blade life prediction methods which use vibration amplitudes in their calculations, (2) allowable frequency margins which need to be justified on the basis of the intensity of resonant stresses computed at low integral orders, and (3) accurate prediction of susceptibility to aeroelastic instabilities. The analytical techniques used in flutter and resonant stress prediction rely on accurate determination of modal characteristics of blades. These characteristics include not only the natural frequencies and mode shapes but also damping available in each mode. Contributions to damping in a vibrating blade arise from aerodynamic sources as well as nonaerodynamic sources. The latter include contributions from material damping, friction damping due to rubbing at interrupted interfaces (shroud to shroud, root to disk), and friction damping due to an external device such as a turbine blade platform-type damper.

Damping, in the context of this report, refers to energy dissipation capacities of the component undergoing vibration. A measure of energy dissipated per vibrational cycle is commonly used to report the extent of damping present in a system. In this report, the extent of damping is reported as the loss factor, which is defined as the ratio of energy lost per cycle of vibration to maximum vibrational energy stored in the appropriate mode divided by  $2\pi$ . Where such a measurement is inadequate or impractical, the extent of damping present is measured indirectly and reported as attenuation of strain in the vibrating components due to the influence of the damping mechanism.

Material or hysteretic damping refers to energy dissipation due to many complex mechanisms within a material, when a volume of the material is subjected to cyclic stresses. Thus, material damping is always present in a vibrating blade. Friction damping at an interface, however, depends on loading, roughness of surfaces, level of external excitation, slip amplitude, geometry of the contacting components, etc. For example, the root structure of a jet engine blade is typically of a dovetail, pin or firtree design, the extent of friction damping being different in each design. In the case of shrouded blades, untwisting of the blades under centrifugal loading brings neighboring blades into contact at shrouds, resulting in a complex "joint" at the interface. Determination of the precise nature of boundary conditions

at such an interface continues to be an unresolved problem defying both analysis and measurement. The condition at the interface may vary from a fully stuck to a freely slipping condition, the extent of friction damping depending on the nature of slipping motion. External dampers are frequently used to reduce stress levels in turbine blades. The two common types of dampers are the so-called blade-to-ground and blade-to-blade dampers. During engine operation, centrifugal forces bring the damper into contact with the blade platform, the extent of friction damping depending on the nature of slipping motion at the contacting surface.

The primary objective of this combined analytical and experimental program was to gain an understanding of the potentials of nonaerodynamic sources of damping in reducing vibration levels in jet engine blades. A critical survey was conducted of the available literature dealing with vibration damping, in general, and damping in jet engine blades, in particular. Though literature on the subject of damping is extensive, relatively few studies appear to be directly applicable to jet engine blades. The list of references given at the end of this report (Refs. 1 through 48) is not meant to be exhaustive and only those studies which are of direct relevance to this program are included in the list. Based on this survey, a series of analytical and experimental efforts were identified for detailed study.

In this program, single blades and blade-like components were analyzed and tested to obtain the contribution from each mechanism of damping. The components included a part-span-shrouded fan blade, a high pressure turbine blade, a blade-like titanium twisted plate, uniform cantilever beams of titanium, and strips of composite material. In addition, small titanium specimens were used in rub tests aimed at determining the nature of dry friction characteristics at an interface.

No single analytical or experimental approach appeared feasible for evaluation of all sources of damping, due to the diversity of mechanisms involved. Analytical efforts encompassed the mathematical modeling and analysis of each mechanism, leading to the solution of many independent problems. Experiments were conducted with the primary goal of highlighting the particular mechanism under study and every care was exercised to minimize contributions from other sources. The environments that needed simulation included centrifugal loading and, to a limited extent, thermal condition. Special fixtures were designed and fabricated for each series of tests. In the case of the twisted plate centrifugal tests were conducted in an evacuated centrifugal test facility.

This report summarizes (1) the principal features of mathematical modeling of the several damping mechanisms, (2) the results obtained from a series of tests leading to the measurement of damping associated with each mechanism, (3) a comparison between results from analyses and corresponding tests, and (4) implications of the results of this study to blade design against resonance and flutter.

## 2. TECHNICAL APPROACH

The fan blade and the turbine blade that were chosen for use in this program are shown in Fig. 1 along with other test components which were used to obtain additional supporting data. The survey of literature (Refs. 1 through 48) indicated that various analytical and experimental approaches were available for the determination of damping in such components. These approaches differed considerably in the level of sophistication, ease of application, and probable time needed to adapt and implement for the component under study. Since no single approach appeared uniquely suitable and advantageous, decisions to consider more than one approach were inevitably made. The final choices in each case depended on later developments, trends observed in tests, and scheduled time and cost. Brief discussions of the technical approaches adopted during the program are provided below.

### 2.1 Analytical Approaches

The mechanisms for which analytical approaches were sought can be broadly divided into two classes; (1) damping caused by material hysteresis, and (2) damping caused by friction forces induced at rubbing surfaces.

#### 2.1.1 Material Damping

Material or hysteretic damping is a material property which is measured by the energy dissipated during cyclic strain in the material. Accurate measurements show that cyclic stress-strain always has a hysteresis loop (Refs. 1 and 2). The analytical approaches for estimating material damping can be broadly divided into (1) formulations which represent the energy loss per unit volume per cycle of vibration in terms of stress amplitude and two material damping constants (Refs. 1 and 2), (2) formulations which model the hysteresis loop by a nonlinear stress-strain law for use in a forced response analysis (Refs. 5, 6, and 7), (3) formulations based on a nonexponential law of decay (Ref. 8), and (4) formulations which express the stress-strain law in terms of a complex modulus; storage and loss modulus (Ref. 10). The first two formulations appeared to be suitable for application in the present program and were selected for detailed study.

Thus, in one approach, the hysteresis loop is modeled by a nonlinear stress-strain law. This law is introduced into the equations of motion of a vibrating component and a forced response solution is obtained for comparison with experimental results. Apart from the inherent difficulties of nonlinear analysis, such an approach is not readily applicable to components having complex geometries. The alternate approach starts with a representation of the

energy dissipated at a point in the material in terms of two material damping constants and the vibratory stress amplitude at the point. Total energy dissipated is obtained by summing the energy dissipated at all points in the component. The procedure calls for a knowledge of vibratory modal stress distribution, which can be determined accurately even for components such as jet engine blades, having complex geometries. In view of its generality, the latter approach was adopted in this program. Subsequently, the approach using the nonlinear stress-strain law was used to develop a procedure for determining the two damping constants.

The ratio of total energy dissipated (D) to the maximum strain energy, (U), during one cycle of vibration, is used as the measure of material damping for a component. Thus, the component "loss factor"  $\eta$  is defined as

$$\eta = \frac{1}{2\pi} \frac{D}{U} \quad (2.1)$$

### 2.1.2 Friction Damping

Depending on conditions at an interface between two contacting components, energy dissipation due to friction may involve different mechanisms. The analytical approaches for estimating friction damping can be broadly classified as follows: (1) macroslip approach (Refs. 13 through 17), and (2) microslip approach (Refs. 23 through 25). In the macroslip approach the entire interface is assumed to be either slipping or stuck. The friction mechanism is either replaced by an equivalent linear viscous model or assumed to be governed by some form of Coulomb's law of dry friction. The effect of friction damping is obtained by determining the forced response of the component. The analysis involved is relatively straightforward and the justification for widespread use of this approach is its effectiveness at predicting the actual response. However, there is some question as to the validity of the macroslip approach when the interface has a large area, and is subjected to a nonuniform load distribution. In the microslip approach a relatively detailed analysis of the stress distribution at the interface is carried out, typically via a finite-element procedure. The extent of local slip, not necessarily throughout the interface, between pairs of contacting points is determined by applying Coulomb's law of friction to the normal and tangential stresses. A detailed knowledge of interface slip dynamics can be obtained from this approach. However, the computational effort needed to modify, iteratively, the interface stress distribution subsequent to local slipping can make the microslip approach unacceptable in a practical application.

In the context of jet engine blades, the macroslip approach was found to be suitable for modeling the friction mechanism and was therefore adopted in this program. Friction damping in jet engine blades arises from slip at the

root, shroud rubbing, and rubbing due to a platform damper. The problem in each case can be described, in a broad sense, as one of determining the effect of friction forces, at some location along the span, on the vibratory motion of the blade. The mathematical model in each case is derived by using a modal approach. The governing equation of motion for a blade can be written as (Ref. 46)

$$[M]\{\ddot{q}\} + [C]\{\dot{q}\} + [K]\{q\} = \{F\}, \quad (2.2)$$

where M, K represent the mass and stiffness matrices. The vector F includes external excitation as well as any friction damping forces. All other damping forces, such as material damping, are included in the equivalent viscous damping matrix C. The free vibration solution of Eq. (2.2) provides natural frequencies, mode shapes, and modal masses. By defining a modal matrix

$$[\Phi] = [\underbrace{\phi^{(1)}}_{\sim}, \underbrace{\phi^{(2)}}_{\sim}, \dots, \underbrace{\phi^{(n)}}_{\sim}], \quad (2.3a)$$

assuming that,

$$\{q\} = [\Phi]\{x(t)\}, \quad (2.3b)$$

and using the orthogonality property of the mode shapes, Eq. (2.2) can be transformed into

$$[m]\{\ddot{x}\} + [c]\{\dot{x}\} + [k]\{x\} = [\Phi]^T\{F\}, \quad (2.4)$$

where modal damping has been assumed.

Assuming that external excitation is harmonic, the main interest is in the case where the excitation frequency is near one of the blade natural frequencies; that is, the near resonance condition. In fact, it is precisely at this near resonance condition that damping plays a crucial role in limiting the otherwise high blade stresses. Since the thrust of this program is toward evaluating the influence of damping on blade responses, attention is focused on a single chosen mode of blade vibration. Thus, the matrix Eq. (2.4), can be reduced to

$$m\ddot{x} + c\dot{x} + kx = P \cos \omega t + F_d, \quad (2.5)$$

where  $m$ ,  $c$ , and  $k$  are modal quantities associated with the mode under consideration.  $P$  is the excitation amplitude,  $\omega$  is the excitation frequency, and  $F_d$  accounts for friction damping forces. Equation (2.5), with appropriate modifications and extensions, forms the basis of study for each of the friction damping mechanisms considered. The precise form of  $F_d$ , of course, depends on the particular source of friction damping (i.e., root slipping, shroud rubbing, and friction due to platform damper).

An assumption which is implicit in the use of Eq. (2.5) is that the friction damping does not drastically alter blade resonant frequency and mode shape, so that attention can be focused on a single chosen mode of vibration. The validity of this assumption is questionable if the analytical model is to cover the entire range of conditions at an interface, the two extremes being the fully stuck (no slip) condition and the freely slipping (zero normal load) condition. However, if the vibratory environment is such that the condition at an interface remains close to one of the extremes, then the assumption made above is valid, and use of Eq. (2.5) is justified.

In this report, the measure of friction damping is given as the increase of loss factor and/or attenuation of blade response over a "baseline" or reference condition. The loss factor is defined in Eq. (2.1) (i.e., proportional to the ratio of energy dissipated to maximum strain energy, during one cycle of vibration). The baseline condition is simply a condition where the vibratory characteristics of the blade (tip amplitude, blade stress) are known. For example, the condition of no slip at the interface (i.e., no friction damping) can serve as a baseline condition.

The principal features of the computer programs developed during the course of this investigation are presented in Appendix A.

## 2.2 Experimental Procedures

The choice of the experimental procedure to measure the contribution of a specific mechanism to the overall damping in a jet engine blade is governed by a number of requirements derived from considerations of the design and operational aspects. The requirements are:

- a. the test item is generally small with a complex shape;
- b. the test item is cantilevered but with the possibility of relative motion at the root;
- c. damping to be measured in a single mode;

- d. some very low damping levels to be expected;
- e. enviromental considerations to include a centrifugal force field, elevated temperatures;
- f. rubbing friction effects at root and shroud to be studied;
- g. air damping effects to be eliminated or accounted for.

This list is not exhaustive but represents the major considerations used when planning the various aspects of the experimental procedures, i.e., (1) fixture design, (2) method of excitation, (3) environmental simulation, and (4) measurement method.

### 2.2.1 Fixture Design

In tests involving the measurement of damping, enormous care needs to be exercised in fixture design so that fixture participation, both in resonant response and damping, can be minimized. In the present program, special fixtures were designed and fabricated with the goals of providing as realistic an environment as possible and highlighting the particular damping mechanism under study.

The basic fixture arrangement used for measuring material damping in blade-like components was a massive root block set in a rigid (within the test frequency range) vacuum chamber and mounted to a slip plate so that vibration could be applied in the horizontal direction. This method was chosen because it provided a convenient way of applying adequate excitation force to the component in an evacuated environment and also for providing means for loading the shrouds and dovetail bearing surfaces of the fan blade. The block, vacuum chamber, slip plate, and shaker armature formed a massive root restraint for the test component.

The component used in the centrifugal tests was a titanium twisted plate having an integral massive root bayonet fitting which locked into the end of the rotating arm; see Figs. 2 and 3. A special locknut arrangement was devised to ensure that the loading in the bayonet fitting did not vary with rotational speed.

The fixture for platform damping investigation was basically a heavy clamp to hold the root of the turbine blade and a mechanical means provided to allow a damper to rub on the platform of the blade; see Fig. 4. The assembly was mounted on top of an electrodynamic shaker. An evacuated environment was considered unnecessary because of the expected small blade amplitude and high damping levels from the external damper.

### 2.2.2 Methods of Excitation

The external excitation on a blade or blade-like component can be provided by a hammer impulse, an initial tip deflection, a sinusoidally varying tip force from a noncontacting magnetic driver or a sinusoidally varying root displacement. For each specific test, the method of excitation and the design of the fixture had to be chosen on the basis of the force levels required, the ease of operation and control, and applicability to the measurement method to be employed. In this program all excitation (except that used in centrifugal tests), was sinusoidally varying root displacement provided by an electrodynamic shaker. In the centrifugal tests, the twisted plate was excited by a noncontacting electromagnetic driver located at the tip.

### 2.2.3 Environment Simulation

Since this program is concerned with evaluation of nonaerodynamic sources of damping, every effort was made to minimize, if not eliminate, air damping effects. Test components were enclosed in a specially designed chamber connected to a vacuum pump. A centrifugal test facility was used to apply centrifugal loading to a twisted plate in an evacuated condition. In an operating engine, centrifugal forces lead to interfacial loading between contacting components. Since all friction damping tests in this program were bench tests, the interfacial loading was applied and controlled by specially designed loading mechanisms. Tests conducted to study the effect of temperature on damping of a fan blade called for the simulation of a typical operational thermal environment. This was done by using blowdrier heater elements to provide radiation heating.

### 2.2.4 Measurement Methods

Measurement methods fall into three general categories, (1) decay measurement, (2) frequency response analysis, and (3) direct measurement. The decay measurement involves the initial excitation of the test item and an analysis of the subsequent response signature when the excitation force is suddenly removed. The form of the transient is a decaying sinusoid for response in a single mode. If the envelope of this response is considered, the loss factor can be determined from a plot of log amplitude versus time (log decrement - Refs. 33 and 34). A variant of this method is to average over a large number of cycles of the quasi-transient behavior of a system subjected to random excitation (random decrement) (see Ref. 34).

The difficulty in decay measurements using the log decrement method is in producing a transient with a single frequency content. The problem is minimized if an initial sinusoidal excitation of a single mode is employed and the modes are well spaced (Ref. 7). More general transients, however, can be analyzed by using fast Fourier transform techniques to obtain frequency response functions. If this response (both magnitude and phase) is examined close to a modal frequency,

the modal damping can be obtained by a "Nyquist" curve fit around the resonance. The procedure for performing this has been automated in computing systems available on the market (see Refs. 35-37, 38).

The frequency response method involves driving the test item through its resonance either by a sinusoidal sweep or dwells at discrete frequencies. Response amplification as well as phase angle between output motion and input force or motion are examined (Ref. 20). One measure of loss factor for single degree of freedom systems is the value of the inverse of transmissibility (Ref. 39). Another, of course, is by way of measuring the bandwidth at half power points (Ref. 40).

The frequency phase method described in Ref. 41 enables the loss factor to be determined by measurement of the input frequency as well as the phase between response and exciting force. These measurements are made at a frequency slightly off resonance. The calculation is independent of the gain setting of the equipment and hence the problem of maintaining constant input level is obviated.

The direct measurement method (Refs. 42 and 43) requires the system to be driven sinusoidally at constant amplitude at or near resonance and the energy input is measured. Since measurement is made at constant amplitude, the energy dissipated per cycle is equal to the average energy input per cycle. The loss factor can be found from the ratio of this value and an independently determined value of the maximum kinetic energy in a cycle. The estimate of the latter may be made analytically.

The Co and Quad (see Refs. 44 and 45) method is similar to the modal analysis (FFT) method in that it separates the response vector (in transfer function form) into its real and imaginary parts and uses a Nyquist plot to determine the modal damping. However, the input in this case is a sine sweep at constant level. Alternatively, the damping factor may also be obtained from the frequencies of the maximum and minimum amplitudes of the quadrature component about a resonance (see Refs. 44 and 45)

Each of the above methods has its own advantages and disadvantages relative to a particular application. One or more of the above methods were used in making measurements of damping in this program. In certain cases, certain modifications were made to these methods and will be described in the appropriate sections of this report.

### 3. MATERIAL DAMPING

The structural configuration of a jet engine blade varies from a nearly uniform, thick, cambered blade of low aspect ratio with little or no twist to a thin, long, twisted and bent aerofoil whose camber, thickness, and cross-sectional area may vary nonuniformly from root to tip. A complex blade geometry subjected to gas and centrifugal loading leads to a complex stress distribution during vibration. For an accurate analytical estimate of material damping (which is a function of vibratory amplitude), vibratory stress calculation must necessarily be made taking full account of blade geometry. An experimental approach may pose its own problems, such as the need to eliminate fixture and air damping effects and the inherent difficulties of measuring small amounts of damping.

Studies dealing with material damping can be found in Refs. 1 through 12. Presented in this chapter, are the results of analysis and testing of a titanium cantilever beam. In addition results from tests conducted on composite material specimens and coated turbine blades are discussed.

#### 3.1 Determination of Material Damping in a Vibrating Blade

Due to the complex geometry of the blade and the resulting complicated stress distribution during vibration, it was found that an effective approach for estimating material damping is the one where energy dissipation is represented in terms of stress amplitude and damping constants; see remarks in Section 2.1.1. An outline of the analytical procedure is given below.

For a vibrating blade, the elastic response at a point in the material is characterized by a hysteresis loop as shown in Fig. 5. The area enclosed by the loop is a measure of the energy dissipated per unit volume per cycle of vibration and is called specific damping energy. The specific damping energy is assumed to be of the form

$$D = J\sigma^n; \quad J = \frac{J^*}{\sigma_e^n} \quad (3.1)$$

where  $\sigma$  is the maximum principal stress,  $\sigma_e$  is the fatigue strength (Ref. 2),  $J$  and  $n$  are material constants. The energy dissipated in the  $i^{\text{th}}$  element (in the sense of an "element" in a finite element program) is given by

$$D_i = J \int_{v_i} \sigma^n dv_i = JA_i \int_z \sigma^n dz, \quad (3.2)$$

where  $v_i$ ,  $A_i$ , and  $h_i$  are the volume, area of the upper/lower surface, and thickness, respectively, of the element (see Fig. 6).

The strain energy in the element is given by

$$U_i = \int_{V_i} \frac{\sigma^2}{2E} dv_i = \frac{A_i}{2E} \int_z \sigma^2 dz, \quad (3.3)$$

where E is the Young's modulus of elasticity

Because of the complicated geometry of a typical fan blade, three cases may arise, depending on the stress distribution across the thickness of the element, as shown in Fig. 6b.

In Case 1, the stress is constant across the thickness. The other two cases have linear stress distributions with the subscripts u and l denoting the upper and lower surfaces, respectively, of the element. For the three cases, it can be shown that Eqs. (3.2) and (3.3) yield the following:

Case 1

$$D_i = J A_i h_i \bar{\sigma}_i^n, \quad U_i = \frac{1}{2E} A_i h_i \bar{\sigma}_i^2, \quad (3.4a)$$

Cases 2 and 3

$$D_i = \frac{J}{n+1} A_i h_i \left( \frac{\bar{\sigma}_u^{n+1} \pm \bar{\sigma}_l^{n+1}}{\bar{\sigma}_u \pm \bar{\sigma}_l} \right)_i, \quad U_i = \frac{1}{6E} A_i h_i \left( \frac{\bar{\sigma}_u^3 \pm \bar{\sigma}_l^3}{\bar{\sigma}_u \pm \bar{\sigma}_l} \right)_i, \quad (3.4b)$$

where the minus signs apply to Case 2 and the plus signs apply to Case 3, and overbars denote absolute values.

Here it is assumed that modal stress distribution of the vibrating blade is available via a finite element analysis. The material damping loss factor for the blade can be written as

$$\eta_s = \frac{1}{2\pi} \frac{\sum_i D_i}{\sum_i U_i} \quad (3.5)$$

where the summations are carried out over all elements in the finite element model of the blade.

A computer program, MATDMP, was written to compute the loss factor for a vibrating blade. The program accepts as input the maximum principal stress on the upper and lower surface of each element, the area and thickness of the element, the material constants, E,  $\sigma_e$ , J\*, n, and magnitude of a reference stress. It is noted that the loss factor for a vibrating blade is associated with a specific reference condition; for example, the maximum stress at the root is to be, say, 60 MPa. The program calculates  $D_i$  and  $U_i$  for each element using the appropriate formulas in Eq. (3.4) and uses Eq. (3.5) to calculate the loss factor.

It is noted that for the special case of  $n=2$ , the loss factor for the blade is independent of the stress distributions and reduces to the simple expression

$$\eta_s = \frac{EJ}{\pi} \cdot \quad (3.6)$$

The procedure given above for calculating material damping in a vibrating blade is quite general and can be used for components having complex geometries. It is noted that modal stress distribution is a standard output from finite element programs such as NASTRAN. However, the accuracy with which the loss factor is determined depends critically on the accuracy of the material damping constants used. The approach developed to obtain the damping constants is presented below.

### 3.2 Determination of Damping Constants J and n

Though the representation of material damping in terms of damping constants has been discussed in the literature (Refs. 1 and 2), reliable values of the constants appear to be unavailable. For example, the damping constants J and n tabulated in Ref. 2 for some materials are based on tests conducted at very low frequencies (0.33 Hz). There is some question as to whether such information obtained at essentially static test conditions can be utilized in a dynamic analysis. Therefore, a need exists for a method of determining the material damping constants accurately over ranges of frequencies expected in application.

The several methods proposed in Ref. 3 for determining the damping constants require the use of a specially designed test fixture. The methods are based on measuring one or more of the following quantities: energy input into the fixture; torsional deflection of a calibrated shaft within the fixture; and strain distribution along a cantilever test specimen. It was felt that a major disadvantage of these methods is the need for a rather complex test setup with its inherent susceptibility to experimental errors. In the present work, a method of determining J and n from a simple test setup, involving vibration of a cantilever beam, is presented. The required analysis is outlined below.

The hysteresis loop, which characterizes material damping, is modeled by a nonlinear stress-strain law. The model is introduced into the differential equation of motion of a vibrating uniform cantilever beam. The forced resonant response to a harmonic excitation is calculated. The solution for the response, which is a function of the excitation and damping, leads to a method of calculating J and n from test results.

The stress-strain law chosen is a modification of the one proposed in Ref. 5, and can be written as

$$\sigma = \sigma_N + \sigma_H, \quad (3.7a)$$

$$\sigma_N = E \xi, \quad (3.7b)$$

$$\sigma_H = \mp \frac{3}{8} E^{n-1} J \xi_0^{n-3} [(\xi_0 \pm \xi)^2 - 2 \xi_0^2], \quad (3.7c)$$

where  $\sigma_N$  is the nominal stress and  $\sigma_H$  is the contribution from material hysteresis. The upper signs refer to the ascending part of the loop, the lower signs to the descending part,  $\xi$  is the strain and  $\xi_0$  is the strain amplitude. It can be shown that the area of hysteresis loop yields Eq. (3.1) (i.e., specific damping energy).

The equation of motion of a uniform cantilever beam undergoing small-amplitude vibrations and subjected to harmonic base excitation is,

$$\bar{E} \bar{I} \frac{\partial^4 \bar{y}}{\partial \bar{x}^4} + \bar{\rho} \bar{A} \frac{\partial^2 \bar{y}}{\partial \bar{t}^2} + \frac{\partial^2 \bar{M}_H}{\partial \bar{x}^2} = \bar{p} \bar{\omega}^2 \cos \bar{\omega} \bar{t}, \quad (3.8)$$

where overbars denote dimensional quantities. Here  $y(x,t)$  is the deflection,  $\rho$  the mass density,  $A$  the area of cross section,  $I$  the cross-sectional area moment of inertia,  $p$  the base excitation amplitude,  $\omega$  the excitation frequency, and  $M_H$  the bending moment due to the presence of material hysteresis. The equation of motion can be nondimensionalized by introducing the following quantities:

$$\bar{x} = x \bar{L}, \quad \bar{y} = y \bar{L}, \quad \bar{p} = \epsilon \rho \bar{L}, \quad \bar{t} = t \left( \frac{\bar{\rho} \bar{A} \bar{L}^4}{\bar{E} \bar{I}} \right)^{\frac{1}{2}}, \quad \bar{\omega} = \omega \left( \frac{\bar{E} \bar{I}}{\bar{\rho} \bar{A} \bar{L}^4} \right)^{\frac{1}{2}} \quad (3.9)$$

$$\epsilon = \frac{9 \bar{E}^{n-1} J}{2^{n+1} (n+1)} \left( \frac{\bar{h}}{\bar{L}} \right)^{n-2}, \quad M_H = \mp [(y_0'' \pm y'')^2 - 2 (y_0'')^2],$$

where the cross section is assumed to be rectangular,  $h$  is the thickness,  $L$  the length, a prime denotes differentiation with respect to  $x$ , and  $y_0$  is the amplitude of vibration. The expressions for the parameter  $\epsilon$ , and the bending moment  $M_H$ , can be obtained by using Eq. (3.7) and the strain-displacement relationship of simple beam theory. The procedure is straightforward and the details are omitted here, for the sake of brevity. The final result is a nonlinear differential equation,

$$\frac{\partial^4 y}{\partial x^4} + \frac{\partial^2 y}{\partial t^2} + \epsilon \frac{\partial^2 M_H}{\partial x^2} = \epsilon \rho \omega^2 \cos \omega t. \quad (3.10)$$

As  $\epsilon \rightarrow 0$ , the linear free vibration problem is recovered. The solution of Eq. (3.10) is sought in the form

$$y(x,t) = \sum_n \phi_n(x) u_n(t), \quad (3.11)$$

where  $\phi_n$  are linear eigenfunctions and  $u_n$  are yet to be determined. Substituting Eq. (3.11) into Eq. (3.10) and using the orthogonality property of  $\phi_n$  leads to

$$\ddot{u}_n + \omega_{0n}^2 u_n = -\frac{\epsilon}{c_{1n}} \left[ \int_0^1 \phi_n'' M_H dx + c_{2n} \rho \omega^2 \cos \omega t \right], \quad (3.12a)$$

where

$$c_{1n} = \int_0^1 \phi_n^2 dx, \quad c_{2n} = \int_0^1 \phi_n dx, \quad (3.12b)$$

and  $\omega_{0n}$  are the natural frequencies.

Due to the presence of the nonlinear hysteresis damping term, an exact solution of Eq. (3.12) cannot be obtained. However, by using the method of averaging (Ref. 47), a first-approximation to the solution can be obtained. As the interest is focussed on the resonant response in a chosen mode of vibration, the subscript  $n$  can be dropped and the solution written in the form

$$u = a(t) \cos [\omega_0 t + \theta(t)] = a \cos \gamma. \quad (3.13)$$

The amplitude and phase are assumed to be functions of time, in contrast with a problem of linear vibrations where  $a$  and  $\theta$  are constants.

The essence of the method of averaging is in the assumption that, if the nonlinearity is small (i.e.,  $\epsilon$  is small), then the amplitude and phase may be treated as constants within a cycle of vibration. Application of the method transforms Eq. (3.13) to a set of first-order differential equations

$$\dot{a} = \frac{\epsilon}{2c_1 \omega_0} [B_1 + c_2 \rho \omega^2 \sin(\gamma - \omega t)], \quad (3.14)$$

$$\dot{\theta} = \frac{\epsilon}{2c_1 \omega_0 a} [A_1 + c_2 \rho \omega^2 \cos(\gamma - \omega t)], \quad (3.15)$$

where  $\omega$  has been assumed to be near  $\omega_0$ , and  $A_1, B_1$  are the first Fourier coefficients in the expansion

$$\int_0^1 \phi'' M_H dx = A_0(a) + \sum_n A_n(a) \cos n\gamma + \sum_n B_n(a) \sin n\gamma. \quad (3.16)$$

By using the expression for  $M_H$  i.e., Eq. (3.9), Eq. (3.10) and Eq. (3.13), the Fourier coefficients can be shown to be, after some algebra,

$$A_1 = -2c_3 a^{n-1}, \quad B_1 = \frac{-8c_3 a^{n-1}}{3\pi}, \quad c_3 = \int_0^1 (\phi')^n dx. \quad (3.17)$$

The problem of obtaining the first-approximation to the steady-state response reduces to the problem of solving two nonlinear algebraic equations

$$q_1 a^{n-1} + \hat{p} \sin \psi = 0, \quad (3.18)$$

$$q_3 \epsilon \sigma a + q_2 a^{n-1} + \hat{p} \cos \psi = 0, \quad (3.19)$$

where

$$\psi = \gamma - \omega t, \quad \omega = \omega_0 (1 + \epsilon \sigma), \quad \hat{p} = \frac{c_2}{c_1} \omega_0^2 \epsilon p,$$

$$q_1 = \frac{8c_3 \epsilon}{\pi c_1}, \quad q_2 = \frac{2c_3 \epsilon}{c_1}, \quad q_3 = 2\omega_0^2.$$

From Eq. (3.18), it is seen that the maximum amplitude,  $\hat{a}$ , for a given excitation, occurs when  $\sin \psi = -1$ , so that,

$$\hat{a}^{n-1} = \frac{\hat{p}}{q_1}. \quad (3.20)$$

The linear eigenfunction of a cantilever beam is

$$\phi = C \left[ (\sin kx - \sinh kx) + \hat{C} (\cos kx - \cosh kx) \right] \quad (3.21a)$$

where

$$\hat{C} = \frac{\cos k + \cosh k}{\sin k - \sinh k} \quad (3.21b)$$

the characteristic number  $k$  is given by,

$$\cos k \cosh k + 1 = 0 \quad ; \quad \omega_0 = k^2 \quad (3.21c)$$

and the normalizing coefficient  $C$  is chosen such that  $\phi(1) = 1$ .

In base excitation tests, it is convenient to measure the strain at some point on the beam, say at the root. The relationship between the root strain,  $\epsilon_0$ , and the tip deflection,  $y_L$ , can be shown to be

$$\bar{y}_L = \frac{\bar{L}^2}{\bar{h} c_4} \epsilon_0, \quad c_4 = -k^2 c \hat{C}. \quad (3.22)$$

Since the objective is to develop a method of determining the damping constants from test results, an equation relating root strain to base excitation amplitude is required. By using relationships defined among the various quantities during the course of the analysis, it can be shown that Eq. (3.20) reduces to

$$c_5 \bar{J} \epsilon_0^{n-1} = \frac{\bar{p}}{\bar{L}}, \quad (3.23a)$$

where

$$c_5 = \frac{12 c_3 \bar{E}^{n-1} \bar{L}}{\pi c_2 \omega_0^2 c_4^{n-1} 2^n (n+1) \bar{h}}. \quad (3.23b)$$

Eq. (3.23a) can be rewritten as

$$\ln \left( \frac{\bar{p}}{\bar{L}} \right) = \ln (c_5 \bar{J}) + (n-1) \ln \epsilon_0. \quad (3.24)$$

Thus by plotting  $(p/L)$  vs  $\epsilon_0$  on a log-log scale, the damping constant  $n$  can be determined. Equation (3.23) can then be used to determine  $J$ .

The test data required for determination of the damping constants consists of excitation levels and corresponding responses for a uniform cantilever beam. A computer program DMPCON was written to generate a linear least-square fit to the test data, and calculate the damping constants. The program accepts as input the geometry of the specimen (length, thickness), material properties (elastic modulus, mass density), test conditions (mode number, location of the strain gage on the specimen), number of test points, and a table of base excitation levels vs strain.

### 3.3 Material Damping Tests

The series of tests that will be discussed in this section focussed on the determination of the characteristics of damping inherent in the titanium alloy (8-1-1). Thus, tests were performed (1) on a uniform cantilever beam to determine damping constants  $J$  and  $n$ , (2) on a twisted plate on the bench as well as in a centrifugal force field to determine damping, (3) on a fan blade to determine its material damping characteristics. All tests were conducted under evacuated conditions to minimize, if not eliminate, air damping effects.

#### 3.3.1 Uniform Cantilever Beam

The objective of this test was to determine the material damping constants  $J$  and  $n$  for a typical titanium alloy in bending and at typical blade response frequencies.

##### 3.3.1.1 Test Approach

In Section 3.2, a relationship between the maximum bending strain and peak input acceleration (sinusoidal forcing function) at the root of a uniform cantilevered beam is derived in terms of the constants  $J$  and  $n$ . The log-log plot of the peak excitation amplitude versus the corresponding maximum root strain has been shown to be a straight line from which the constants can be determined. The approach chosen therefore was to tightly clamp a beam test piece at one end and subject it to harmonic excitation measuring the strain at a point close to the root for a range of peak excitation amplitudes and in each of its first three modes. The root strain was derived from the measured strain using the standard beam functions (Ref. 48).

The test piece, as shown in Fig. 7a, was designed and built incorporating the following criteria some of which were in accordance with Ref. 39.

- a) Titanium 8-1-1 alloy to be used,
- b) Single cantilevered beam configuration,
- c) The clamped length of the beam to be at least one tenth the beam length and have a thickness of at least three times the beam thickness to minimize clamping effects,
- d) The aspect ratio to be at least 6:1 to minimize Poisson's ratio effects,
- e) The root radius to be equal to the beam thickness to minimize the stress concentration factor,
- f) The uniformity of thickness and width along the beam length to be better than 1%,
- g) The first three resonant frequencies to be in the range 60 to 1200 Hz,

- h) The piece to be machined from bar stock with successively reduced cuts to minimize residual stresses,
- i) Surfaces to be finely ground.

A special clamp (see Fig. 7b) was designed to enable the test piece to be rigidly held in the vacuum chamber of the basic fixture assembly described in Appendix B. A torque of 27 m.N was found to be sufficient to clamp the test piece, as no change in beam response (vibrating in first mode in air) was observed as the torque was increased further. The input control accelerometer was mounted directly on the clamp near the root of the beam.

#### 3.3.1.2 Instrumentation

The instrumentation system used is basically the same as that discussed in detail in Appendix B with the exception that the X-Y plotter was used only to record steady state strain levels (unfiltered, rms) with no horizontal sweep time base involved. The signal from the input control accelerometer (VSS Type 101, SN105) was amplified 20 dB prior to entering the servo control unit during excitation of the first beam bending mode so that the required low acceleration levels ( $g < .1$ ) could be applied. The response of the blade was obtained from a strain gage (Micro-Measurements Type EA-15-062AK-120) mounted 17.2 mm from the root. The gage lead-in wires were routed and epoxied in such a way as to minimize any damping or mass effects.

#### 3.3.1.3 Test Results

A fixture check out confirmed that there were no fixture resonances near the blade modal frequencies of interest. There was, however, a high frequency component noted in the input acceleration signal. This was eliminated by the use of a 50 Hz bandwidth tracking filter inserted in the excitation circuit between the signal conditioner and the servo control unit.

Owing to the very low damping in the beam ( $\eta \sim .0002$ ) the maximum response amplitude of the beam was difficult to obtain. The signal generator instability generally exceeded the half power bandwidth of the response. However, by careful tuning procedures using a Lissajous figure displayed on an oscilloscope and repeated attempts, a reliable value for the peak response was obtained. When the peak value of the response was considered to have been obtained, the strain gage level was read off the digital voltmeter and also recorded on the X-Y plotter. The excitation period was noted when the response ellipse axis on the scope was vertical.

All tests were performed with the pressure inside the chamber reduced to 15 torr. The final set of response data for each of the three beam modes is shown in Table I. These data were reduced using the expressions given in Appendix B and using the following equipment settings and other data:

Input accelerometer conditions setting	41.8 mv/g
Strain gage and lead in wire resistance	120.5 $\Omega$
Gage factor	1.995
Strain gage translator setting	3.6
Assumed modulus of elasticity	124 GPa

### 3.3.2 Twisted Plate - Bench and Spin Tests

Using the analysis of Section 3.1, the loss factor for a bladelike structure having a complex shape may be computed from the maximum principal stresses in a given mode. As a first step in applying this method to an actual fan blade, a uniform, twisted plate was chosen. The test objectives were to measure the forced response of the plate and to determine its loss factors both on the bench and with the plate subjected to a centrifugal force field.

#### 3.3.2.1 Test Approach

The analysis of Section 3.1 requires the determination of the principal stresses throughout the component. However, if the responses are modal then the stress at one point can be used to scale the modal stress distribution. Therefore the test method chosen was to harmonically excite the plate which was held rigidly at its root in a massive block and measure the strain response using miniature strain gages at its root for various levels of forcing. The loss factors were estimated from root strain transient response curves resulting from abrupt cut off of the harmonic excitation, i.e., in an essentially single mode response. The application of an overall steady force field was obtained by mounting the plate on the end of a centrifuge arm and spinning it. For this series of tests, the harmonic excitation was provided by means of an electromagnetic driver located at the tip of the plate.

The test specimen was a titanium alloy 8-1-1 plate of aspect ratio, 3. The dimensions were 15.24 x 5.08 x .25 cm with the plate linearly twisted to give a twist of 30.5° (actual) relative to the root. Similar design and fabrication guidelines to those used for the uniform beam were used in this case (see Section 3.3.1). However, the root attachment of the centrifuge arm required a special design. The final design shown in Fig. 3, incorporated the following features:

1. A root mass that was large compared with that of the plate.
2. A minimum of mating surface area at the connection between the root and centrifuge arm.

3. Preloaded mating surfaces using a special locknut arrangement (torque to 680 Nm) such that the load remained constant over the range of test speeds.
4. Integral plate and root bayonet fitting.

A steel shim, 0.1 mm thick, was glued near the tip of the plate to permit magnetic excitation, see Fig. 2. The magnetic driver was attached to the arm by means of a steel tube surrounding the test piece. The test assembly in the centrifuge is shown in Fig. 8. The plate tip radius was 72.59 cm.

For bench tests, the plate was mounted in the fixture/vacuum chamber as shown in Fig. 9 and described in Appendix B, using a clamp adapter. This clamp was mounted on the massive steel root-block and held the bayonet fitting of the plate by means of four large bolts. The root chord of the plate was positioned vertically.

The plate was instrumented with two longitudinal strain gages (Micromasurements Type EA-06-062AK-120) mounted 0.64 cm from the root and edges of the plate as shown in Fig. 2. These positions corresponded with the root edge elements used in the finite element structural analysis model shown in Fig. 10. The length of wire on the actual plate was minimal with the wire routed along the radius and then up through a hole in the root. The wire was epoxied in place.

#### 3.3.2.2 Instrumentation

The instrumentation system used in the centrifugal tests is shown in a block diagram in Fig. 11. The plate was excited by means of a small electromagnetic driver located near the tip of the plate (see Fig. 2). Power for the driver was provided via slip rings by an MB Electronics power amplifier and the frequency was controlled by a B&K sweep oscillator. A Fluke counter provided an accurate readout of the input signal period. The plate strain gages were wired through slip rings to a pair of strain gage translators. These provided a calibrated signal to a narrow band pass filter and amplifier. The signal with high and low frequency noise removed was recorded on a B&K level recorder operating in the peak mode. Decays were obtained on this recorder and loss factors determined using the method described in Appendix B. The recording system used for the bench testing is essentially the same as the system described in Appendix B except that the narrow band filter was not required since the noise level was considerably lower. The excitation system used is described in Appendix B with the amplifier in the input circuit to enable the very low ( $< 0.02g$ ) acceleration levels to be applied. The input control accelerometer (VSS type 101, S/N 105) was mounted directly onto the thickened root (bayonet fitting) of the plate test piece as shown in Fig. 8. For both tests, all output voltage rms readings were taken from a digital voltmeter and that level was noted on the charts.

### 3.3.2.3 Testing and Results

Prior to testing in the centrifuge, the arm was carefully balanced using finely adjustable counter balance weights. Testing consisted of exciting the plate at each of its first three natural modes, namely first bending, second bending and first torsion modes, in air (at 0 rpm only) and in partial vacuum (5 torr) at rotational speeds up to 1508 rpm. The procedure used was to bring the plate to resonance, as indicated by a steady maximum response, and abruptly cut-off the excitation, thus obtaining a record of decaying signals from strain gages mounted near the root. The magnet had to be repositioned to obtain maximum response in each mode. The system used was found to be susceptible to noise from the slip rings and interference from neighboring rigs. However, by repeating the tests at each test point a number of times, reasonably consistent results were obtained. In all, data were recorded from a total of 120 tests in a partially evacuated environment of 5 torr. A summary of the results obtained from these tests is given in Table II, and actual test data are plotted in Fig. 12. Sample decay curves are given for tests performed at zero speed in Fig. 13 and at 1000 rpm in Figs. 14 and 15.

Bench testing of the plate consisted of exciting the plate in air and in partial vacuum in each of its first three modes with a base excitation, noting the peak response of the plate and then obtaining a decay curve after an abrupt cut-off of the excitation. The input levels needed to obtain adequate strain levels in the first mode were very low ( $< .02g$ ) and required a signal amplifier in the input circuit. Even with this technique, the range for which values could be obtained was very limited. The second mode was difficult to tune because of a possible fixture interaction, but above a certain input level, consistent results were obtained. These results are summarized in Table II. Owing to small asymmetry of the plate, the first torsion mode was also excited but in this case the response to various inputs could not be realistically compared with analysis and so only the loss factor data are given. The values for loss factor in each of the modes from bench test are also plotted in Fig. 12 and provide a good comparison with values obtained from the centrifuge test.

### 3.3.3 Typical Fan Blade in Ambient and Thermal Environments

Using the analysis of Section 3.1, the loss factor for a component vibrating in a given resonant mode may be computed from the maximum principal stress distribution. In order to verify the theory, a part span shrouded titanium fan blade was subjected to vibration testing. The test objectives were to measure the material damping in the blade for its first three resonant modes and also to assess the effects of elevated temperature on the damping characteristics of the blade.

### 3.3.3.1 Test Approach

The analysis of Section 3.1 requires the determination of the principal stresses throughout the component. However, if the responses are modal, then the stress at a reference point on the blade can be used to scale the modal stress distribution. Therefore the test method chosen was to harmonically excite the fan blade which was welded at its root to a massive block and measure the strain response for various levels of forcing using miniature foil strain gages mounted at high axial stress locations near the root and the A.S.M.T. position. The loss factors for the first flap mode were estimated from frequency sweep response plots using the half power method. For the two higher modes the loss factors were estimated from strain transient curves resulting from abrupt cut-off of the harmonic excitation (i.e., in an essentially single mode response). The basic damping data were obtained with the blade vibrating in evacuated conditions. However, for the tests in a thermal environment, evacuated conditions were considered unnecessary since the measurements of any changes in damping characteristics due to temperature would provide the desired information. The tests were therefore performed in air with temperatures on the blade of the order of 150°C.

The test specimen was an advanced part span shrouded titanium (Ti) fan blade with dovetailed root configuration. The same blade was used throughout the program to obtain measurements of damping at root as well as at shroud interfaces.

For this test series, the blade was welded into a massive titanium block at its root by machining the dovetail off and replacing it with weldment (see Figs. 16 and 17). The root was oriented in the block such that the applied excitation vector was normal to the tip chord. The system was mounted in the fixture/vacuum chamber vibration set up described in Appendix B.

The test arrangement for the thermal testing is shown in Fig. 18. It was basically the same as that used for the "cold" blade except that the airtight aluminum lid was replaced by a fiberglass cover and two 1 kW blowdrier heater elements were installed to provide radiation heating. The heaters were freely suspended from a separate bracket arrangement such that they were approximately 215 cm from the blade profile. Three thermocouples were used, one inside the dovetail of the blade, one near the shroud, and one close to the tip. A VARIAC voltage controller was used in all the tests and a prolonged soak (three hours) assured a stabilizing of the temperature profile from root to tip. The two TCs on the blade touched the blade surface before the tests started so that the temperatures recorded were actual metal temperatures, but were moved away during vibration.

### 3.3.3.2 Instrumentation

The blade was instrumented with two high temperature strain gages (BLH

Electronics, Type FSM 12-35-S6). The lead wires were originally attached using M BOND G100 high temperature cement which proved to be too brittle and was replaced with RTV 106. The choice of gage location was directed by the need for high axial strains in all three modes and a NASTRAN dynamic analysis was used to determine the optimum locations. These locations, as shown in Fig. 16 and 17, were near the root at the leading edge and above the shroud near the maximum thickness position.

The instrumentation system used in the tests was the basic system described in Appendix B. An amplifier was required in the input circuit to enable the low ( $< 0.1g$ ) acceleration levels to be applied. The input control accelerometer was mounted outside the fixture at the root location (see Fig. 18). For the tests, all output voltage RMS readings were taken from the digital voltmeter and these levels were noted on the data charts.

#### 3.3.3.3 Testing and Results

Testing at ambient temperature consisted of exciting the blade at each of its first three natural modes of vibration under evacuated conditions down to 10 torr and recording the strain response. Decay tests in the first mode (first flap) were not feasible owing to difficulties experienced in achieving a total arrest of input motion upon abrupt cut-off of the excitation. This difficulty was caused by the inertial forces of the vibrating blade being sufficiently large to induce vibratory motion in the shaker armature after the input was cut-off. Thus a modified procedure using a frequency sweep over the resonance and determination of the bandwidth at the "half power point" at various degrees of pressurization and evacuation was utilized. The pressure was gradually reduced until the damping limit imposed by the available minimum sweep rate (0.0136 octave/minute) was reached. This damping value was calculated to be  $\eta = 0.0022$ . The loss factor for material damping, being much smaller, was obtained by extrapolation of the data points to zero pressure. The values obtained for the first mode loss factor and frequency are shown plotted against the pressure ratio in Figs. 19 and 20 respectively. The loss factor value obtained by extrapolation can be seen to be between 0.003 and 0.00085 for a range of "root" stresses of 56 to 110 MPa. These results, together with the data for the two higher modes are tabulated in Table III. It should be noted that the loss factors for modes 2 and 3 were obtained from the average slope between points 1 and 4 dB down from the maximum value on the decay curves. Figure 21 shows a comparison of the test results (loss factor) with the theoretical values for the first three modes.

In the thermal environment, the loss factors in the first mode were high enough, because of air damping, to be derived directly from the slow frequency sweep response data. Results for the first mode are shown in Fig. 22. Two input levels, namely 0.075 g and 0.15 g, were applied and loss factors were determined using the "half power method." As can be seen, the temperatures

dropped during the test as a result of air being pumped around inside the chamber by the blades and being cooled by the surfaces of the chamber. "Hot" and "cold" peak decay curves for the second and third modes are shown superimposed for comparison in Fig. 23 and 24.

#### 3.3.4 Composite Material Damping

In addition to the several mechanisms of damping discussed so far, two additional mechanisms, viz. (1) composite materials and (2) coatings typically used in turbine blading, were examined to determine the potential, if any, of damping available. The effort related to composite materials is discussed below.

Potentials of damping in composite material were evaluated by tests conducted on two materials: Boron/Aluminum (50% by volume of Boron filaments in a 6061 Aluminum matrix); and Boron/Aluminum/Titanium (0.076 mm thick titanium cladding on two sides amounting to approximately 6% by volume titanium). The specimens were flat strips (see Fig. 25) of nominal size of 20.32 x 2.54 x 0.25 cm. Two of each specimens were tested as cantilever beams (see Fig. 26) and data were obtained in their first two modes. All tests were conducted in a vacuum chamber, exciting the beams at their resonances and recording the decay of vibrations upon abrupt cutoff of input excitation. The strain signals from a gage mounted 0.64 cm from the root were filtered before being recorded on a level recorder.

Before the final sets of data were recorded to obtain an estimate of damping, it was found necessary to conduct tests to (1) determine the clamping torque above which the fixture participation could be considered to be minimum and (2) establish the level of maximum strain below which the material behavior is linear. Based on this series of tests, a clamping torque of 60 Nm was found to be adequate and about 500 micro strain at the root of the cantilevered specimen was found to be the desired limit. During these initial tests the material characteristics of the specimens appeared to undergo continuous change and this necessitated subjecting one B/Al test piece and one B/Al/T test piece to prolonged testing over a wide range of input levels. In doing so, it was suspected that these two beams were overstressed and thus were not used to obtain the final results. The results presented in Fig. 27 were obtained for bending strains within the linear range.

Using the carefully measured values of resonant frequencies and from a knowledge of the beam characteristic numbers, the modulus of elasticity for B/Al and B/Al/Ti specimens were calculated to be 199 GPa and 166 GPa, respectively. Figures 27a and 27b show the measured loss factors as a function of maximum root strain. Factors obtained from characteristic beam functions (Ref. 48) were used to estimate the root strain from the measured strain. For both the specimens, the loss factor in mode 2 was found to be smaller than that in mode 1. The variation of damping with strain level is small indicating that the value of  $n$  in the relationship  $D = J\sigma^n$  is close to 2. Even with limited maximum strain

levels, repeatability, particularly in the first mode, was found to be difficult as is evident from a comparison of results for mode 1 obtained before and after measuring mode 2.

### 3.3.5 Tests on Turbine Blades With Thermal Barrier Coatings

The objective of this series of tests was to evaluate the damping potential, if any, of some typical coatings currently in use on turbine blades. In general, these coatings are used for thermal protection and to inhibit corrosion. The coatings are applied to the blade airfoil and upper surface of the platform.

#### 3.3.5.1 Test Approach

The approach was to measure the loss factors of blades (before and after applying a coating) using response decay techniques. Two turbine blades, similar to that used for the platform damping tests (Section 6) were prepared and tested. The following treatments were used in preparing the blades for these tests.

Treatment # 1 - Two blades

Strip (20% HNO<sub>3</sub>) and vapor blast

Treatment # 2 - Blade #1

Diffusion Aluminide coat (pack cementation process) to a thickness of 76 microns.

Diffusion heat treat at 1079°C/4 hrs/Argon

Treatment # 3 - Blade #2

Sputter coat with NiCoCrAlY to a thickness of 126 microns.

Diffusion heat at 1079°C/4 hrs/Argon

Treatment # 4 - Both Blades

Overcoat (plasma spray) with Y<sub>2</sub>O<sub>3</sub>-ZrO<sub>2</sub> to a thickness of 250 microns using a 76 microns thick bond coat of NiCr/Al composite.

Before each test, the blades were instrumented with a strain gage (MM Type EA-06-062AK-120) at the root of the shank.

Each blade was tested in the same fixture as was used in the platform damping tests (see Fig. 4), but in these tests, additional care was taken to make the fixture participation an absolute minimum and torquing procedures were standardized. Even with this additional effort, the fixture participation and root effects were

still significant. However, initial tests indicated that small changes in blade damping could be detected with the setup as long as the torquing procedures were followed.

Strain gage signals were conditioned using the strain gage translator and were recorded on the level recorder. Calibration of the level recorder was performed by exciting the blade with the shaker and reading the output levels on a digital voltmeter.

Decays were obtained by impacting the blade with a 'soft' hammer rather than by using the decay from resonance technique as tuning was impractical with the extremely low damping levels prevailing.

### 3.3.5.2 Test Results

The ranges of loss factor and response frequency for the blades following a treatment are shown below for a stress range of 17 MPa - 55 MPa.

Treatment #	<u>Blade #1</u>		<u>Blade #2</u>	
	Frequency Hz	Loss Factor	Frequency Hz	Loss Factor
1	520.17-520.09	.00030-.00031	523.25	.00029-.00037
2	521.16	.00022-.00029	—	—
3	--	--	521.27	.00024-.00036
4	496.52	.00090-.00128	501.76	.00068-.00106

## 3.4 Numerical Results and Discussion

In this section, numerical results relevant to the evaluation of material damping in titanium are presented. Theoretical results are compared to those obtained from tests.

### 3.4.1 Damping Constants

The measured data from tests on the uniform cantilever beam are given in Table I. The dimensions of the beam are given in Fig. 7a. The following properties have been assumed for titanium, the beam material:  $E = 1.27 \times 10^5$  MPa;  $\rho = 4370 \text{ kg/m}^3$ ,  $\sigma_e = 590$  MPa. Use of the test data (excitation vs response) in the computer program DMPCON yields the following results:

Mode	Frequency (Hz)		n	$\frac{J^*}{\text{kN.m/m}^3} / \text{Cycle}$
	Theory	Test		
1	67.1	68.4	1.89	1.30
2	420	427	2.05	2.40
3	1178	1196	2.02	1.03
Average Values $\approx$ 2				1.58

It is noted that n is very close to 2 for titanium.

An analysis of data from tests on the uniform cantilever beam indicates that the value of the damping constant n is very close to 2, for titanium, suggesting that material damping is essentially independent of stress. This value of n is in general agreement with the value quoted in Ref. 2. However, the value of  $J^* = 1.58 \text{ kN.m/m}^3 / \text{cycle}$  that was obtained in this program, is an order of magnitude less than that noted in Ref. 2 ( $J^* = 14$ ). This considerable difference could be attributed, among other factors, to differences in test frequencies. It is noted that values of damping constants in Ref. 2 were obtained from tests conducted at 0.33 Hz, essentially static conditions. It is necessary, however, to emphasize that no final conclusions should be drawn from this limited study. Only a thorough program solely devoted to a study of material damping constants for a set of selected engine blade materials can serve to establish the magnitudes of these constants for use in design considerations.

### 3.4.2 Twisted Plate

As indicated in Section 3.1, the procedure for calculating material damping calls for the modal stress distribution of the component. The NASTRAN finite element model of the twisted plate is shown in Fig. 10. The model consists of 48 QUAD4 type of elements. Figure 28 shows, for the first three modes, the spanwise distribution of modal principal stresses near the midchord of the plate. A comparison of the measured and theoretical (NASTRAN) frequencies (Hz) is shown below:

Mode	Zero Speed		500 rpm		1000 rpm		1500 rpm	
	Theory	Test	Theory	Test	Theory	Test	Theory	Test
1	97.8	101	100	103	107	109	118	119
2	540	550	542	553	548	558	557	568
3	670	667	670	677	671	677	672	678

A theoretical loss factor of 0.00018 is obtained by using  $J^* = 1.58$  and  $n = 2$ . Figure 29 shows the test results of the forced resonant response of the twisted plate. It is possible to estimate the extent of material damping by using the forced response results; what is required is an equation relating the material damping loss factor, blade stress, and the base excitation level. Such an equation has been derived in Ref. 42 for the case of a uniform cantilever beam. The necessary analysis involves the computation of the work done by the shear force at the root and the strain energy stored during one cycle of vibration. For the case of the twisted plate these quantities were calculated by using modal information (frequency, mode shape and modal stress) obtained from a NASTRAN analysis. An analysis similar to the one in Ref. 42 was carried out and the results from Fig. 29 were used to compute the material damping loss factors as follows: 0.0001 for the first mode and 0.00016 for the second mode.

The results of calculating the damping constants by using the uniform cantilever beam tests indicate that  $n$  is very close to 2 for titanium. This implies that material damping for any component made of titanium is essentially independent of stress; suggesting that the detailed procedure developed in Section 3.1 is essentially redundant if the blade material is titanium. However, in order to study the sensitivity of the theoretical results to possible variation in the value of  $n$ , and to check out the computer program, MATDMP, loss factors for the twisted plate were calculated by using the modal stress distributions obtained from NASTRAN. The results for a reference root stress of 68.49 MPa are summarized below.

Mode	Theoretical Loss Factor ( $\eta$ ); $J^* = 1.58$		
	$n = 1.9$	$n = 2.0$	$n = 2.1$
1	.00024	.00018	.00014
2	.00024	.00018	.00014
3	.00023	.00018	.00015

For the twisted plate, centrifugal forces caused an apparent increase in material damping in the first two modes (see Fig. 12) possibly due to some participation by the fixture. No such increase was observed in the third mode (torsion) indicating a more complete restraint of the fixture against torsion. Data were taken at vibratory stress levels not exceeding 46 MPa. Attempts at testing at higher stress levels were thwarted by tip deflection limitations (driver proximity) in the first mode and driver power limitations for the higher modes. This small stress range does not enable the nature of dependence of damping on stress to be established.

### 3.4.3 Fan Blade

A NASTRAN finite element analysis was carried out to determine the natural frequencies, mode shapes, and modal stress distribution for the first three modes of a typical fan blade. A comparison of theoretical and test frequencies is shown below:

Frequency (Hz)	Mode 1	Mode 2	Mode 3
Theory	77.3	242	497
Test	77.9	250	482

The test results for material damping (loss factors) for the fan blade are shown in Fig. 21. A theoretical loss factor of 0.00018 is obtained by using  $J^* = 1.58$  and  $n = 2$  for titanium.

For the fan blade, test results in the first mode indicate some spread in data, possibly due to the method that had to be used to obtain these results; i.e., the method of measuring damping by vibrating the blade in a pressurized chamber and extrapolating the results to vacuum conditions. Measurements in modes 2 (second bending) and 3 (first torsion) were obtained more directly by observing the decay of vibrations in vacuum.

Tests performed on the fan blade in a thermal environment indicate that, for titanium, the differences in material damping between "cold" and "hot" conditions are insignificant. This appears to confirm the results of Ref. 12. The observed drop in resonant frequency in each mode, with increase in temperatures, is attributable to the decrease in modulus of elasticity at higher temperatures.

B/AL and B/AL/Ti specimens tested show loss factors between .001 and .002, although repeatability of tests was a major problem. Tests performed on turbine blades coated with typical corrosion inhibitor coatings show no change in damping levels. However, for blades having a 250 microns thick thermal coating, an increase in damping of 300 to 400 percent was noted.

#### 4. DAMPING DUE TO SLIPPING AT ROOT

The root structure of a jet engine blade is typically of a dovetail, pin or firtree design. The root slides into a corresponding slot on the rotor disk, and centrifugal forces provide a tight fit during engine operation. Major parameters which control the extent of friction damping at the root to disk interface are: centrifugal loading, roughness of surfaces, level of external excitation, and root geometry. Studies which address the specific problem of root damping in a jet engine blade can be found in Refs. 18-22. Presented in this Chapter, are the results of analysis and testing of a fan blade having a dovetail root.

##### 4.1 Forced Response of a Fan Blade with Slip at the Root

Based on an assessment of different available analytical approaches, the approach of Ref. 20 was chosen for detailed study and application. The analysis presented in this Section is based on the following assumptions; see also remarks in Section 2.1.2:

1. Friction mechanism is of macroslip-type, and governed by Coulomb's law of dry friction.
2. Friction damping does not drastically alter blade resonant frequency and mode shape, so that attention can be focussed on a single chosen mode of vibration.
3. For the mode under consideration, the modal stiffness and modal stress are normalized to unit tip displacement of the blade, and are computed for the case when there is no slip at the root.

For a vibrating blade with slip at the dovetail root, the total motion may be considered as a combination of rigid body motion and elastic vibratory motion as shown in Fig. 30a. If attention is focused on a single mode of vibration, then the governing equation of vibratory motion can be written as

$$m_1 \ddot{x}_1 + k(x_1 - x_2) + c(\dot{x}_1 - \dot{x}_2) = P \cos \omega t . \quad (4.1)$$

Here,  $m_1$ ,  $k$ , and  $c$  are modal quantities,  $P$  is the external excitation amplitude,  $\omega$  is the excitation frequency,  $x_1$  is the tip amplitude, and  $x_2$  accounts for blade rigid body motion. For the rigid body motion the equation is

$$I_0 \ddot{\theta} + M_f \operatorname{sgn}(\dot{\theta}) + M_v = 0, \quad (4.2)$$

where  $I_0$  is the mass moment of inertia of the blade about the root,  $M_f$  is the frictional moment due to slip, and  $M_v$  is the moment due to vibratory forces. Letting,

$$\begin{aligned} I_0 &= m_2 L^2, & x_2 &= \theta L, \\ M_f &= R \mu N \cos \alpha, & \kappa &= (R/L) \cos \alpha, \end{aligned} \quad (4.3)$$

where  $L$  is the length of the blade,  $\mu$  is the coefficient of friction,  $N$  is the axial pull on the blade,  $\alpha$  is the dovetail angle, and  $R$  is the "effective radius" to the rubbing surface (Fig. 30b), the equations of motion for the blade are

$$\begin{aligned} \bar{m}_1 \ddot{\bar{x}}_1 + \bar{k}(\bar{x}_1 - \bar{x}_2) + \bar{c}(\dot{\bar{x}}_1 - \dot{\bar{x}}_2) &= P \cos \bar{\omega} t, \\ \bar{m}_2 \ddot{\bar{x}}_2 - \bar{k}(\bar{x}_1 - \bar{x}_2) - \bar{c}(\dot{\bar{x}}_1 - \dot{\bar{x}}_2) + \mu \kappa \bar{N} \operatorname{sgn}(\dot{\bar{x}}_2) &= 0, \end{aligned} \quad (4.4)$$

where overbars denote dimensional quantities. It is convenient to non-dimensionalize the equations of motion by introducing the following quantities

$$\begin{aligned} \beta &= \bar{m}_2 / \bar{m}_1, \quad x_1 = \bar{x}_1 / \bar{x}_0, \quad x_2 = \bar{x}_2 / \bar{x}_0, \quad \bar{\omega}_0^2 = \bar{k} / \bar{m}_1, \quad t = \bar{t} \bar{\omega}_0, \\ \omega &= \bar{\omega} / \bar{\omega}_0, \quad F = \mu \kappa \bar{N} / \bar{k} \bar{x}_0, \quad p = \bar{P} / \bar{k} \bar{x}_0, \quad \zeta = \bar{c} / 2 \bar{m}_1 \bar{\omega}_0, \end{aligned} \quad (4.5)$$

where  $\bar{x}_0$  is some characteristic length and the governing equations in dimensionless form are,

$$\begin{aligned} \ddot{x}_1 + (x_1 - x_2) + 2\zeta(\dot{x}_1 - \dot{x}_2) &= p \cos \omega t, \\ \beta \ddot{x}_2 - (x_1 - x_2) - 2\zeta(\dot{x}_1 - \dot{x}_2) + F \operatorname{sgn}(\dot{x}_2) &= 0. \end{aligned} \quad (4.6)$$

Assuming a solution of the form

$$\begin{aligned} x_1 &= a \cos(\omega t + \phi - \delta), \\ x_2 &= b \cos(\omega t + \phi), \\ \operatorname{sgn}(\dot{x}_2) &\approx - (4/\pi) \sin(\omega t + \phi), \end{aligned} \quad (4.7)$$

leads to

$$\begin{aligned}
 \eta \alpha_1 + (1 - \omega^2) \alpha_2 - Q_2 &= \cos \phi, \\
 (\omega^2 - 1) \alpha_1 + \eta \alpha_2 - \eta Q_2 &= -\sin \phi, \\
 \eta \alpha_1 + \alpha_2 - (1 - \beta \omega^2) Q_2 &= 0, \\
 \alpha_1 - \eta \alpha_2 + \eta Q_2 + G &= 0,
 \end{aligned} \tag{4.8}$$

where,

$$\begin{aligned}
 \eta &= 2\zeta\omega, \quad Q_2 = b/p, \quad G = 4F/\pi p, \\
 \alpha_1 &= (a/p) \sin \delta, \quad \alpha_2 = (a/p) \cos \delta.
 \end{aligned} \tag{4.9}$$

Equations (4.8) are set of algebraic equations in the unknowns,  $\alpha_1$ ,  $\alpha_2$ ,  $\phi$ , and  $\delta$ . The last two equations of the set can be shown to yield

$$\begin{aligned}
 \alpha_1 &= -(\eta\beta\omega^2 Q_2 + G)/(1 + \eta^2), \\
 \alpha_2 &= [(1 + \eta^2 - \beta\omega^2) Q_2 + \eta G]/(1 + \eta^2)
 \end{aligned} \tag{4.10}$$

so that,

$$Q_1 = a/p = (\alpha_1^2 + \alpha_2^2)^{1/2} \quad \text{and} \quad \tan \delta = \alpha_1/\alpha_2. \tag{4.11}$$

Substitution of Eqs. (4.10) in the first two equations of Eq. (4.8) leads to,

$$\tan \phi = (\omega^2 \alpha_1 + G)/(\alpha_2 + \beta Q_2) \omega^2, \tag{4.12}$$

and after some algebra, a quadratic equation, the solution of which yields,

$$Q_2 = -C_2 G + [(C_2 G)^2 - C_1(C_3 G^2 - C_4)]^{1/2}, \tag{4.13}$$

where

$$\begin{aligned}
 C_1 &= \eta^2(1 + \beta)^2 + (1 + \beta - \beta\omega^2)^2, \quad C_2 = \eta/C_1, \\
 C_3 &= [(1 - \omega^2)^2 + \eta^2]/\omega^4 C_1, \quad C_4 = (1 + \eta^2)/\omega^4 C_1.
 \end{aligned}$$

It is noted that  $Q_1$  is a measure of the blade response and  $Q_2$  a measure of the slip amplitude at the root. From Eq. (4.12), the condition for slip to occur (i.e.,  $Q_2 > 0$ ) is

$$(C_3 G^2 - C_4) < 0; \quad G < \left\{ (1 + \eta^2) / \left[ (1 - \omega^2)^2 + \eta^2 \right] \right\}^{1/2}. \quad (4.14)$$

When there is no slip at the root, the solution is given by

$$\begin{aligned} Q_2 &= 0, \\ Q_1 &= \left[ (1 - \omega^2)^2 + \eta^2 \right]^{1/2}. \end{aligned} \quad (4.15)$$

The analysis and solution developed above is applicable to the case of direct excitation of the blade. If the excitation is applied at the base of the blade, as was done for tests performed in this program, the analysis follows along similar lines to the one given above. The necessary modifications to the analysis and solution are as follows:

$$p = \bar{p} / \bar{x}_0, \quad C_4 = 1, \quad (4.16)$$

$$\begin{aligned} \alpha_1 &= -(1 + \beta - \beta \omega^2) G / C_1, \\ \alpha_2 &= \left[ \eta (1 + \beta) G / C_1 \right] + Q_2, \end{aligned} \quad (4.17)$$

where  $\bar{p}$  is the displacement amplitude of the base excitation.

The influence of friction at the root can be expressed as a loss factor, defined as

$$\eta_f = \frac{1}{2\pi} \frac{D}{U} \quad (4.18)$$

where  $D$  is the energy dissipated per cycle of vibration and  $U$  is the peak strain energy in the blade. The two energies are given by

$$D = 4\mu\kappa \bar{N} \bar{x}_2, \quad U = \frac{1}{2} \bar{k} \bar{x}_1^2, \quad (4.19)$$

so that, in terms of dimensionless quantities

$$\eta_f = G Q_2 / Q_1^2, \quad (4.20)$$

and total loss factor for the blade is,

$$\eta_b = \eta_0 + \eta_f, \quad (4.21)$$

where  $\eta_0$  accounts for damping from sources other than friction, such as, material hysteresis and air damping.

The major interest is in obtaining the maximum blade response at resonance. One approach is to calculate the response for different values of the nondimensional frequency,  $\omega$  and pick out the maximum amplitude. However, for the damping levels expected in the problem being studied, maximum response occurs when the excitation frequency is near the natural frequency (i.e.,  $\omega \approx 1$ ) so that a good approximation to the maximum response is obtained by simply getting  $\omega = 1$  in the solution.

The blade tip deflection can be related to the blade stress by specifying a baseline or reference condition where the blade vibration characteristics are fully known. If the baseline tip deflection of the blade is chosen as the characteristic length  $\bar{x}_0$  used for nondimensionalization in Eq. (4.5), then it can be shown that

$$\sigma = a \sigma_0, \quad (4.22)$$

where  $\sigma_0$  is the blade stress in the baseline condition and  $\sigma$  is the blade stress at any other condition. In the present study, the condition of no slip at the root is chosen as the baseline condition so that the baseline blade stress is the same as the modal blade stress.

A computer program, ROTDMP was written to compute blade loss factor and blade stress (near the root) as a function of blade axial load. The program calculates the resonant response by using Eqs. (4.10) through (4.13), the loss factor by Eqs. (4.18) through (4.21), and the blade stress by Eq. (4.22). The input to the program includes: frequency in Hz; blade axial load, N; coefficient of friction  $\mu$ ; dovetail correction factor  $\kappa$ ; mass ratio  $\beta$ ; modal stiffness  $k$ ; baseline (modal) stress  $\sigma_0$  and non-friction damping loss factor  $\eta_0$ .

## 4.2 Experimental Investigation of Damping at Blade Root

The objectives of this series of tests were to estimate the potentials of damping available in a root structure of dovetail design and to compare the results with the trends established by analysis.

### 4.2.1 Experimental Approach

Section 4.1 describes the analysis of the forced response of a single fan blade with slipping in a dovetail configured root. Since the major effect of the centrifugal loading of a typical blade is to increase the reactive forces on the mating surfaces of the dovetail, the approach taken in this investigation was to test a single dovetailed blade and simulate, as closely as possible, the root loading by means of a special fixture. Sinusoidal excitation was applied at the blade root and the blade response was monitored via strain gages mounted at high stress points. Since the major interest was in obtaining the maximum blade response at resonance, the tests were run at steady state at a resonant frequency and transient decays were obtained by abruptly cutting off the excitation. The level of damping was estimated from the slope of the resulting decay curve.

The test piece used was another specimen of the titanium fan blade used in the material damping tests. The blade was mounted in the fixture, described in the next section, using two titanium alloy (8-1-1) clamps with mating surfaces having geometry and dimensions exactly the same as those of the blade root slot in an actual disc. Blade strain response was measured by two strain gages, one mounted near the leading edge at the root and the other at the above-shroud-maximum-thickness position. These were the same locations used in the material and shroud damping investigations.

The basic fixture, slip plate and shaker arrangement, as described in APPENDIX B, was used. A new steel root block was designed to provide a dovetail slot for the blade root and a means of applying an axial load to the blade root. The arrangement is shown in Fig. 31.

The rubbing surfaces were provided by two titanium clamping blocks bolted to the steel fixture block. The width dimension of the dovetail cutout is maintained by a loading block separating the two clamping blocks. The loading block is a sliding fit between them. Strain gaged loading screws acting on the block provided a measure of the load along the axis of the blade. The load is transferred to the blade root via a small diameter roller bearing located on the centerline of the loading block. The assembly was then bolted into the vacuum chamber (see Fig. 32), which in turn was mounted on the slip plate driven by the electrodynamic shaker.

The load bolts were designed to provide adequate axial stiffness at the root, yet be sensitive enough to be able to apply accurate loads as monitored by means of strain gage output. The steel bolt "working" section was 2.54 cm long and 0.32 cm in diameter. Two strain-gages were used on each bolt and arranged to minimize bending effects. As a result of calibration tests, .695 microstrain per Newton was determined.

#### 4.2.2 Instrumentation

The same type of strain gages as previously used in the material damping tests were used on this blade. The instrumentation system used was the same as that discussed in APPENDIX B except that the X-Y recorder was not required. All strain gage responses were recorded as unfiltered and filtered signals. The Krohnkite filter was set at 100 Hz in the low pass mode to obtain the filtered results.

The two strain gaged loading bolts were connected through a 3 pole switch to a portable balance bridge and strain indicator unit as shown in Fig. 33.

#### 4.2.3 Test Results

All tests were performed with the pressure in the chamber reduced to 15 torr.

After several preliminary tests and developing the technique of adjusting the load bolts, the first mode responses were obtained with root loading varied from 576 to 2879 Newtons and with excitation levels of 0.2, 0.5 and 1.0 g applied. The results of the final test series are tabulated in Table IV. Typical decay curves are shown in Fig. 34 for the minimum root load applied and in Fig. 35 for the maximum root load. The loss factors were calculated from the average slope between points 1 and 4 dB down from maximum on the decay curves. Figures 36, 37 and 38 show how the loss factor, root stress and response frequency vary with axial load at root and input excitation level.

### 4.3 Discussion of Results

In this section, a comparison of the numerical results from analysis and testing of a fan blade with a dovetail root is presented. Values of the parameters used in computation are as follows:

Blade Length, L . . . . .	0.28 m (11 in)
Mass moment of inertia about root, $I_0$ . . . . .	(0.066 slugs-in <sup>2</sup> /12)
Dovetail angle, $\alpha$ . . . . .	45 deg.
Dovetail effective radius, R . . . . .	8.26 mm (0.325 in)
Dovetail correction factor, $\kappa$ . . . . .	0.0209
Coefficient of friction, $\mu$ . . . . .	0.3, 0.35
Non-friction damping loss factor, $\eta_0$ . . . . .	0.0005
Frequency, (Test) . . . . .	74 Hz
Modal mass, $m_1$ . . . . .	(2.734E-3 slugs/12)
Modal stiffness, k . . . . .	11.21 kN/m (64 lb/in)
Modal stress near root, $\sigma_0$ . . . . .	298 MPa (4.35E+4 psi)
Mass ratio, $\beta$ . . . . .	2

The modal information is for the first mode, and normalized to unit tip deflection of the blade.

The theoretical and test results of blade loss factor as a function of blade axial load are shown in Fig. 36 from which the following observations can be made.

- (1) Loss factors decrease rapidly with increase in axial load.
- (2) For low axial loads, higher levels of excitation lead to higher levels of friction damping. With increased axial loads, this dependence on excitation is reduced.
- (3) Loss factors begin to level off at moderate axial loads, asymptotically approaching the non-friction damping loss factors; i.e., the blade tends to reach the condition of essentially no slip at the root.
- (4) At high axial loads, relative macroslip at the root interface is unlikely to be present and friction damping, if any, may be governed by microslip or local slip.

Figure 37 shows the theoretical and test results of blade stress near the root as a function of blade axial load. It is seen from the figure that, for a given axial load, the theoretical blade response (hence blade stress) is independent of the excitation level. This is in agreement with the results published in Ref. 20. However, test results from the present program indicate that, for a given axial load, blade stress is dependent on the excitation level. This discrepancy between theoretical and test results is possibly due to the idealized nature of the analytical model. As the analytical model considers only macroslip motion, an increase in excitation level leads to an increase in slip amplitude at the interface. The resulting increase in friction damping tends to maintain a constant blade stress. The dependence of stress on excitation level, as indicated by test results, implies that during tests the slip motion at the interface may have been predominantly of the microslip type.

## 5. DAMPING DUE TO RUBBING AT SHROUD INTERFACES

In the case of part-span shrouded blades, untwisting of the blades under centrifugal pull brings neighboring blades into contact at the shrouds. Determination of the precise nature of conditions at such an interface continues to be an unresolved problem defying both analysis and measurement. Major parameters which control the nature and extent of friction damping at the shroud to shroud interface are: centrifugal loading, roughness of surfaces, level of external excitation, shroud location on the blade, blade geometry, and shroud geometry. Studies which address the specific problem of shroud damping can be found in Refs. 25-29. Presented in this chapter are the results of analysis and testing of a part-span shrouded fan blade with rubbing at its shroud faces.

### 5.1 Forced Response of a Fan Blade With Rubbing at the Shrouds

Uncertainties in the precise nature of vibratory kinematics and kinetics at the shroud faces during rubbing, demanded that different analytical approaches be explored to determine their suitability. The microslip approach was abandoned in favor of the macroslip approach, after a NASTRAN finite element analysis confirmed the need for an iterative-type solution to obtain accurate quantitative results; see remarks in Section 2.1.2, and also Ref. 25. Apart from some questions as to its utility in a practical application such an iterative-type solution was beyond the scope of the present program in terms of time and cost schedule. In the macroslip approach, initial efforts consisted of modeling the rather high inplane stiffness of the shroud as a spring in series with the friction forces at the shroud faces. Such a modeling procedure leads to the following result: for a given excitation level, there is a rapid decrease in blade stress with increase in shroud normal load. However, test results indicated precisely the opposite trend, i.e., an increase of blade stress with increase in shroud normal load, for a given excitation; thus revealing the inadequacy of the initial analytical model. The difficulty is one of proper modeling of the physics of a vibrating blade having rubbing at the shrouds. Details of the model that was finally adopted and the associated analysis are given below.

Schematics of a part span shrouded fan blade, and shroud rubbing surfaces are shown in Fig. 39a and Fig. 39b. The following assumptions are made; see also remarks in Section 2.1.2,

1. Friction damping is of macroslip-type, and governed by Coulomb's law of dry friction.

2. Friction damping does not drastically alter blade resonant frequency and mode shape, so that attention can be focused on a single chosen mode of vibration.
3. For the mode under consideration, the modal stiffness and modal stress are normalized to unit tip displacement of the blade, and are computed for the case when there is no friction at the interface.
4. Shrouds are infinitely rigid and shroud load is uniformly distributed over the rubbing surfaces.
5. Slipping motion is resisted by the static stiffness of the blade below the shrouds.

Under the assumptions made, the equations of motion can be written as (see Fig. 40)

$$\bar{m}\ddot{\bar{x}}_1 + \bar{k}(\bar{x}_1 - \bar{x}_2) + \bar{c}\dot{\bar{x}}_1 = \bar{P} \cos \bar{\omega} \bar{t}, \quad (5.1)$$

$$\beta \bar{k} \bar{x}_2 + 2\mu \bar{N} \operatorname{sgn}(\dot{\bar{x}}_2) - \bar{k}(x_1 - x_2) = 0,$$

where overbars denote dimensional quantities,  $m$ ,  $k$ , and  $c$  are modal quantities,  $x_1$  is the blade tip deflection,  $x_2$  denotes the slip at the shroud,  $P$  is the excitation amplitude,  $\omega$  is the excitation frequency,  $\mu$  is the coefficient of friction, and  $N$  is the normal load. The quantity  $\beta k$  is the static stiffness of the blade below the shrouds and resists the slipping motion. Thus, the parameter  $\beta$  accounts for changes in the stiffness of the system during slipping motion. It is convenient to nondimensionalize the equations of motion by introducing the following quantities:

$$x_1 = \bar{x}_1 / \bar{x}_0, \quad x_2 = \bar{x}_2 / \bar{x}_0, \quad \bar{\omega}_0^2 = \bar{k} / \bar{m}_1, \quad \omega = \bar{\omega} / \bar{\omega}_0, \quad t = \bar{t} \bar{\omega}_0, \quad (5.2)$$

$$\zeta = \bar{c} / 2\bar{m}_1 \bar{\omega}_0, \quad F = 2\mu \bar{N} / \bar{k} \bar{x}_0, \quad p = \bar{P} / \bar{k} \bar{x}_0,$$

where  $\bar{x}_0$  is some characteristic length. The equations in dimensionless form are

$$\begin{aligned} \ddot{x}_1 + (x_1 - x_2) + 2\zeta \dot{x}_1 &= p \cos \omega t, \\ \beta x_2 + F \operatorname{sgn}(\dot{x}_2) - (x_1 - x_2) &= 0. \end{aligned} \quad (5.3)$$

Assuming a solution of the form

$$\begin{aligned}
 x_1 &= a \cos(\omega t + \phi - \delta), \\
 x_2 &= b \cos(\omega t + \phi), \\
 \text{sgn}(\dot{x}_2) &\approx -(4/\pi) \sin(\omega t + \phi),
 \end{aligned}
 \tag{5.4}$$

leads to a set of algebraic equations,

$$\begin{aligned}
 \eta a_1 + (1 - \omega^2) a_2 - Q_2 &= \cos \phi, \\
 (\omega^2 - 1) a_1 + \eta a_2 - \eta Q_2 &= -\sin \phi, \\
 (1 + \beta) Q_2 - a_2 &= 0 \\
 G + a_1 &= 0
 \end{aligned}
 \tag{5.5}$$

where

$$\begin{aligned}
 \eta &= 2\zeta\omega, \quad Q_2 = b/p, \quad G = 4F/\pi p, \\
 a_1 &= (a/p) \sin \delta, \quad a_2 = (a/p) \cos \delta.
 \end{aligned}
 \tag{5.6}$$

The last two equations of Eq. (5.5.) yield,

$$a_1 = -G, \quad a_2 = (1 + \beta) Q_2,
 \tag{5.7}$$

so that,

$$Q_1 = a/p = (a_1^2 + a_2^2)^{1/2} \quad \text{and} \quad \tan \delta = a_1/a_2.
 \tag{5.8}$$

Substitution of Eq. (5.7) into the first two equations of Eq. (5.5) leads to

$$\tan \phi = \left[ \eta(1 + \beta) Q_2 + (1 - \omega^2) G \right] / \left[ (\beta + \beta \omega^2 + \omega^2) Q_2 - \eta G \right],
 \tag{5.9}$$

and after some algebra, a quadratic equation, the solution of which yields,

$$Q_2 = -C_2 G + \left[ (C_2 G)^2 - C_1(C_3 G^2 - C_4) \right]^{1/2},
 \tag{5.10}$$

where

$$C_1 = (\omega^2 + \beta \omega^2 - \beta) + \eta^2 (1 + \beta)^2, \quad C_2 = \eta / C_1,$$

$$C_3 = [(1 - \omega^2)^2 + \eta^2] / C_1, \quad C_4 = 1 / C_1$$

It is noted that  $Q_1$  is a measure of the blade response, and  $Q_2$  a measure of the slip amplitude at the shroud interface, from Eq. (5.9) the condition for slip to occur, i.e.,  $Q_2 > 0$ , is

$$(C_3 G^2 - C_4) < 0; \quad G < [(1 - \omega^2)^2 + \eta^2]^{1/2} \quad (5.11)$$

The analysis and solution developed above is applicable to the case of direct excitation of the blade. If the excitation is applied at the base of the blade, as was done for tests performed in this program, the analysis follows along similar lines to the one given above, the only modifications being a redefinition of the nondimensional excitation amplitude,

$$p = \bar{p} / x_0, \quad \text{and} \quad C_4 = \omega^4 / C_1,$$

where  $\bar{p}$  is the displacement amplitude of the base excitation.

The influence of friction at the shrouds can be expressed as a loss factor, defined as

$$\eta_f = \frac{1}{2\pi} \frac{D}{U}, \quad (5.12)$$

where  $D$  is the energy dissipated per cycle of vibration and  $U$  is the peak strain energy in the blade. The two energies are given by

$$D = 8\mu \bar{N} \bar{x}_2, \quad U = \frac{1}{2} \bar{k} \bar{x}_1^2, \quad (5.13)$$

so that, in terms of dimensionless quantities

$$\eta_f = G Q_2 / Q_1^2, \quad (5.14)$$

and total loss factor for the blade is,

$$\eta_b = \eta_o + \eta_f, \quad (5.15)$$

where  $\eta_o$  accounts for damping from sources other than friction, such as, material hysteresis and air damping.

The major interest is in obtaining the maximum blade response at resonance. One approach is to calculate the response for different values of the nondimensional frequency,  $\omega$ , and pick out the maximum amplitude. However, for the damping levels expected in the problem being studied, maximum response occurs when the excitation frequency is near the natural frequency (i.e.,  $\omega \approx 1$ ) so that a good approximation to the maximum response is obtained by simply setting  $\omega = 1$  in the solution.

The blade tip deflection can be related to the blade stress by specifying a baseline or reference condition where the blade vibration characteristics are fully known. If the baseline tip deflection of the blade is chosen as the characteristic length  $\bar{x}_o$  used for nondimensionation in Eq. (5.2), it can be shown that

$$\sigma = \alpha \sigma_o, \quad (5.16)$$

where  $\sigma_o$  is the blade stress in the baseline condition and  $\sigma$  is the blade stress at any other condition. In the present study, the condition of no friction at the shroud interfaces is chosen as the baseline condition so that the baseline blade stress is the same as the modal blade stress.

A computer program SHDDMP was written to compute blade loss factor and blade stress as a function of base excitation level in g-units. The program calculates the resonant response by using Eqs. (5.7) through (5.10), the loss factor by Eqs. (5.12) through (5.15), and the blade stress by Eq. (5.16). The input to the program includes: frequency in Hz; shroud normal load N; coefficient of friction  $\mu$ ; stiffness ratio  $\beta$ ; modal stiffness k; baseline (modal) blade stress  $\sigma_o$ , and; nonfriction damping loss factor  $\eta_o$ .

## 5.2 Experimental Investigation of Damping at Shrouds

The objectives of this series of tests were to examine the nature of the response characteristics of a shrouded fan blade and to obtain a measure of damping available due to shroud rubbing.

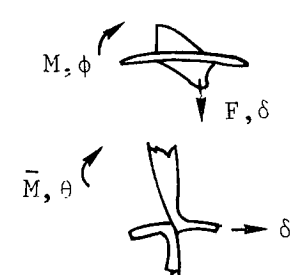
### 5.2.1 Test Approach

The method described in Section 5.1 enables the calculation of maximum response of a single blade subjected to excitation at its base and whose shrouds rub on rigid surfaces under a given normal load. The fan blade used in these tests was welded at its root to a massive block and provided with a means for applying a static normal load on the shroud surfaces. The whole assembly was mounted in a vacuum chamber and subjected to harmonic excitation. The shroud normal loads and input acceleration levels were varied and the stress response at the ASMT (Above-Shroud-Maximum-Thickness) position was monitored. Damping levels were estimated from transient response curves resulting from abrupt cut off of input signals.

The fan blade used in these tests was the same titanium blade used in material damping tests. The loading platens (Fig. 41) which were used to apply normal loads on the shrouds, have a rectangular rubbing surface designed to mate with the curved perimeter of the shroud interface. The platens were made of titanium alloy 8-1-1 and hardfaced with tungsten carbide to be compatible with the surface treatment on the shroud interfaces.

The loading disc holding the load platens (Fig. 41) was positioned around the blade so that the platens rested on the shroud surfaces. The cable and weight system shown in Fig. 42 was used to impose a normal load on the shrouds. The cables were positioned 11.4 cm apart on the loading disk. Upon reaching the required torque (and hence, the required normal load on the shroud interfaces), the disk was locked in position and the cables were removed. Complete air tightness was achieved by capping the access holes on the fixture. The above setup assured constant shroud loading through the series of tests.

Actual flexural and torsional stiffness of the blade at the shroud location were measured and were used in the design of the shroud loading mechanism. The measurements of these force and moment coefficients were made in a series of static loading tests. Moments were applied via rigid extensions glued to the shrouds and displacements were measured using dial indicators. The following results were obtained for the several stiffnesses.

		Stiffness Coefficient	Measured Value
		$K_{F\delta}$	114000 N/m
		$K_{M\phi}$	743 Nm/rad
		$K_{\bar{M}\delta}$	5694 Nm/m
		$K_{\bar{M}\theta}$	412 Nm/rad
<p><math>M, \bar{M}</math> Applied Moments: <math>F</math> Applied Force  <math>\theta, \phi</math> Angular Displacement: <math>\delta</math> Linear displacement</p>			

### 5.2.2 Instrumentation

The instrumentation system used was the basic system shown in Fig. 43, and described in Appendix B. All data recording was done on the level recorder with steady state strain gage millivolt readings taken directly from the digital voltmeter. The response of the blade was obtained from a single high temperature strain gage (BLH Electronics Type FSM-12-35-36, 3.18 mm) mounted in the above-shroud-maximum-thickness position (see Fig. 17). To monitor the shroud motion, two miniature accelerometers (Endevco 2250 and Vibrametrics M1000) were mounted on a small nonmetallic block which was then epoxied to the shroud (see Fig. 44). The accelerometers monitored the out of plane (axial) motion and the in plane motion parallel to the rubbing surfaces. Filtering of the accelerometer signals was required at times to assess the magnitude of the fundamental component. This was done using the Krolmwhite variable filter in the low pass mode. A preliminary survey of the blade response was conducted over a wide frequency range, measurements for which were made via a miniature accelerometer mounted at the blade tip.

### 5.2.3 Test Results

Several preliminary frequency sweeps were performed to locate the major modal responses. The response plot for tip flapwise acceleration of one such sweep is shown in Fig. 45. This was performed at a relatively low applied torque (5.2 Nm) and so the boundary conditions at the shroud interface represented neither a fully locked nor a freely slipping condition. In fact, during tests at this low normal load on the shrouds, a rattling type of motion was observed at the shroud location. This resulted in a number of peaks occurring as a result of the inherently nonlinear nature of the constraint forces at the shroud interfaces. However, within the range of frequencies swept, the observed modes included three predominantly above-shroud modes. Because of the low shroud load, these modes occurred at 260 Hz (bending), 475 Hz (second bending) and 880 Hz (torsion). Decay tests were performed from which the damping levels in each of these modes were measured. Upon increasing the applied torque, it was noted that the number of nonlinear responses diminished. Also, the three above-shroud modes manifested themselves (see Fig. 46) at 278 Hz (bending), 1110 Hz (torsion) and 1440 Hz (second bending). It was also noted that the response included some participation from the "free" blade bending mode at 93 Hz.

Subsequent testing was focused only on the above-shroud bending and the above-shroud torsion modes. These tests were performed with a reduced pressure of 16 torr inside the chamber. Two methods of obtaining the responses to various input levels were used. The first was to employ a slow frequency sweep at constant input level for a given shroud load. The frequency range was just large enough to at least include the half power points. The sweep

rate was chosen to be low enough not to distort the response curve at the existing modal damping levels. A characteristic of these curves was a flat peak over a significant bandwidth around the resonance, as shown in Fig. 47. The second method was to tune the frequency to obtain the maximum response for a given mode. After the maximum strain value had been recorded (Digital Voltmeter reading - mv rms) the input was abruptly cut off and the decay curve recorded on the peak level recorder. It was noted that this latter method produced higher (generally less than 1 dB) maximum blade responses than the sweep method. The steady state results were used for comparison with analysis and are tabulated in Table V. Shroud acceleration data obtained for certain test points are given in Table V. The loss factor for each test point was determined from the decay curves and was obtained from the mean slope between the 1 dB and 4 dB points down from the maximum value as described in Appendix B. A sampling of the decay curves obtained for mode 1 is shown in Figs. 48 and 49. Figure 48 shows how the decay pattern changes as the input level is increased for a given shroud load and Fig. 49 shows the manner in which the decaying signal changes with shroud load and input level. Figures 50 and 51 give the ASMT stress as a function of shroud normal load for modes 1 and 2.

After testing, the platens were removed and their rubbing surfaces examined. As can be seen in Fig. 52, the majority of wear took place at the outer corners of the surfaces. This occurred even though initially the surfaces were true and tight against the entire length. It is likely that initially some of the new hardfacing may have quickly worn off allowing the load to move outward and concentrate on a small area since the loading device was not able to automatically adjust to the new contact condition. The distance between these contact points was 5.08 cm. However, the fact that the shroud load acted on a very narrow region enabled its value to be determined from the applied torque.

### 5.3 Discussion of Results

In this section, a comparison of the numerical results from analysis and testing of a part-span-shrouded fan blade with rubbing at the shroud faces is presented. Values of parameters used in computation are as follows:

Coefficient of friction, $\mu$ . . . . .	0.3, 0.35
Nonfriction damping loss factor, $\eta_0$ . . . . .	0.0005
Frequency (Test). . . . .	280 Hz
Static stiffness of blade below shrouds . . . . .	113.8 kN/m (650 lb/in.)

Modal stiffness, k . . . . .	79.15 kN/m (425 lb/in.)
Modal stress, ASMT (Above-Shroud-Max.-Thickness) . . . . .	1003 MPa (1.464 x 10 <sup>6</sup> psi)
Stiffness ratio, $\beta$ . . . . .	1.44

It may be recalled that the analysis focuses attention on a single chosen mode of vibration of the blade with rubbing at the shroud faces. The identification of this mode, for obtaining modal parameters, is made difficult by the complex kinematics and kinetics at the shroud rubbing surfaces. Several NASTRAN runs were made to study the effect of different boundary conditions on frequencies and mode shapes of the fan blade. The runs included the cases of shrouds unrestrained, shrouds fully restrained at the shroud faces, and shrouds freely slipping at the shroud faces. Also, vibration tests provided insight into the dynamics of shrouds during vibration; for example, the mode shape, and the out-of-plane motion of the shrouds observed suggested that the second bending mode of the blade with shrouds unrestrained is the appropriate mode of vibration to model. Therefore, values of modal stiffness and modal stress from this mode were used in the analysis.

The following observations are made upon a close examination of Figs. 45 through 52:

- (1) The modes of interest correspond to those in which the motion is essentially above the shroud (see Figs. 45 and 46).
- (2) The stress amplitude at slip resonance (see flat top in Fig. 47) is proportional to shroud load (N) and excitation level (g). Off resonance, however, the stress amplitude is proportional to excitation level only. An increase in shroud load at a given g level, increases the frequency and response amplitude at which macroslipping would begin. For a given shroud load, an increased g level hastens the slipping action and leads to a wider bandwidth of frequencies in which damping can be effective. At a given frequency and g level, an increase in shroud load leads to an increase in stress level.
- (3) Reference to Figs. 48 and 49 suggests that slipping increases with g levels as indicated by the progressively steeper slopes at the start of the decay. However, the decay curves superpose at lower stress levels indicating damping levels which are essentially independent of initial conditions.

(4) Reference to Fig. 50 suggests that, for a given shroud normal load, the blade stress approaches a constant asymptotic value with increase in excitation level; i.e., distinct macroslip conditions. The analysis predicts an abrupt transition, at low g levels, from a region of no friction damping to the macroslip region. The test results indicate a smoother transition at about 1 g for 150 N, about 2 g for 300 N, and about 3 g for 400 N; the smoothness of the transition indicating a region of partial macroslip conditions.

Analysis suggests that blade stresses are sensitive to the coefficient of friction; higher the coefficient of friction, higher the stresses at which transition to macroslip occurs. The ability of the analytical model to predict blade stress appears to improve with reduction in shroud normal load and/or increase in excitation level, i.e., conditions representing macroslip motion.

Measurements made in the above-shroud-torsion mode indicate damping levels substantially lower than those in the above-shroud-bending mode. The vibratory motion in the torsion mode causes a slipping motion (rotational) that is different from that caused in a bending mode (translational). In the tests performed, the rubbing action at the interfaces in the torsion mode may have been microscopic as no trend to reach a constant stress level could be observed as g levels increased up to 4 g (compare Figs. 50 and 51).

It would appear that in these tests, dry friction damping was more effective in the bending mode than in the torsion mode. This is most likely due to the restraint against torsional motion in the present setup being different from that offered by neighboring blades in an assembly.

The wear pattern shown in Fig. 52 suggests that the shroud contact during vibration occurs over a very narrow region and even this minimal contact is sufficient to cause changes in mode shapes as well as to provide adequate damping.

#### 5.4 Characteristics of Sliding Friction

Observations made in the shroud damping tests indicate that slip occurred between the mating surfaces of the shrouds. Accelerometers located on the shroud monitored the shroud motion.

The analysis of Section 5.1 employs the normal coulomb damping model for dry friction damping at the shrouds with an estimated equivalent coefficient of friction of 0.3 to 0.35. The purpose of this series of tests was to examine the friction force-slip relationship due to the surface contact interaction of two test pieces representative of the shrouds of a typical fan blade. From this investigation, the value of equivalent sliding friction coefficient was to be derived.

#### 5.4.1 Test Approach

The approach chosen for this investigation was to provide sinusoidal relative motion between two test pieces which were held together with a constant normal force and to measure the resulting frictional forces directly. The range of normal loads, frequencies, and relative velocities to be imposed were to be consistent with those pertaining to the shroud damping investigation (see Section 5.2.3).

The test pieces chosen were a pair of load platen pieces as used in the shroud damping investigation. These were rectangular prisms (22.35 x 32.00 x 6.35 mm) made from titanium (Ti) 8.1.1 alloy with the rubbing face (6.35 x 22.35 mm) flame sprayed with tungsten carbide (see Fig. 52). One piece was gripped with its rubbing surface horizontal in a special clamp mounted on a slip plate attached to an electrodynamic shaker such that motion could be applied parallel to the long side of the rubbing surface (see Fig. 53). The other piece (shown in Fig. 54 as stationary upper test piece) was mounted at the end of a pivoted area attached to the shaker support frame (see Figs. 53 and 54). The upper test piece was supported longitudinally by two strain gaged bolts (previously used in the root damping investigation) and the normal load was applied via roller bearings along the top surface of the test piece. Lateral stabilization was achieved by locating the tips of the load bolts in shallow indentations in the fore and aft faces of the test piece. The strain gaged bolts were preloaded to 575 N. The sensitivity of the load measuring arrangement was 347 microstrain/kN. The input motion of the lower test piece was monitored by an accelerometer mounted on the clamp. The normal load was applied by putting the required weights on the loading platform as shown in Fig. 53.

Testing consisted of setting the required frequency and input acceleration and recording the frictional force-slip loop on an oscilloscope for a range of normal loads.

#### 5.4.2 Instrumentation

The excitation control system used is described in Appendix B along with a 50 Hz bandwidth tracking filter to condition the control accelerometer signal. The strain gages on one of the load bolts were connected to a bridge amplifier with internal calibration capability. The filtered input acceleration control signal was connected by the horizontal axis of an oscilloscope and the output of the bridge amplifier was connected to the vertical axis of the oscilloscope. The horizontal axis was calibrated by putting in a known acceleration and the vertical axis was calibrated using the bridge amplifier integral calibrator.

### 5.4.3 Testing and Results

The nominal condition for testing was defined as a displacement of 0.127 mm DA at a frequency of 280 Hz with normal loads ranging from about 250 to 700 N. Three loads were used, based on the weights available and the dead load of the upper arm; these were 271, 492, and 672 N. The displacement was varied from 0.056 to 0.132 mm DA and frequencies of 80, 140, 280 and 420 Hz were input.

Initially, the time varying signals from the two accelerometers and strain gages were examined on the scope. A composite picture of a typical set of traces for one condition is given in Fig. 55. The magnitude of the noise in the quiescent system can be seen in the uppermost trace. As can be seen, the upper test piece acceleration has a high frequency component. This high frequency may be due to the surface rubbing or possibly to impacting of loose roller bearings in the upper arm. The component usually accompanied the results using the lowest normal load. Using a 250 Hz low pass filter, this component was removed and the magnitude of the fundamental can be seen compared with that of the input signal. A friction force-slip loop is shown superimposed for comparison. The results for all tests performed are given in Table VI.

The equivalent friction coefficient was determined from the measured area of the recorded (photograph of oscilloscope picture) loop and a knowledge of the input frequency and displacement. The resulting values for friction coefficient are plotted against normal load, input frequency, and relative maximum velocity in Fig. 56.

## 6. DAMPING DUE TO PLATFORM-DAMPERS

Platform-type dampers are frequently used in gas turbine blade design to dissipate energy through friction generated at the interface between the damper and blade platform. The type of damper considered in this program is the so-called blade-to-ground damper (Fig. 4). During engine operation, centrifugal forces bring one end of the damper into contact with the blade platform, the other end being attached to a relatively static component such as a cover plate. Major parameters which control the extent of friction damping at the damper to platform interface are: contact load, roughness of surfaces, level of external excitation, location of platform on the blade, and stiffness of the damper. Studies which address the specific problems of damping at a blade platform can be found in Refs. 30-32. Presented in this chapter are the results of analysis and testing of a turbine blade subjected to friction damping at its platform.

### 6.1 Forced Response of a Turbine Blade with a Platform Damper

Generic models which can be used to analyze blade-to-ground type of platform dampers can be found in Ref. 16 and 17. The analytical approach used in this Section closely follows that of Ref. 30, the generic model being essentially the same as the one in Ref. 17. The following assumptions are made; see remarks in Section 2.1.2:

1. Friction damping is of macroslip-type, and governed by Coulomb's law of dry friction;
2. Friction damping does not drastically alter blade resonant frequency and mode shape, so that attention can be focussed on a single chosen mode of vibration;
3. For the mode under consideration, the modal stiffness, and modal stress are normalized to unit tip displacement of the blade, and are computed for the case when the damper is not in contact with the blade platform.

A schematic sketch of a turbine blade with a platform damper is shown in Fig. 57a, and the associated analytical model in Fig. 57b. The equation of motion can be written as

$$\bar{m} \ddot{\bar{x}} + \bar{k} \bar{x} + \bar{c} \dot{\bar{x}} = \bar{P} \cos \bar{\omega} \bar{t} - \phi_d \bar{F}_d, \quad (6.1)$$

where overbars denote dimensional quantities,  $m$ ,  $k$ , and  $c$  are modal quantities,  $P$  is the excitation amplitude,  $\omega$  is the excitation frequency,  $x$  is the blade tip displacement,  $\phi_d$  is the modal displacement at the platform, and  $F_d$  is the force due to the damper.

Denoting the blade displacement at the platform by  $q_d$ , the damper spring displacement by  $\hat{q}_d$ , and introducing

$$q_d = \phi_d x, \quad \hat{q}_d = \phi_d y, \quad (6.2)$$

it can be shown that

$$F_d = \phi_d k_d \begin{cases} \bar{x} + \bar{y}_m - \bar{x}_m, & 0 < \bar{\omega} \bar{t} < \tau \\ -\bar{y}_m, & \tau < \bar{\omega} \bar{t} < \pi \end{cases} \quad (6.3)$$

$$\bar{y}(\bar{t}) = -\bar{y}(\bar{t} + \pi), \quad \cos \tau = 1 - (2\bar{y}_m/\bar{x}_m), \quad \bar{y}_m = \mu \bar{N} / \phi_d \bar{k}_d, \quad (6.4)$$

where subscript  $m$  denotes peak value,  $N$  is the damper normal load, and  $\mu$  is the coefficient of friction.

The damper force is a discontinuous function of time, and is shown in Fig. 58a as a function of the blade displacement at the platform. Figure 58b shows the blade displacement at the platform and the damper spring displacement over one cycle of vibration. It is noted that the slip amplitude at the damper to platform interface is  $(x_m - y_m)$ .

It is convenient to nondimensionalize Eqs. (6.1) - (6.4) by introducing

$$x = \bar{x}/\bar{x}_0, \quad a = \bar{x}_m/\bar{x}_0, \quad y = \bar{y}/\bar{x}_0, \quad b = \bar{y}_m/\bar{x}_0, \quad \bar{\omega}_0^2 = \bar{k}/\bar{m}, \quad \omega = \bar{\omega}/\bar{\omega}_0, \quad (6.5)$$

$$t = \bar{t}\bar{\omega}_0, \quad \epsilon = \phi_d^2 \bar{k}_d/\bar{k}, \quad \zeta = \bar{c}/2\bar{m}\bar{\omega}_0, \quad \rho = \bar{P}/\bar{k}\bar{x}_0$$

where  $\bar{x}_0$  is some characteristic length. The result is

$$\ddot{x} + x + 2\zeta\dot{x} = \rho \cos \omega t - \epsilon y, \quad (6.6)$$

$$y = \begin{cases} x + b - a, & 0 < \omega t < \tau \\ -b, & \tau < \omega t < \pi \end{cases} \quad (6.7)$$

$$y(t) = -y(t + \pi), \quad \cos \tau = 1 - (2b/a), \quad b = \mu \bar{N} / \phi_d \bar{k}_d \bar{x}_0.$$

From the equations developed above, two limiting cases can be identified as follows: damper free (no contact with the platform),  $\tau = 0$ ,  $b = 0$ , and damper stuck (no slip at the platform),  $\tau = \pi$ ,  $b = a$ .

Due to the nonlinear (discontinuous) nature of the function,  $y$ , the solution of Eq. (6.6) is obtained by using the method of averaging, a perturbation method (Ref. 47). The essence of the method is the assumption that, if the nonlinearity is small (i.e.,  $\epsilon$  is small), then the amplitude and phase of the response may be treated as constants within a cycle of vibration. A solution is sought in the form

$$x = a(t) \cos [t + \theta(t)] = a \cos \gamma, \quad (6.8)$$

where the amplitude and phase are assumed to be functions of time. Application of the method of averaging transforms Eq. (6.6) to a set of first-order differential equations,

$$\begin{aligned} \dot{a} &= (1/2\pi) [-2\pi\zeta a - \epsilon a \sin^2 \tau - \pi p \sin(\gamma - \omega t)], \\ \dot{\theta} &= (1/2\pi a) [a\tau - (a/2) \sin 2\tau - \pi p \cos(\gamma - \omega t)], \end{aligned} \quad (6.9)$$

where the case of near resonance, i.e.,  $\omega \approx 1$ , has been assumed.

Equations (6.9) yield the steady-state response as a set of nonlinear algebraic equations,

$$\begin{aligned} -2\zeta a + R(\epsilon, a, \tau) &= p \sin \psi, \\ -2\delta a + S(\epsilon, a, \tau) &= p \cos \psi, \end{aligned} \quad (6.10)$$

where

$$\psi = \gamma - \omega t, \quad \delta = \omega - 1, \quad (6.11)$$

$$R = -(\epsilon a / \pi) \sin^2 \tau, \quad S = (\epsilon a / 2\pi) (2\tau - \sin 2\tau), \quad (6.12)$$

Though Eqs. (6.10) are nonlinear equations, due to their special structure, it is possible to calculate the maximum response by some algebraic manipulations; see Ref. 17. Some of the steps are outlined below.

Squaring and adding Eqs. (6.10) yields a quadratic equation for  $\delta$ , the solution of which is

$$\delta = (1/2a) \left\{ S \pm [p^2 - (R - 2\zeta a)^2]^{1/2} \right\}. \quad (6.13)$$

Since  $\delta$  is a frequency parameter, the maximum response occurs when  $\delta$  has a double root; that is,

$$p^2 - (R - 2\zeta a)^2 = 0. \quad (6.14)$$

By using the definitions for  $\tau$  and  $R$  given by Eqs. (6.4) and (6.11), respectively, it can be shown that Eq. (6.14) leads to a quadratic equation for the maximum amplitude. The final results are

$$Q_m = (1/2\pi\eta_0) \left\{ (\pi - 4\epsilon G) + [(\pi - 4\epsilon G)^2 + 16\epsilon\pi\eta_0 G^2]^{1/2} \right\}, \quad (6.15)$$

$$\omega_m = 1 + (\epsilon/4\pi)(2\tau_m - \sin \tau_m); \quad \tau_m = \cos^{-1} [1 - (2G/Q_m)], \quad (6.16)$$

where  $Q_m$  is the maximum response and  $\omega_m$  is the frequency at which the maximum occurs, and

$$Q_m = a/p, \quad G = b/p, \quad \eta_0 = 2\zeta.$$

Further, it is seen from Eq. (6.15) that  $Q_m$  is a function of  $\eta_0$ ,  $\epsilon$ , and  $G$  which in turn is a function of the normal load on the platform; see Eq. (6.7). The optimum value of the damper normal load can be determined by minimizing Eq. (6.15) with respect to  $G$ ; that is

$$\frac{dQ_m}{dG} = 0,$$

which leads to

$$G^* = \pi / [2(\epsilon + \pi\eta_0)], \quad (6.17)$$

where  $G^*$  is the optimum value. The associated optimum response and frequency can be shown to be

$$Q_m^* = 2G^* \quad , \quad \omega^* = 1 + (\epsilon/4) \quad . \quad (6.18)$$

The analysis and solution developed above is applicable to the case of direct excitation of the blade. If the excitation is applied at the base of the blade, as was done for tests performed in this program, the analysis follows along similar lines to the one given above, the only modification being a redefinition of the nondimensional excitation amplitude,

$$p = \bar{p}/\bar{x}_0,$$

where  $\bar{p}$  is the displacement amplitude of the base excitation.

The influence of friction at the platform can be expressed as a loss factor, defined as

$$\eta_f = \frac{1}{2\pi} \frac{D}{U} \quad , \quad (6.19)$$

where  $D$  is the energy dissipated per cycle of vibration and  $U$  is the peak strain energy in the blade. The two energies are given by

$$D = 4\mu\bar{N}\phi \left| \bar{x}_m - \bar{y}_m \right|, \quad U = \frac{1}{2} \bar{k} \bar{x}_m^2, \quad (6.20)$$

so that in terms of dimensionless quantities

$$\eta_f = (4\epsilon/\pi)G (Q_m - G)/Q_m^2, \quad (6.21)$$

and total loss factor for the blade is,

$$\eta_b = \eta_0 + \eta_f, \quad (6.22)$$

where  $\eta_0$  accounts for damping from sources other than friction, such as, material hysteresis and air damping.

The blade tip deflection can be related to the blade stress by specifying a baseline or reference condition where the blade characteristics are fully known. If the baseline tip deflection of the blade can be chosen as the characteristic length  $\bar{x}_0$  used for nondimensionalization in Eq. (6.5), then it can be shown that

$$\sigma = \alpha \sigma_0, \quad (6.23)$$

where  $\sigma_0$  is the blade stress in the baseline condition and  $\sigma$  is the blade stress at any other condition. In the present study, the damper free condition (no contact between damper and platform) is chosen as the baseline condition.

It was found, from tests in the damper free condition, that the blade shank stress is a nonlinear function of the base excitation level; see Fig. 61. In other words, damping due to sources other than platform friction,  $\eta_0$ , is a function of the excitation level. It can be shown that,

$$\eta_0 = \bar{p} \sigma_m / \sigma_0, \quad (6.24)$$

where  $\sigma_m$  is the modal stress.

A computer program PLTDMP was written to compute blade loss factor, resonant frequency and blade shank stress as a function of the normal load on the platform. The program calculates the baseline damping loss factor by using Eq. (6.24), resonant response by Eq. (6.15), resonant frequency by Eq. (6.16), loss factor by Eqs. (6.19) through (6.22), and blade shank stress by Eq. (6.23). The program terminates if the resonant frequency changes from the baseline frequency by a specified amount. The input to the program includes: frequency in Hz; base excitation level in g-units; coefficient of friction  $\mu$ ; damper stiffness  $k_d$ ; modal displacement at the platform  $\phi_d$ ; modal stiffness  $k$ ; modal stress  $\sigma_m$ ; baseline stress  $\sigma_0$  and; allowable frequency shift, expressed as a fraction of the baseline frequency.

## 6.2 Platform Damping Tests

The analysis of Section 6.1 was developed for application to blade-to-ground type platform dampers. The forced response of a bladelike structure having such a damper is determined in terms of the modal quantities of the structure, the normal load applied through the damper, the stiffness of the damper and the frictional characteristics of the rubbing interface. In order to verify the analysis, a turbine blade with a suitable platform configuration was chosen for the test program and a means was devised to provide damping at the platform.

The test objective was to obtain the frequency response of the blade for various levels of input excitation and damper load. The effect of damper stiffness was also to be determined.

### 6.2.1 Test Approach

In an operating engine, centrifugal forces acting on the damper provide the contact load between the damper and the blade platform. In this test series, the contact load was applied and controlled by a lever and weight mechanism as shown in Fig. 4. The blade was rigidly clamped in a steel fixture and excitation was provided at the root by a powerful electrodynamic shaker. This method was chosen so that sufficiently high input force was available to overcome the large damping forces expected and to obtain realistically high stresses in the shank of the blade. The modal response of the blade was measured using strain gages located at the blade root on the shank and at the airfoil root on the centerline through the shank.

The test method chosen was to apply a selected damper load and excite the blade sinusoidally at a given input level in the vicinity of the blade's first mode frequency. The frequency was then tuned to produce the maximum blade response.

Since the level of damping produced by the platform damper far exceeds the contributions from other sources, the tests were performed in air. The test piece was a second stage high pressure turbine blade having a three teeth fir tree root configuration and a platform located at approximately 27.7 percent blade span as measured from the shank root. The platform had a generous trailing edge overhang which was convenient for accommodating the damper. The blade material was a nickel chromium high temperature alloy. The basic blade geometry is given in Fig. 59.

The damper was a rectangular prism integral with, and cantilevered from a T416 stainless steel loading arm. The free end was arranged to rub on the underside of the platform, with the load vector normal to the platform and damper end face surfaces. Two dampers were made, both with a length of 10.1 mm and thickness of 3.2 mm. Their depth measurements were 7.6 mm and 4.2 mm giving nominal stiffnesses at the free ends of 10.3 and 48.6 MN/m respectively. However, a static test of the smaller damper indicated a stiffness, in the

fixture, of 5.5 MN/m. This figure was used in the analysis. The area of the rubbing surface was made the same for both dampers, i.e. 2 mm x 2 mm. The damper and loading arms were heat treated to HRC 41 to match the hardness of the blade. The basic fixturing requirements were that the blade be held rigidly at its root with negligible root damping and that it provide a means of applying a damper load up to 900N on the blade platform with no free motion in the clamping mechanism. The fixture used is shown in Fig. 4 and comprises a two piece clamp bolted to an adapter base plate mounted on the shaker. The clamp has steps machined in its upper and lower pieces, which contact the peaks of the two outer lobes of the blade root fir tree. Four 3/8 inch bolts, each torqued to 48 Nm, allowed the blade to be tightly gripped between the two clamp blocks. The loading arm of the damper mechanism was pivoted on a pin mounted in the lower clamp block. The pivot was designed to be self adjusting and no free play was possible. The mechanical advantage of the loading mechanism was 4:1 with the lever loaded horizontally at the top using a cable pulley and hanging weight system. A counter balance was attached to the base plate to prevent lateral loading of the shaker armature.

#### 6.2.2 Instrumentation

The blade was instrumented with two strain gages (Micro Measurements type EA-06-062AK-120), one mounted at the shank root and the other at the airfoil root as shown in Fig. 59. Both gages were on the center line of the shank. Another strain gage of the same type, was mounted diagonally on the side of the large damper.

The instrumentation system used in this test series was the basic system described in Appendix B. For the final tests, the output from the blade strain gages was read directly from the digital volt meter and tabulated together with the input g level and frequency readings.

#### 6.2.3 Testing and Results

Prior to vibration testing, the stiffness of the small damper was estimated with the loading arm mounted on the fixture by statically loading the damper tip and measuring the tip displacement using a dial indicator. The measured stiffness was 5.5 MN/m.

During early exploratory vibration testing, the strain gage on the large damper was monitored. An example of the traces obtained is shown in Fig. 60. It may be noted that at a constant normal load of 89N on the platform, the damper strain gage response changes from nearly sinusoidal to one with a much more complex wave form as the excitation level is increased from 2.4 g pk. At 15 MPa shank stress, the signal clearly shows the periodic loss of contact with

the platform. At this point acoustical noise was emitted from the blade. At 4.6 g pk input level, the signal distortion is more pronounced and the noise level is increased.

An initial test was performed to examine the blade alone response characteristics and to assess the extent of the root damping. The blade response to input g levels from 0.06 to 0.9 are tabulated in Table VII and shown plotted in Fig. 61.

Final testing consisted of setting the platform damper load and input acceleration level and exciting the blade in the vicinity of its fundamental (first flap) mode. It was found that there was a threshold of both frequency and input level below which the blade showed no significant response. Once the threshold had been crossed then the blade vibration would continue even with reduction in input level back into the threshold region. Thus, this region could not be clearly defined but every effort was made to obtain these threshold results in a consistent manner. For the highest levels of platform load (>50 N) the resonant response frequency varied significantly from that of the fundamental mode of the lightly loaded blade. This required an increase in the range of frequencies to include any other resonant modes in the response. The response results for the small and large dampers are given in Tables VIII and IX respectively. Plots showing the variation of blade stresses with input level for the range of platform normal loads are given in Figs. 62 and 63. It should be noted in Figs. 62 and 63 that the faired curves used to connect the test points are to aid in identification of the various load cases and do not represent theoretical results. On Fig. 64 the shank stress is shown plotted against the applied platform normal load for input values of 0.5g, 0.7g, and 1.0g. Test and theoretical values are shown for comparison.

### 6.3 Discussion of Results

In this section, a comparison of the numerical results from analysis and testing of a turbine blade with a blade-to-ground platform damper are presented. Values of the parameters used in computation are as follows:

Coefficient of friction . . . . .	0.15, 0.3
Frequency, (Test) . . . . .	515 Hz
Damper stiffness, $k_d$ . . . . .	5472 kN/m (31250 lb/in)
Modal stiffness, $k$ . . . . .	245 kN/m (1400 lb/in)
Modal displacement at platform, $\phi_d$ . . .	0.12
Modal shank stress, $\sigma_m$ . . . . .	2293 MPa (3.348E+5 psi)
Baseline conditions . . . . .	see Fig. 61

The modal information is for the first mode and normalized to unit tip displacement of the blade.

Figure 64 shows the theoretical and test results of blade shank stress as a function of normal load for three base excitation levels and two values of friction coefficient. For the theoretical results shown, the change in resonant frequency is less than one percent of the baseline frequency. From Fig. 64 the following observations can be made.

- (1) The theoretical results for the case of  $\mu = 0.15$  are in general agreement with the test results.
- (2) Higher excitation levels and/or lower values of friction coefficient imply lower rates of stress attenuation,
- (3) For the relatively high stiffness of the damper used in the present program, the rate of stress attenuation is essentially linear.

The influence of damper stiffness on the response characteristics is shown in Fig. 65, where the blade shank stress is plotted as a function of normal load, for a given excitation level and for four values of damper stiffnesses. For all the results shown in Fig. 65, the change in resonant frequency is less than one percent of the baseline frequency. It can be seen that for smaller values damper stiffness, there is an optimum normal load where the stress is a minimum. For normal loads higher than the optimum, there is a gradual increase in shank stress.

Devices such as the platform damper belong to a class of inherently nonlinear damping mechanisms similar to those of shroud damping. As in the case of shroud damping, the vibration characteristics depend on the nature and extent of contact between the damper and the blade platform, as well as the excitation level imposed on the system. The traces shown in Fig. 60 are a clear indication of the changes taking place at the contact region; a nearly sinusoidal response changing to one which emitted audible noise.

Examination of Figs. 62 and 63 suggest that until a certain combination of  $g$  levels and normal loads are attained, the blade response would be practically not measureable. Upon reaching those levels, the response of the blade would depend on the magnitude of the normal load. If the latter is "high", the response mode may correspond to a "stuck damper" condition as is evident from slightly higher frequencies measured. If the  $g$  levels continued to increase, then a condition in which the damper breaks contact may be reached. Under these conditions the blade "plunges" into a lower mode resulting in the jumps in stress as shown in Figs. 62 and 63.

A careful examination of Figs. 62 and 63 also reveals that the airfoil stresses which begin being lower than that measured on the shank gradually become higher for "larger" loads and at higher g levels. This is a clear indication of a change in mode shape which points to the need to include more than a single mode in the mathematical model.

## 7. GENERAL CONCLUSIONS AND RECOMMENDATIONS

The series of analytical and experimental programs discussed in this report have generated data which forms the basis for understanding the potential of nonaerodynamic damping in limiting blade vibration levels. This investigation begins to address the designer's need to be able to set speed margins of rotors on the basis of predicted damping levels at low order resonances. As the exciting forces acting on rotors vibrating at a resonant speed are counteracted entirely by damping forces, only an accurate estimate of available damping can influence the decision in regard to the range of acceptable speeds of the machine. Similarly rotor speeds at which blade flutter is likely cannot be accurately predicted without a knowledge of the contributions from all sources of damping.

All test data and analyses in this report are generated for single blades and an attempt has been made to outline procedures to extend the results for application to an assembly of blades. Undoubtedly future programs must be aimed at verifying these procedures and develop a more firm data base that will serve as a guideline to the designer.

Throughout the present program, the tests underscored the importance of fixture design. Enormous care had to be exercised to make sure that the fixtures designed and fabricated were rugged enough to withstand the vibration levels and to contribute the barest minimum to damping being measured. These are tough requirements and cannot always be fully met. Even with the care that was exercised in this program, it was clear that the root restraint for the twisted plate was found to be less than adequate in the bending modes.

Measurements of damping of aerofoil type components must always be made in vacuum as the contributions from air can lead to order of magnitude increments in measured damping. While this requirement sounds simple to implement, considerable difficulties in measurement can arise for components with extremely low levels of damping. In fact, material damping measurements for the fan blade tested in the program required the use of a pressurized chamber. Data taken at gradually decreasing pressure levels had to be extrapolated to estimate damping under complete vacuum conditions.

Material damping evaluation was made by testing a beam, a twisted plate and an advanced fan all made of a titanium alloy. Material damping constants ( $J$  and  $n$ ) were determined from test data which indicated a value close to  $n=2$ .

The latter is in general agreement with earlier reports but the value of  $J$  found in this program is different from published results by nearly an order of magnitude. The initial conclusions are that this difference may be attributed to the differences in frequencies of vibration between the tests conducted in this program (50 to nearly 600 Hz) and essentially static conditions used in earlier reports. These are, of course, preliminary conclusions. Only a thorough program solely devoted to a study of damping constants for a set of selected engine blade materials can serve to establish the magnitudes of these constants for use in design considerations.

Testing in a limited thermal environment showed that the differences in damping between "cold" and "hot" conditions are insignificant. Similar conclusions are drawn for the differences in damping between zero speed and at speed. The latter reached nearly 1500 rpm and any changes in damping observed is attributed to possible fixture participation.

The general conclusion (that can be drawn from all the studies on material damping conducted in this program) is that damping due to hysteresis in titanium is very low; the loss factor being of the order of  $2 \times 10^{-4}$  to  $5 \times 10^{-4}$ . If  $n = 2$ , the same values apply for a whole assembly. This suggests that damping due entirely to this source should not be accounted for in design against flutter and resonant vibration.

Insofar as damping available at dovetail type root structure is concerned, the data shows that rapid reduction in damping loads occur with increasing normal load on the root. Thus, in actual practice, for an advanced fan under operating conditions the centrifugal pull acting on blades is so high that little or no relative motion at the root-disc interface is likely. Thus, contributions from this source of damping at operating speeds is projected to be very minimal. Unless design changes incorporating retention techniques which permit relative motions at the root location can be examined and introduced, damping from this source should be viewed to be of little importance for design considerations.

Damping at shrouds and at blade platforms due to rubbing represent by far, the most complex mechanism to model analytically in view of the inherently nonlinear nature of these mechanisms. Testing to measure contributions from these mechanisms presents its own problems in view of the continuously changing boundary conditions at the interfaces as the loading and frequency on the device are varied.

Damping at shroud interfaces appears to be the most likely available source of damping for shrouded titanium blades. The level of damping available from the rubbing action is difficult to estimate. However, calculations made using the analytical model developed in this program indicate that the

principal governing parameters are the excitation (g) levels to which the blades are subjected and the normal loads acting at the interfaces. Calculations show that a loss factor of about .003 can be achieved under a normal load of 500 N and a 5 g loading resulting in a vibratory stress of 190 MPa. These numbers are valid for a single blade and no extensions to an assembly can be made without a knowledge of a modal analysis of a fan assembly vibrating in a given nodal diameter pattern.

Experience in regard to platform damping suggests that the important parameters are the damper stiffness and normal load on the damper. Stress reductions of nearly 50 percent can be attained with this mechanism. Stress attenuation in turbine blades can occur either due to damping and/or due to a change of mode shape. The latter arises due to restraint provided by the platform damper.

Under certain combinations of excitation levels and normal load, changes in blade mode shapes were observed in this program. Thus, future programs in this area must be aimed at including several modes in the mathematical model.

Tests conducted on composite material specimens undoubtedly show the damping capacities inherent in composites but the principal difficulty in testing composites lies in obtaining repeatability and consistency. Only a large number of tests can serve to establish reliable information taking into consideration scatter levels.

The program on coating effects was limited to the study of increase in damping, if any, that can be obtained by the use of thermal barrier coatings. Test data indicated that the differences in damping before and after the coating was applied to a turbine blade could be significant but the overall damping levels were still very low.

Although all the tests were conducted on single blades and appropriate mathematical models were developed to represent the several mechanisms of damping, procedures to apply this data to predict damping levels in an assembly of blades have been developed and discussed.

## 8. REFERENCES

1. Lazan, B. J.: Damping of Materials and Members in Structural Mechanics. Pergamon Press, N.Y., 1968.
2. Goodman, L. E.: Material Damping and Slip Damping. Shock and Vibration Handbook, Ed. Harris, C. M. and Crede, C. E. Second Edition, McGraw-Hill Book Co., N.Y., 1976, Chptr. 36.
3. Bert, C. W.: Material Damping: An Introductory Review of Mathematical Models, Measures and Experimental Techniques, Jour. Sound and Vibration, 29(2), pp. 129-153, 1973.
4. Crandall, S. H.: The Role of Damping in Vibration Theory, Jour. Sound and Vibration, 11(1), pp. 3-18, 1970.
5. Pisarenko, G. S.: Vibrations of Elastic Systems Taking Into Account of Energy Dissipation in the Material. Wright-Patterson Air Force Base, WADD TR60-580, 1962.
6. Arnoldi, R. A.: Internal Friction Damping of Mechanical Vibrations, Ph.D. Thesis 1953. Polytechnic Institute of Brooklyn.
7. Baker, W. E., Woolam, W. E. and Young, D.: Air and Internal Damping of Thin Cantilever Beams, Int. Jour. Mechanical Sci., Vol. 9, pp. 743-766, 1967.
8. Dawson, T. H.: Continuum Description of Hysteresis Damping of Vibrations, Int. Jour. Solids and Structures, Vol. 14, pp. 457-464, 1978.
9. Myklestad, N. O.: The Concept of Complex Damping, ASME Jour. Applied Mechanics, pp. 284-286, Sept. 1952.
10. Snowdon, J. C.: Transverse Vibration of Beams with Internal Damping. Journal of the Acoustical Society of America, Vol. 35, No. 12, 1963.
11. Mead, D. J. and Mallick, A. K.: Material Damping Under Random Excitation, Jour. Sound and Vibration, 45(4), pp. 487-494, 1976.
12. Clark, J. W. and Hagel, W. C.: Influence of Static Stress and Temperature on Internal Damping, Trans. American Society of Metals, Vol. 52, pp. 95-115, 1960.
13. Den Hartog, J. P.: Forced Vibrations with Combined Coulomb and Viscous Friction, Trans. ASME, APM-53-9, pp. 107-115, 1931.
14. Ruzicka, J. E.: Resonance Characteristics of Unidirectional Viscous and Coulomb-Damped Vibration Isolation Systems, ASME Jour. Engineering for Industry, pp. 729-740, Nov. 1967.

## 8. REFERENCES (Cont'd)

15. Schlesinger, A.: Vibration Isolation in the Presence of Coulomb Friction, Jour. Sound and Vibration, 63(2), pp. 213-224, 1979.
16. Levithan, E. S.: Forced Oscillation of a Spring-Mass System Having Combined Coulomb and Viscous Damping, Jour. Acoustical Society of America, Vol. 32, No. 10 pp. 1265-1269, 1960.
17. Caughey, T. L.: Sinusoidal Excitation of a System with Bilinear Hysteresis, ASME J. of Applied Mech., Vol. 27, pp. 640-643, Dec. 1960.
18. Hanson, M. P.: A Vibration Damper for Axial-Flow Compressor Blading, Proc. S.E.S.A., Vol. 14, No. 1, pp. 155-162, 1955.
19. Hanson, M. P., Meyer, A. J. and Manson, S. S.: A Method of Evaluating Loose-Blade Mounting as a Means of Suppressing Turbine and Compressor Blade Vibration, Proc. S.E.S.A., Vol. 10, No. 2, pp. 103-116, 1953.
20. Jones, D. I. G. and Muszynska, A.: Vibrations of a Compressor Blade with Slip at Root. The Shock and Vibration Bulletin, No. 48, pp. 53-61, Sept. 1979.
21. Jones, D. L. G. and Muszynska, A.: Design of Turbine Blades for Effective Slip Damping at High Rotational Speeds. Paper presented at the Shock and Vibration Symposium, Washington, D.C., October 1978.
22. Bezhenov, A. I.: "Influence of Some Factors on GTE Turbine Blade Vibrational Energy Dissipation". Izvestia VUZ, Aviatsionnaya Tekhnika, Vol. 20, No. 3, pp. 117-121, 1977.
23. Hartley, R., Sturgess, C. E. N and Rowe, G. W.: Friction in Finite-Element Analyses of Metalforming Processes, Int. Jour. Mechanical Sci., Vol. 21, pp. 301-311, 1979.
24. Goodman, L. E., and Klumpp, J. H.: Analysis of Slip Damping with Reference to Turbine-Blade Vibration, ASME Jour. Applied Mechanics, pp. 421-429, Sept. 1956.
25. Bielawa, R. L.: An Analytical Study of the Energy Dissipation of Turbomachinery Bladed-Disk Assemblies Due to Inter-Shroud Segment Rubbing, ASME Paper No. 77-DET-73, Sept. 1977.
26. Srinivasan, A. V., Lionberger, S. R. and Brown, K. W.: Dynamic Analysis of An Assembly of Shrouded Blades Using Component Modes, ASME Jour. Mechanical Design, Vol. 100, No. 3, pp. 520-527, 1978.
27. Earles, S. W. E. and Williams, E. J.: A Linearized Analysis for Frictionally Damped Systems, Jour. Sound and Vibration, 24(4), pp. 445-458, 1972.

## 8. REFERENCES (Cont'd)

28. Williams, E. J. and Earles, S. W. E.: Optimization of the Response of Frictionally Damped Beam Type Structures with Reference to Gas Turbine Compressor Blading, ASME Jour. Engineering for Industry, pp. 471-476, May 1974.
29. Rimkunas, D. A. and Frye, H. M.: Investigation of Fan Blade Shroud Mechanical Damping, Wright-Patterson Air Force Base, Aero Propulsion Lab. Report # FR-11065, 1979.
30. Griffin, J. H.: "Friction Damping of Resonant Stresses in Gas Turbine Engine Airfoils". ASME Paper #79-GT-109, March 1979.
31. Allen, R. E. and Sidenstick, J. W.: "Turbine Blade Technology-Present and Future", ASME Paper #80-C2 Aero-10, August 1980.
32. Dickerson, E. O.: Turbine Blade Structural Dynamic Analysis, AIAA Paper No. 80-0782.
33. Plunkett, R.: Measurement of Damping, Structural Damping ASME, 1959.
34. Plunkett, R.: Problems in Damping Measurement and Analysis, Course Notes, Vibration Damping Short Course, Univ. of Dayton Research Institute, Dayton, Ohio, Oct. 1978.
35. Ramsey, K. A.: Effective Measurements for Structural Dynamics Testing, Sound and Vibration, Nov. - Dec. 1975.
36. Drake, M. L.: Fast Fourier Transform Methods, Course Notes - Vibration Damping Short Course, University of Dayton Research Institute, Dayton, Ohio, Oct. 1978.
37. Halvorsen, W. O. and Brown, D. L.: Impulse Technique for Structural Frequency Response Testing. Sound and Vibration, Nov. 1977.
38. Klosterman, A., and Zimmerman, R.: Modal Survey Activity Via Frequency Response Functions. S.A.E. Paper 751063.
39. Granick, N. and Stern, J.: Material Damping of Aluminum by a Resonant-Dwell Technique, NASA TN D-2893.
40. Parin, M. L.: Material Property Measurements and Data Reduction, Resonant Beam Measurement Techniques, Course Notes - Vibration Damping Short Course. Univ. of Dayton Research Institute, Dayton, Ohio, Oct. 1978.
41. Smith, G. M. and Berns, H. D.: Frequency Phase Method for Measuring Material Damping. Materials Research and Standards, May 1964.
42. Gibson, R. F. and Plunkett, R.: A Forced Vibration Technique for Measurement of Material Damping, Paper presented at the SESA Spring Meeting, Dallas, Texas, May 1977.

## 8. REFERENCES (Cont'd)

43. Gibson, R. F.: Dynamic Mechanical Behavior of Fiber-Reinforced Composites: Measurement and Analysis, J. Composite Materials, Vol. 10, Oct. 1976.
44. Stahle, C. V. Jr.: Phase Separation Technique for Ground Vibration Testing, Aerospace Engineering, July 1962.
45. Keller, A. C.: Vector Component Techniques: A Modern Way to Measure Modes. Sound and Vibration, Marc. 1969.
46. Meirovitch, L.: Analytical Methods in Vibrations, MacMillon Co., New York, Chapter 4, 1967.
47. Nayfeh, A. H.: Perturbation Methods, Wiley Interscience, Chapter 5, 1973.
48. Young, D. and Felgar, R. P.: Tables of Characteristic Functions Representing Normal Modes of Vibration of a Beam. The University of Texas Publication, No. 4913, July 1, 1949.

## APPENDIX A

### COMPUTER PROGRAMS

Numerical results from the analyses developed during the present study were obtained by using several simple computer programs written in FORTRAN. Following are brief descriptions of the programs, source listings, examples of input and examples of output.

#### Material Damping

In material damping studies, two computer programs were used, one for calculating damping constants and the other for estimating the extent of material damping in a vibrating blade.

#### DMPCON

Objective: To determine material damping constants  $J^*$  and  $n$

Description: The program generates a linear least-squares fit to data obtained from tests on a uniform cantilever beam having a rectangular cross section. The test data is a table of base excitation  $g$ -levels vs strain. The integrations needed for evaluating some of the constants in Eq. 3.23 are performed in a separate subroutine SIMPS by using Simpson's rule.

#### List of Major Variables:

FORTRAN Symbol	Report Symbol	Units	Description
L	L	in.	Length of beam
H	h	in.	Thickness of beam
E	E	psi	Modulus of elasticity
RHO	$\rho$	slugs/12/in. <sup>3</sup>	Mass density
SIGF	$\sigma_e$	psi	Fatigue strength
SGL		in.	Strain gage location: distance from root
MODE			Mode number
NPT			Number of test points
G(I)			Base excitation $g$ -level
EPS(I)			Strain
FREQ		Hz	Frequency
N	$n$		Damping constant
JS	$J^*$	in.-lb/in. <sup>3</sup> /cycle	Damping constant

Input:

L, H, E, RHO, SIGF	(5E10.4)
SGL, MODE, NPT	(E10.4, 2I10)
G(1), EPS(1), G(2), EPS(2), G(3), EPS(3)	(6E10.4)

·  
·  
·

MATDMP

Objective: To estimate material damping loss factor for a vibrating blade, for a given reference blade stress.

Description: The program uses modal stress distribution of the blade, obtained from a finite element program such as NASTRAN. For each element, the energy dissipated and the peak strain energy are calculated by using Eq. 3.4. Summation of the energies over all the elements and using Eq. 3.5 yields the loss factor for the blade.

List of Major Variables:

FORTTRAN Symbol	Report Symbol	Units	Description
E	E	psi	Modulus of elasticity
SIGF	$\sigma_e$	psi	Fatigue strength
N	n		Damping constant
JS	$J^*$	in.-lb/in. <sup>3</sup> /cycle	Damping constant
SREF		psi	Reference blade stress
NREF			Element number where SREF is defined
NELE			Total number of elements
ID			Element number
H	$h_i$	in.	Element thickness
A	$A_i$	in. <sup>2</sup>	Element surface area
SIGU	$\sigma_u$	psi	Maximum principal stress: upper
SIGL	$\sigma_l$	psi	Maximum principal stress: lower
ETA	$\eta$		Loss factor

Input:

E, SIGF, N, JS, SREF, NREF, NELE	(5E10.4, 2I5)
ID, H(ID), A(ID), SIGU(ID), SIGL(ID)	(I5,4E15.7)

·  
·  
·

## Friction Damping

In friction damping studies, three programs were used, one for each of the following: slipping at the root of a fan blade, rubbing at the shroud faces of a fan blade, and rubbing between an external damper and the platform of a turbine blade. A list of the major variables used in the three programs, ROTDMP, SHDDMP and PLTDMP, is shown below.

List of Major Variables: ROTDMP, SHDDMP, PLTDMP

FORTRAN Symbol	Report Symbol	Units	Description	Program		
				ROTDMP	SHDDMP	PLTDMP
FREQ		Hz	Frequency	x	x	x
EXIG			Base excitation			
MU	$\mu$		g-level	x	x	x
KAP	$\kappa$		Coefficient of dry friction	x	x	x
BETA	$\beta$		Factor of dovetail geometry	x		
K	k	lbs/in.	Mass Ratio/(Stiffness Ratio)	x	(x)	
KD	$k_d$	lbs/in.	Modal stiffness	x	x	x
PHID	$\phi_d$		Damper stiffness			x
N	N	lbs	Modal displacement at platform			x
N1,N2		lbs	Normal load	x	x	x
G1,G2			Range of normal loads	x		x
SIGO	$\sigma_o$	psi	Range of base excitation g-levels		x	
SIGM	$\sigma_m$	psi	Baseline blade stress	x	x	x
ETO	$\eta_o$		Modal blade stress			x
ETA	$\eta_b$		Baseline loss factor	x	x	x
EPS	$\epsilon$		Total blade loss factor	x	x	x
NPT			Parameter			x
FTOL			Number of points calculated	x	x	x
KODE			Tolerance on baseline frequency: Expressed as a fraction			x
			Output Control { 0 = Print & plot } { 1 = print only } { 2 = plot only }	x	x	x

ROTDMP

Objective: To calculate the total blade loss factor and blade stress as a function of blade axial load, for a fan blade with slip at its dovetail root.

Description: The program calculates the resonant response of the blade by using Eqs. 4.10 through 4.13, the loss factor by Eqs. 4.18 through 4.21, and the blade stress by Eq. 4.22.

Input:

FREQ, EXIG, MU, KAP, BETA, K	(6E10.4)
------------------------------	----------

SIGO, ETO, N1, N2, NPT, KODE	(4E10.4, 2I10)
------------------------------	----------------

SHDDMP

Objective: To calculate the total blade loss factor and blade stress as functions of base excitation level, for a shrouded fan blade with rubbing at the shroud faces.

Description: The program calculates the resonant response of the blade by using Eqs. 5.7 through 5.10, the loss factor by Eqs. 5.12 through 5.15, and the blade stress by Eq. 5.16.

Input:

FREQ, N, MU, BETA, K	(5E12.4)
----------------------	----------

SIGO, ETO, G1, G2, NPT, KODE	(4E12.4, 2I6)
------------------------------	---------------

PLTDMP

Objective: To calculate the blade loss factor, resonant frequency, and blade stress as a function of normal load, for a turbine blade with rubbing between the blade platform and an external damper.

Description: The program calculates baseline damping loss factor by using Eq. 6.25, the resonant response of the blade Eq. 6.15, loss factor by Eqs. 6.19 through 6.23, and blade stress by Eq. 6.24. The program terminates if the resonant frequency changes from the baseline frequency by more than a specified amount. Also the optimum response is calculated by using Eq. 6.18.

Input:

FREQ, EXIG, MU, KD, PHID, K	(6E10.4)
-----------------------------	----------

SIGM, SIGO, FTOL, N1, N2, NPT, KODE	(5E10.4, 2I5)
-------------------------------------	---------------

```

1  RSS*DAMP(1).DMPCON
2  REAL K, KX, JS, N, L
3  DIMENSION F2(55), F3(55), G(50), EPS(50), A(2,2), R(2), XK(5)
4  DATA A, R/6*0.0/
5  DATA XK /1.875, 4.694, 7.855, 11.00, 14.14/
6  PI=3.1415927
7  READ(5, 11) L, H, E, RHO, SIGF, SGL, MODE, NPT,
8  (G(I), EPS(I), I=1, NPT)
9  WRITE(6, 11) L, H, E, RHO, SIGF, SGL, MODE, NPT,
10 (G(I), EPS(I), I=1, NPT)
11 C
12 K=XK(MODE)
13 WD=K**2
14 WD2=WD**2
15 WCE=(E**H**2/(12.*RHO*L**4))**0.5
16 FQ=WD**WC/(2.*PI)
17 C
18 C
19 C
20 C
21 C
22 C
23 SK=SIN(K)
24 CK=COS(K)
25 SHK=SINH(K)
26 CHK=COSH(K)
27 C=(SHK-SK)/(2.*SK*SHK)
28 CH=(CK+CHK)/(SK-SHK)
29 C2=2.*C/K
30 C4=-WD*C*CH
31 C
32 SCALE FACTORS FOR STRAIN AND EXCITATION
33 Z=K*SGL/L
34 SCA1=2.*CH/(SIN(Z)+SINH(Z))+CH*(COS(Z)+COSH(Z))
35 SCA2=(32.174*12./(2.*PI*FQ)**2)/L
36 C
37 DO 5 I=1, NPT
38 X=ALOG(EPS(I))*SCA1
39 Y=ALOG(G(I))*SCA2
40 A12=A12+X
41 R1=R1+Y
42 R2=R2+X*Y
43 A11=NPT
44 A22=A12
45 DET=A11*A22-A12*A21
46 SLOPE=(A11*R2-A21*R1)/DET
47 XINT=(A22*R1-A12*R2)/DET
48 NJ=EXP(XINT)

```

```

49          C          C          C          C          C          C          C          C          C          C
50          C          C          C          C          C          C          C          C          C          C
51          C          C          C          C          C          C          C          C          C          C
52          C          C          C          C          C          C          C          C          C          C
53          C          C          C          C          C          C          C          C          C          C
54          C          C          C          C          C          C          C          C          C          C
55          C          C          C          C          C          C          C          C          C          C
56          C          C          C          C          C          C          C          C          C          C
57          C          C          C          C          C          C          C          C          C          C
58          C          C          C          C          C          C          C          C          C          C
59          C          C          C          C          C          C          C          C          C          C
60          C          C          C          C          C          C          C          C          C          C
61          C          C          C          C          C          C          C          C          C          C
62          C          C          C          C          C          C          C          C          C          C
63          C          C          C          C          C          C          C          C          C          C
64          C          C          C          C          C          C          C          C          C          C
65          C          C          C          C          C          C          C          C          C          C
66          C          C          C          C          C          C          C          C          C          C
67          C          C          C          C          C          C          C          C          C          C
68          C          C          C          C          C          C          C          C          C          C
69          C          C          C          C          C          C          C          C          C          C
70          C          C          C          C          C          C          C          C          C          C
71          C          C          C          C          C          C          C          C          C          C
72          C          C          C          C          C          C          C          C          C          C
73          C          C          C          C          C          C          C          C          C          C
74          C          C          C          C          C          C          C          C          C          C
75          C          C          C          C          C          C          C          C          C          C
76          C          C          C          C          C          C          C          C          C          C
77          C          C          C          C          C          C          C          C          C          C
78          C          C          C          C          C          C          C          C          C          C
79          C          C          C          C          C          C          C          C          C          C
80          C          C          C          C          C          C          C          C          C          C
81          C          C          C          C          C          C          C          C          C          C
82          C          C          C          C          C          C          C          C          C          C
83          C          C          C          C          C          C          C          C          C          C
84          C          C          C          C          C          C          C          C          C          C
85          C          C          C          C          C          C          C          C          C          C

CONSTANTS C1, C3, C5
NN=50
NP=NN+1
XN=NN
DX=1./XN
DO 1 I=1, NP
XIM=I-1
SX=K*XIM*DX
SX=SIN(KX)
CX=COS(KX)
SHX=SINH(KX)
CHX=COSH(KX)
PHI=C*((SX-SHX)+CH*(CX-CHX))
PHIS=-C*(K**2)*((SX+SHX)+CH*(CX+CHX))
F2(I)=PHI*PHI
F3(I)=ABS(PHIS)**N
C1=SIMPS(DX, NN, F2)
C3=SIMPS(DX, NN, F3)
Z1=12.*C3*L*E**(N-1.)
Z2=PI*C2*W02*ABS(C4)**(N-1.)
Z3=(2.**N)*(N+1.)*H
C5=Z1/(Z2*Z3)
JS=(XJ/ABS(C5))*SIGF**N
WRITE(6,21) L,H,SGL,E,RHO,SIGF,FQ,N,JS
11 FORMAT (5E10.4/E10.4, 2I10/(6E10.4))
21 FORMAT (//: ** DAMPING CONSTANTS **://
15X, 'L' =, E12.4/5X, 'H' =, E12.4/5X, 'SGL' =, E12.4//
25X, 'E' =, E12.4/5X, 'RHO' =, E12.4/5X, 'SIGF' =, E12.4//
35X, 'FREQ' =, E12.4//5X, 'N' =, E12.4/5X, 'JS' =, E12.4)
STOP
END

RSS*DAMP(1).SIMPS
FUNCTION SIMPS(H,N,F)
DIMENSION F(55)
S1=0.
S2=0.
DO 1 I=2, N, 2
S1=S1+F(I-1)
S2=S2+F(I)
1 SIMPS=(-F(1)+F(N+1)+2.*S1+4.*S2)*H/3.
RETURN
END

```

```

RSS*DAMP(1), DMPCON-DATA
1 .8000E+01 .1250E+00 .1850E+08 .4090E-03 .8614E+05 .0702E-02
2 .6400E+00 .0511E-02 .1200E-01 .0662E-02 .1400E-01 .1276E-02
3 .1000E-01 .0822E-02 .1650E-01 .0933E-02 .1800E-01 .1293E-02
4 .1500E-01 .1178E-02 .2200E-01 .1276E-02 .2300E-01 .
5 .2000E-01 .1320E-02 .
6 .2500E-01 .

```

```

@XQT DMPCON

```

```

@ADD, P, DMPCON-DATA
.8000+01 .1250+00 .1850+C8 .4090-03 .8614+C5 .7020-03
.6400+00 .0511-02 .1200-01 .0662-02 .1400-01 .1076-02
.1000-01 .0822-03 .1650-01 .0933-03 .1800-01 .1293-02
.1500-01 .1178-02 .2200-01 .1276-02 .2300-01 .
.2000-01 .1320-02 .
.2500-01 .

```

```

** DAMPING CONSTANTS **

```

```

L      = .8000+01
H      = .1250+00
SGL    = .6400+00

E      = .1850+08
RHO    = .4090-03
SIGF   = .8614+05

FREQ   = .6709+C2

N      = .1890+01
JS     = .1862+00

```

```

1  RSS*DAMP(1).MATDMP
2  REAL N,JS
3  DIMENSION SIGU(400),SIGL(400),H(400),A(400)
4  PI=3.1415927
5  READ(5,10) E,SIGF,N,JS,SREF,NPEF,NELE
6  DO 5 I=1,NELE
7  READ(5,11) ID,H(ID),A(ID),SIGU(ID),SIGL(ID)
8  SUM1=0.0
9  SUM2=0.0
10 XN=N+1.
11
12 SR1=ABS(SIGU(NREF))
13 SR2=ABS(SIGL(NREF))
14 SF=AMAX1(SR1,SR2)/SREF
15
16 DO 1 I=1,NELE
17 SU=SIGU(I)/SF
18 SL=SIGL(I)/SF
19 HH=H(I)
20 AA=A(I)
21 AU=ABS(SU)
22 AL=ABS(SL)
23 A1=AU**XN
24 A2=AL**XN
25 A3=AU**3
26 A4=AL**3
27
28 IF(SU*SL .GT. 0.0) GO TO 2
29 D=AU+AL
30 SUM1=SUM1+AA*HH*(A1+A2)/D
31 SUM2=SUM2+AA*HH*(A3+A4)/D
32 GO TO 1
33
34 2 IF(ABS(SU-SL) .LT. .01*SU) GO TO 3
35 D=AU-AL
36 SUM1=SUM1+AA*HH*(A1-A2)/D
37 SUM2=SUM2+AA*HH*(A3-A4)/D
38 GO TO 1
39
40 3 SUM1=SUM1+AA*HH*(AU**N)*XN
41 SUM2=SUM2+AA*HH*(AU**2)**3.
42
43 1 CONTINUE
44
45 ETA=(3.*E*(JS/SIGF**N)/(XN*PI))*(SUM1/SUM2)
46
47 WRITE(6,21) E,SIGF,N,JS,NELE,NREF,SREF,ETA
48
49

```

ORIGINAL PAGE IS  
OF POOR QUALITY

```

50
51
52
53
54
55
56
57
10 FORMAT(SE10.4,2I5)
11 FORMAT(I5,4E15.7)
21 FORMAT(//,,* MATERIAL DAMPING *//,
,E12.4//5X, SIGF = ,E12.4//5X, N
15X, ,E
25X, ,JS
35X, ,SREF = ,E12.4//5X, ,ETA = ,E12.4)
STOP
END
= ,I12/
= ,I12/

```

```

RSS*DAMP(1).MATDMP-DATA
.1850E+08
1 .8614E+05 .190CE+01 .230CE+00 .1000E+05 3 48
2 .1000000+00 .1000000+01 .8428057+05 --.8417259+05
3 .1000000+00 .1000000+01 .9787132+05 --.9581361+05
4 .1000000+00 .1000000+01 .9581388+05 --.9787160+05
5 .1000000+00 .1000000+01 .8417687+05 --.8428486+05
6 .1000000+00 .1000000+01 .8097715+05 --.8115996+05
7 .1000000+00 .1000000+01 .7927311+05 --.7758624+05
8 .1000000+00 .1000000+01 .7758687+05 --.7927374+05
9 .1000000+00 .1000000+01 .8116409+05 --.8098127+05
10 .1000000+00 .1000000+01 .6908156+05 --.6929569+05
: :
: :
: :

```

@XQT MATDMP

@ADD,P MATDMP-DATA

\*\* MATERIAL DAMPING \*\*

```

SIGF = .1850+08
      = .8614+05
JS    = .1900+01
      = .2300+00
NELE =          48
NREF =          3
SREF = .1000+05
ETA  = .2432-03

```

```

1  RSS*DAMP(1).ROTDMP
2  DIMENSION X(100),Y1(100),Y2(100)
3  REAL MU, KAP, K, N1, N2
4  PI=3.1415927
5
6  READ (5,10) FREQ,EXIG,MU,KAP,BETA,K,SIGO,ETO,
7  1N1,N2,NPT,KODE
8  WRITE(6,10) FREQ,EXIG,MU,KAP,BETA,K,SIGO,ETO,
9  1N1,N2,NPT,KODE
10
11  QO=1./ETO
12  P=(32.174*12.*EXIG)/(2.*PI*FREQ)**2
13  FAC=(4.*MU*KAP)/(PI*K*P)
14  XNPT=NPT
15  DN=(N1-N2)/XNPT
16  N=N1+DN
17  NP=0
18
19  C1=1.+(ETO*(1.+BETA))**2
20  C2=ETO/C1
21  C3=ETO**2/C1
22  C4=1.
23
24  DO 1 I=1,NPT
25  N=N-DN
26  G=N*FAC
27
28  IF(G*G .GE. C4/C3) GO TO 2
29
30  Q2=-C2*G+((C2*G)*(C2*G)-(C3*G*G-C4))**0.5
31  A1=-G/C1
32  A2=Q2 + (ETO*(1.+BETA))*G/C1
33  Q1=(A1**2+A2**2)**0.5
34  Q3=(A1**2+(A2-Q2)**2)**0.5
35  GO TO 3
36
37  Q3=00
38  Q2=0.0
39  3 ETA=ETO+G*Q2/Q3**2
40
41  X(I)=N
42  Y1(I)=Q3*P*SIGO
43  Y2(I)=ETA
44  NP=NP+1
45
46  1 CONTINUE
47
48  WRITE(6,21) FREQ,EXIG,MU,KAP,BETA,K,SIGO,ETO,N1,N2

```

```

49 IF (KODE .EQ. 2) GO TO 9
50 DO 4 J=1,NP
51 WRITE(6,22) X(J),Y1(J),Y2(J)
52
53 C
54 9 IF (KODE .EQ. 1) GO TO 8
55 CALL PLOT(NP,X,Y1)
56 CALL PLOT(NP,X,Y2)
57
58 C
59 10 FORMAT(6E10.4/4E10.4,2I10)
60 21 FORMAT(//: ## ROOT DAMPING **: //
61 15X, 'FREQ =',E12.4/5X, 'EXIG =',E12.4//5X, 'MU =',E12.4/
62 25X, 'KAP =',E12.4/5X, 'BETA =',E12.4/5X, 'K =',E12.4//
63 35X, 'SIGO =',E12.4/5X, 'ETO =',E12.4//5X, 'N1 =',E12.4/
64 45X, 'N2 =',E12.4//5X, 'N', 'N', '10X, 'STRESS',8X, 'ETA'//)
65 22 FORMAT(F10.3,2E12.4)
66 8 STOP
67 END

```

RSS\*DAMP(1).PLOT

```

1 1
2 2
3 3
4 4
5 5
6 6
7 7
8 8
9 9
10 10
11 11
12 12

```

```

SUBROUTINE PLOT(NPT,X,Y)
DIMENSION X(100),Y(100)
CALL INITTT(240)
CALL BINITTT
CALL NPPTS(NPT)
CALL CHECK(X,Y)
CALL DSPLAY(X,Y)
CALL TINPUT(I)
CALL TSEND
CALL FINITTT(G,700)
RETURN
END

```

```

RSS*DAMP(1).ROTDAMP-DATA
1 .7400E+02 .1000E+01 .3000E+00 .2089E-01 .2000E+01 .6400E+02
2 .4350E+05 .5000E-03 .1100E+04 .1000E+03 10

```

@XQT ROTDMP

@ADD,P ROTDMP-DATA  
.7400+02 :1000+01 :3000+00 :2089-01 :2000+01 :.6400+02  
.4350+05 :5000-03 :.1100+04 :.1000+03 :10  
1

\*\* ROOT DAMPING \*\*

FREQ = 7400+02  
EXIG = 1000+01  
MU = 3000+00  
KAP = 2089-01  
BETA = 2000+01  
K = 6400+02  
SIGO = 4350+05  
ETO = 5000-03  
N1 = 1100+04  
N2 = 1000+03

N	STRESS	ETA
1100.000	.5966+04	.1302-01
1000.000	.5423+04	.1432-01
900.000	.4881+04	.1592-01
800.000	.4339+04	.1791-01
700.000	.3796+04	.2046-01
600.000	.3254+04	.2387-01
500.000	.2712+04	.2865-01
400.000	.2169+04	.3581-01
300.000	.1627+04	.4775-01
200.000	.1085+04	.7162-01

```

1  RSS*DAMP(1).SHDDMP
2  DIMENSION X(100),Y1(100),Y2(100)
3  REAL K, MU, N
4  PI=3.1415927
5
6  READ (5,10) FREQ,N,MU,BETA,K,SIGO,ETO,G1,G2,NPT,KODE
7  WRITE(6,10) FREQ,N,MU,BETA,K,SIGO,ETO,G1,G2,NPT,KODE
8
9  Q0=1./ETO
10 XNPT=NPT
11 DG=(G1-G2)/XNPT
12 EXIG=G1+DG
13 NPEO
14
15 C1=1.+(ETO*(1.+BETA))**2
16 C2=ETO/C1
17 C3=ETO**2/C1
18 C4=1./C1
19
20 DO 1 I=1,NPT
21 EXIG=EXIG-DG
22 P=(32.174*12.*EXIG)/(2.*PI*FREQ)**2
23 FACE=(8.*MU)/(PI*K*P)
24 G=N*FACE
25
26 IF(G*G .GE. C4/C3) GO TO 2
27
28 Q2=-C2*G+((C2*G)*(C2*G)-(C3*G*G-C4))**0.5
29 A1=-G
30 A2=(1.+BETA)*Q2
31 Q1=(A1**2+A2**2)**0.5
32 Q3=(A1**2+(A2-Q2)**2)**0.5
33 GO TO 3
34
35 2 Q3=Q0
36 Q2=0.0
37 3 ETA=ETO+G*Q2/Q3**2
38
39 X(I)=EXIG
40 Y1(I)=Q3*P*SIGO
41 Y2(I)=ETA
42 NP=NP+1
43
44 1 CONTINUE
45
46 WRITE(6,21) FREQ,N,MU,BETA,K,SIGO,ETO,G1,G2

```

```

47 IF (KODE.EQ.2) GO TO 9
48 DO 4 J=1,NP
49 WRITE(6,22) X(J),Y1(J),Y2(J)
50
51 C
52 9 IF (KODE.EQ.1) GO TO 8
53 CALL PLOT(NP,X,Y1)
54 CALL PLOT(NP,X,Y2)
55
56 C
57 10 FORMAT(5E12.4/4E12.4,2I6)
58 21 FORMAT(///,*,* SHROUD DAMPING *,*//
59 15X,*,FREQ =,*,E12.4/5X,*,N =,*,E12.4/5X,*,MU =,*,E12.4/
60 25X,*,BETA =,*,E12.4/5X,*,K =,*,E12.4/5X,*,G1 =,*,E12.4/5X,*,G2 =,*,E12.4/
61 35X,*,ETA =,*,E12.4/5X,*,G1 =,*,E12.4/5X,*,G2 =,*,E12.4/
62 4//6X,*,G,*,8X,*,STRESS,*,8X,*,ETA,*,//)
63 22 FORMAT(F10.3,2E12.4)
      8 STOP
      END

```

RSS\*DAMP(1).PLOT

```

1 SUBROUTINE PLOT(NPT,X,Y)
2 DIMENSION X(100),Y(100)
3 CALL INITI(240)
4 CALL FINIT(1)
5 CALL NPTS(NPT)
6 CALL CHECK(X,Y)
7 CALL DSPLAY(X,Y)
8 CALL TINPUT(I)
9 CALL TSEND
10 CALL FINIT(0,700)
11 RETURN
12 END

```

```

RSS*DAMP(1).SHDDMP-DATA
1 .2800E+03
2 .1464E+06
.3000E+02
.5000E-03
.3500E+00
.0000E+00
.1440E+01
.2000E+01
.4520E+03
10
1

```

@XQT SHDDMP

@ADD,P SHDDMP-DATA  
:2800+03 :3000+02 :3500+00 :1440+01 :4520+03  
:1464+06 :5000-03 :0000 :2000+01 :10

\*\* SHROUD DAMPING \*\*

FREQ = :2800+03  
N = :3000+02  
MU = :3500+00  
BETA = :1440+01  
K = :4520+03  
SIGO = :1464+06  
ETO = :5000-03  
G1 = :0000  
G2 = :2000+01

G	STRESS	ETA
.000	.0000	.5000-03
.200	.7305+04	.5000-03
.400	.8660+04	.8435-03
.600	.8660+04	.1265-02
.800	.8660+04	.1687-02
1.000	.8660+04	.2109-02
1.200	.8660+04	.2530-02
1.400	.8660+04	.2952-02
1.600	.8660+04	.3374-02
1.800	.8660+04	.3796-02

```

RSS*DAMP(1).PLTDMP
1 DIMENSION X(100),Y1(100),Y2(100),Y3(100)
2 REAL MU,KD,K,N1,N2,N,NOP
3 PI=3.1415927
4
5 READ (5,10) FREQ,EXIG,MU,KD,PHID,K,SIGM,SIGO,FTOL,
6 1 N1,N2,NPT,KCODE
7 WRITE(6,10) FREQ,EXIG,MU,KD,PHID,K,SIGM,SIGO,FTOL,
8 1 N1,N2,NPT,KODE
9
10 EPS=PHID**2*KD/K
11 P=(32.174**12.*EXIG)/(2.*PI*FREQ)**2
12 FAE=MU/(PHID*KD*P)
13 ETO=EP*SIGM/SIGO
14 XNPT=NPT
15 DN=(N2-N1)/XNPT
16 N=-DN
17 NP=0
18
19 DO 1 I=1,NPT
20 N=N+DN
21 G=N*FAC
22 C1=PI-4.*EPS*G
23 C2=16.*PI*EPS*ETO*G**2
24 QM=(C1+(C1*C1+C2)**0.5)/(2.*PI*ETO)
25 IF (G .GE. QM) GO TO 2
26 TAU=ACOS(1.-(2.*G/QM))
27 WM=1.+(EPS/(4.*PI))*(2.*TAU-SIN(2.*TAU))
28 IF (ABS(1.-WM) .GT. FTOL) GO TO 2
29 ETA=ETO+(4.*EPS/PI)*G*(QM-G)/OM**2
30 X(I)=N
31 Y1(I)=WM*FREQ
32 Y2(I)=QM*P*SIGM
33 Y3(I)=ETA
34 1 NP=NP+1
35
36 2 WRITE(6,21) FREQ,EXIG,MU,KD,PHID,K,SIGM,SIGO,ETO,
37 1 FTOL,N1,N2,EPS
38
39 IF(EPS .GT. 4.*FTOL) GO TO 4
40 GOP=PI/(2.*(EPS+PI*ETO))
41 NOP=(GOP/FAC)
42 SIGOP=(2.*GOP)*P*SIGM
43 WMOP=(1.+(EPS/4.))*FREQ
44 ETAOP=ETO+EPS/PI
45
46 4 IF (KODE.EQ.2) GO TO 9
47 DO 3 J=1,NP
48 3 WRITE(6,22) X(J),Y1(J),Y2(J),Y3(J)

```

```

49 IF(EPS .GT. 4.*FTOL) GO TO 9
50 WRITE(6,23) NOP,WMOP,SIGOP,ETAOP
51 IF(KODE .EQ. 1) GO TO 5
52 CALL PLOT(NP,X,Y1)
53 CALL PLOT(NP,X,Y2)
54 CALL PLOT(NP,X,Y3)
55
56 C
57 10 FORMAT(6E10.4/5E10.4,2I5)
58 21 FORMAT(//): ** PLATFORM DAMPING **//
59 15X, 'FREQ' =, E12.4/5X, 'PHID' =, E12.4/5X, 'K' =, E12.4/
60 35X, 'SIGM' =, E12.4/5X, 'SIGO' =, E12.4/5X, 'ETO' =, E12.4/
61 45X, 'FTOL' =, E12.4/5X, 'N1' =, E12.4/5X, 'N2' =, E12.4/
62 55X, 'EPS' =, E12.4//6X, 'N', 'ICX', 'FREQ', '6X', 'STRESS',
63 68X, 'ETA'//)
64 22 FORMAT(F10.3,3E12.4)
65 23 FORMAT(/IX, 'OPTIMUM VALUES'// F10.3,3E12.4)
66 5 STOP
67 END

```

RSS\*DAMP(1).PLOT

```

1 SUBROUTINE PLOT(NPT,X,Y)
2 DIMENSION X(100),Y(100)
3 CALL INIIT
4 CALL BINITT
5 CALL NPTS(NPT)
6 CALL CHECK(X,Y)
7 CALL DISPLAY(X,Y)
8 CALL TINPUT(I)
9 CALL TSEND
10 CALL FINIIT(0,700)
11 RETURN
12 END

```

```

RSS*DAMP(1).PLTDMP-DATA
1 .5150E+03 .1000E+01 .1500E+00 .3125E+05 .1200E+00 .1400E+04
2 .3348E+06 .3533E+05 .1000E-01 .0000E+00 .5000E+01 .10

```

@XQT PLTDMP

@ADD,P PLTDMP-DATA  
.5150+03 .1000+01 .1500+00 .3125+05 .1200+00 .1400+04  
.3348+06 .3533+05 .1000-01 .0000 .5000+01 .10

\*\* PLATFORM DAMPING \*\*

ERFQ = .5150+03  
MU = .1500+00  
KD = .3125+05  
PHID = .1200+00  
K = .1400+04  
SIGM = .3348+06  
SIGO = .3533+05  
ETO = .3494-03  
FTOL = .1000-01  
N1 = .0000  
N2 = .5000+01  
EPS = .3214+00

N	FREQ	STRESS	ETA
.000	.5150+03	.3533+05	.3494-U3
.500	.5150+03	.2749+05	.4491-03
1.000	.5150+03	.1966+05	.6281-03
1.500	.5150+03	.1184+05	.1042-02
2.000	.5151+03	.4162+04	.2966-02
2.500	.5198+03	.3129+03	.3945-01

ORIGINAL PAGE IS  
OF POOR QUALITY

## APPENDIX B

### TEST ASSEMBLIES, INSTRUMENTATION AND DATA REDUCTION

#### B.1 Test Assemblies

The test program discussed in this report required the design and fabrication of a number of test components and fixtures. Table B-1 presents a complete listing of the major components of the test assembly used in each test series. Design office assembly drawings and parts lists are referenced by number for each assembly. Fabrication engineering orders, other than those associated with a particular parts list, are also referenced.

Whenever possible, fixtures were used for more than one test series with minor modification. The basic test arrangement used for most of the testing comprised a massive root block, onto which the test piece was either clamped or welded, bolted into an aluminum plate vacuum chamber and mounted on a slip plate so that vibration could be applied horizontally by a Ling Dynamic Systems electrodynamic shaker. The slip plate moved on a film of oil spread between the plate and the flat horizontal surface of a granite block. For the material damping tests on a fan blade, the root block was made of titanium alloy 8-1-1 with the blade welded into it (see Figs. 1, 16-18). A fixture checkout was performed with this test assembly and with the blade restrained at its tip. Frequency response sweeps were performed from 60 to 1000 Hz at input acceleration levels of up to 3 g. These sweeps showed a large axial resonance of the fixture at 550 Hz. However, by locating the input control accelerometer on the root block as shown in Fig. 18, this mode could be controlled to give a flat response at both the input location and directly adjacent to the blade root from 60 to 1000 Hz. This frequency range was adequate for the free blade vibration tests.

For the shroud damping investigation, a shroud loading disk arrangement, (see Fig. 41), was placed around the blade and bolted in position to lugs on the fixture side and base plates. Since the torsion mode of the blade with shrouds restrained was found to be at about 1100 Hz, additional fixture checkout runs were performed up to 2000 Hz. Again, with the control accelerometer on the outside of the root block, a flat input level could be maintained at the blade root up to 1600 Hz.

For the root damping tests, a steel root block was inserted in place of the titanium block and provision was made to clamp the fan blade at its dovetail with a variable axial load (see Figs. 31 and 32). Response frequencies of less than 500 Hz were to be investigated and hence no further fixture checks were required.

The twisted plate, uniform cantilevered beam and composite beam specimens were attached to the steel block individually by special clamps. Because of the cantilevered design of these clamps, the input control accelerometer was mounted directly on each clamp to ensure correctness of input level.

The fixturing for the remaining test series is discussed in the body of the report in the sections referenced in Table B-1.

Supporting mechanical equipment to provide the environmental conditions and applied loads are included in the list of test equipment given in Table B-2.

## B.2 Instrumentation

The electronic equipment used for excitation control and for response signal conditioning and recording during the test program are included in the list of test equipment given in Table B-2.

The basic control system for all shaker excited tests is shown in Fig. 43. The servo level and frequency control was provided by a B & K Automatic Vibration Exciter Controller which was connected into the shaker and matched power amplifier circuit. Test piece input acceleration levels were sensed by a VSS Type 101 accelerometer. The accelerometer signal was conditioned by a charge amplifier located in the LDS Vibration Meter. The output, normalized to 10 mv/g, was passed through a 50 Hz bandwidth tracking filter provided by the SD Dynamic Analyzer. This ensured that the fundamental component of the input signal had the desired level. For inputting very low g levels ( $< 0.1$ ), a Krohnkite amplifier was interposed between the tracking filter and the controller to enable the input signal to be amplified to a level acceptable to the controller. The filtered control signal was also amplified, as required, and connected into the horizontal axis of the oscilloscope in order to obtain Lissajous figures. Logarithmic frequency sweeping was provided by the controller with rates down to 0.0136 octave/minute. A Fluke counter provided an accurate readout of the input signal period.

The basic data collection, conditioning and recording system is also shown in Fig. 43. Signals from the single strain gage (per channel) mounted on the test piece were conditioned by a strain gage translator. This module provided the potentiometric bridge balance resistor, bridge excitation voltage and amplification of the normalized strain gage signals to the required signal level for recording. By setting the correct K-factor on the input dial a normalized signal was obtained equal to 12.5 mv rms per 1000 psi (6.895 MPa) peak stress. The factor is given by:

$$K = \frac{0.009065 \times E \times (R_G + R_B + R_L)^2}{G_F \times R_G \times R_B}$$

where RG = Strain gage resistance, ohms  
 RB = Balance resistance (=500 ohms)  
 RL = Lead wire resistance (ohms)  
 E = Youngs Modulus of specimen material (GPa)  
 GF = Gage Factor

The calibrated strain signal level was read directly on a digital voltmeter. This was possible since most testing required resonance dwell techniques. From the translator, the signal was fed through a Krohnkite variable filter/amplifier and then to a B & K level recorder operating in the peak detection logarithmic level mode for permanent chart recording. Alternate recording systems were provided by the oscilloscope and the log converter/X-Y plotter. Calibration of the recorders was performed by recording a signal of known millivolt level, as determined by the voltmeter, and using the 20 and 40 dB amplification switches on the Krohnkite amplifier to cover the range required.

Signal conditioning for the response accelerometers was provided either by the second channel charge amplifier on the vibration meter or by integral electronics and a separate conditioning unit depending on the type of accelerometer used. Acceleration levels were read off the vibration meter and recorded on the level recorder.

### B.3 Data Reduction

Two types of data plotting were used in the test program, namely, response peak logarithmic level decay with time at constant frequency and response peak logarithmic level variation with time for time varying input frequency (logarithmic sweep about a resonance). From these presentations it was required to determine the modal loss factor and frequency data.

#### Loss Factor From Decay Curves

Assuming an equivalent linear viscous damping in a system, the exponential envelope of the peaks of a decaying response is given by

$$x = x_0 e^{-\pi \eta t / \tau_n} \tag{B.1}$$

where x is the amplitude at time t,  $x_0$  is the initial or reference amplitude,  $\eta$  is the loss factor, and  $\tau_n$  is the period of vibration. The level recorder gives the change in amplitude in terms of decibels referenced to  $x_0$ . Denoting the record level at time t by  $L_x$ ,

$$\begin{aligned}
L_x &= 20 \log_{10}(x/x_0) \\
&= -20\pi (\log_{10} e) \eta t / \tau_n = -27.3 \eta t / \tau_n
\end{aligned}
\tag{B.2}$$

and

$$\frac{dL_x}{dt} = -27.3 \eta / \tau_n
\tag{B.3}$$

Equation (B.3) can be rewritten as

$$\frac{dL_x}{dt} = \frac{dL_x}{d\ell} \cdot \frac{d\ell}{dt} = S \cdot P = -27.3 \eta / \tau_n
\tag{B.4}$$

where S is the instantaneous slope (dB/mm) of a curve on the chart,  $\ell$  is the length (mm) on the chart and P is the paper speed (mm/sec) of the recorder. The loss factor can be calculated by using Eq. (B.4) as

$$\eta = SP \tau_n / 27.3
\tag{B.5}$$

In practice, the decays were not true straight lines, i.e.,  $\eta$  varied with strain level and initial transients caused some distortion at the start of the decay. An average loss factor was then determined from the slope between amplitude levels of 1 and 4 dB down from the initial peak level. Thus, the critical region for damping, i.e., the peak to half power level, was spanned.

#### Loss Factor From Frequency Response Plots

The frequency sweep is of the form

$$f(t) = f_0 e^{\alpha t}
\tag{B.6}$$

where  $f_0$  is the initial or reference frequency  
 $f(t)$  is the frequency at time t, and  
 $\alpha$  is a constant for a given sweep rate.

Let  $\bar{\Delta t}$  be the time taken for an octave change in frequency,

Then 
$$\frac{f(t + \bar{\Delta t})}{f(t)} = 2 = e^{\alpha \bar{\Delta t}}$$

From which

$$\alpha = \ln 2 / \bar{\Delta t} \quad (B.7)$$

Hence, given the sweep rate (octaves/second), chart paper speed P (mm/sec) and a reference frequency  $f_o$ , the frequency during the sweep can be determined from

$$f(t) = f_o e^{\alpha \Delta \ell / P} \quad (B.8)$$

where  $\Delta \ell$  is the measured length (mm) on the chart between  $f_o$  and  $f(t)$ .

The loss factor is given by

$$\eta = \frac{\Delta f}{f_n} \quad (B.9)$$

where  $\Delta f$  is the half power bandwidth about the resonant frequency,  $f_n$ . If  $\Delta f$  is swept in time  $\Delta t$  and assuming the response curve is symmetrical about the peak, then

$$\begin{aligned} \Delta f &= 2(f_n e^{\alpha \Delta t / 2} - f_n) \\ &= 2 f_n (e^{\alpha \Delta t / 2} - 1) \end{aligned} \quad (B.10)$$

$$\doteq f_n \alpha \Delta t \quad \text{for small } \alpha \Delta t$$

An estimate of loss factor is therefore given by using (B.9)

$$\eta = \alpha \Delta t \quad (B.11)$$

Now the measured chart length  $\Delta \ell$ , corresponding to the change in time  $\Delta t$  is given by

$$\Delta\ell = P \cdot \Delta t \quad (\text{B.12})$$

where P is the chart paper speed.

Therefore, the loss factor can be determined using equations (B.11) and (B.12) as

$$\eta = \frac{\alpha \Delta\ell}{P} \quad (\text{B.13})$$

In practice, the slowest sweep rate available was chosen, namely  $2.2598 \times 10^{-4}$  octaves/sec, giving a value for  $\alpha$  of 0.00015664. The loss factors were determined by measuring the distance between points 3 dB down from the maximum response and taking the resonant frequency as the frequency midway between these points.

## APPENDIX C: DAMPING IN AN ASSEMBLY OF BLADES

The present program dealt exclusively with single blades and blade-like components. An attempt was made to extend the analyses developed, and results obtained in the present program to predict damping levels in an assembly. In this Chapter, procedures (based on single blade analyses and results) are developed for determining the damping levels in an assembly. At the minimum, these procedures should yield results which are good approximations to the actual levels of damping in an assembly of blades.

The following assumptions are made.

1. The assembly is vibrating in a single mode characterized by a nodal diameter pattern and a constant interblade phase angle.
2. The following modal quantities associated with the mode of vibration are known: frequency, modal mass, modal stiffness, and modal stress distribution of the reference blade (defined as the blade having the maximum amplitude).
3. All modal quantities are normalized to unit tip displacement of the reference blade.

### 7.1 Material Damping

The procedure for determining the assembly material damping loss factor is analogous to the one used in Section 3.1 for a single blade. The loss factor can be written as

$$\eta^* = \frac{1}{2\pi} \frac{\sum_{j=1}^{N^*} D_j}{\sum_{j=1}^{N^*} U_j}, \quad (C.1)$$

where (\*) refers to the assembly,  $j$  is the blade number,  $D$  the energy dissipated,  $U$  the strain energy, and  $N^*$  the number of blades in the assembly. The energy dissipated is a function of blade stress and damping constants. The strain energy is a function of blade stress and modulus of elasticity. The stress at a point on the  $j^{\text{th}}$  can be written as

$$\sigma_j = \sigma_R \cos j\beta^*, \quad \beta^* = 2\pi \rho / N^*, \quad (C.2)$$

where  $\sigma_R$  is the stress at the corresponding point on the reference blade,  $p$  is the number of nodal diameters, and  $\beta^*$  is the interblade phase angle. Equations (C.2) and (3.4) lead to

$$D_j = D_R (\cos j\beta^*)^n, \quad U_j = U_R (\cos j\beta^*)^2, \quad (C.3)$$

where  $n$  is the damping constant.

Substitution of Eq. (C.3) into (C.1) and introduction of

$$C_\eta = \frac{\sum_{j=1}^{N^*} \cos^n j\beta^*}{\sum_{j=1}^{N^*} \cos^2 j\beta^*}, \quad \eta_R = \frac{1}{2\pi} \frac{D_R}{U_R}, \quad (C.4)$$

leads to

$$\eta^* = C_\eta \eta_R, \quad (C.5)$$

where  $\eta_R$  is the material damping loss factor for the reference blade, computed by using the blade modal stress distribution for the assembly mode of vibration and the analysis of Section 3.1. Clearly, for  $n = 2$ ,  $C_\eta = 1$  so that the loss factors for a reference blade and an assembly are identical.

## 7.2 Friction Damping

The friction damping effects considered in this section are those due to slipping at blade roots and rubbing at shroud interfaces. An assembly mode of vibration which is characterized by modal quantities can be thought of as a single degree of freedom, acted on by friction forces. Thus, the possibility of using the analyses developed for single blades, with some modifications, to predict the effects of friction damping in an assembly of blades is explored here. In particular, the idea is to use the computer programs ROTDMP and SHDDMP developed for single blades, with suitable modifications to the input information to reflect the dynamics of the vibrating assembly. Brief descriptions of the necessary modifications to the input information are as follows.

### (1) Modal Information:

The modal parameters; frequency  $f^*$ , modal stiffness  $k^*$ , and modal mass  $m^*$  are those that characterize the assembly mode of vibration.

### (2) Baseline Condition:

The baseline condition is assumed to be condition of no friction damping.

The baseline stress  $\sigma^*$  is the blade modal stress at some point on the reference blade. The baseline damping loss factor  $\eta_0^*$  is assumed to be known.

(3) Base Excitation Level in g-units,  $n_g$

Typically, this information is unavailable for an assembly of blades. However,  $n_g$  can be estimated provided some additional information pertaining to assembly is given as follows:

(a) Given  $P^*$ , the excitation force amplitude,

$$n_g = \frac{P^*}{k^*} \frac{(2\pi f^*)^2}{g} \quad (C.6)$$

where  $g$  is the acceleration due to gravity ( $9.81 \text{ m/sec}^2$ )

(b) Given  $x_0^*$ , baseline tip deflection of reference blade,

$$n_g = \frac{x_0^* \eta_0^*}{C_m} \frac{(2\pi f^*)^2}{g} \quad (C.7)$$

where  $C_m$  is a constant depending on the mode of vibration. For example, for a uniform cantilever beam  $C_m = 1.566$  for the first mode (Ref. 39). However, in the case of an assembly  $C_m$  may have to be determined from tests.

(4) Interface normal load, coefficient of friction:

In single blade analysis the energy dissipated due to friction at an interface is computed as,

$$D = 4\mu N x_s \quad , \quad (C.8)$$

where  $N$  is the normal load,  $\mu$  the coefficient of friction, and  $x_s$  the slip amplitude. In an assembly, all the blades are not equally active due to the existence of a nodal diameter pattern. The total energy dissipated in the assembly can be estimated as

$$D_f^* = 4\mu N x_s \sum_{j=1}^{N^*} |\cos j \beta^*| \quad . \quad (C.9)$$

Thus, a convenient way of accounting for the dynamics of the assembly is to define an equivalent coefficient of friction,

$$\mu^* = C_\mu \mu; \quad C_\mu = \sum_{j=1}^{N^*} \cos j \beta^* . \quad (C.10)$$

(5) Mass Ratio,  $\beta$  (Root Damping)

For a single blade the mass ratio is defined as

$$\beta = (I_0/L^2)/m_1 , \quad (C.11)$$

where  $I_0$  is the blade mass moment of inertia about the root,  $L$  the blade length, and  $m_1$  the modal mass. For an assembly, the total mass moment of inertia about the disk circumference can be written as

$$I_0^* = I_0 N^* , \quad (C.12)$$

so that, an equivalent mass ratio for the assembly is,

$$\beta^* = (I_0^*/L^2)/m^* . \quad (C.13)$$

(6) Stiffness ratio  $\beta$ , (Shroud Damping)

For a single blade the stiffness is defined as

$$\beta = \hat{k}/k , \quad (C.14)$$

where  $\hat{k}$  is the static stiffness of the blade below the shrouds. In an assembly, this static stiffness is not the same as that for a single blade due to the influence of neighboring blades. However, the appropriate value of the static stiffness, can be obtained from static tests on the assembly, so that an equivalent stiffness ratio can be defined as

$$\beta^* = \hat{k}^*/k^* . \quad (C.15)$$

TABLE I

## TITANIUM CANTILEVER BEAM TEST RESULTS

Mode	Input Level <sup>1</sup> g pk	Period sec	Response Level <sup>2</sup> microstrain
1	0.010	0.0146220	511
	0.012	0.0146216	662
	0.014	0.0146158	702
	0.015	0.0146160	822
	0.0165	0.0146200	933
	0.018	0.0146196	1076
	0.020	0.0146190	1178
	0.022	0.0146187	1276
	0.023	0.0146206	1293
	0.025	0.0146186	1320
2	0.05	0.0023390	138
	0.08	0.0023392	222
	0.10	0.0023390	262
	0.15	0.0023391	409
	0.16	0.0023395	427
	0.20	0.0023392	498
	0.20	0.0023397	520
	0.22	0.0023399	591
	0.24	0.0023398	609
	0.25	0.0023395	609
	0.26	0.0023401	680
	0.28	0.0023401	716
	0.30	0.0023391	733
	0.32	0.0023401	778
	0.34	0.0023402	827
	0.35	0.0023402	911
	0.36	0.0023401	867
0.40	0.0023405	1093	
3	0.10	0.00083618	71
	0.20	0.00083598	147
	0.20	0.00083622	147
	0.30	0.00083618	222
	0.40	0.00083610	293
	0.50	0.00083636	369
	0.55	0.00083620	400
	0.60	0.00083630	440
	0.70	0.00083651	507
	0.80	0.00083649	564
1.00	0.00083675	680	
1.20	0.00083709	791	

## NOTES:

<sup>1</sup>Sinusoidal vibration applied at root of cantilever<sup>2</sup>Axial strain measured at 8% span

TABLE II

## SUMMARY OF TWISTED PLATE TEST RESULTS

Nominal Rotational Speed, rpm	Centr. Force N	Mode No.	Freq., Hz	Stress <sup>1</sup> Range MPa (pk)	Vibratory to Static		Loss Factor		
					Stress Ratio	Range	Range	Average	
<u>Centrifugal Test</u>									
0 (in air)	0	{	1	100.7	16.2-27.6	-	.0014	-.0017	.0016
			2	549	27.0-39.4	-	.00040	-.00071	.00059
			3	677	35.3	-	.00030	-.00031	.00031
0 (in vac)	0	{	1	101	27.6	-	.00049	-.00051	.00050
			2	550	27.6	-	.00040	-.00042	.00040
			3	677	39.0	-	.00015	-.00017	.00016
500	211	{	1	103	13.8-27.6	8.3 16.6	.00050	-.00071	.00060
			2	553	27.6-33.0	16.6 19.9	.00055	-.00065	.00060
			3	678	30.0-39.6	18.1 23.9	.00020	-.00022	.00020
1000	845	{	1	109	13.8-27.6	2.1 4.2	.00055	-.00102	.00080
			2	559	11.0-46.0	1.7 6.9	.00060	-.00079	.00070
			3	677	13.0-24.8	2.0 3.7	.00019	-.00022	.00021
1200	1220	{	1	113	27.6-30.9	2.9 3.2	.00093	-.00104	.00097
			2	-	-	-	-	-	-
			3	-	-	-	-	-	-
1400	1650	{	1	117	9.9	0.76	.00080	-.00104	.00093
			2	566	9.9-19.9	0.76 1.5	.00067	-.00085	.00074
			3	678	7.2-13.2	0.55 1.0	.00019	-.00025	.00022
1500	1900	{	1	119	8.8-11.6	0.59 0.78	.00085	-.00111	.00099
			2	568	9.9-12.7	0.66 0.85	.00040	-.00060	.00051
			3	678	9.9-22.2	0.66 1.5	.00018	-.00023	.00020
<u>Bench Test<sup>2</sup></u>									
(in air)	0	{	1	101	9.3-86	-	.00056	-.00088	.00070
			2	548	25-97	-	.00076	-.00107	.00097
			3	679	5.8-30	-	.00013	-.00014	.00014
(in vac)	0	{	1	101	66-104	-	.00049	-.00054	.00052
			2	549	21-95	-	.00027	-.00036	.00032
			3	680	7.9-41	-	.000092	-.0000104	.000097

NOTES: 1 Stress value assuming E - 128 GPa

2 Steel shim removed from tip

TABLE III

## SUMMARY OF DATA FOR FAN BLADE MATERIAL DAMPING TESTS

Pressure Ratio <sup>1</sup> P/P <sub>s</sub>	Input Acceleration g	Mode	Response Frequency Hz	Root Stress MPa	ASMT Stress MPa	Loss Factor
0.02	ND	1(1F)	77.88 <sup>4</sup>	56	28	.00030 <sup>2</sup>
	ND		77.89	110	52	.00085
	0.19	2(2F)	250.38	47	32	.00024 <sup>3</sup>
	0.56		250.39	145	98	.00027
	0.83		250.37	207	141	.00027
	0.6	3(1T)	483.09	36	47	.00011
	1.0		482.91	58	76	.00012
	2.8		481.39	126	165	.00014
	6.0		480.35	159	207	.00015
	0.26	ND	1(1F)	77.80	56	ND
ND		77.77		110	ND	.0023
0.38		2(2F)	250.29	68	ND	.00032
0.85			250.29	128	ND	.00049
1.7			250.29	200	ND	.00062
2.5		3(1T)	482.46	65	ND	.00029
7.0			481.19	123	ND	.00048
1.0	ND	1(1F)	77.57	56	ND	.0040
	ND		77.44	110	ND	.0062
	0.75	2(2F)	250.09	62	ND	.00067
	2.0		249.96	133	ND	.00109
	4.0		249.96	196	ND	.00130
	5.7	3(1T)	481.72	53	70	.00087
	7.0		481.74	63	82	.00095
	10.0		481.58	72	95	.00102

- NOTES: 1. P<sub>s</sub> = 760 Torr  
2. Loss factors for mode 1 derived from frequency sweep data  
3. Loss factors for modes 2 and 3 derived from decay data  
4. Frequencies estimated from Figure 20

TABLE IV

## SUMMARY OF ROOT DAMPING TEST DATA

Total Bolt Load N	Excitation Level g(pk)	Root Stress MPa(pk)	Response Frequency Hz	Loss Factor $\eta$
576	0.2	5.4	68.311	.0374
	0.2	5.5	68.353	.0374
	0.5	9.9	66.445	.0501
	0.5	9.9	66.454	.0501
	1.0	11.0	64.135	.0846
	1.0	11.0	64.144	.0815
1152	0.2	6.1	72.396	.0259
	0.2	6.1	72.369	.0234
	0.2	6.1	72.369	.0259
	0.5	12.1	69.989	.0436
	0.5	12.4	70.013	.0436
	1.0	17.4	68.871	.0515
	1.0	17.4	68.890	.0550
	1.0	17.4	68.899	.0469
1727	0.2	11.5	73.910	.0129
	0.2	11.2	73.915	.0132
	0.2	11.2	73.893	.0135
	0.5	14.8	72.516	.0289
	0.5	15.2	72.490	.0285
	0.5	15.4	72.543	.0273
	1.0	21.2	71.367	.0446
	1.0	21.2	71.408	.0433
2303	0.2	18.0	74.460	.0089
	0.2	17.8	74.555	.0088
	0.2	18.1	74.560	.0088
	0.5	23.9	73.719	.0149
	0.5	24.4	73.735	.0135
	0.5	24.4	73.719	.0147
	1.0	28.8	72.690	.0263
	1.0	28.8	72.690	.0265
	1.0	28.8	72.690	.0284
2879	0.2	21.9	74.794	.0073
	0.2	21.9	74.800	.0073
	0.5	31.0	74.173	.0113
	0.5	30.9	74.184	.0113
	1.0	38.4	73.341	.0207
	1.0	38.9	73.341	.0208
	1.0	38.8	73.346	.0198

TABLE V

## SUMMARY OF SHROUDED BLADE RESPONSE TEST DATA

<u>Shroud</u> <u>Normal</u> <u>Load N</u>	<u>Input</u> <u>Accel.</u> <u>g(pk)</u>	<u>Excit.</u> <u>Period</u> <u>ms</u>	<u>ASMT</u> <u>Stress</u> <u>MPa(pk)</u>	<u>Loss</u> <u>Factor</u> <u><math>\eta</math></u>	<u>Shroud O.O.P.<sup>2</sup></u> <u>Acceleration g</u>		<u>Shroud I.P.<sup>3</sup></u> <u>Acceleration, g</u>	
					<u>Unfilt<sup>4</sup></u>	<u>Filt.</u>	<u>Unfilt</u>	<u>Filt.</u>
First Flap Mode Results								
150	0.5	3.566	41	.0034	2.5	2.5	1.8	1.2
	1.0	3.574	54	.0038	2.9	2.9	2.7	1.8
	2.0	3.589	59	.0056	3.6	3.6		
	3.0	3.589	60	.0054				
	4.0	3.579	63	.0053				
300	0.5	3.563	61	.0024	3.8	3.8	1.7	1.6
	1.0	3.566	103	.0023	7.2	7.0	2.1	1.7
	2.0	3.574	124	.0036	8.8	8.8	4.0	3.2
	3.0	3.575	128	.0044	9.6	9.1	5.2	2.6
	4.0	3.580	134	.0036	10.0	7.6	9.0	3.6
500	0.25	3.558	39	.0031				
	0.5	3.551	56	.0026	4.0	4.0		
	0.5	3.558	60	.0024			1.5	1.4
	1.0	3.556	102	.0027	6.8	6.8		
	1.0	3.559	124	.0022				
	2.0	3.560	154	.0034	12.0	11.0		
	2.0	3.564	163	.0031			4.7	3.1
	3.0	3.562	178	.0031	13.0	11.0		
	3.1	3.566	182	.0034			8.2	
	4.0	3.565	186	.0031	14.0	14.0		
	4.0	3.565	195	.0032				
First Torsion Mode Results								
150	0.5	0.8932	5.5	.00052	2.6	2.1	2.0	1.8
	1.0	0.8940	9.2		3.8	3.6	3.0	2.7
	2.0	0.8944	12.0	.00080	5.6	5.0	1.3	0.9
300	0.5	0.8932	6.1	.00058	3.4	3.4	0.9	0.8
	1.0	0.8935	11.0	.00055	5.8	5.2	2.4	1.2
	2.0	0.8933	15.0	.00075	4.0	3.6	3.0	1.3
	3.0	0.8940	20.0	.00082	14.0	9.9	9.9	3.5
500	0.5	0.8910	7.7	.00040	4.4	3.8	1.5	1.4
	1.0	0.8912	13.0	.00045	6.2	6.2	1.9	1.7
	2.0	0.8918	17.0	.00059	8.4	8.4	3.8	3.0
	3.0	0.8924	23.0	.00074		11.0	3.2	3.1
	4.0	0.8933	28.0	.00084	14.0	13.0	3.2	1.8

- Notes: 1. Slope of decay taken between the 1 and 4dB points  
2. O.O.P = Out of plane (normal to shroud plane)  
3. I.P = In plane (normal to shroud plane)  
4. Low pass filter

TABLE VI

## SUMMARY OF FRICTION TEST RESULTS

Input Accel g	Input Freq. Hz	Relative Disp. mm(pk-pk)	Maximum Velocity mm/sec(pk)	Normal Load N	Work Done Per Cycle mJ	Equivalent Friction Coefficient
1.7	80	0.132	33.2	271	14.6	0.407
1.7	80	0.132	33.2	494	22.3	0.341
1.7	80	0.132	33.2	672	28.1	0.317
3.0	140	0.076	33.5	271	10.7	0.517
3.0	140	0.076	33.5	494	15.7	0.417
3.0	140	0.076	33.5	672	18.9	0.370
5.0	140	0.127	55.9	271	17.5	0.509
5.0	140	0.127	55.9	494	27.2	0.434
5.0	140	0.127	55.9	672	33.7	0.395
10.0	280	0.064	55.9	271	7.7	0.445
10.0	280	0.064	55.9	494	11.5	0.378
10.0	280	0.064	55.9	672	14.0	0.329
20.0	280	0.127	112	271	16.6	0.482
20.0	280	0.127	112	494	24.4	0.390
20.0	280	0.127	112	672	30.4	0.357
20.0	420	0.056	73.7	271	7.4	0.487
20.0	420	0.056	73.7	494	10.6	0.382
20.0	420	0.056	73.7	672	13.1	0.345

TABLE VII

## SUMMARY OF TURBINE BLADE RESPONSE TEST RESULTS

<u>Input Level g(pk)</u>	<u>Input Frequency Hz</u>	<u>Shank Stress MPa(pk)</u>	<u>Root Stress MPa(pk)</u>
0.06	515.498	34	25
0.10	515.328	53	42
0.20	515.291	97	79
0.30	515.286	133	108
0.40	515.129	139	110
0.50	515.132	181	146
0.60	515.137	197	158
0.70	515.137	209	169
0.79	515.145	220	179
0.9	515.002	236	191

TABLE VIII

## SUMMARY OF TURBINE BLADE PLATFORM DAMPING TEST RESULTS ("SMALL DAMPER")

Normal Load N	Input Level g(pk)	Input Frequency Hz	Shank Stress MPa(pk)	Root Stress MPa(pk)	Normal Load N	Input Level g(pk)	Input Frequency Hz	Shank Stress MPa(pk)	Root Stress MPa(pk)
1.65	0.29	515.892	41	30	26.4	3.9	516.025	44	37
	0.40	515.573	109	88		4.1	515.868	259	204
	0.50	515.591	136	111	33	3.0	515.198	12	-
	0.60	515.467	149	120		4.0	516.377	26	22
	0.70	515.331	164	135		5.0	516.649	88	67
	0.80	515.374	178	138		6.0	516.646	> 300	> 300
	1.0	515.294	193	157					
3.3	0.55	515.969	99	79	88.9	1	562.212	18	19
	0.70	515.498	153	123		2	561.325	29	30
	0.85	515.464	168	137		3	558.438	39	41
	1.0	515.315	194	157		4	560.601	38	40
						5	561.558	38	40
4.9	0.70	515.921	72	-	6	563.304	38	40	
	0.77	516.396	66	47	7	566.640	35	36	
	0.85	515.871	135	112	8	568.971	33	34	
					8	515.039	47	40	
	1.0	515.565	175	152	9	515.464	55	47	
6.6	1.1	515.783	129	101	9	577.247	26	31	
	1.5	515.778	200	160	10	575.530	29	33	
					10	515.198	56	50	
13.2	1.8	515.823	7	-					
	2.0	515.879	215	182					
19.8	2.6	515.464	7	7	178	2	565.576	20	25
	2.8	515.464	12	10		4	559.059	45	52
	3.0	515.703	210	182		4	565.323	65	73
						6	558.090	77	85
						8	557.302	85	93
				10	554.416	89	99		

TABLE IX

## SUMMARY OF TURBINE BLADE PLATFORM DAMPING TEST RESULTS ("LARGE" DAMPER)

Normal Load N	Input Level g(pk)	Input Frequency Hz	Shank Stress MPa(pk)	Root Stress MPa(pk)	Normal Load N	Input Level g(pk)	Input Frequency Hz	Shank Stress MPa(pk)	Root Stress MPa(pk)			
1.65	-0.255	517.786	39	28	19.8	2.1	516.486	20	ND			
	0.28	516.028	41	30		2.2	516.134	160				
	-0.30	515.903	73	60		2.3	516.129	215				
	0.315	515.730	79	63		26.4	2.8	ND		11		
	-0.34	515.735	83	69				3.0		516.145	18	
	0.36	515.730	96	77				3.2		515.951	243	
	-0.40	515.663	108	88				88.9		2	557.072	17
	-0.45	515.695	119	94						3	540.003	22
	-0.51	515.453	140	114						4	524.084	24
	0.55	515.419	155	125						5	510.618	28
	0.60	515.382	144	118		6	511.546	35		21		
	0.65	515.347	154	118		7	511.339	36		ND		
	0.70	515.305	154	123		8	507.261	47		38		
	0.80	515.315	173	137		9	515.265	>300		ND		
3.3	0.45	516.630	42	ND	10	516.156	>300	ND				
	0.55	516.332	73	ND	178	2	584.669	23	28			
	0.70	515.573	143	116		3	581.727	40	ND			
6.6	0.85	515.959	113	ND		4	580.649	47	ND			
	0.90	515.919	126	ND	5	574.511	44	ND				
	1.0	515.969	147		6	574.511	52	61				
	9.9	0.9	516.140		79	7	574.260	52	59			
1.1		516.165	140		8	ND	50	57				
1.3		516.134	164	10	574.548	56	61					
13.2	1.5	516.097	93-124	ND	178	2	584.669	23	28			
	1.9	516.129	195			3	581.727	40	ND			

TABLE B-1

TEST COMPONENTS AND OTHER HARDWARE DESIGNED  
AND FABRICATED FOR THE TEST PROGRAM

Item No.	<u>Item Description</u>	<u>Design and Fabrication Refs.</u> <u>Drawing Nos/Engineering Order Nos.</u>	<u>Section Ref.</u>
I	Material Constants Determination		3.3.1
	1. Test Piece (Uniform Cantilever Beam)	EOI513005	
	2. Adapter Clamp	EOI513003&4	
	3. Steel Root Block	As For Item V-2	
	4. Vacuum Chamber	As For Item III-2	
II	Twisted Plate-Centrifuge & Bench Tests		3.3.2
	1. Test Piece (Twisted Plate)	} DRG 1794-1 Parts List 48300 + EOI513000 Unlisted DRG DTD 7-31-79 EOI513007 As For Item V-2 As For Item III-2	
	2. Support Assembly		
	3. Driver Magnet Assembly		
	4. Adapter Clamp		
	5. Steel Root Block		
	6. Vacuum Chamber		
III	Fan Blade-Evacuated & Thermal Tests		
	1. Test Piece (Blade Welded in Titanium - Root Block)	} (Blade Furnished by P&WA) DRG1794-2 Parts List 48466	3.3.3
	2. Vacuum Chamber		
	3. Thermal Lid		
IV	Shrouded Fan Blade Tests		5.2.1
	1. Test Piece (Fan Blade Welded at Root)	} (Blade Furnished by P&WA) DRG1794-2 Parts List 48466	
	2. Load Platens		
	3. Vacuum Chamber		
	4. Load Mechanism Assembly		
V	Root Damping Tests		4.2.1
	1. Test Piece (Fan Blade)	} (Blade Furnished by P&WA) DRG1794-2 Parts List 48466 + EOI513009	
	2. Steel Root Block		
	3. Root Attachment Assembly		
	4. Load Measurement Bolts		
VI	Platform Damping Tests		6.2.1
	1. Test Piece (Turbine Blade)	} (Blade Furnished by P&WA) DRG1794-3 Parts List 48595	
	2. Fixture-Root Clamp and Base Plate		
	3. Loading Arm Includes Damper (2 Made)		
VII	Composite Beam Damping		3.3.4
	1. Test Piece (Flat Strip-4 Specimens)	Furnished by UTRC S/N 3491A/B&3492A/B	
	2. Adapter Clamp	Unlisted DRG	
	3. Steel Root Block	As For Item V-2	
	4. Vacuum Chamber	As For Item III-2	
VIII	Blade Coating Investigation		3.3.5
	1. Test Piece (Turbine Blade)	As For Item VI-1 Stripped & Coated	
	2. Fixture	As For Item VI-2	
IX	Friction Evaluation Tests		5.3.1
	1. Test Piece (1 Pair Load Platens)	As For Item IV-2	
	2. Fixture Assembly	EOI513017 thru 021	
	3. Load Measurement Bolts	As For Item V-4	

TABLE B-2

## EQUIPMENT USED IN TEST PROGRAM

<u>Item No.</u>	<u>Equipment</u>	<u>Model or Type No.</u>	<u>Serial No.</u>	<u>Manufacturer</u>
Environmental, Load and Input Excitation Equipment				
1	Electro-Dynamic Vibrator (5300 N)	724	128	L.D.S
2	Power Amplifier 2 kW (used with Item 1)	MPA 2	139	L.D.S
3	Power Amplifier 400 W	2250 MB		MB Electronics
4	Magnetic Driver 75 W	-	-	Built In-house
5	Centrifuge (1.73 m dia, 3000 rpm)	-	-	UTRC Rig
6	Vacuum Pump	3164 A	-	Kinney
7	Load Bolts (1500 N capacity)	-	-	Built In-house
8	Automatic Vibration Exciter Control	1025	199899	B & K
9	Vibration Meter	DVA	270	L.D.S
10	Dynamic Analyser 50 Hz BW Tracking Filter	SD101B	84	Spectral Dynamics
11	Variable Filter/Amplifier (40 dB)	3322	139	Krohnkite
12	Variac (2)	W5	-	G. R.
13	TC Readout Meter	2165 A	0960046	Fluke
14	Vacuum Gage	FA160	YY10223	Wallace & Tiernan
15	Portable Strain Indicator	P350	2486	Budd
16	Strain Gage Bridge Amplifier	BAM 1B	14194	Vishay Instr.
17	Counter/Timer	1953 A	2195003	Fluke
18	Counter/Timer	5532A	209-00170	H.P.
19	Accelerometers	101	105/106	V.S.S.
20	Strain Gages (on load bolts - Item 7)	EA-06-050-AH-120		MM
21	Thermocouples Chromel/Alumel	-	-	Built In-house
Response Data Collection, Conditioning and Recording Equipment				
22	Accelerometers: Sensitivity 41.8/46.5 pcmb/g	101	105/106	V.S.S.
23	Sensitivity 10 mv/g	M1000	6008	Vibrametrics, Inc.
24	Sensitivity 5 mv/g	2250	N195	Endevco
25	Strain Gages: Miniature Foil Type	EA-05-062-AK-120		MM
26	Miniature Foil Type	EA-06-062-AK-120		MM
27	Mid Temperature Type	FSM-12-35-S6		BLH
28	Vibration Meter	As for Item 9		L.D.S.
29	Signal Conditioner (used with Item 23)	LP15-3	393	Vibrametrics, Inc.
30	Signal Conditioner (used with Item 24)	4416	AB27	Endevco
31	Strain Gage Translators	ED1127-8	128/133	Built In-house
32	Strain Gage Bridge Amplifier	As for item 16		
33	Variable Amplifier Filter	As for Item 11		
34	Log Converter	7562A	1211A01693	H.P.
35	Level Recorder	2305	240896	B & K
36	Digital Voltmeters	8000A	0645437	Fluke
37	Counter/timer	As for items 17 & 18		
38	X-Y Recorder	7035B	1722A13849	H.P.
39	Oscilloscope with camera	533	001791	Tektronix
40	Time Base Unit (used with Item 38)	17108A	938A011.00	H. P.
41	Digital Multimeter	7004A	2878	Systron Donner

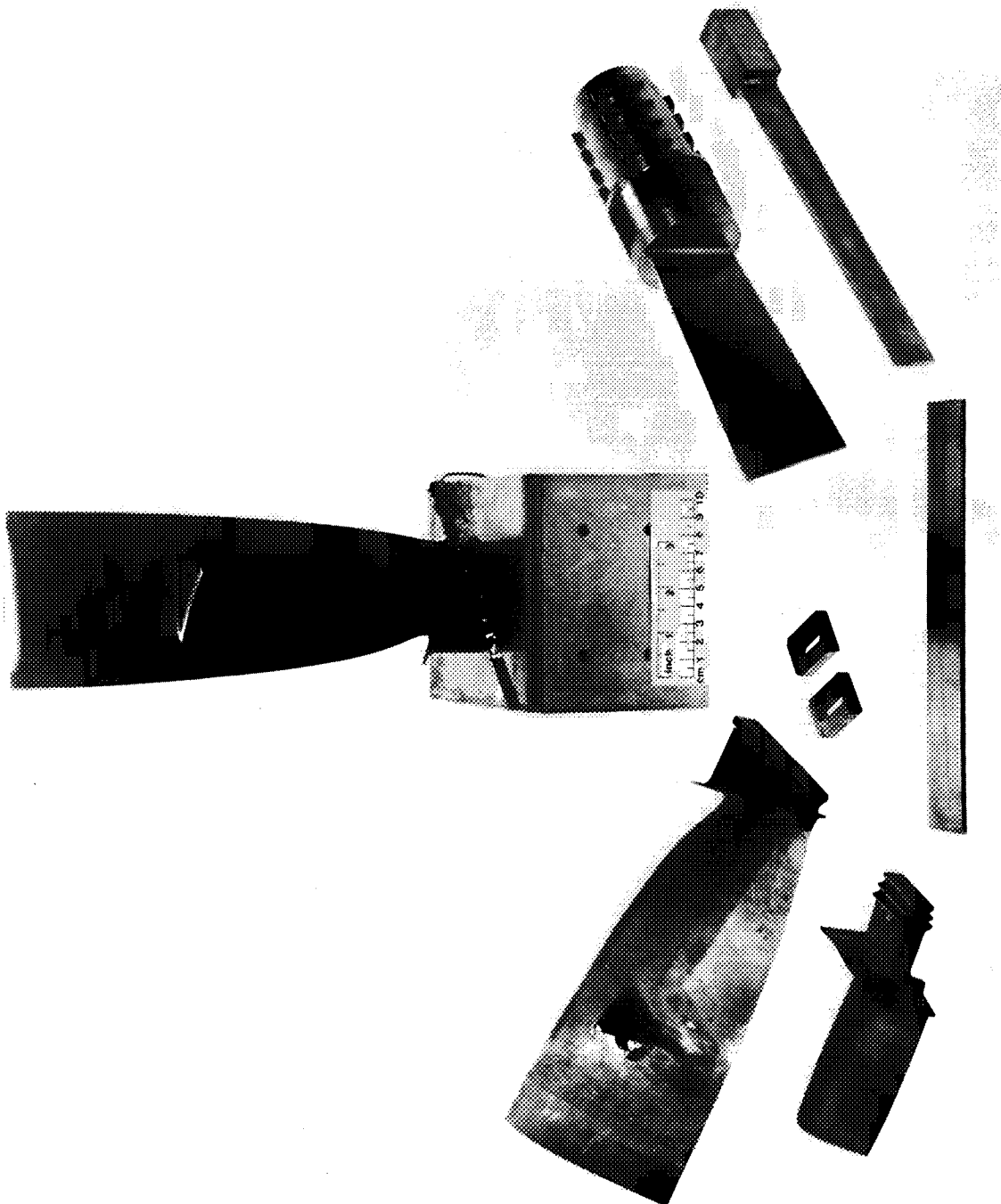


Figure 1 Blades and Other Test Components Used in the Program

ORIGINAL PAGE IS  
OF POOR QUALITY

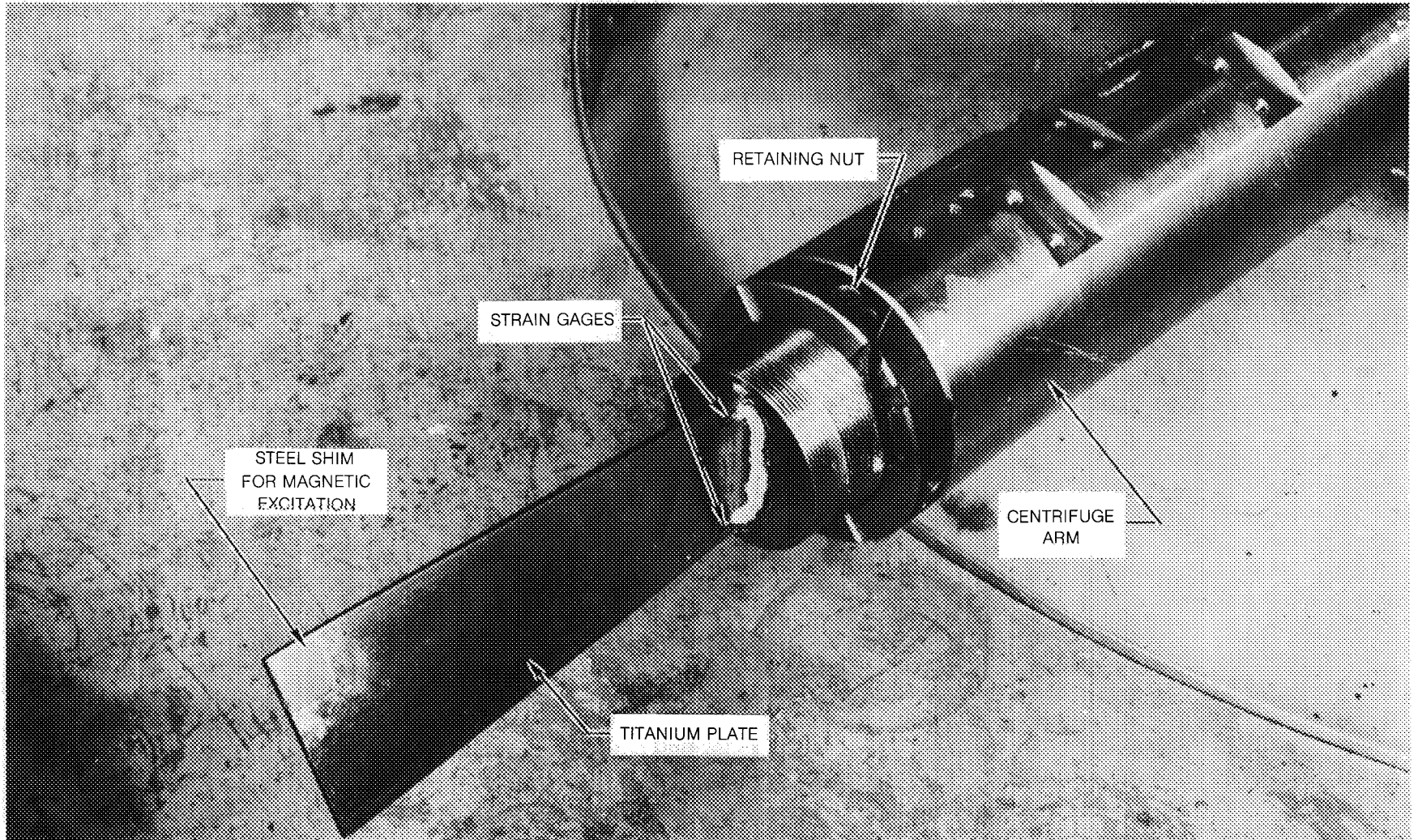
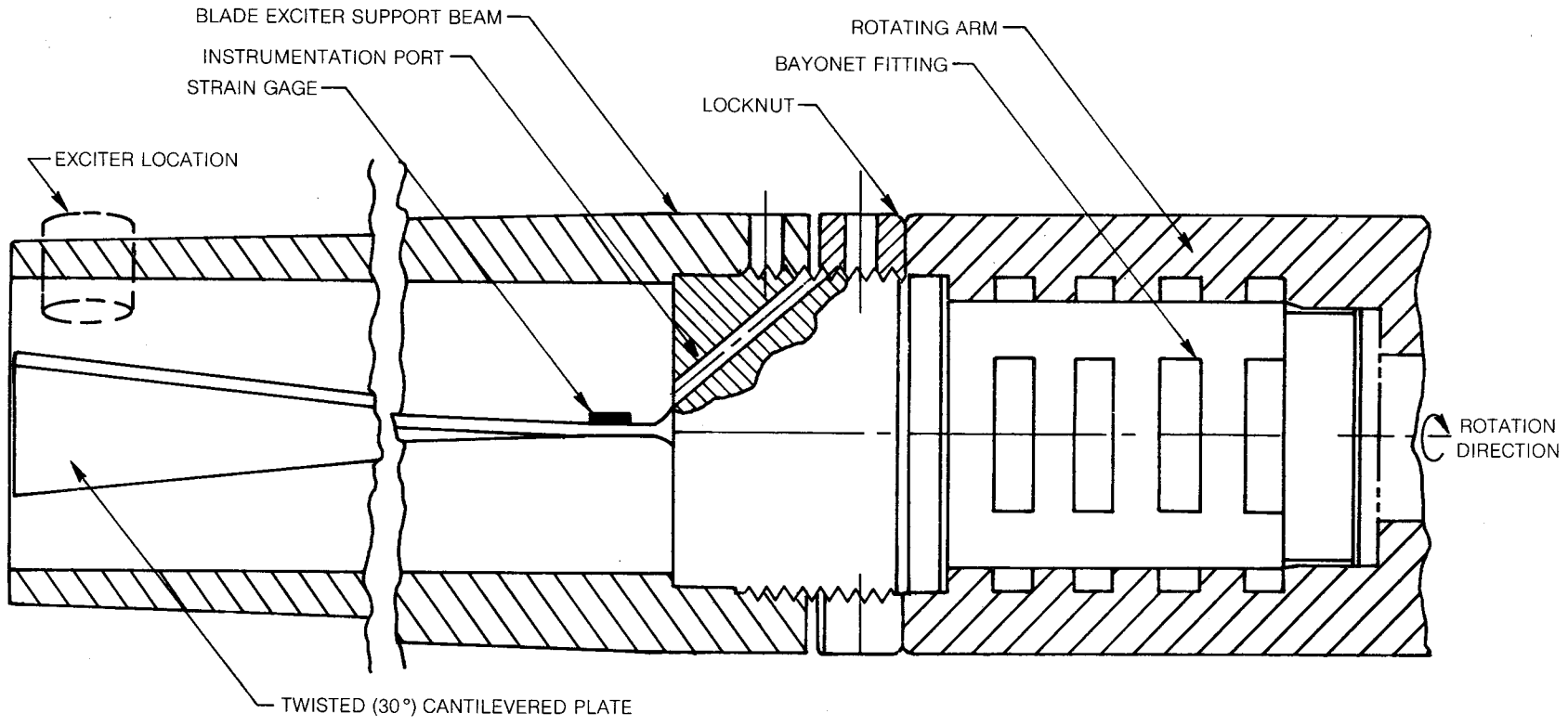


Figure 2. Twisted Plate Mounted on Centrifuge Arm



**Figure 3. Twisted Plate Installation for Centrifugal Test**

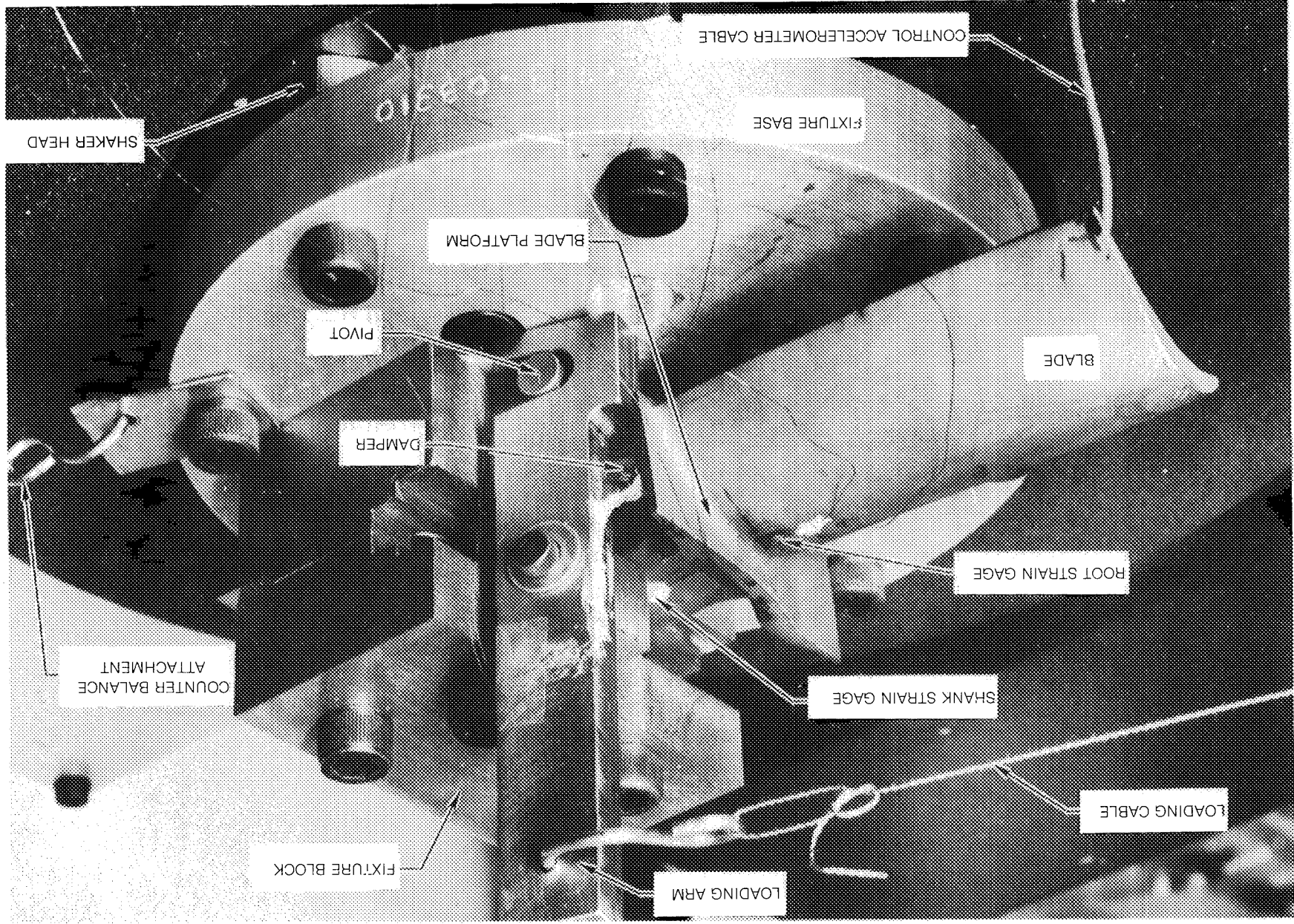


Figure 4. Turbine Blade/Platform Damper Vibration Test Set Up

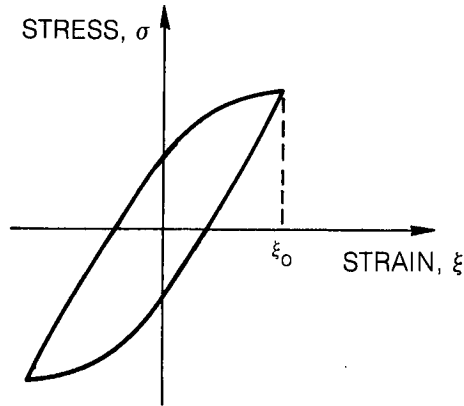


Figure 5. Hysteresis Loop for Material Damping

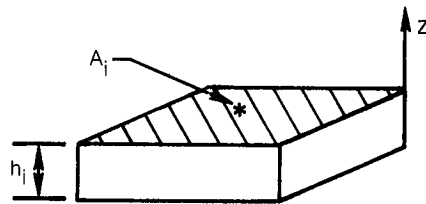


Figure 6a. Typical Blade Element

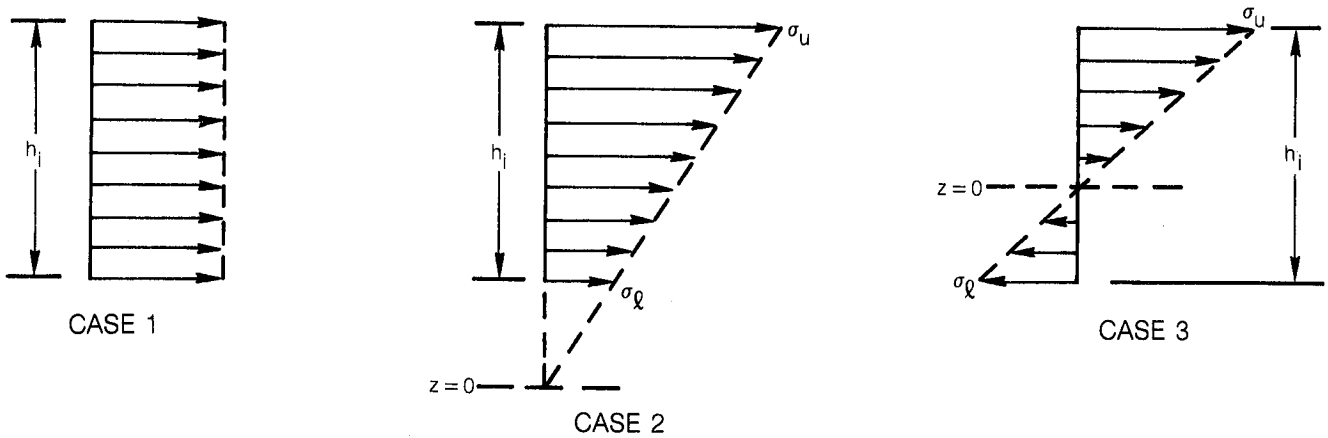
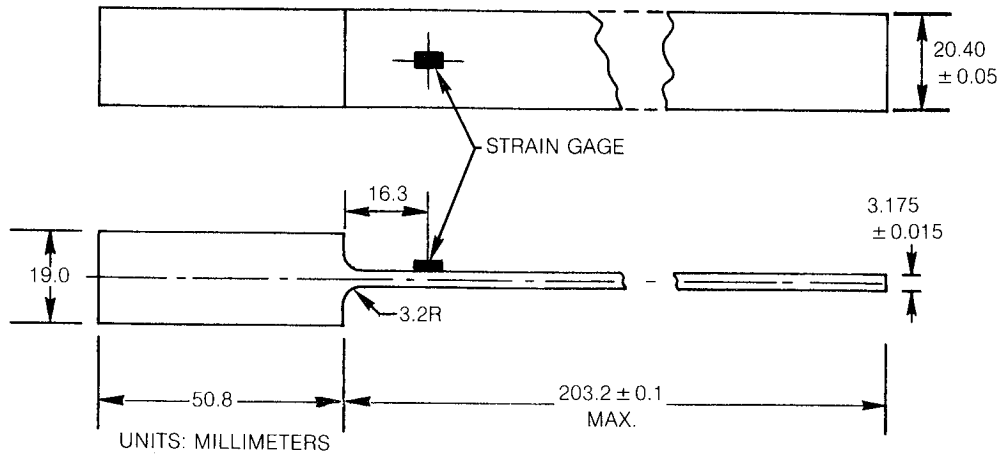
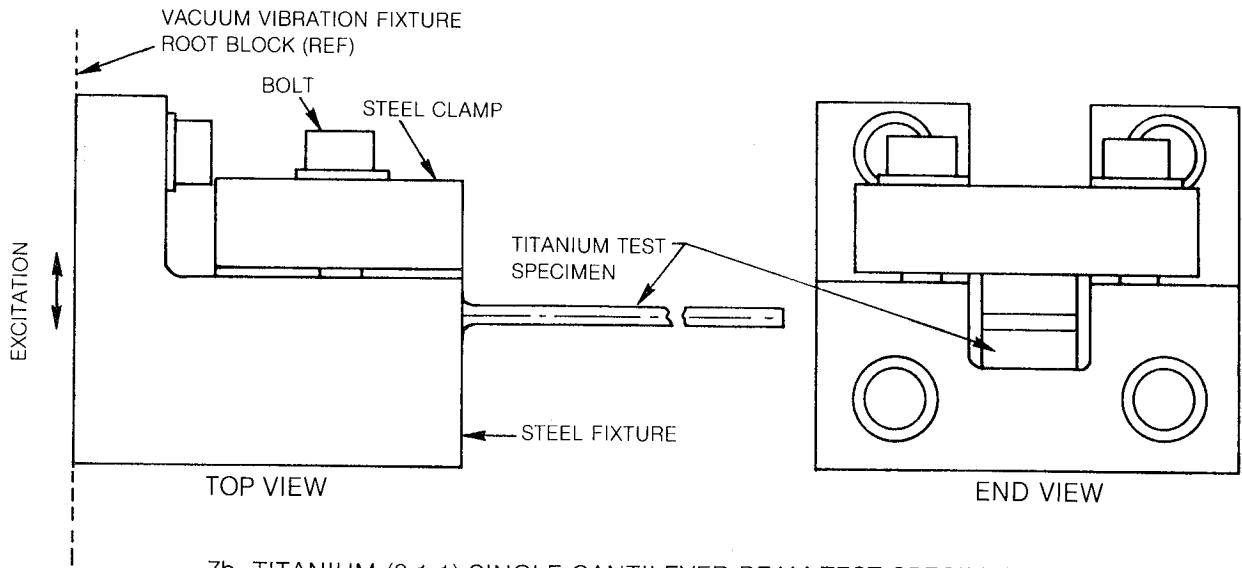


Figure 6b. Stress Distribution Across Element Thickness



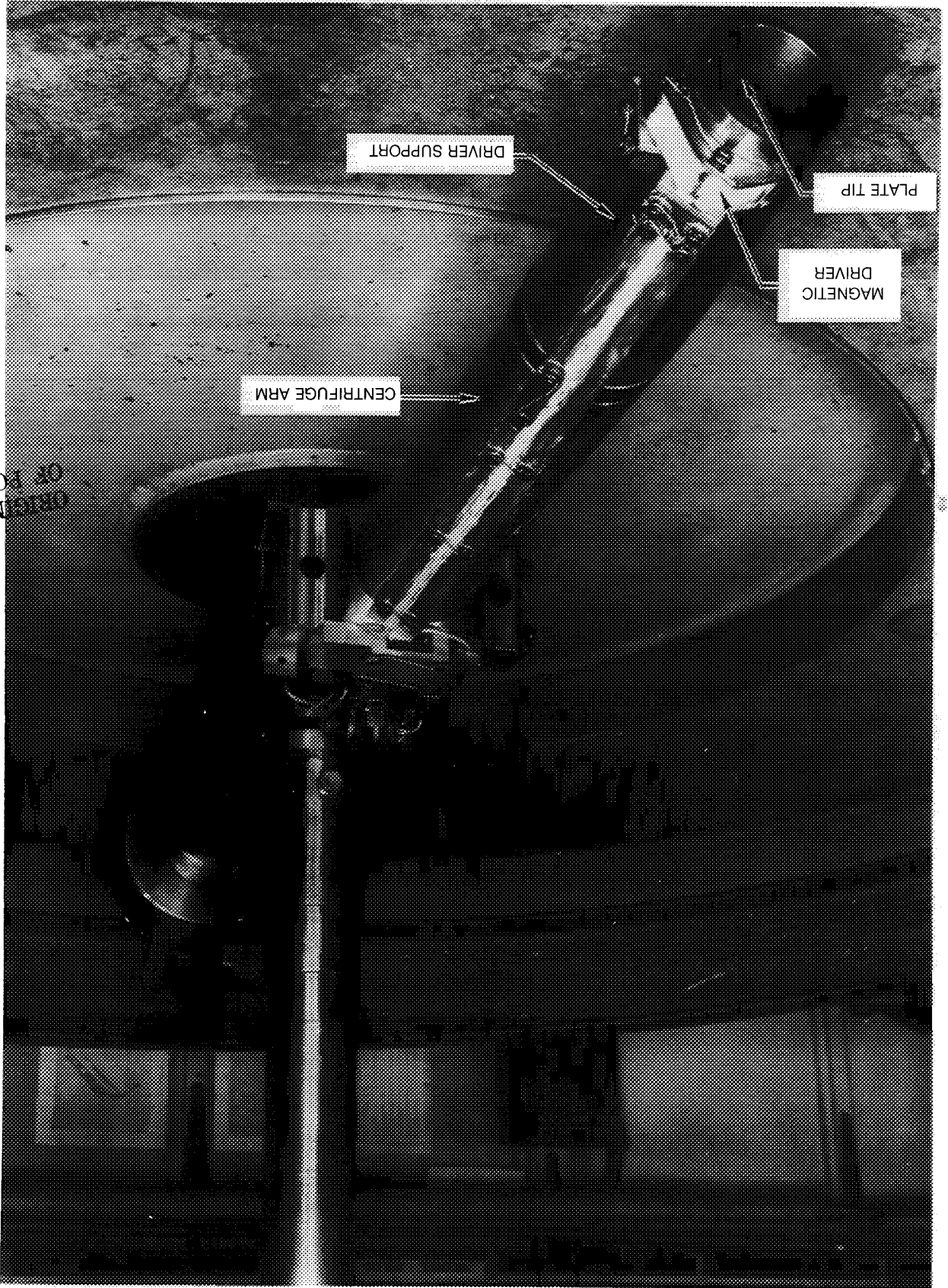
7a. GENERAL ARRANGEMENT OF TEST SET-UP



7b. TITANIUM (8-1-1) SINGLE CANTILEVER BEAM TEST SPECIMEN

**Figure 7. Material Damping Constant Measurement Test Hardware**

Figure 8. Assembly of Centrifugal Test Rig for the Twisted Plate



ORIGINAL PAGE IS  
OF POOR QUALITY

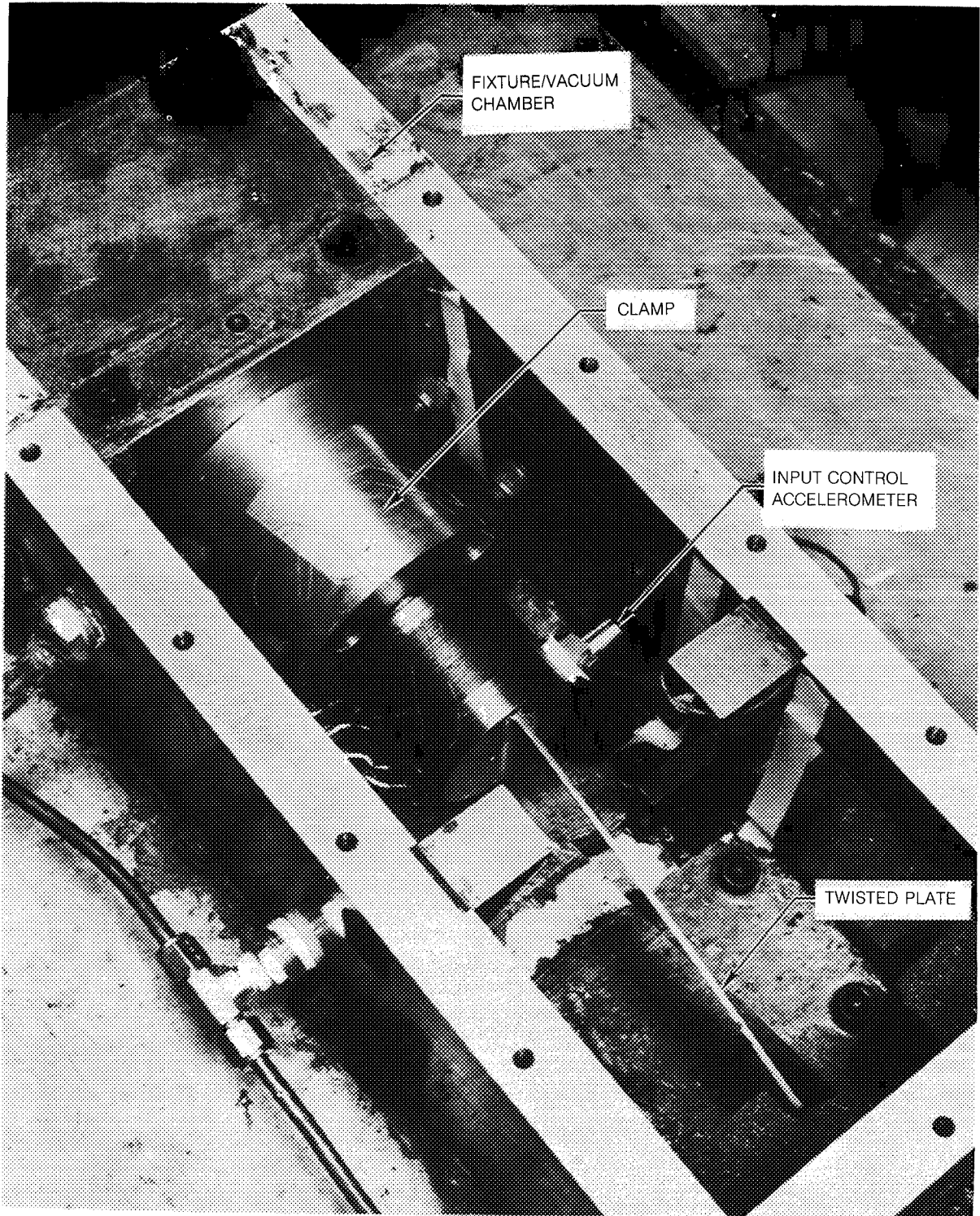


**Figure 9. Twisted Plate Mounted in Bench Test Fixture**

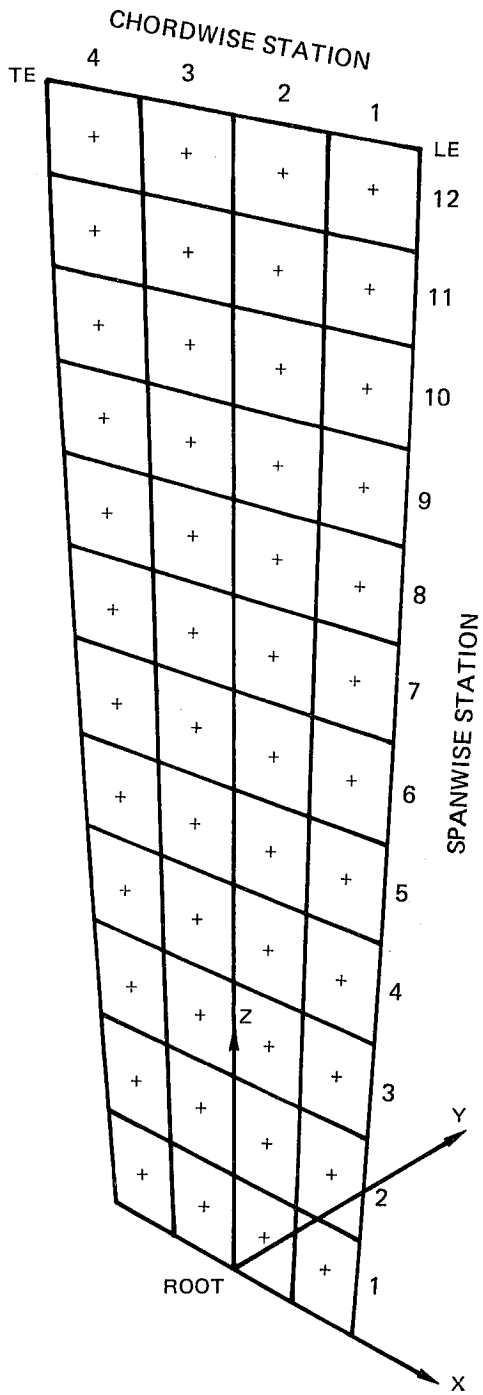
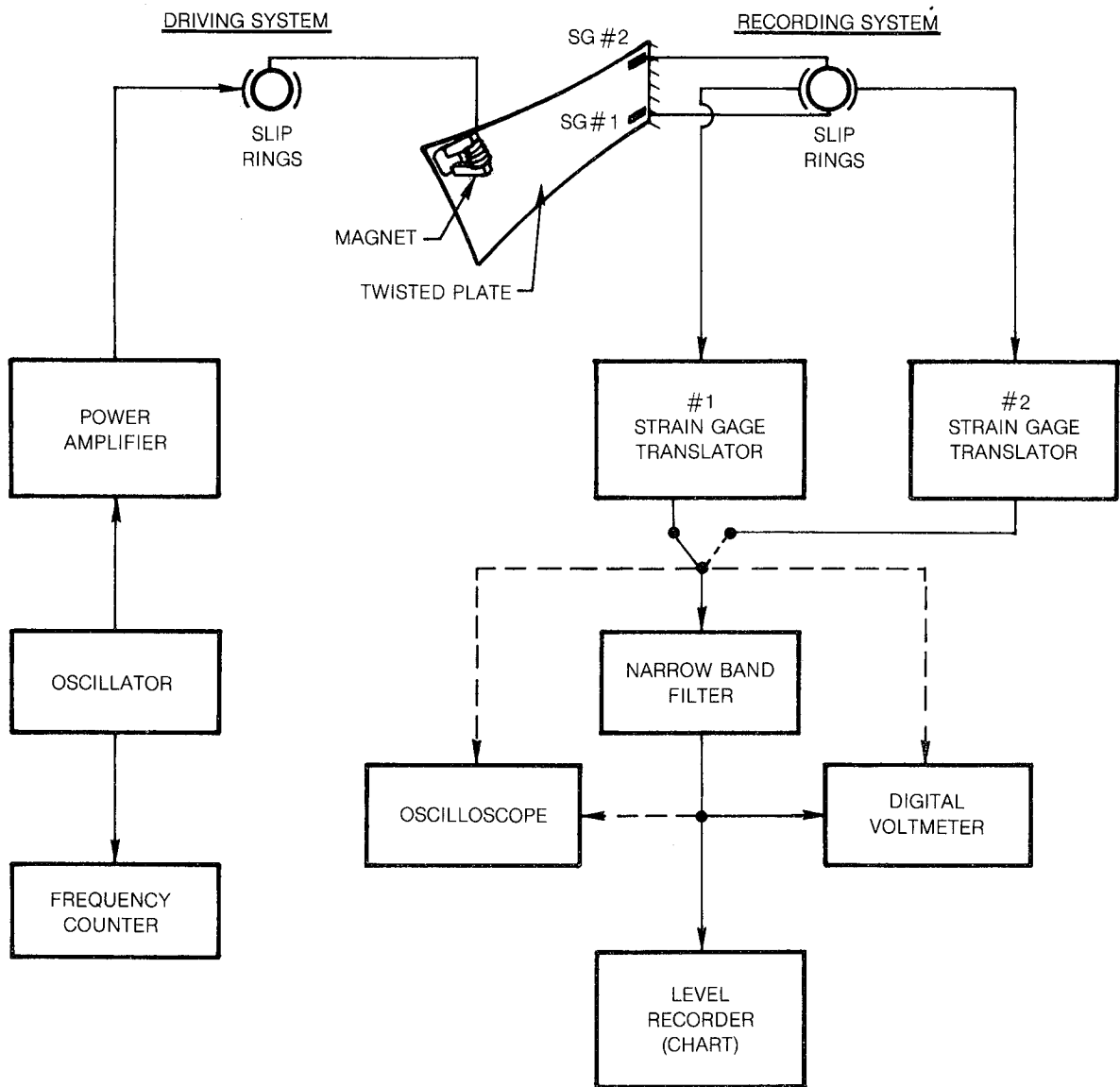
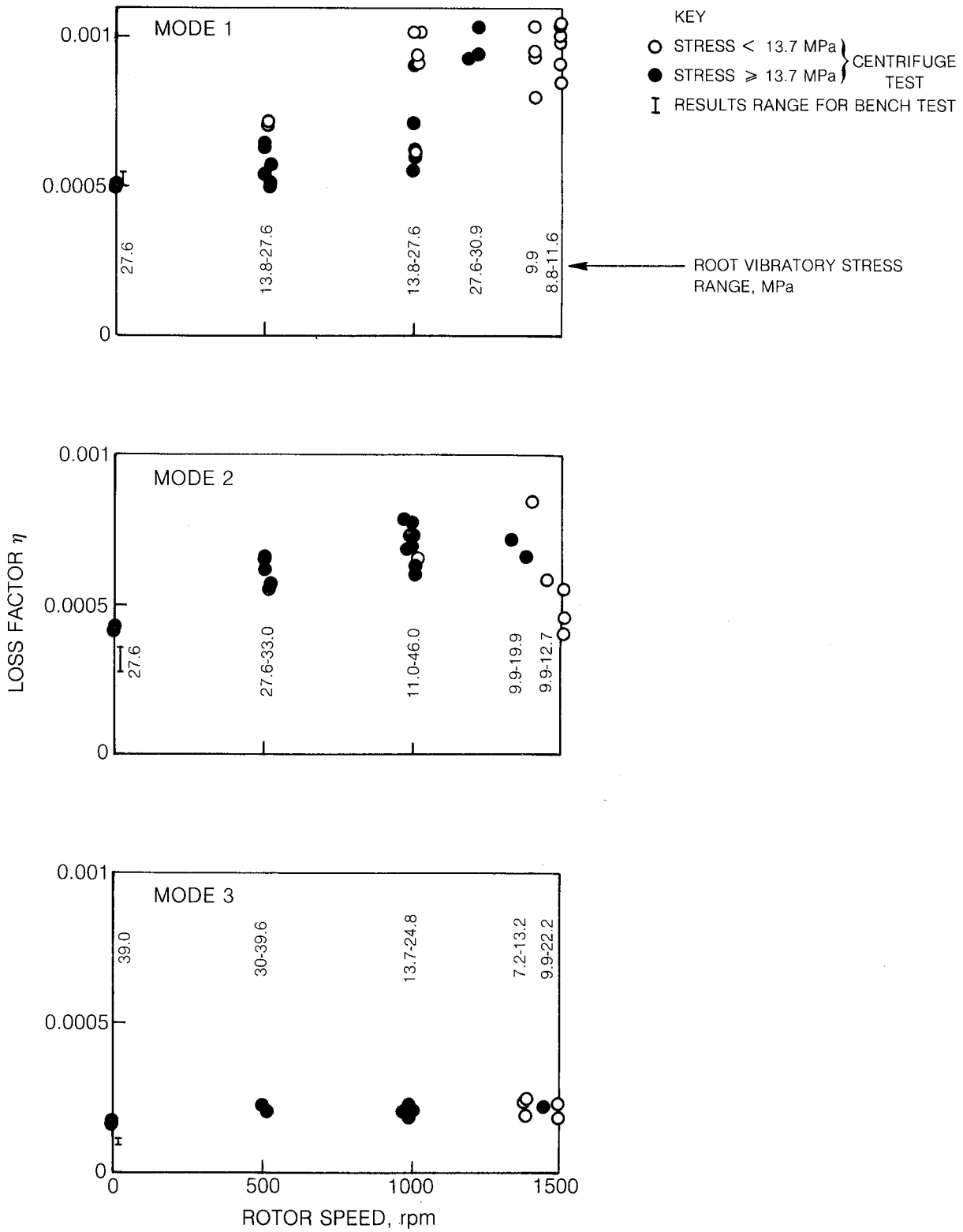


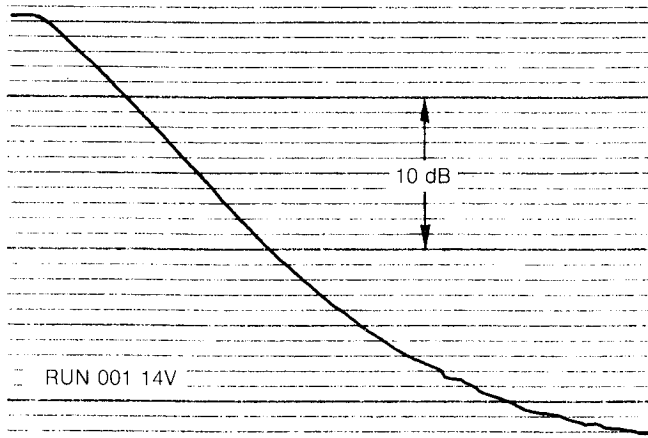
Figure 10. NASTRAN Finite Element Model for the Twisted Plate



**Figure 11. Block Diagram of the Driving and Recording Systems used to Obtain Vibration Decay Data for the Twisted Plate on the Centrifuge**

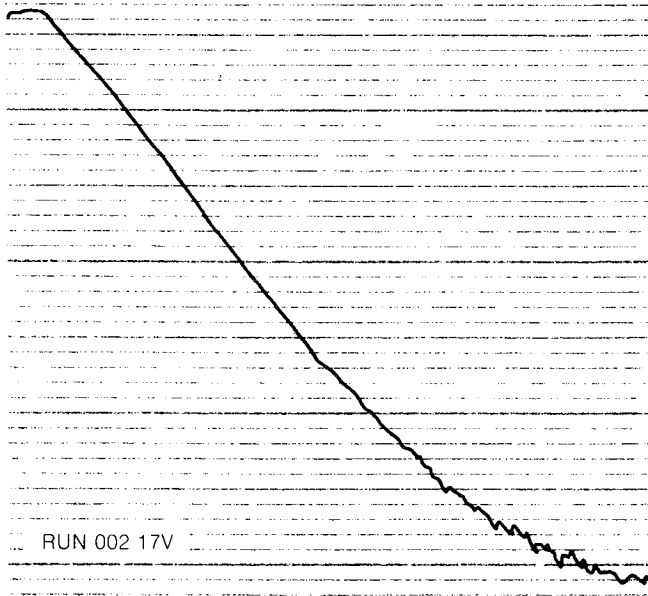


**Figure 12. Variation of Modal Damping (Loss Factor) with Rotational Speed for Titanium Twisted Plate in Partial Vacuum (5 torr)**



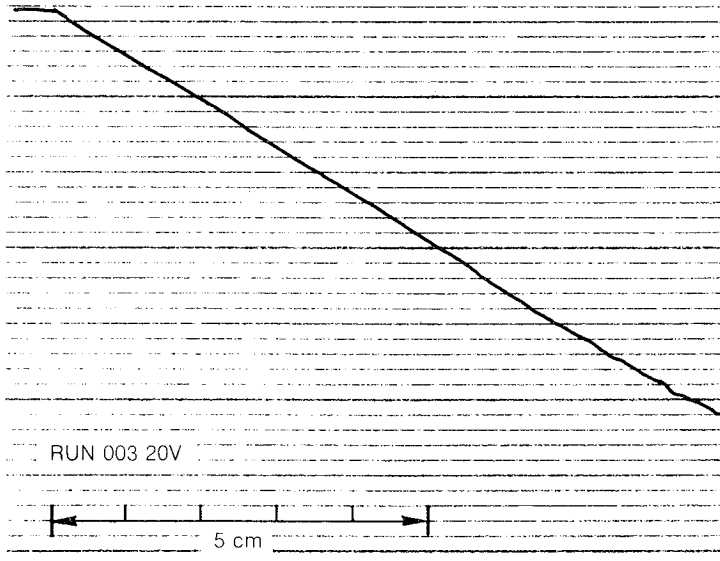
MODE 1 (1F)  
 FREQUENCY = 101.1 Hz  
 MAX STRESS = 27.6 MPa  
 LOSS FACTOR = 0.00049

WRITING SPEED 50 mm/sec  
 PAPER SPEED 3 mm/sec



MODE 2 (2F)  
 FREQUENCY = 550.3 Hz  
 MAX STRESS = 27.6 MPa  
 LOSS FACTOR = 0.00042

WRITING SPEED 200 mm/sec  
 PAPER SPEED 10 mm/sec



MODE 3 (1T)  
 FREQUENCY = 677.2 Hz  
 MAX STRESS = 27.6 MPa  
 LOSS FACTOR = 0.00016

WRITING SPEED 200 mm/sec  
 PAPER SPEED 10 mm/sec

**Figure 13. Decay Characteristics of Twisted Plate Vibrating in Its First Three Modes at Zero Speed in Vacuum**

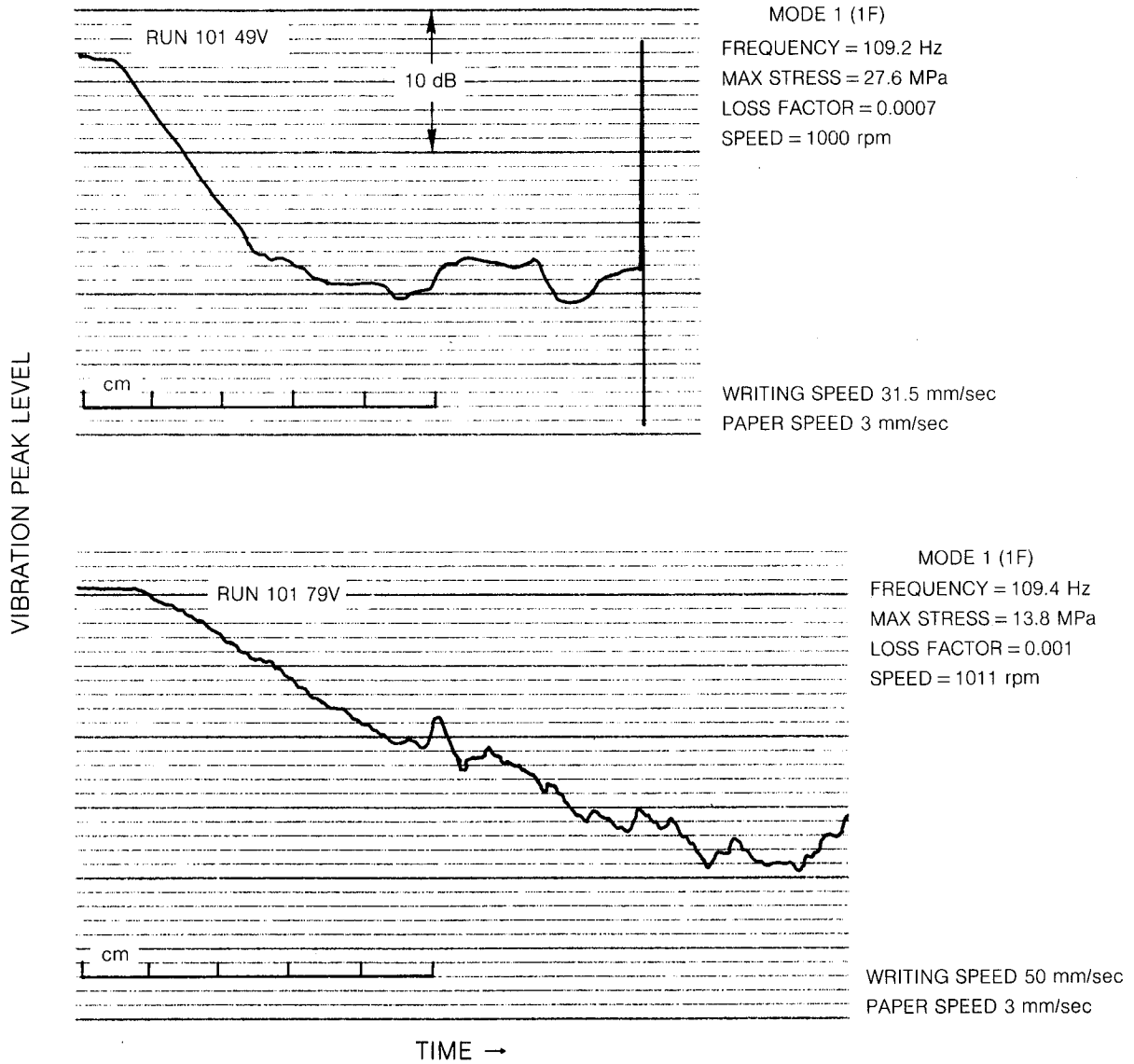


**Figure 14. Decay Characteristics of Twisted Plate Vibrating in Its First Mode at Speed in Vacuum. (Two Samples)**

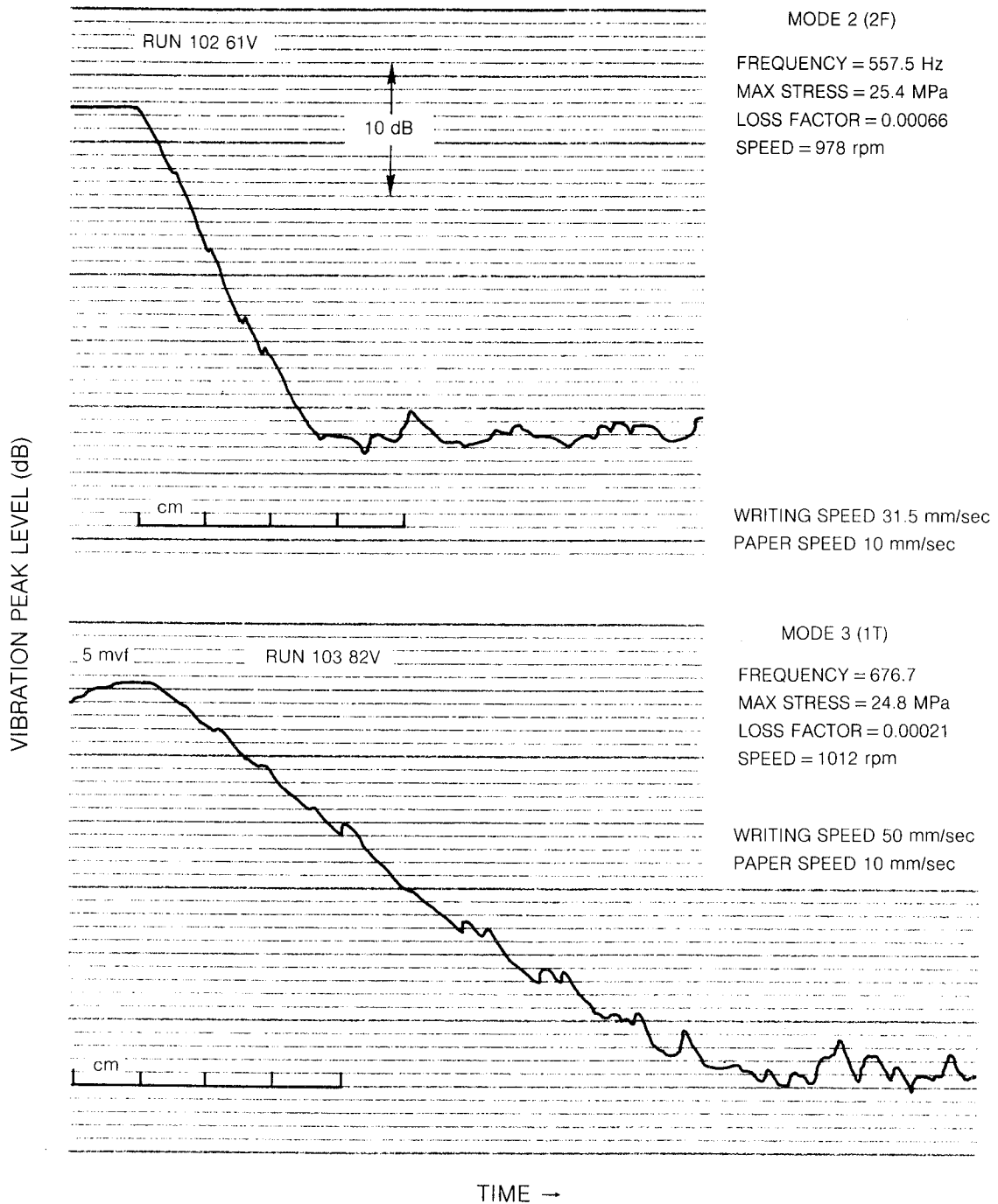


**Figure 15. Decay Characteristics of Twisted Plate Vibrating in Its Second and Third Modes at Speed in Vacuum. (5 torr)**

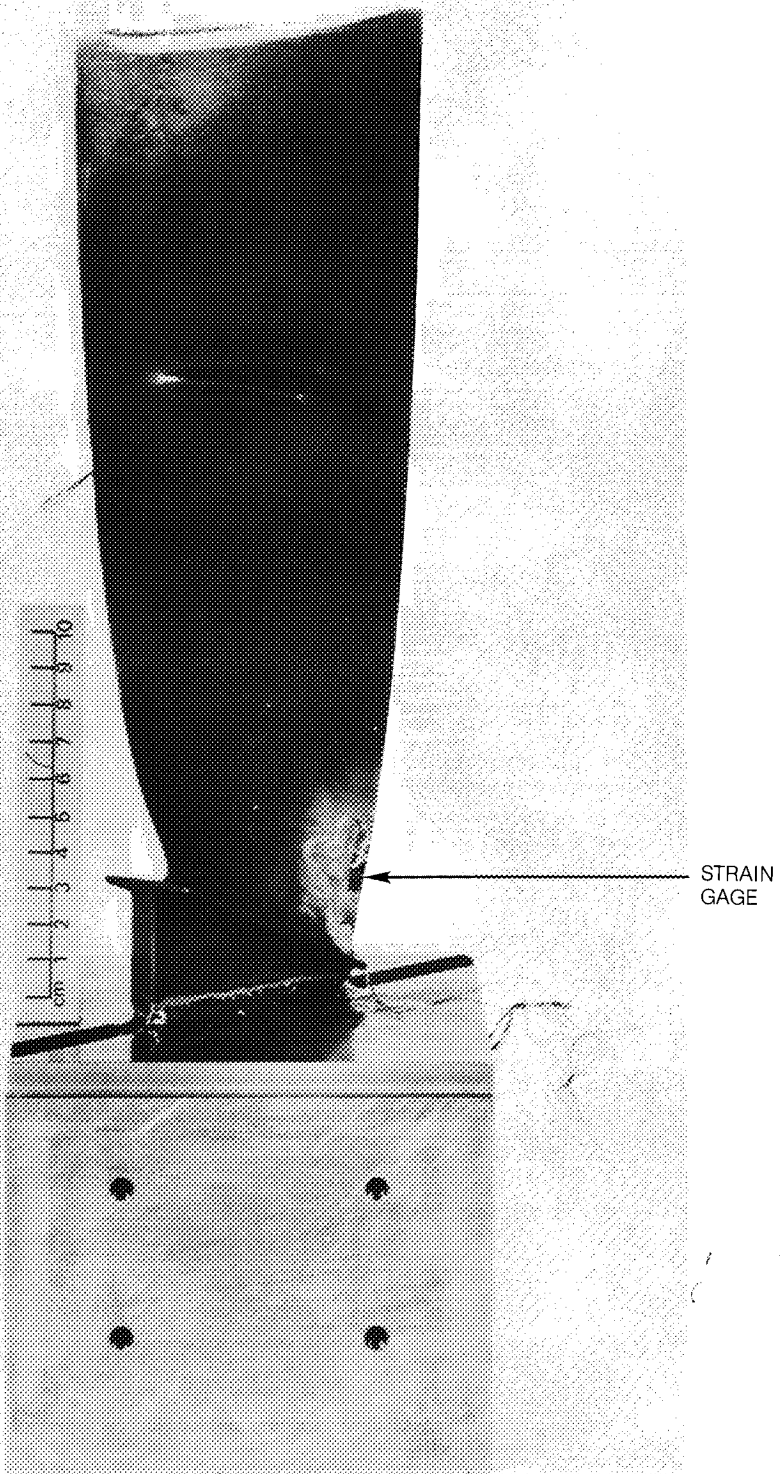


**Figure 16. Instrumented Fan Blade Showing "Root" Strain Gage**

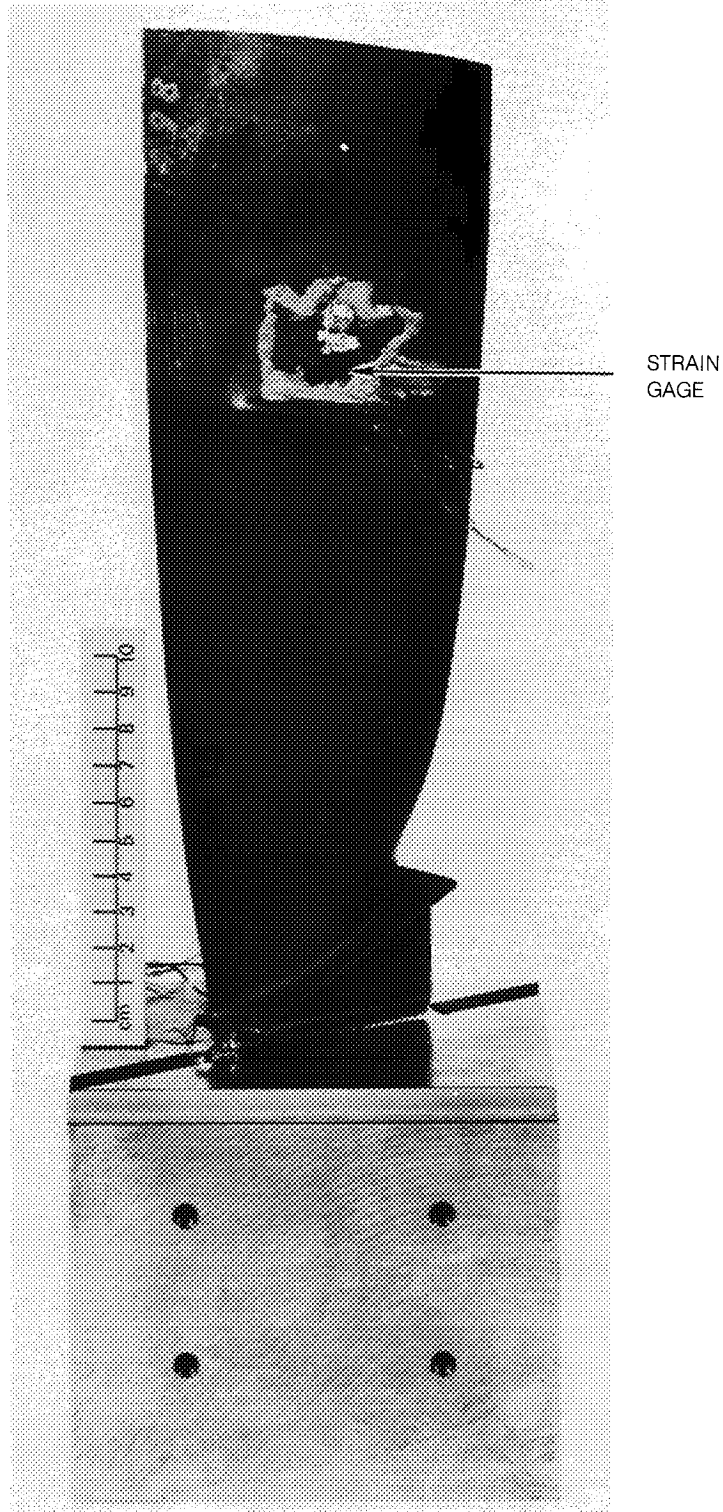


**Figure 17. Instrumented Fan Blade Showing A.S.M.T. Strain Gage**

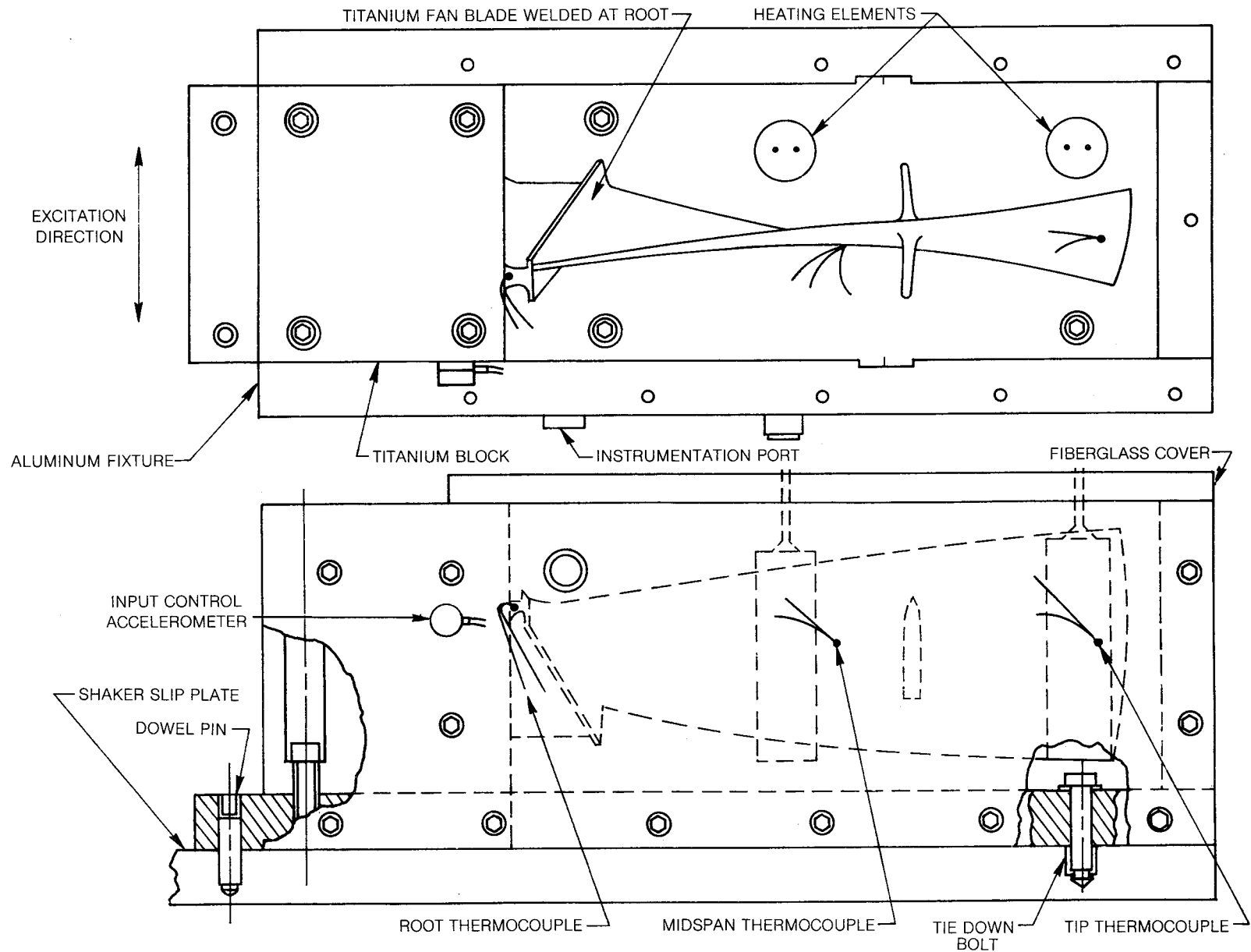
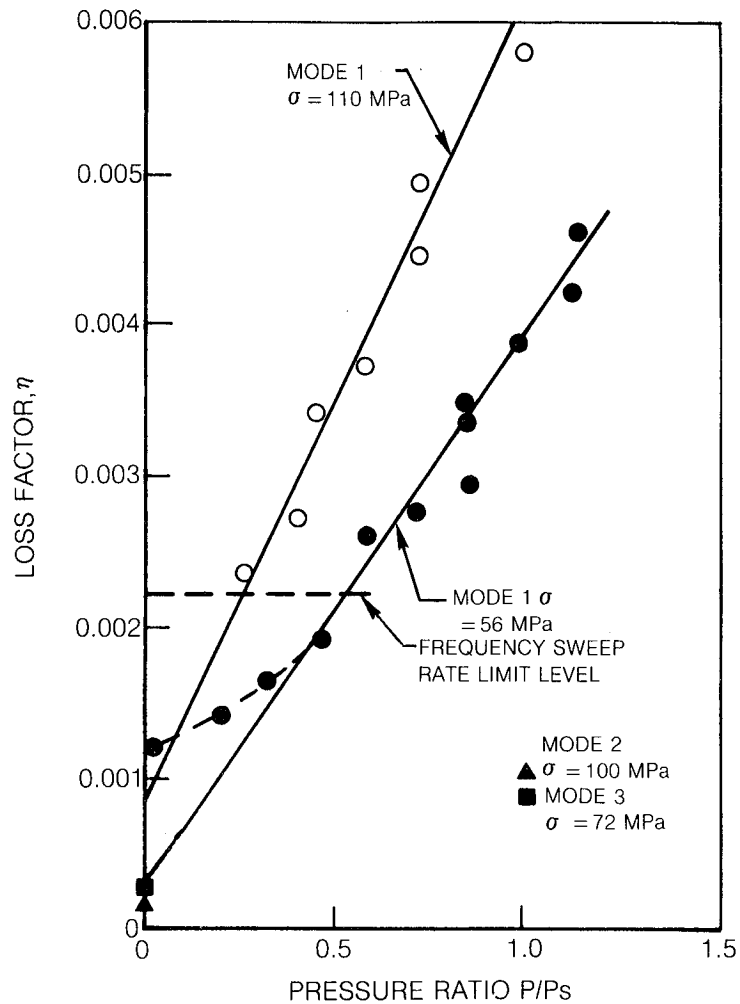
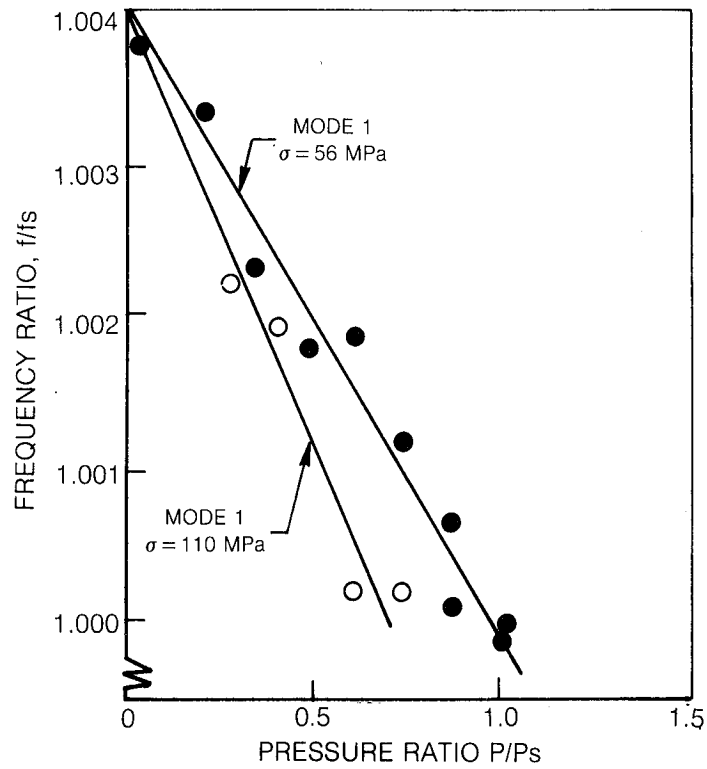


**Figure 18. Test Set-Up for Fan Blade Material Damping Investigation at Elevated Temperatures**



NOTES:  
 $P_s = 760$  TORR  
 $\sigma =$  MAXIMUM OF STRESSES MEASURED AT BLADE ROOT ( $E = 124$  GPa)  
 FREQUENCY SWEEP RATE = MINIMUM AVAILABLE (0.0136 OCTAVE PER MINUTE) ALLOWS  $< 5\%$   
 DEVIATION FROM STEADY STATE FOR  $\eta > 0.0022$

**Figure 19. Variation of Measured Modal Damping with Air Pressure for Fan Blade**



NOTES:

$P_s = 760$  TORR

$f_s = 77.5795$  Hz (MEASURED FREQUENCY AT ATMOSPHERIC PRESSURE, 755 TORR)

$\sigma =$  MAXIMUM STRESS MEASURED AT BLADE ROOT ( $E = 124$  GPa)

**Figure 20. Variation of Measured First Mode Frequency Ratio with Air Pressure for Fan Blade**

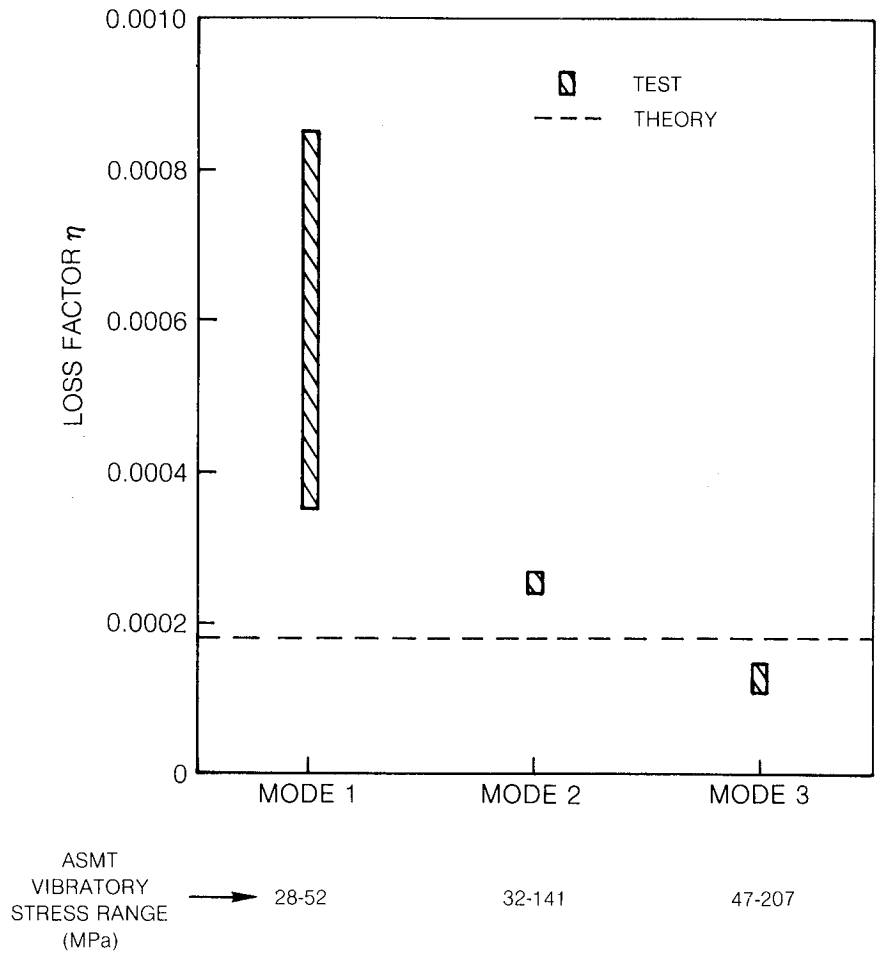


**Figure 21. Material Damping in a Typical Fan Blade**

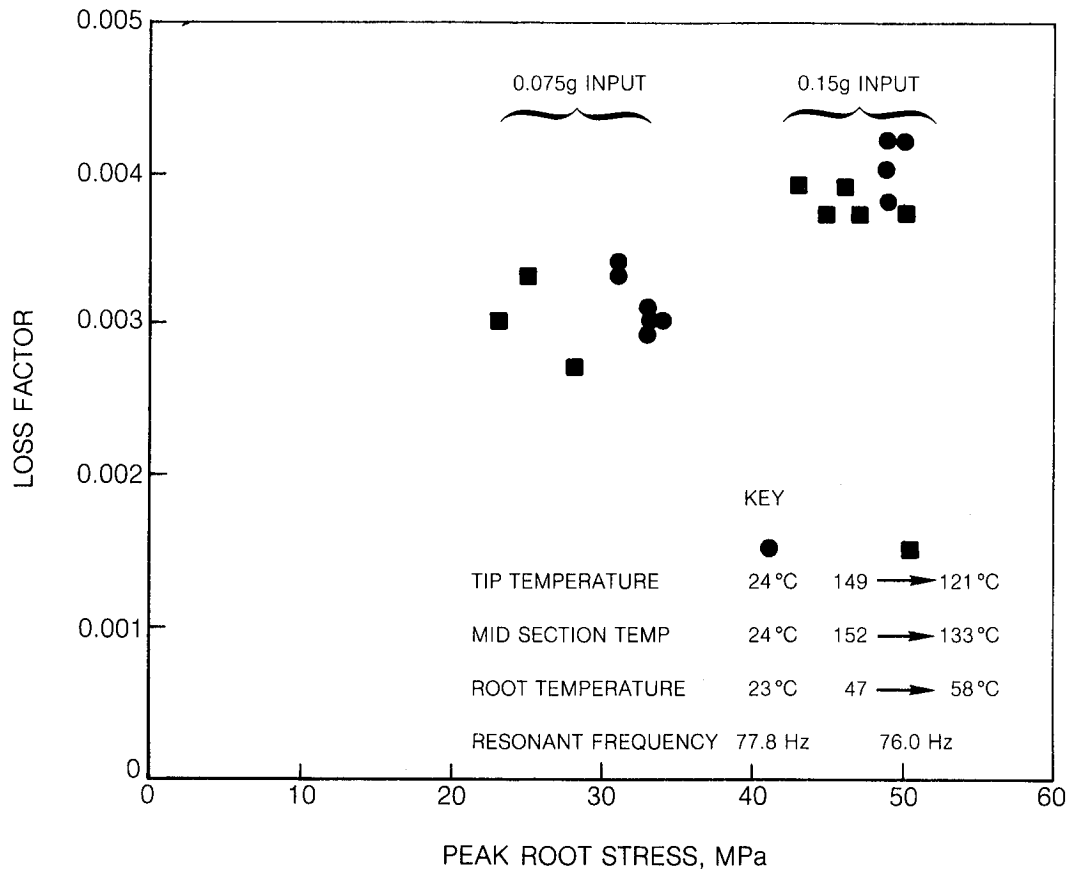


**Figure 22. Variation of Loss Factor with Root Stress and Soak Temperature**

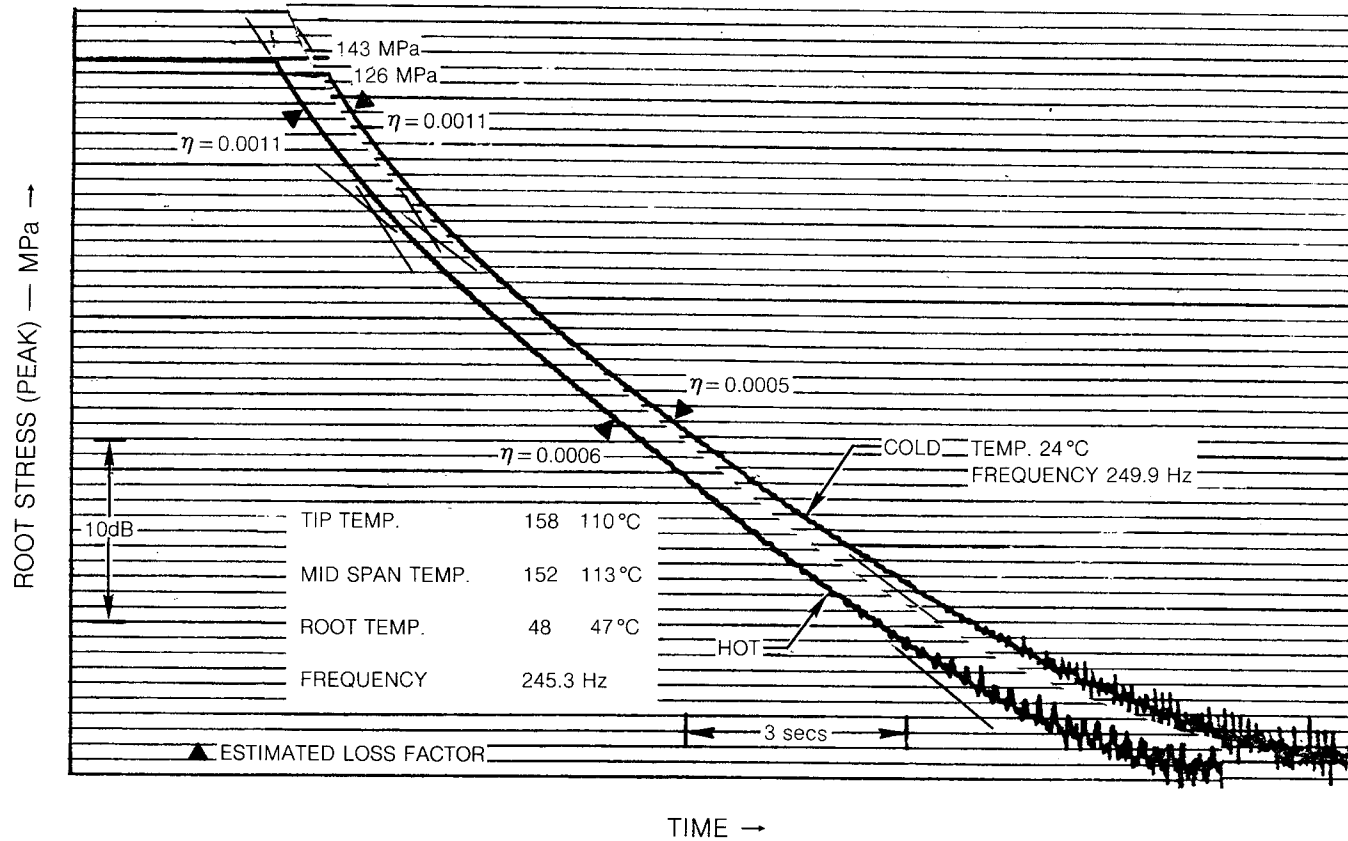
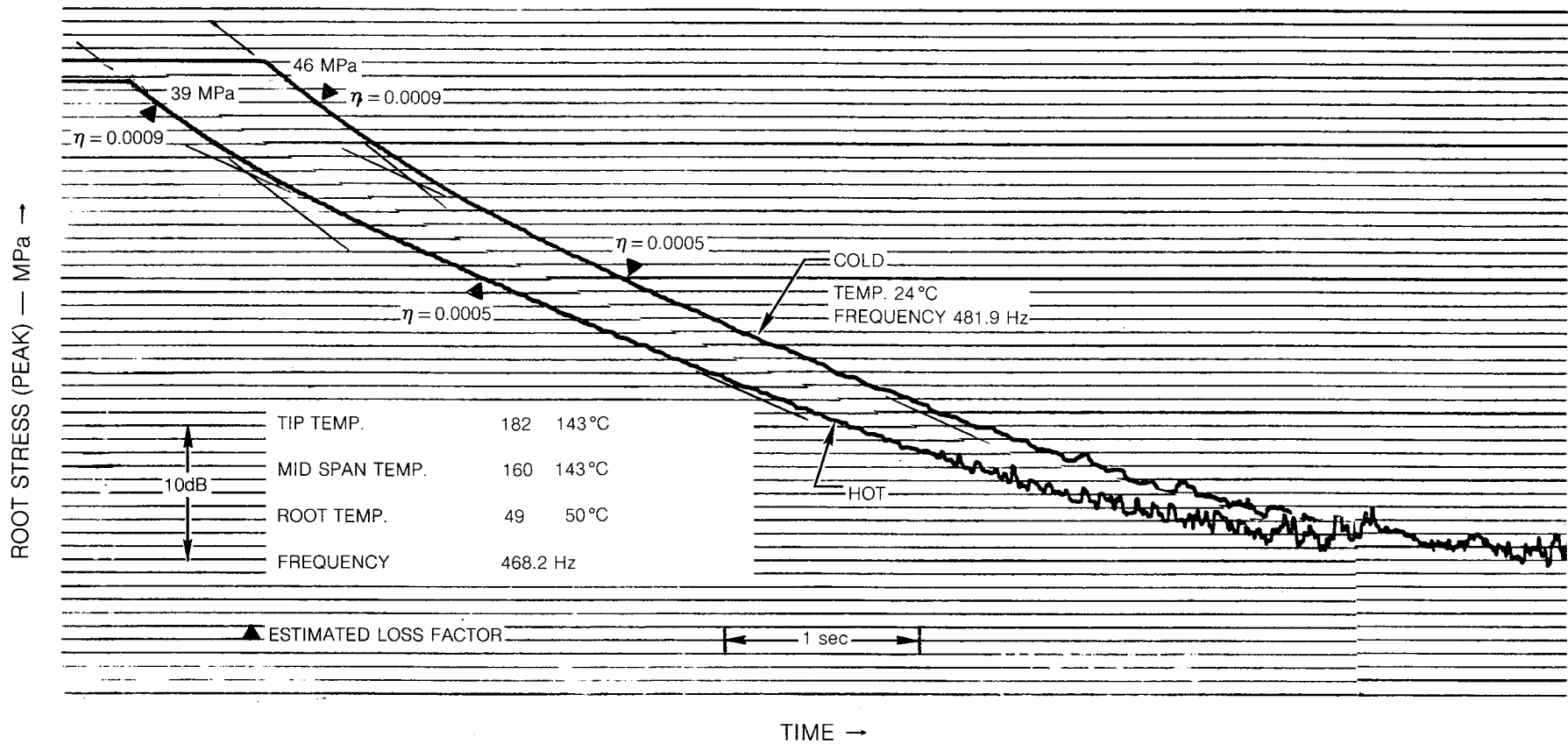
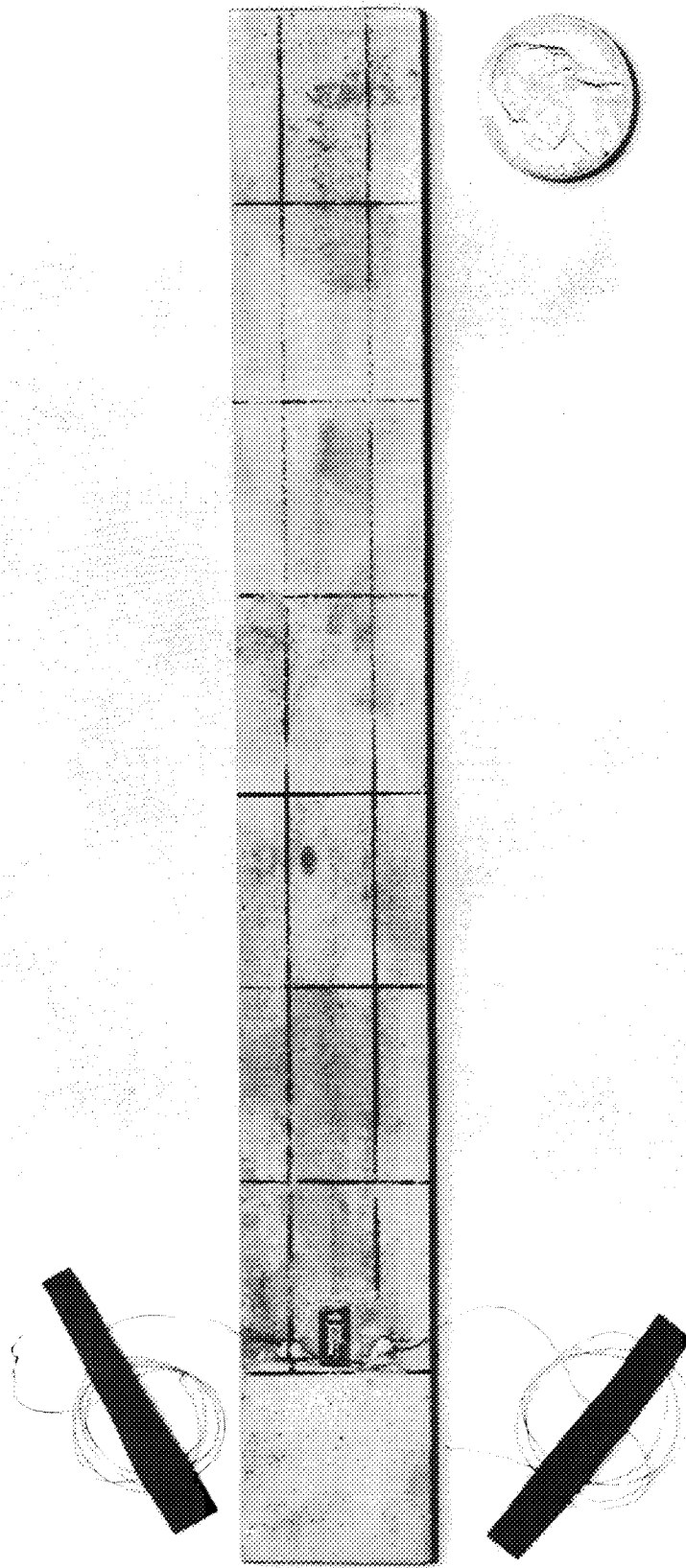


Figure 23. Stress Amplitude Decay Curves for a Fan Blade Vibrating in Air In Its Second Bending Mode for Two Temperature Conditions



**Figure 24. Stress Amplitude Decay Curves for a Fan Blade Vibrating in Air in Its First Torsion Mode for Two Temperature Conditions**



**Figure 25. Typical Composite Material Test Piece**

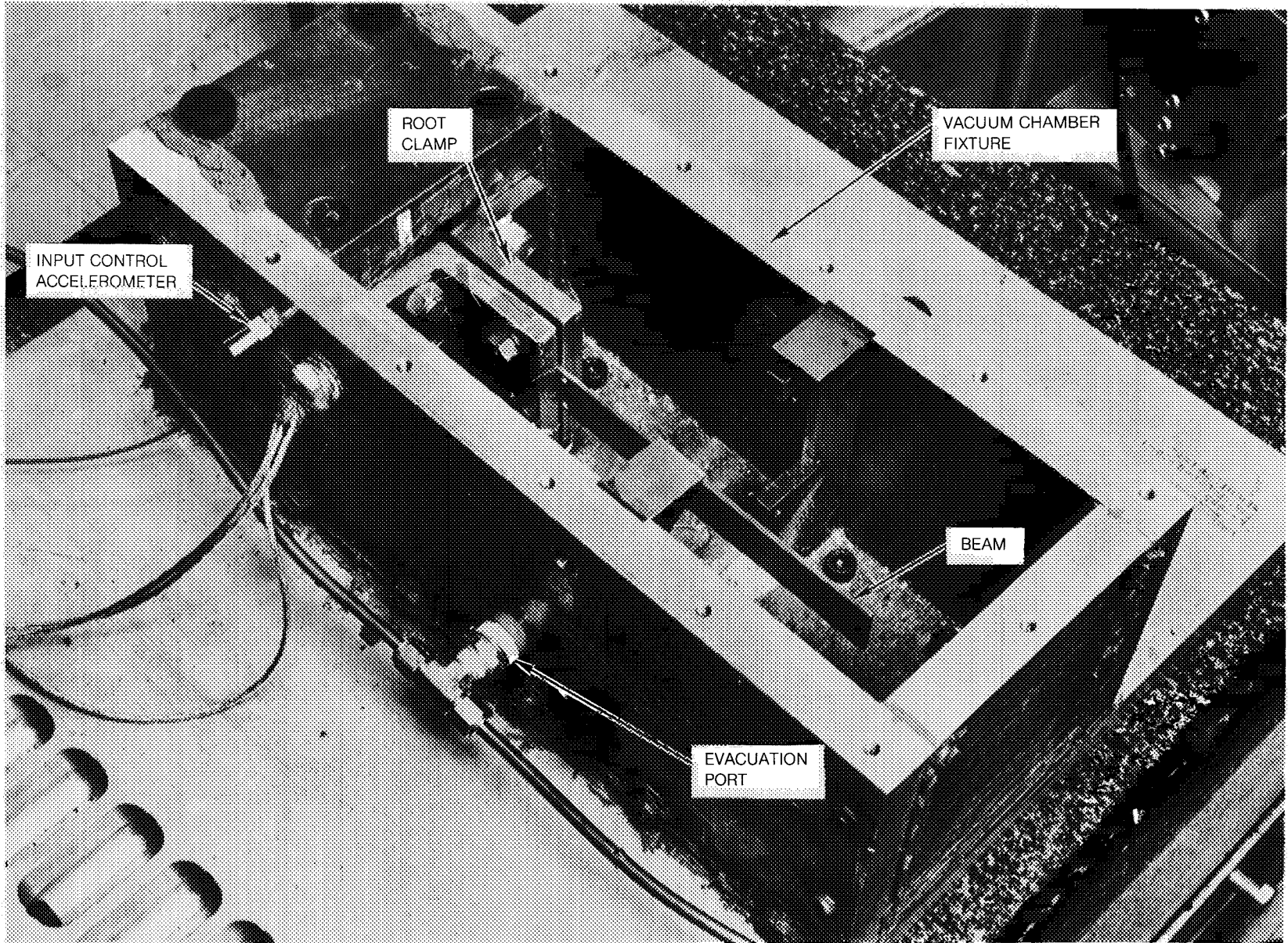


Figure 26. Composite Material Cantilevered Beam Vibration Test Set Up

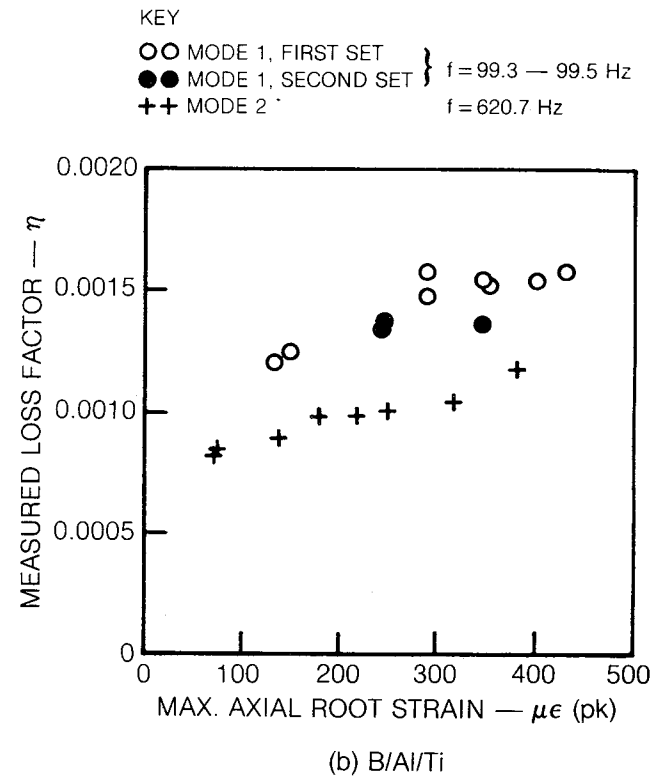
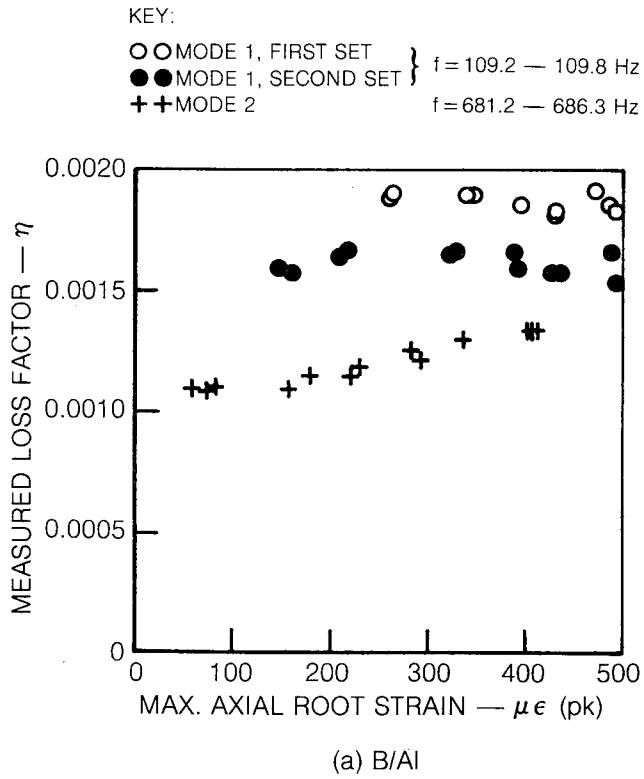
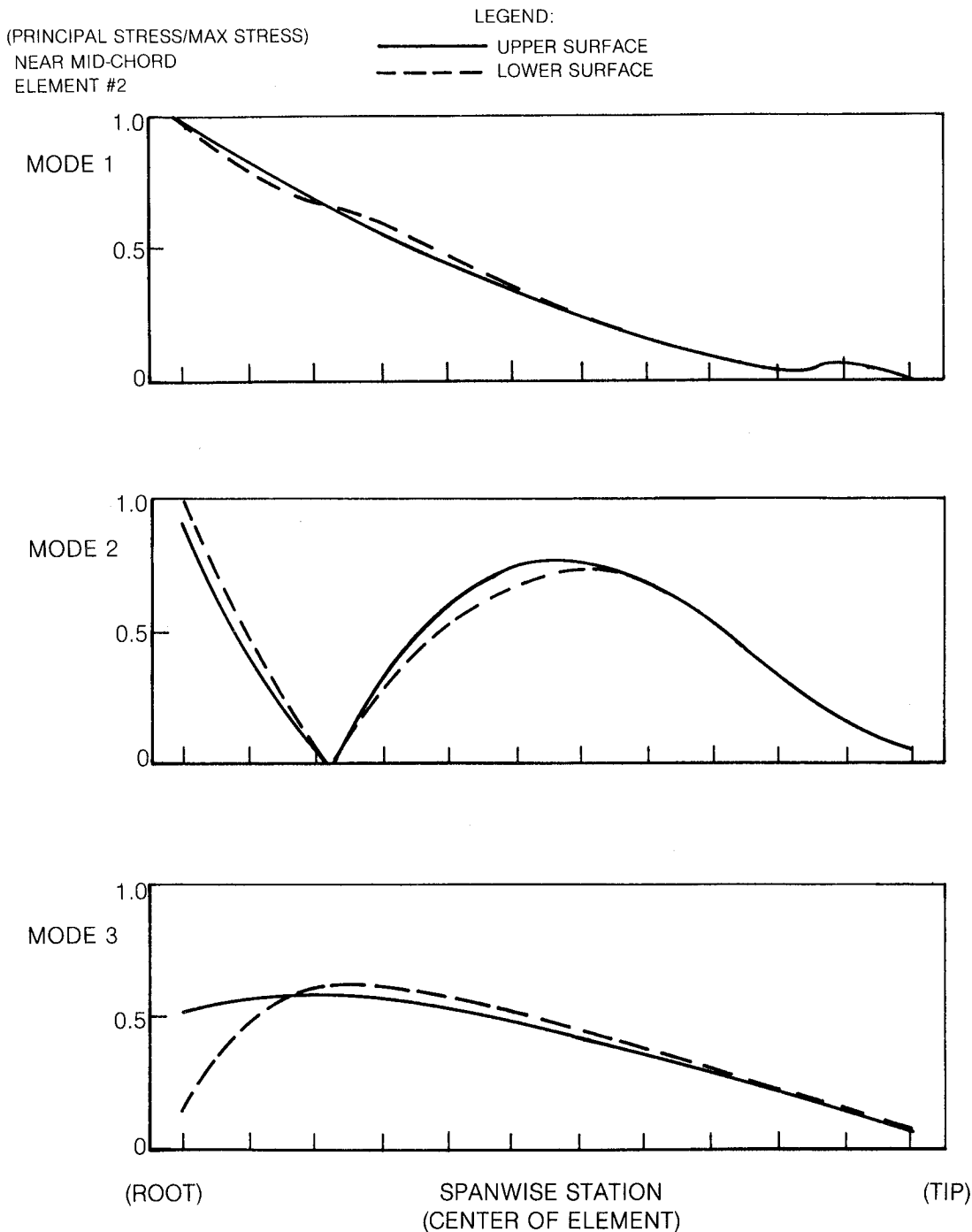
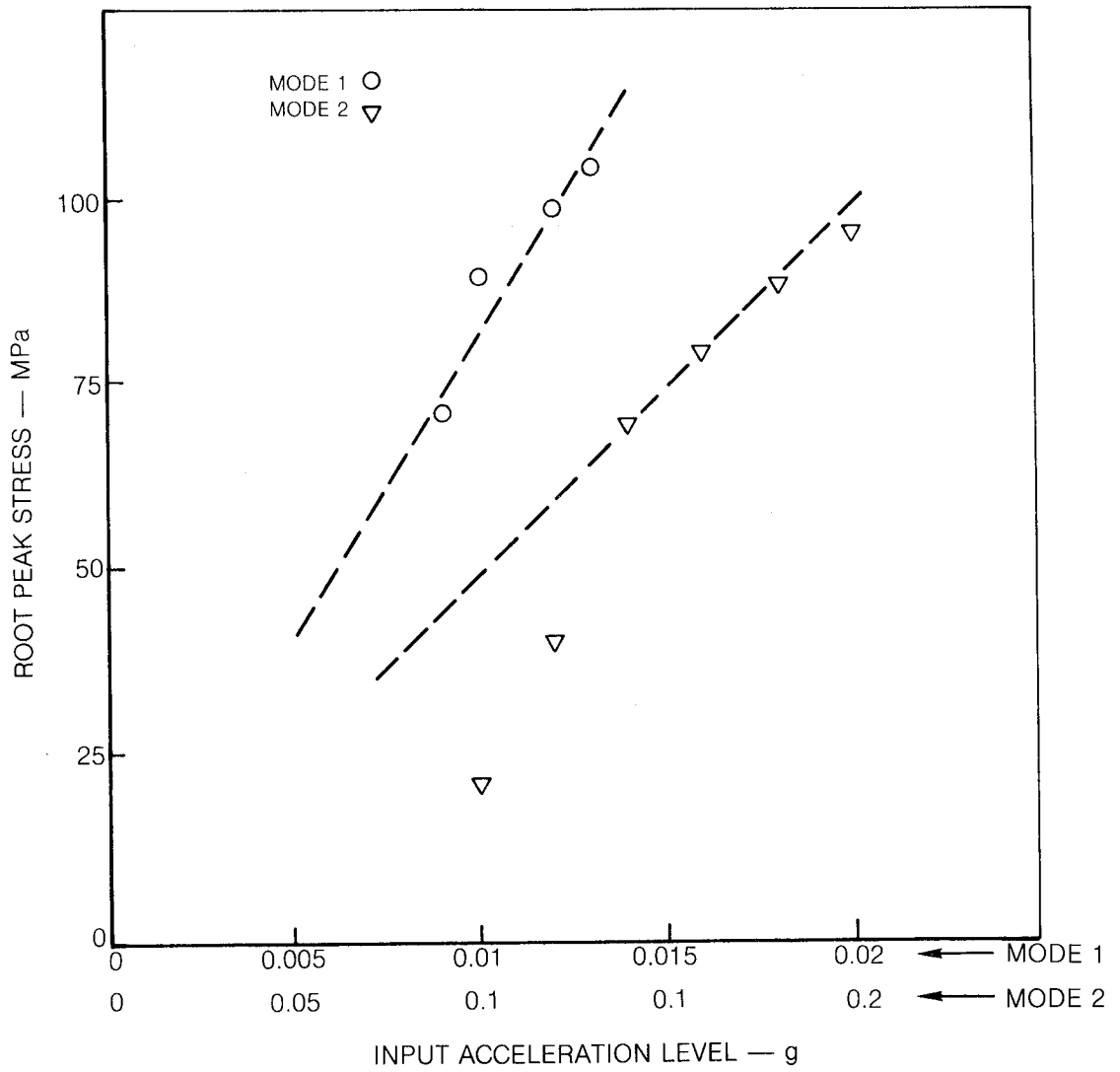


Figure 27. Composite Material Damping



**Figure 28. Spanwise Distributions of Outer Fiber Major Principal Stresses for Twisted Plate**



**Figure 29. Twisted Plate Forced Response in Partial Vacuum (10 Torr)**

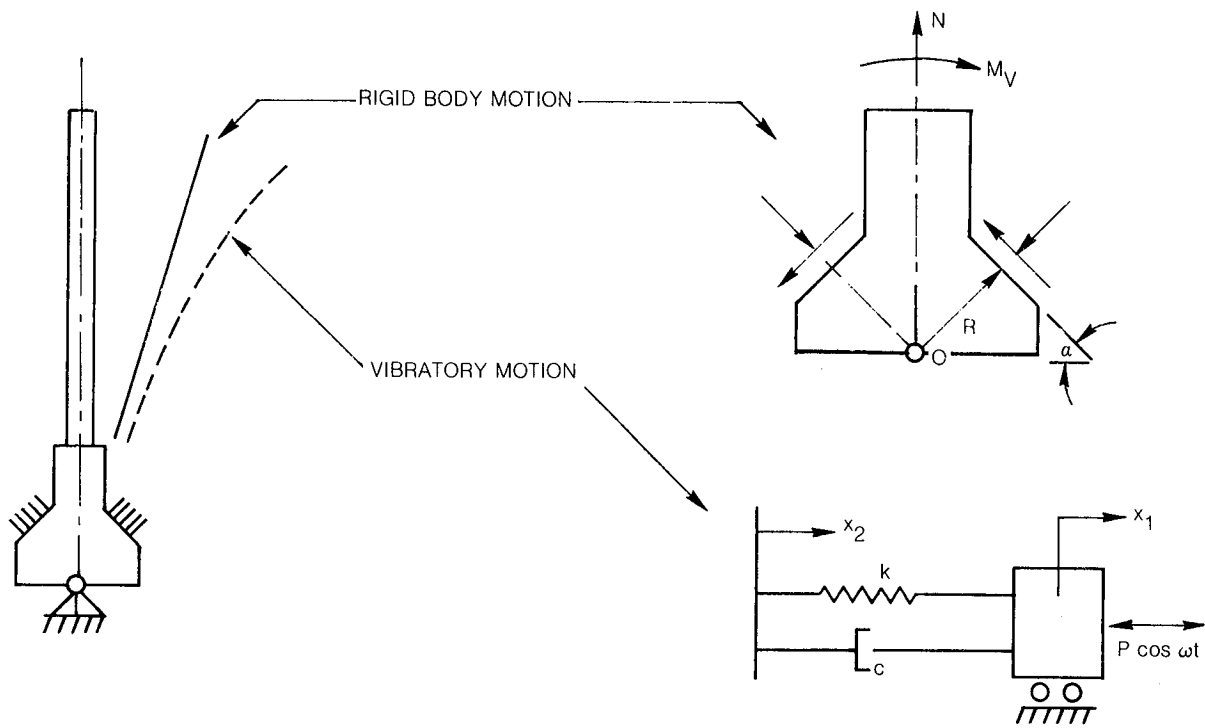


**Figure 30a. Motions of Blade with Slip at Root**

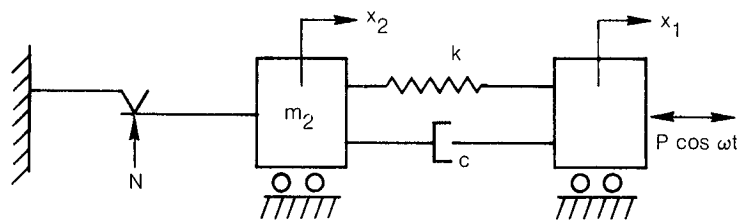


**Figure 30b. Analytical Model of Blade with Slip at Root**

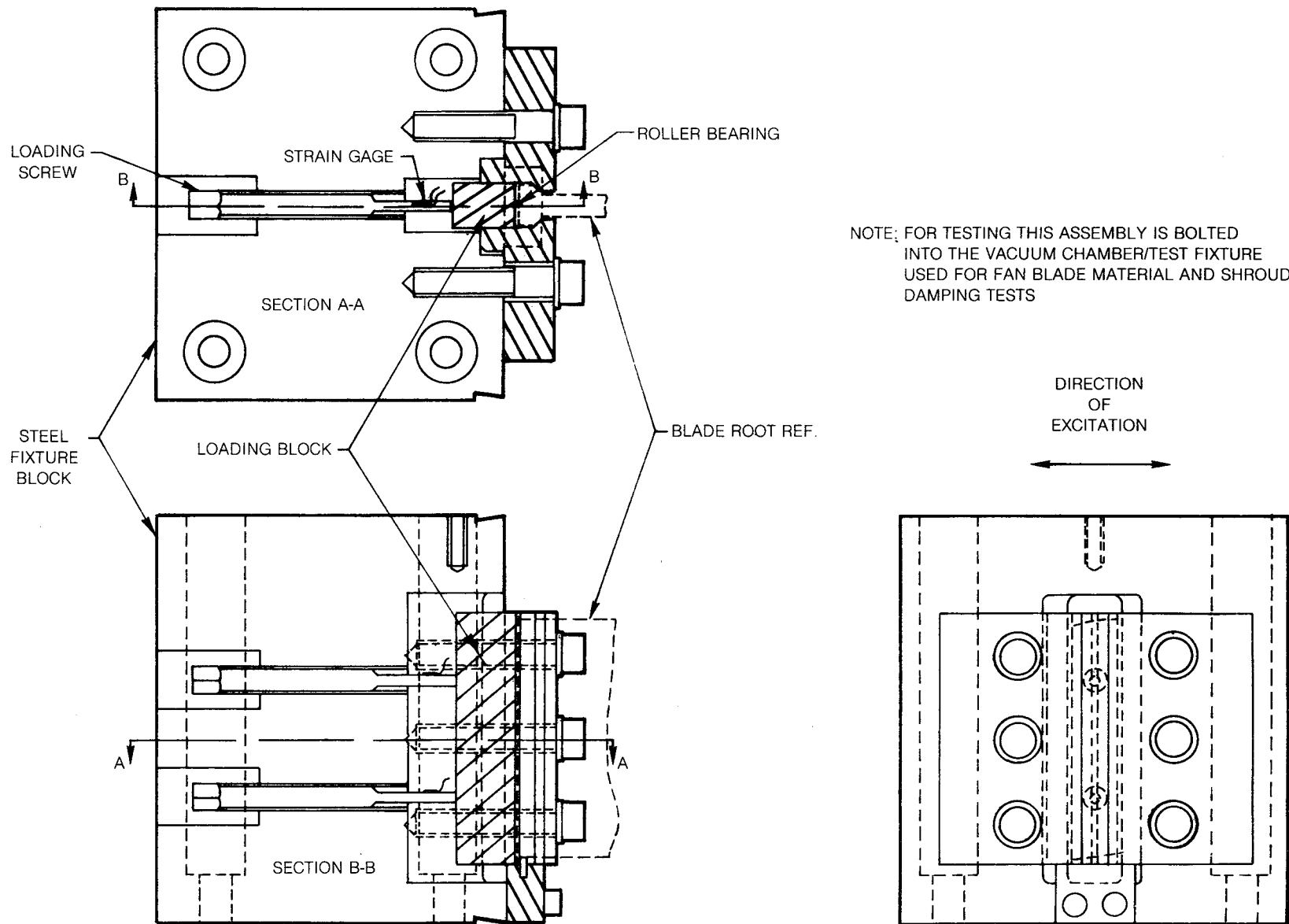
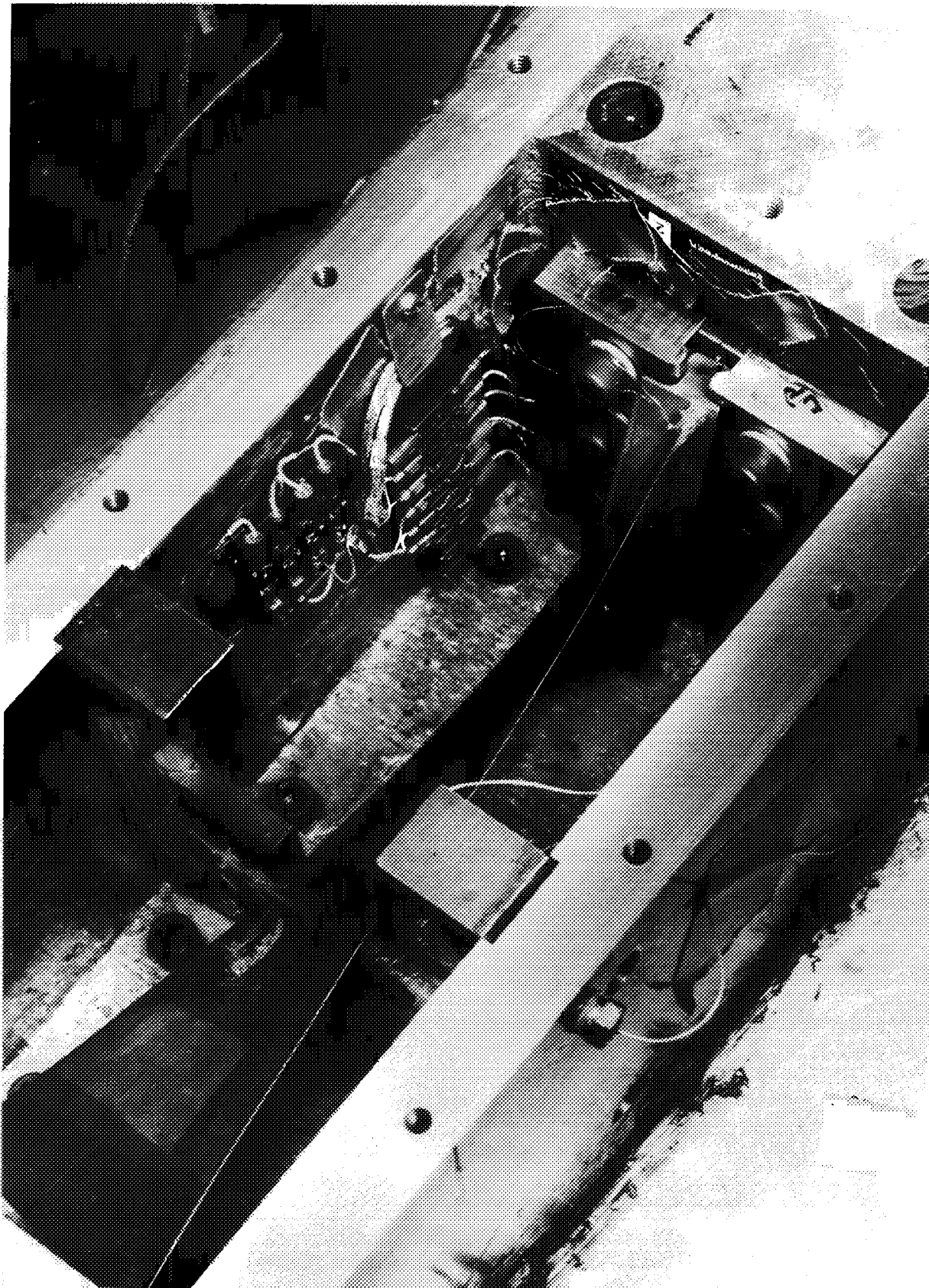
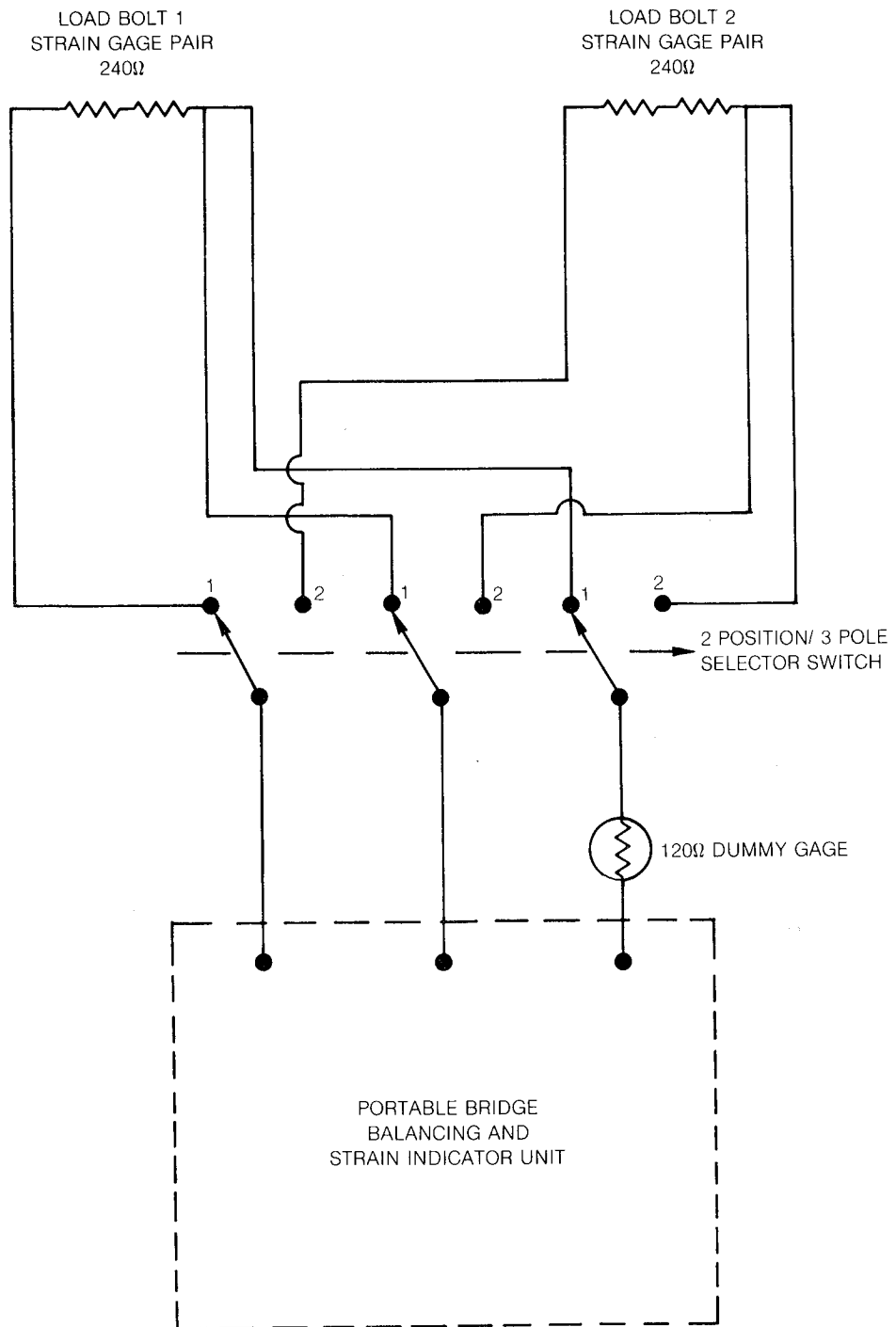


Figure 31. Test Fixture and Root Loading Device for Fan Blade Root Damping Tests



**Figure 32. Fan Blade/Fixture Test Assembly for Root Damping Investigation**



**Figure 33. Circuit and Switching Arrangement for Strain Gage Load Bolts**

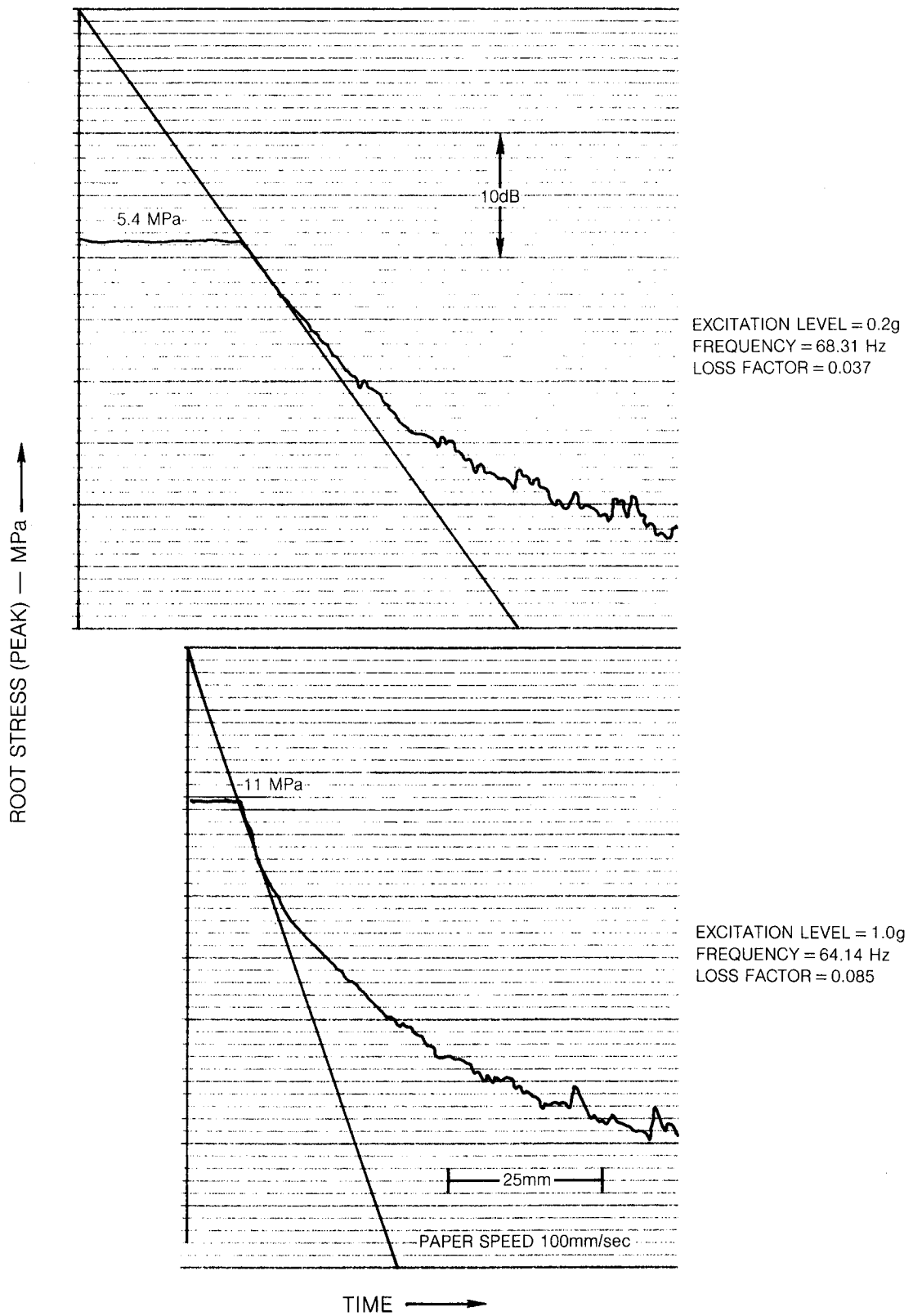
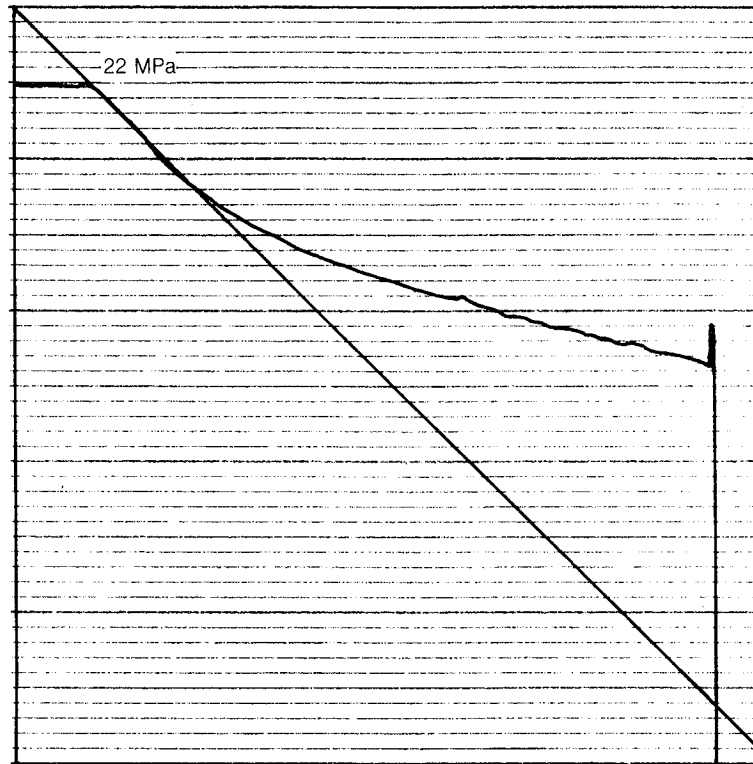
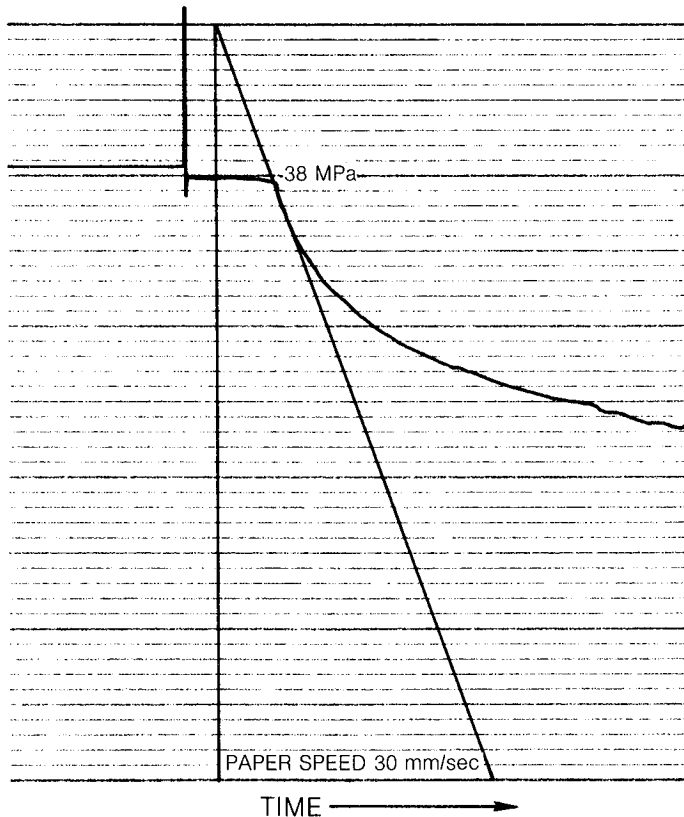


Figure 34. Decays of Blade Response with an Applied Root Loading of 576N.

ROOT STRESS (PEAK) — MPa



EXCITATION LEVEL = 0.2g  
FREQUENCY = 74.79 Hz  
LOSS FACTOR = 0.0072



EXCITATION LEVEL = 1.0g  
FREQUENCY = 73.34 Hz  
LOSS FACTOR = 0.0207

Figure 35. Decays of Blade Response with an Applied Root Loading of 2879N

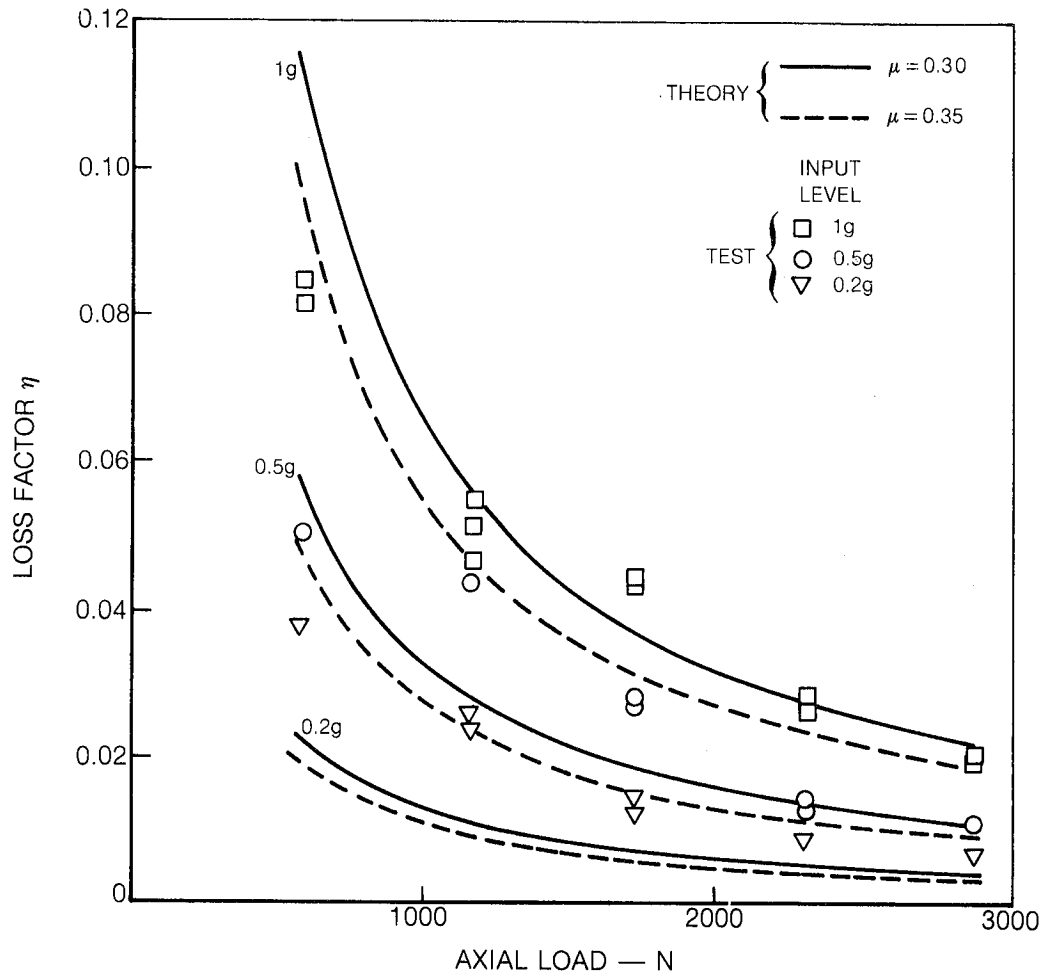


**Figure 36. Damping at Fan Blade Root**

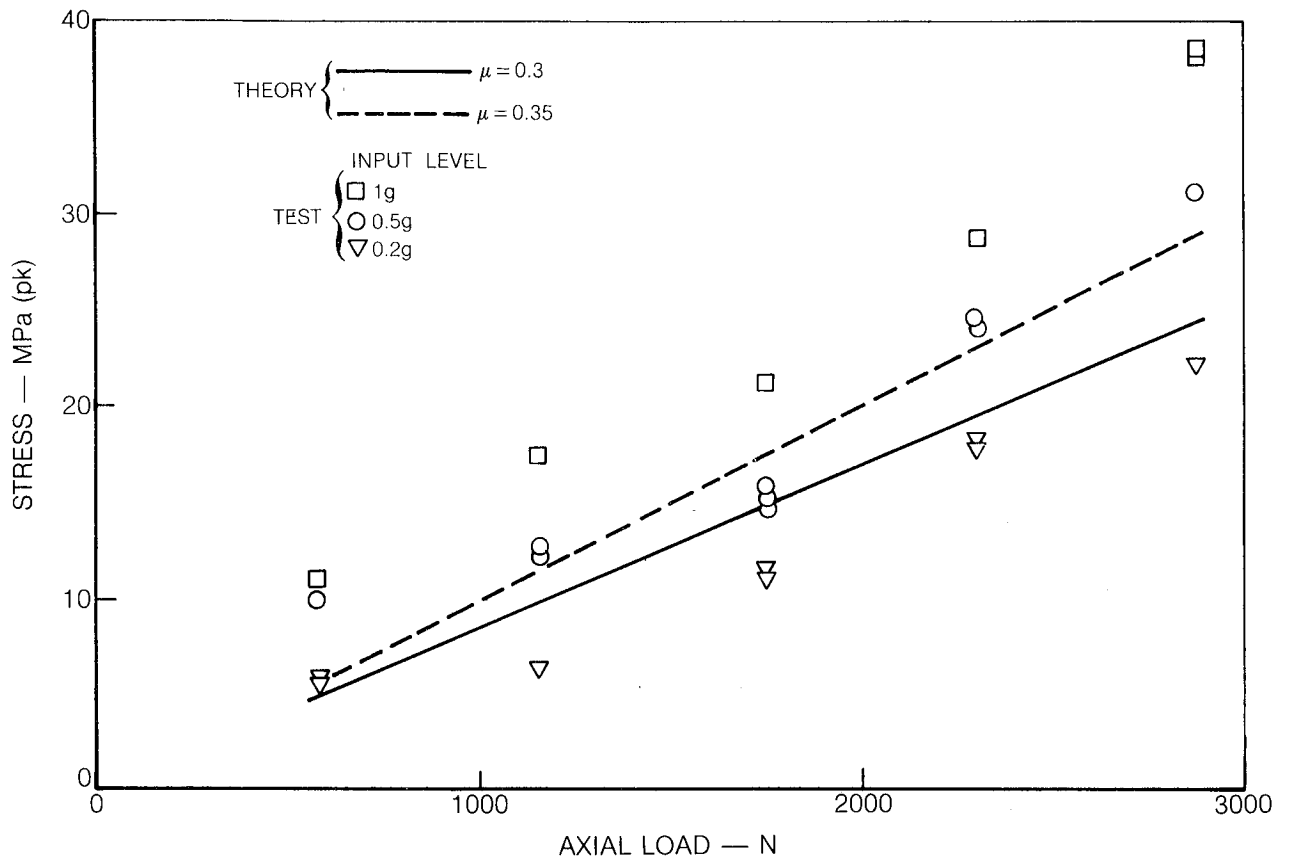
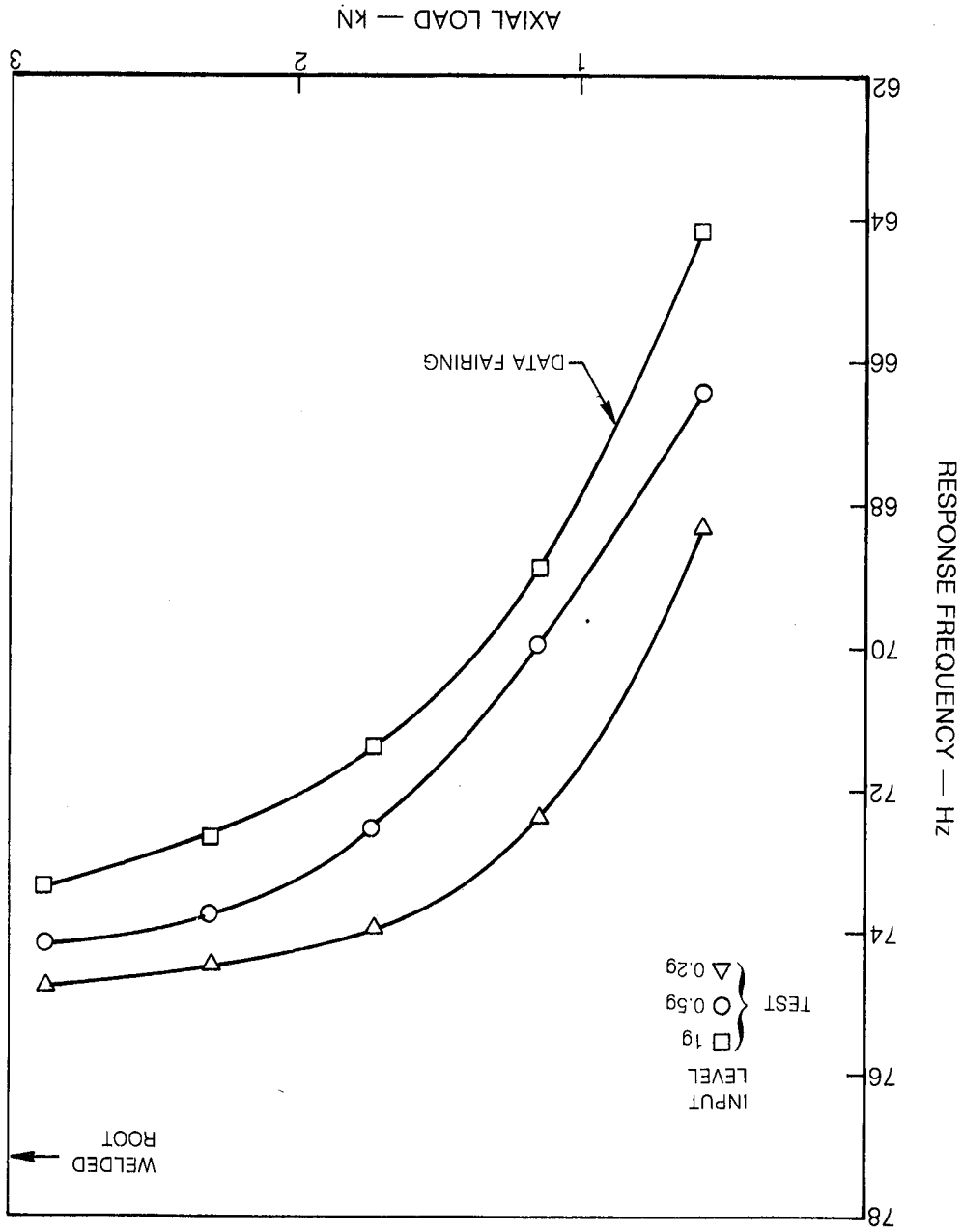


**Figure 37. Variation of Root Vibratory Stress with Root Loading**

Figure 38. Variation of Blade Response Frequency with Root Normal Load for Various Excitation Levels



RESPONSE FREQUENCY — HZ

AXIAL LOAD — KN

INPUT LEVEL  
1g  
0.5g  
0.2g

DATA FAIRING

WELDED ROOT

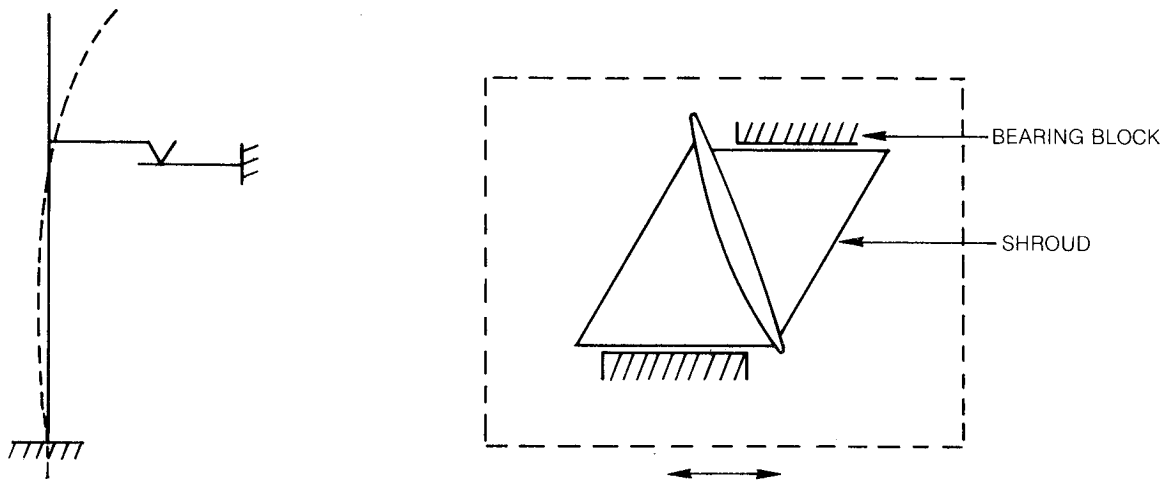


Figure 39a,b. Schematic of Shroud Rubbing

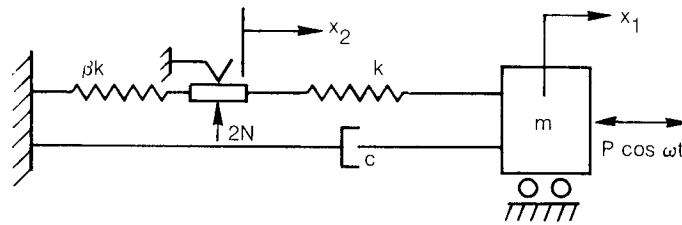


Figure 40. Analytical Model for Shroud Rubbing

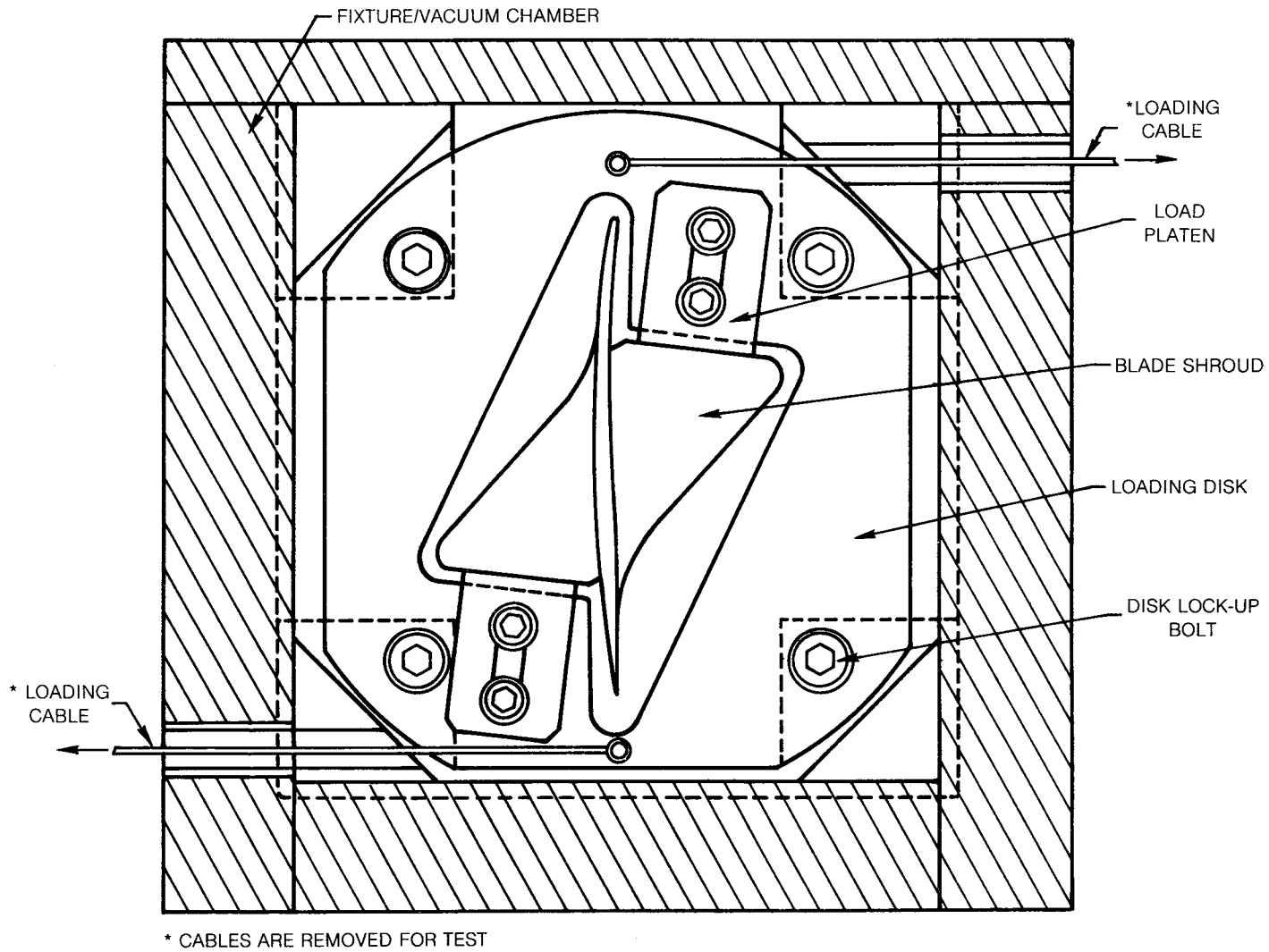


Figure 41. Shroud Loading Device for Investigation of Fan Blade Shroud Damping Mechanism

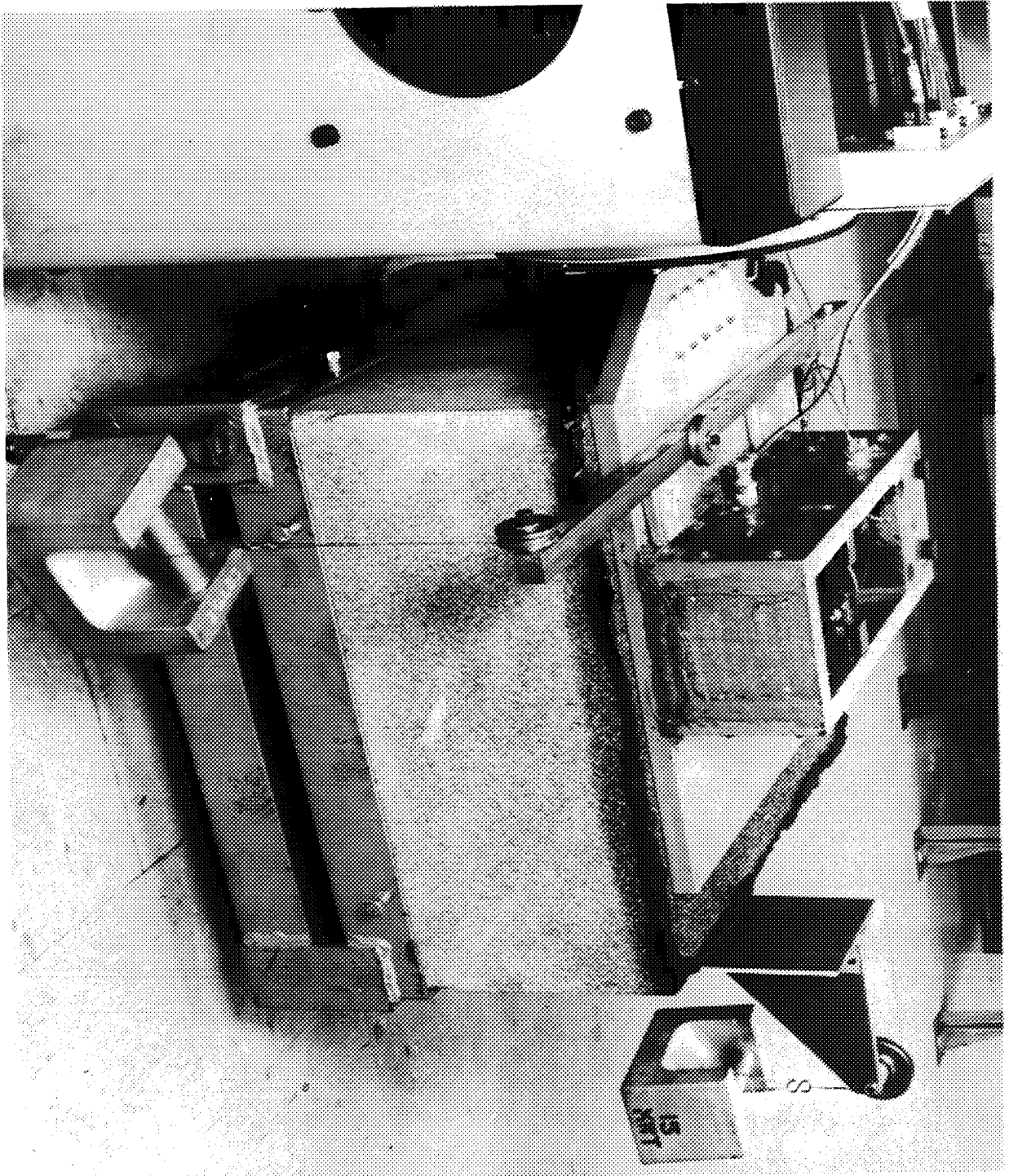
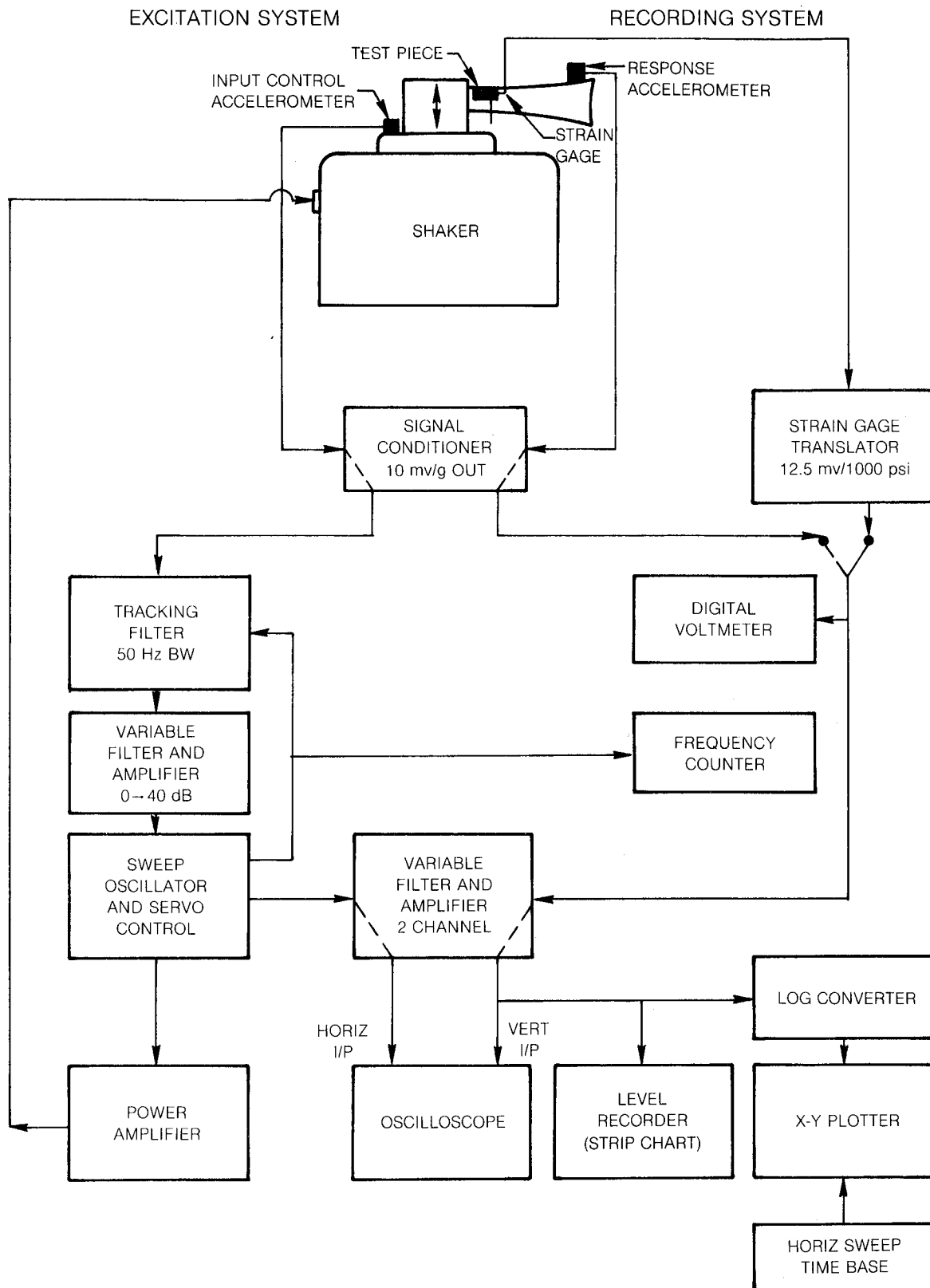


Figure 42. Shroud Loading Mechanism



**Figure 43. Block Diagram of Basic Excitation and Recording Systems Used to Obtain Strain and Acceleration Response Data from Test Items Excited by the Electro-dynamic Shaker**

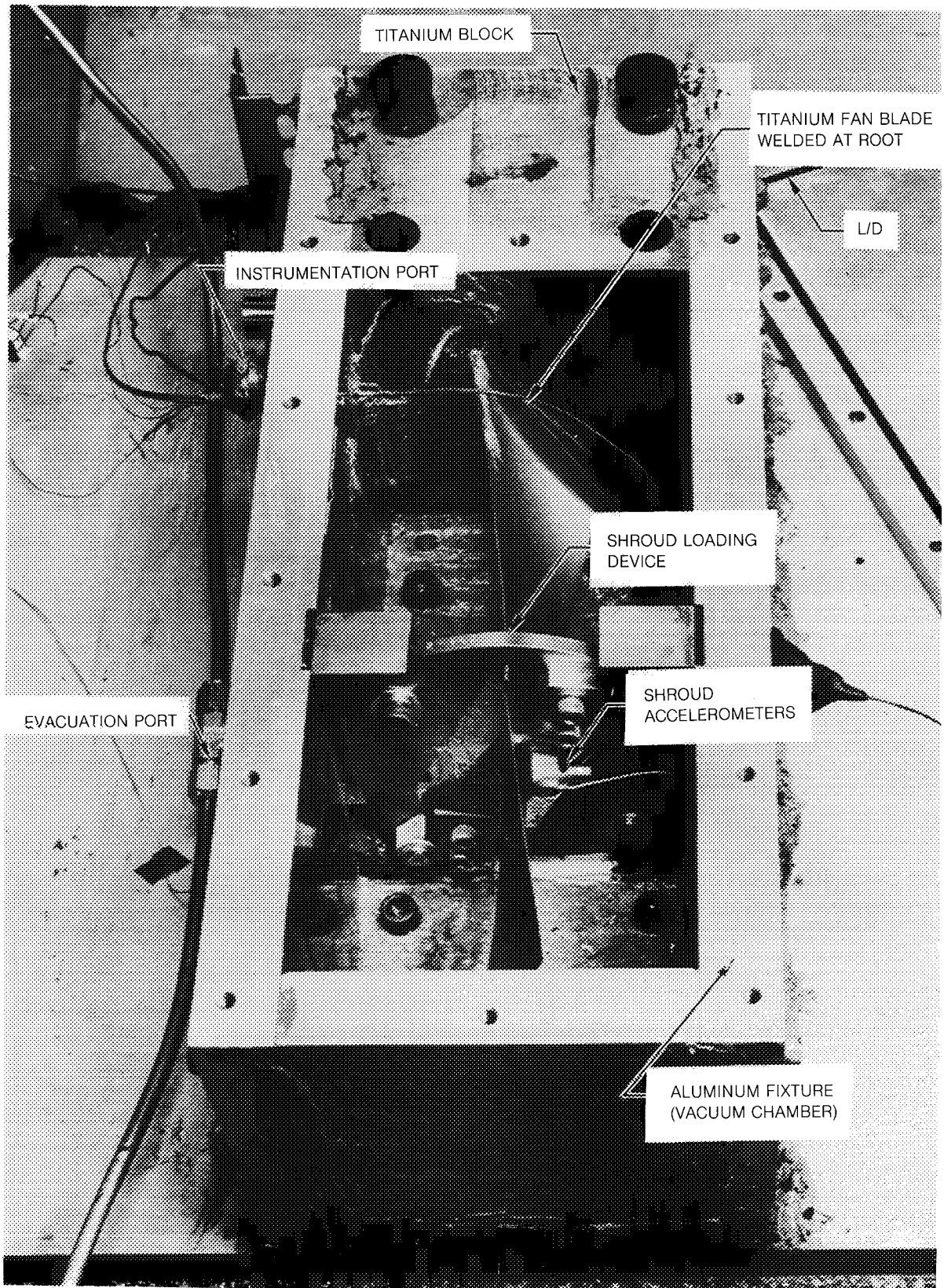
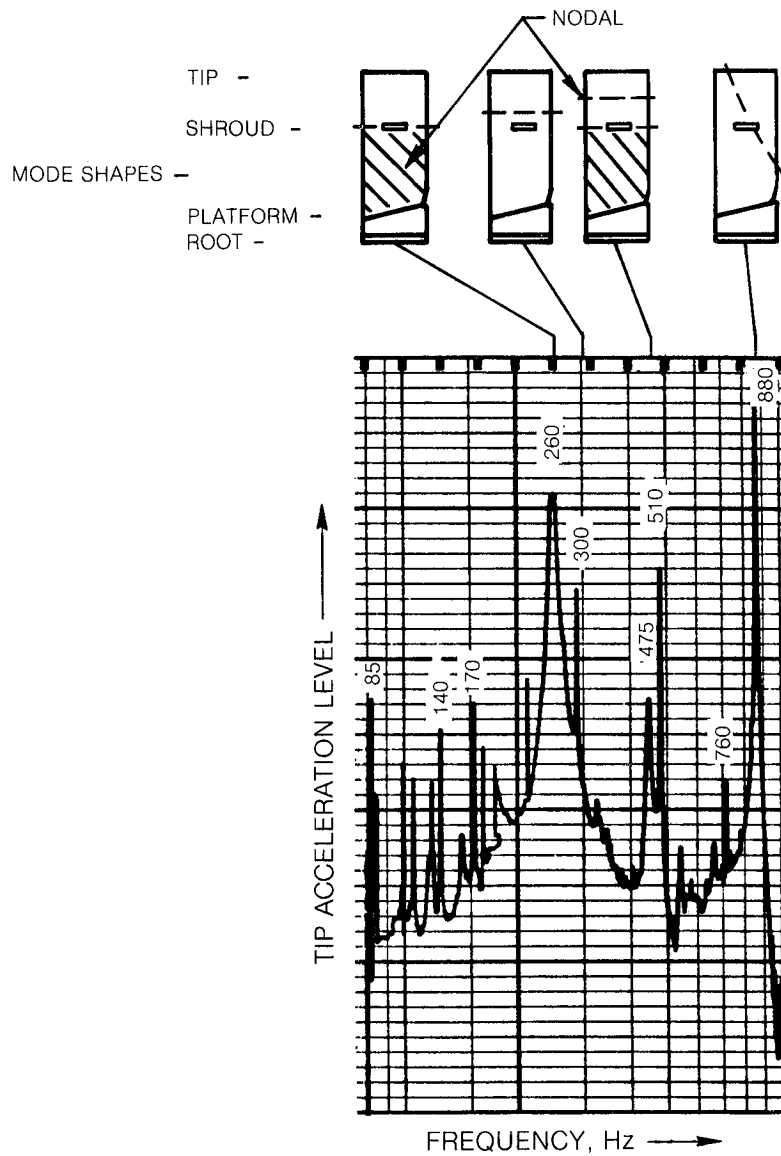
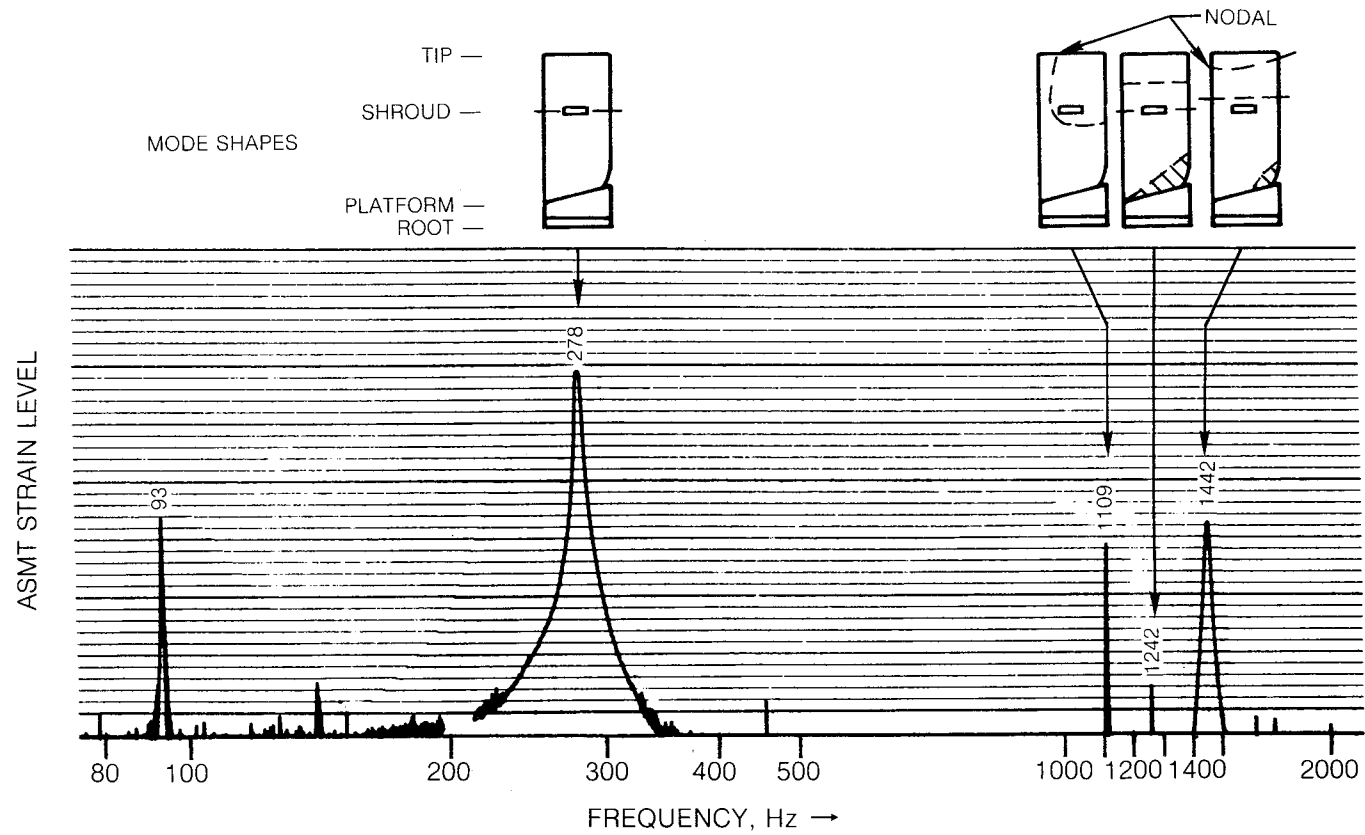


Figure 44. Test Set-Up for Shroud Damping Investigation



FREQUENCY, Hz	RESPONSE DESCRIPTION
85	NONLINEAR — MODIFIED FIRST FREE BLADE BENDING MODE
140	NONLINEAR — HIGH FREQUENCY RESPONSE
170	NONLINEAR — HIGH FREQUENCY RESPONSE
260	ABOVE SHROUD BLADE BENDING (FLAP) MODE ( $\eta = 0.003$ )
300	NONLINEAR — MODIFIED SECOND FREE BLADE BENDING MODE
475	ABOVE SHROUD BLADE SECOND BENDING MODE ( $\eta = 0.003$ )
510	NONLINEAR — HIGH FREQUENCY RESPONSE
760	NONLINEAR — HIGH FREQUENCY RESPONSE
880	ABOVE SHROUD BLADE TORSION ( $\eta = 0.001$ )

**Figure 45. Fan Blade Response Characteristics from a 2g Level Exploratory Sweep — Shrouds Loaded with 102N**



FREQUENCY, Hz	RESPONSE DESCRIPTION
93	NONLINEAR — MODIFIED FIRST FREE BLADE BENDING MODE
278	ABOVE SHROUD BLADE BENDING (FLAP) MODE
1109	ABOVE SHROUD BLADE TORSION
1242	NONLINEAR — MODIFIED SECOND BENDING MODE
1442	ABOVE SHROUD SECOND BENDING MODE

**Figure 46. Fan Blade Response Characteristics from a 2g Level Exploratory Sweep — Shrouds Loaded with 150 N**

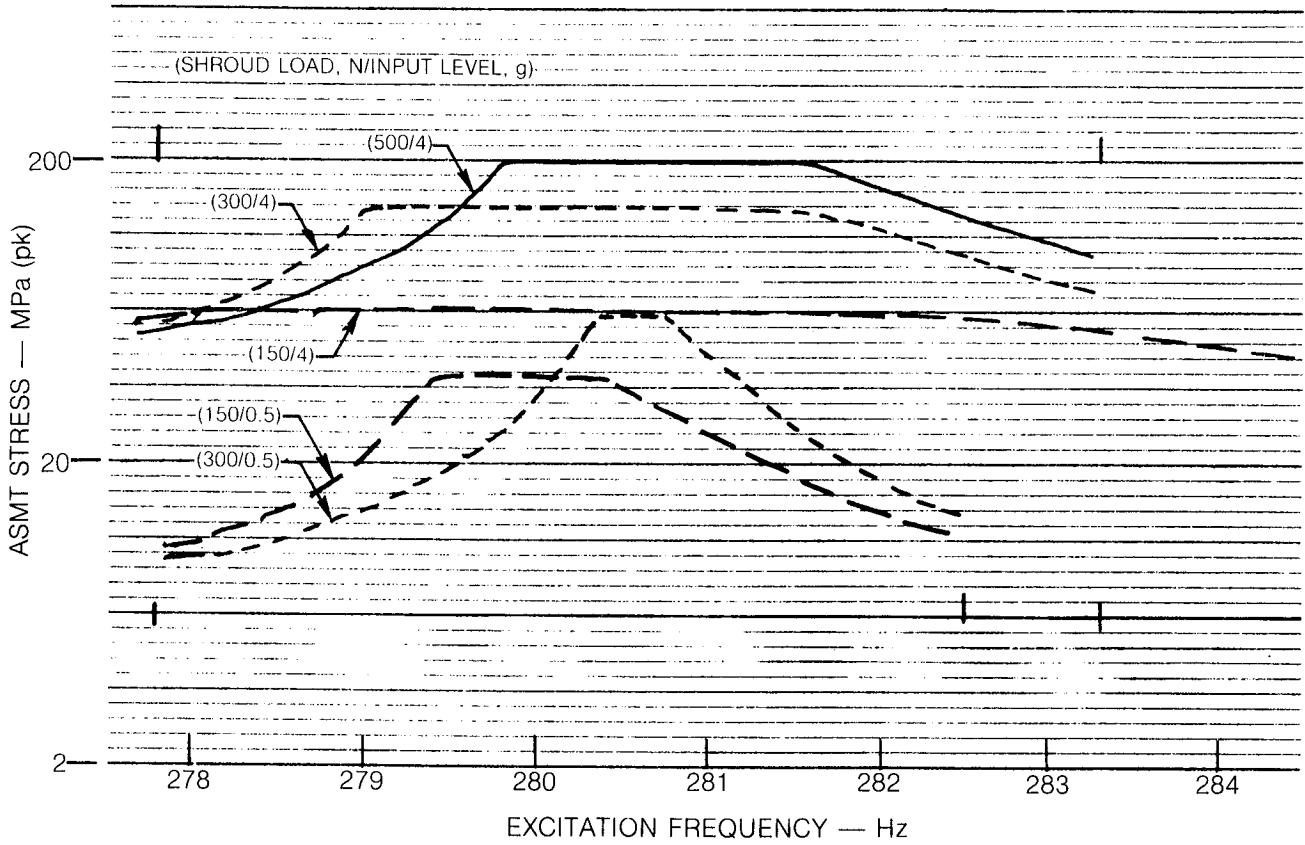


**Figure 47. First Flap Mode Response to a Slow Frequency Sweep at Constant Input Acceleration Levels**

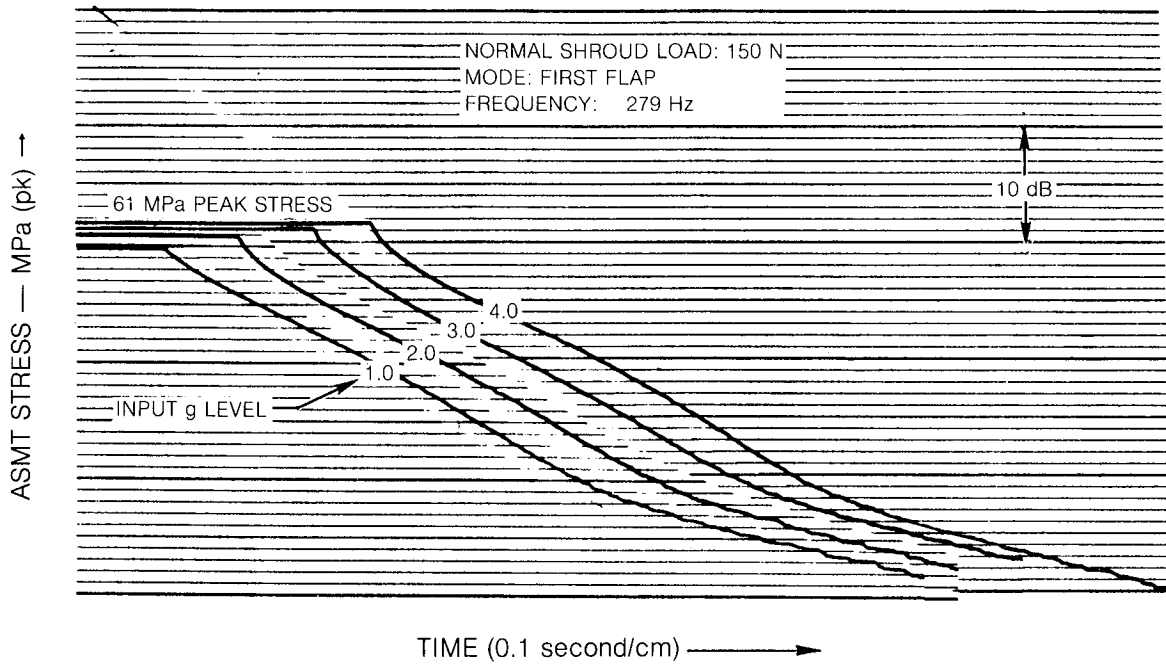


**Figure 48. Damping Due to Rubbing at Shroud for a Typical Fan Blade — Variation of Response Decay with Initial Stress**

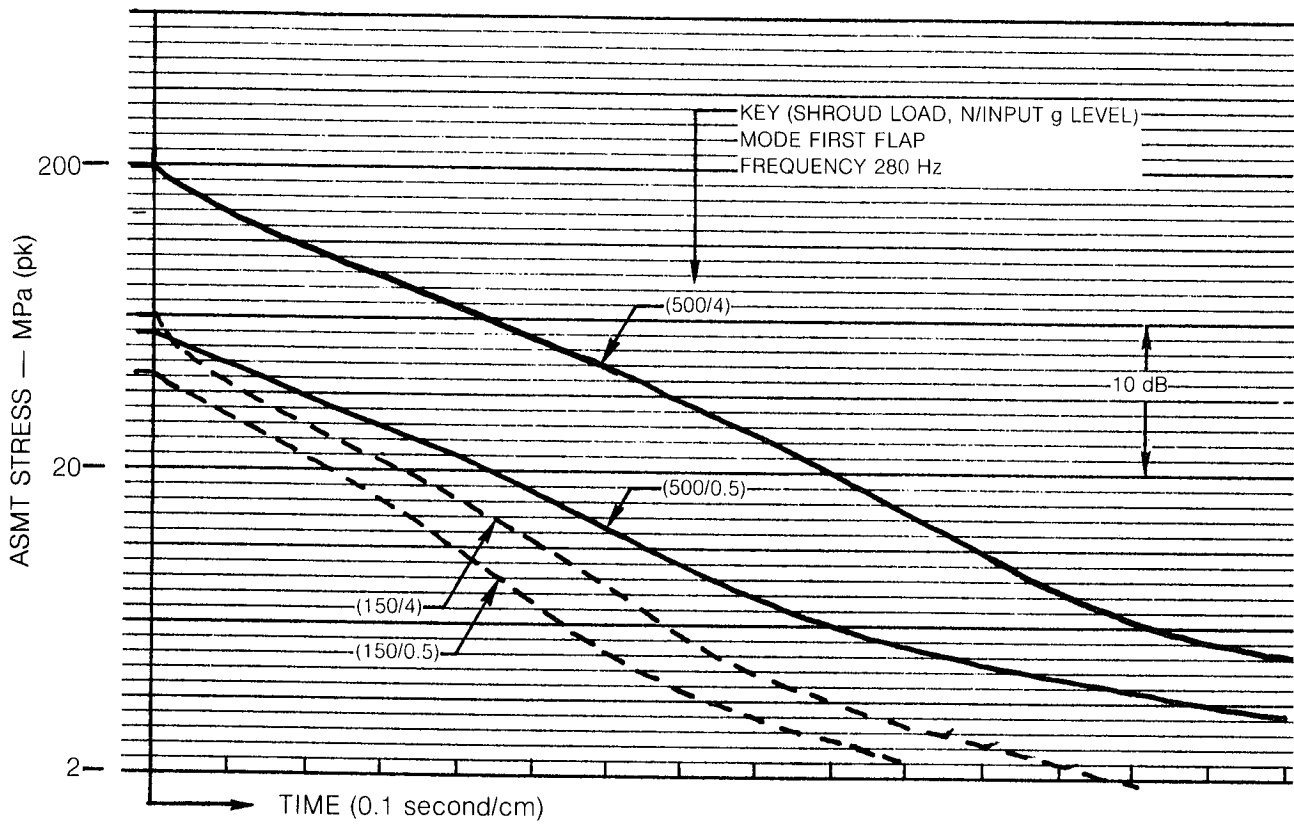


**Figure 49. Damping Due to Rubbing at Shroud for a Typical Fan Blade — Variation of Response Decay with Shroud Load and Initial Stress**

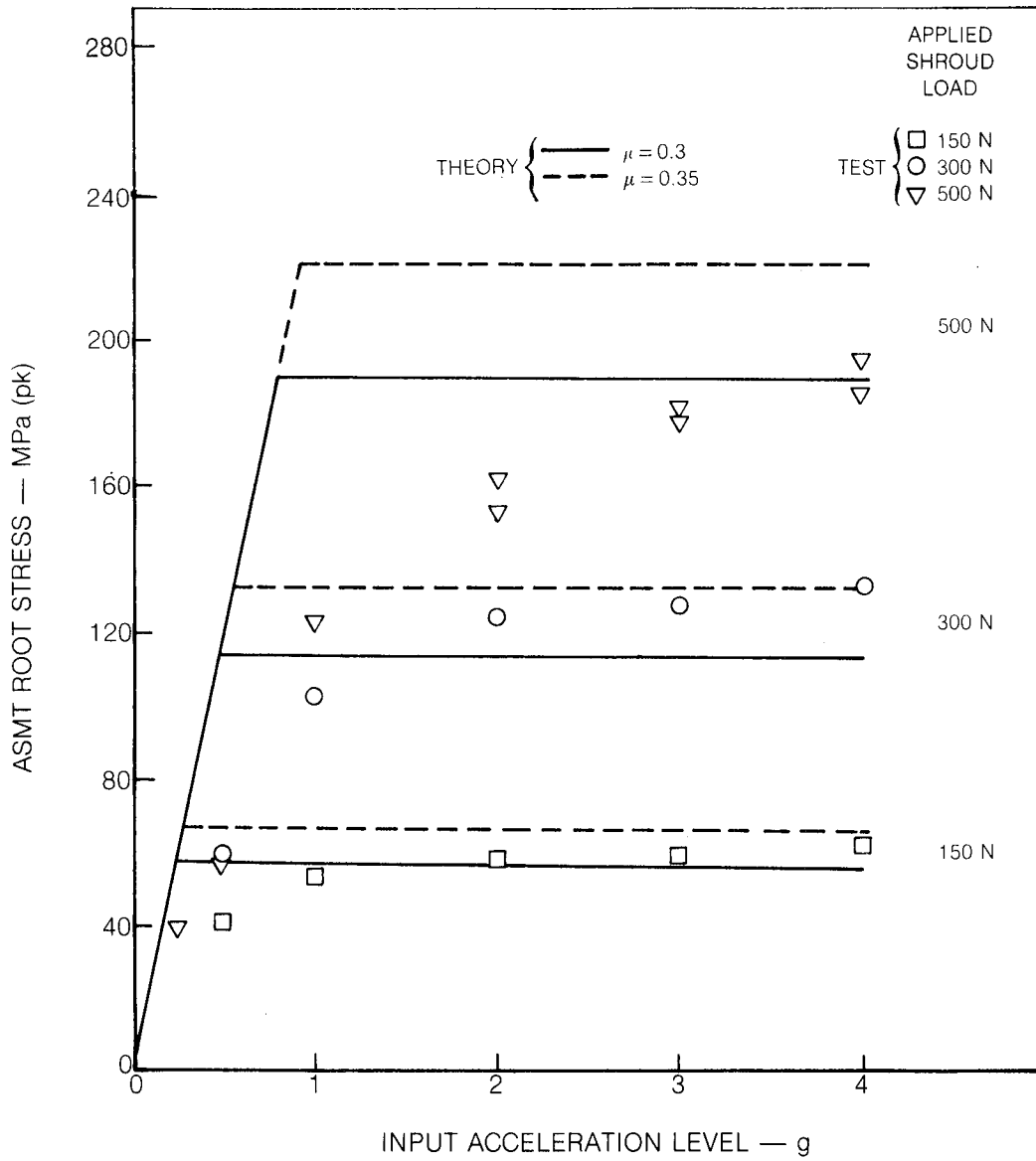
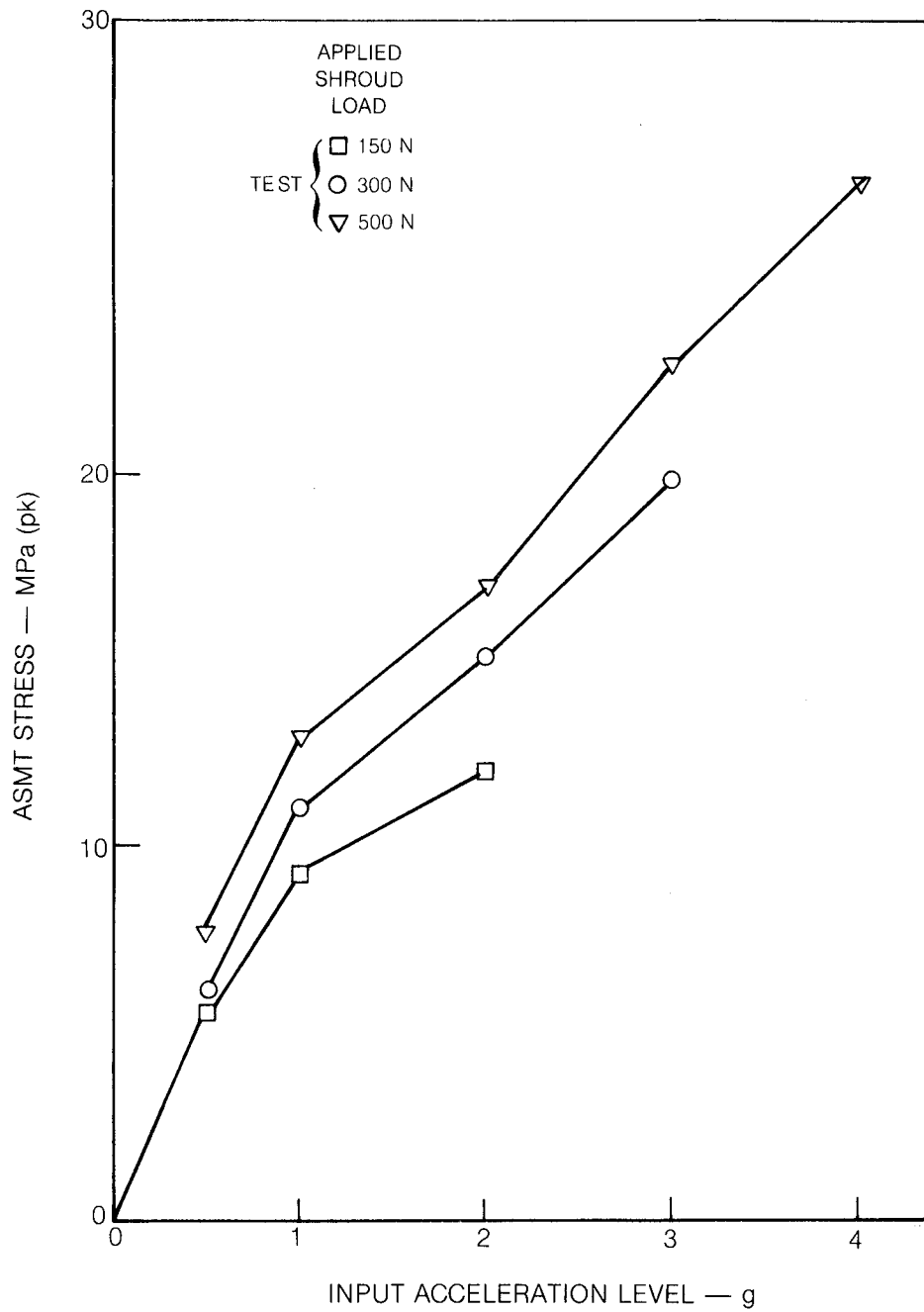
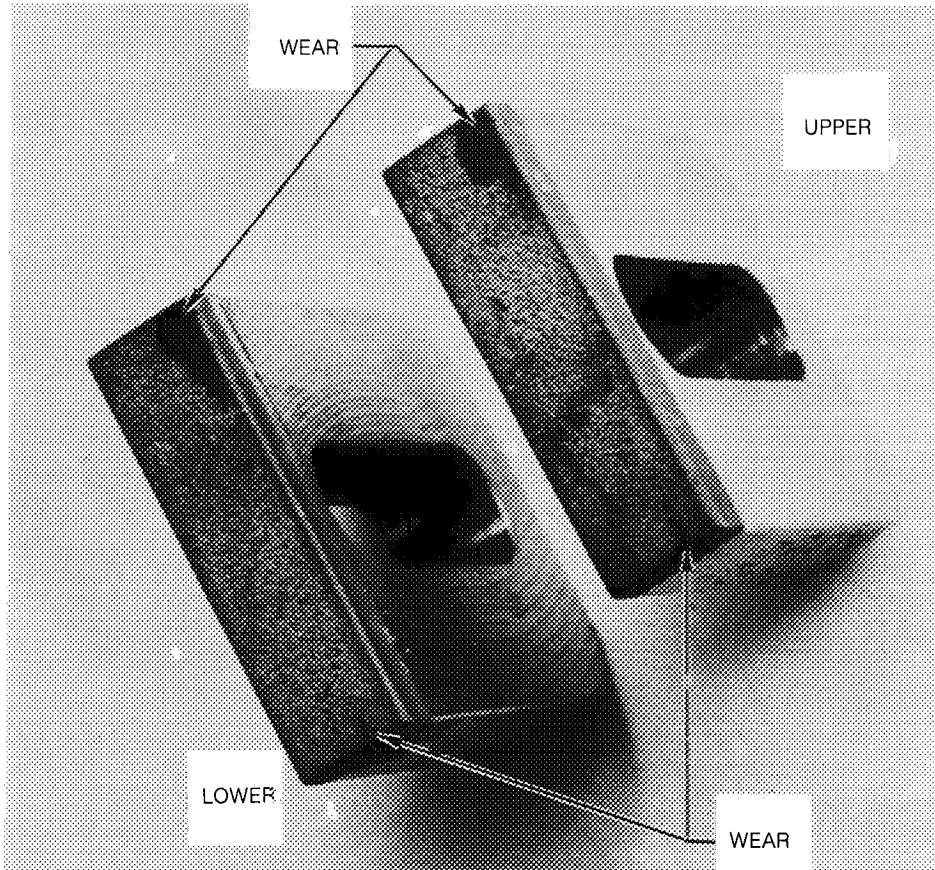


Figure 50. Shroud Damping Effects on Blade Response (First Flap Mode ~ 280 Hz)



**Figure 51. Blade Response in the Above-Shroud-Torsion Mode**



**Figure 52. Wear Areas on Shroud Load Platens**

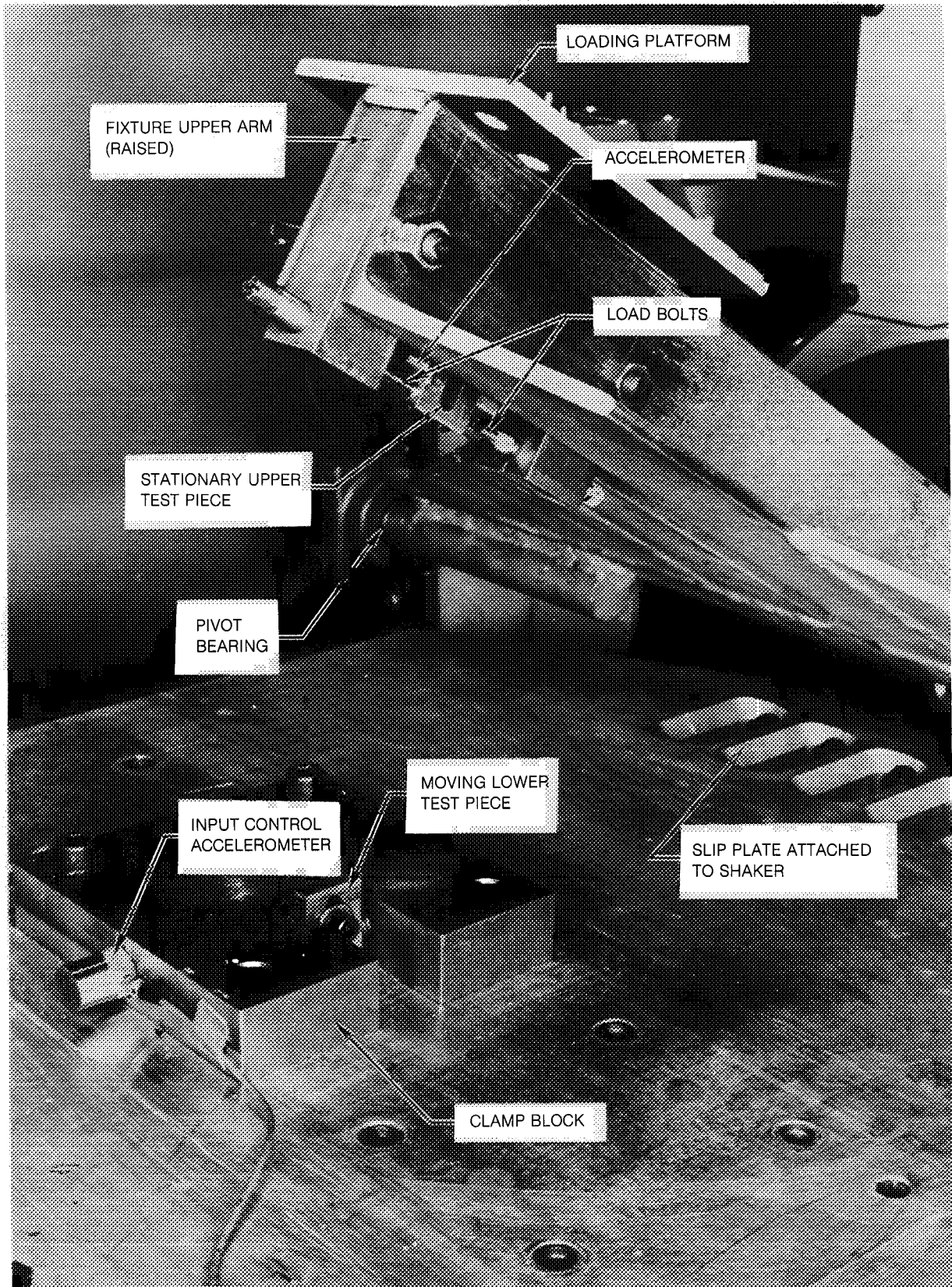


**Figure 53. Friction Test Assembly (Upper Arm Raised)**

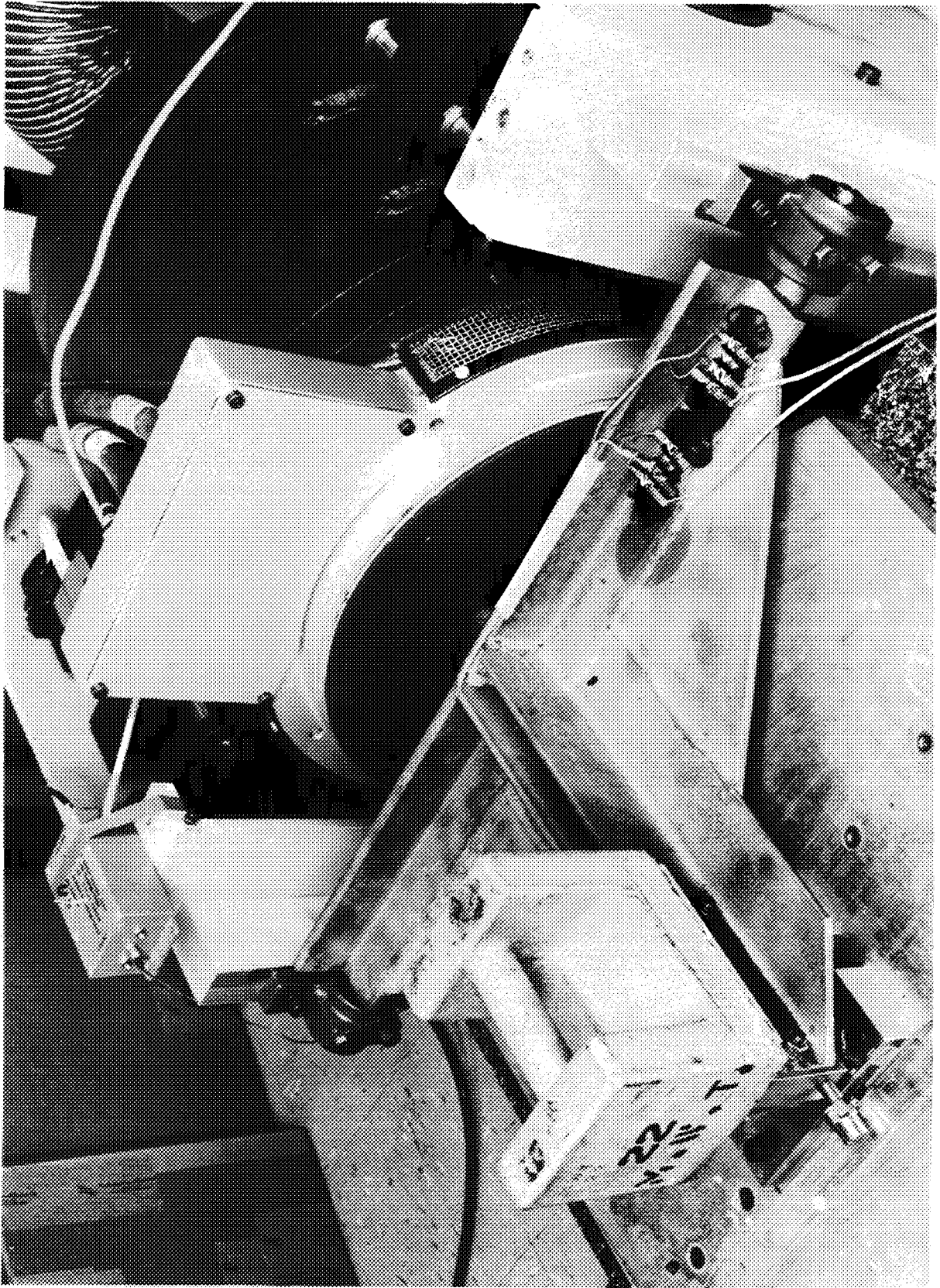
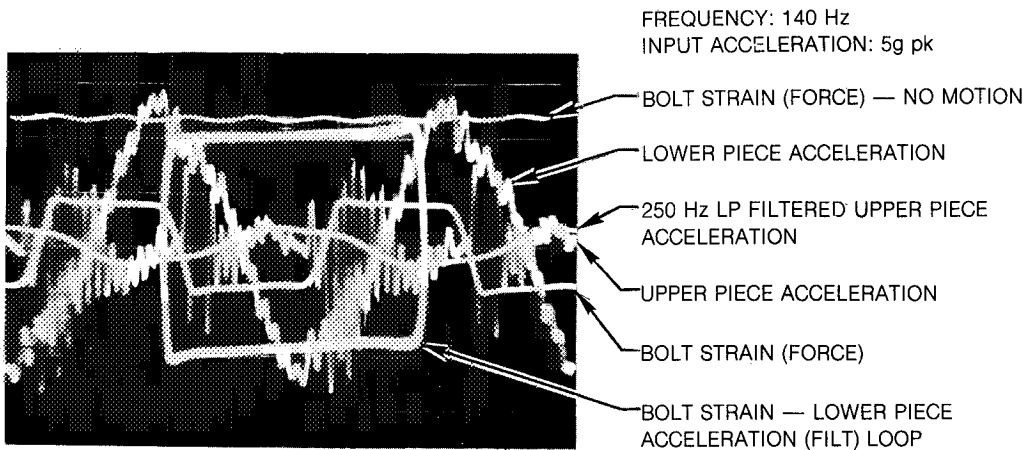
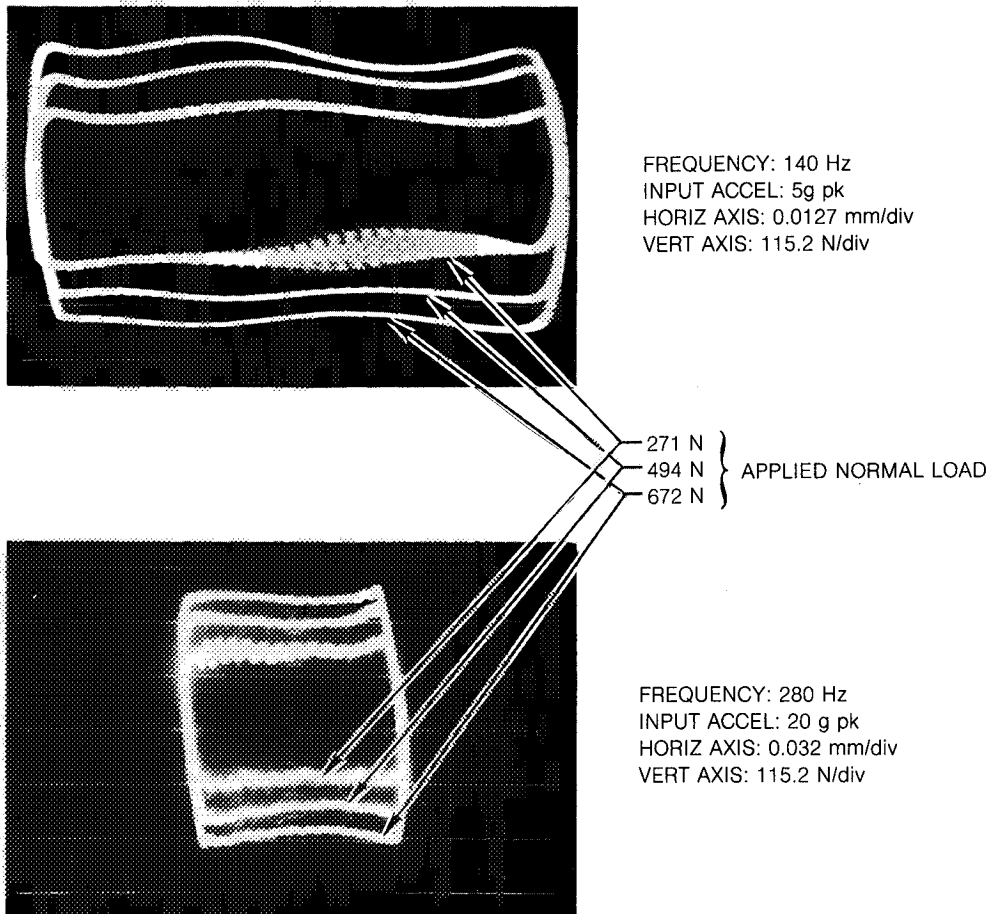


Figure 54 Friction Test Assembly



**Figure 55a. Typical Signals from Acceleration and Force Transducers**



**Figure 55b. Typical Measured Friction Force — Slip Loops**

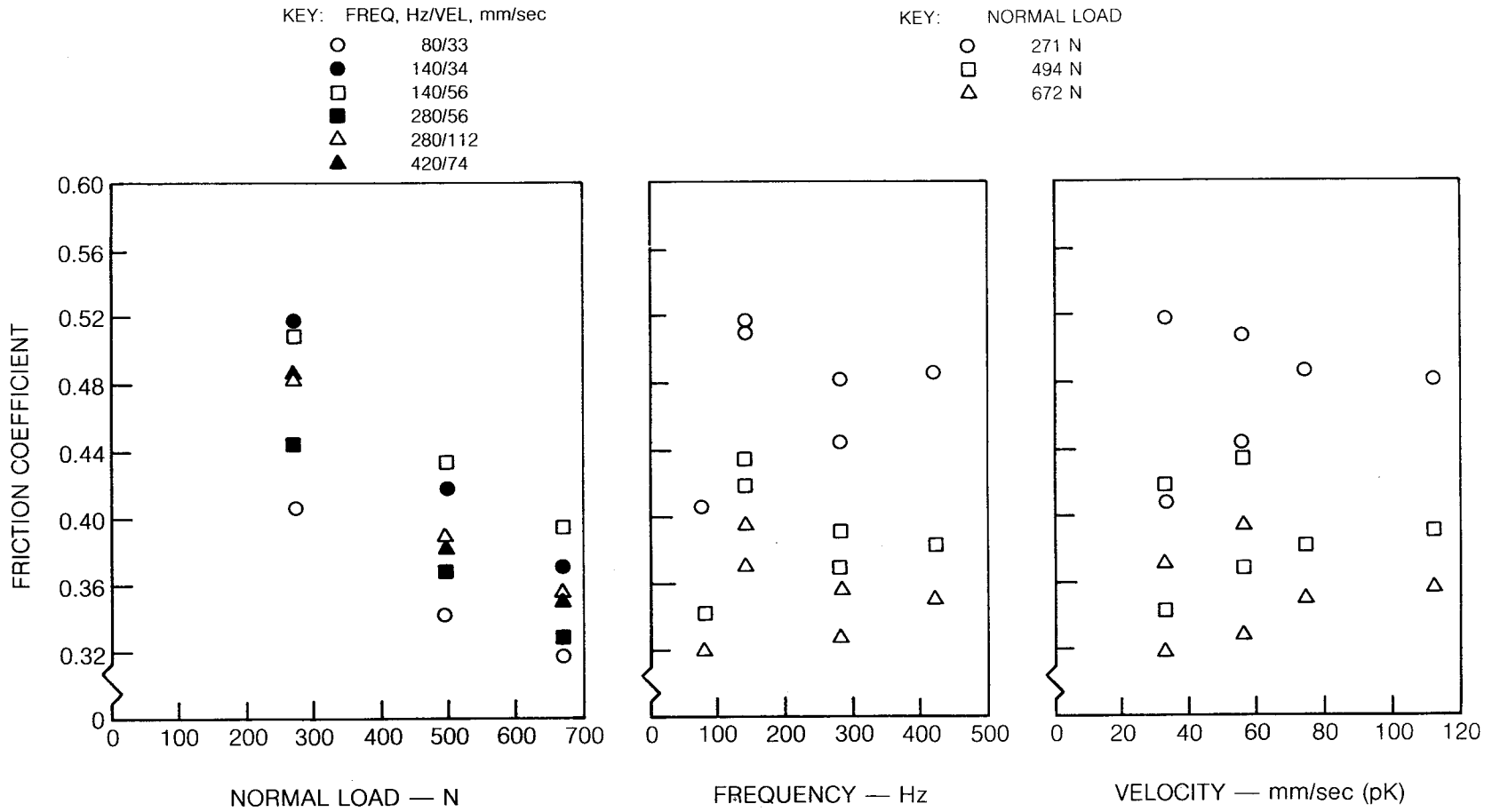


**Figure 56 Variation of Equivalent Friction Coefficient During Sinusoidal Motion With Normal Load, Frequency and Maximum Relative Velocity**

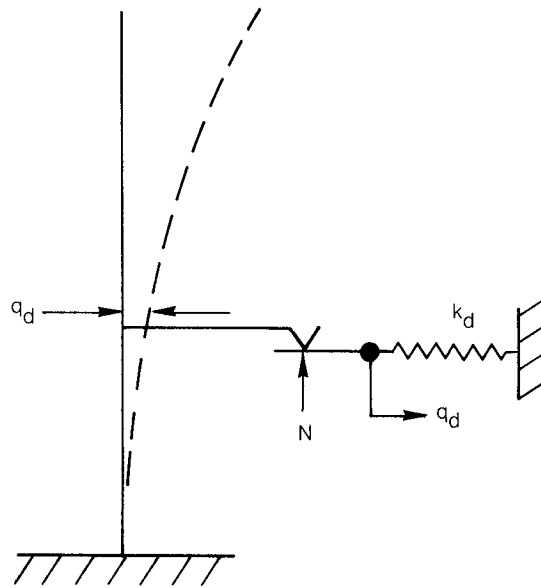


**Figure 57a. Schematic of Turbine Blade and Platform Damper**

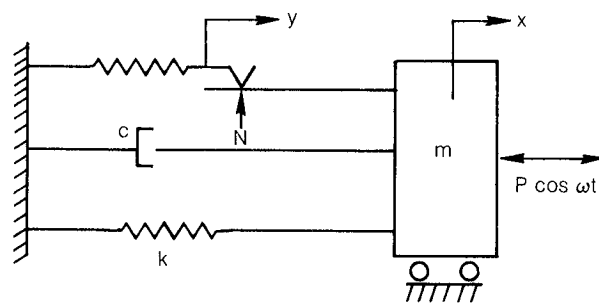


**Figure 57b. Analytical Model for Platform Damping**



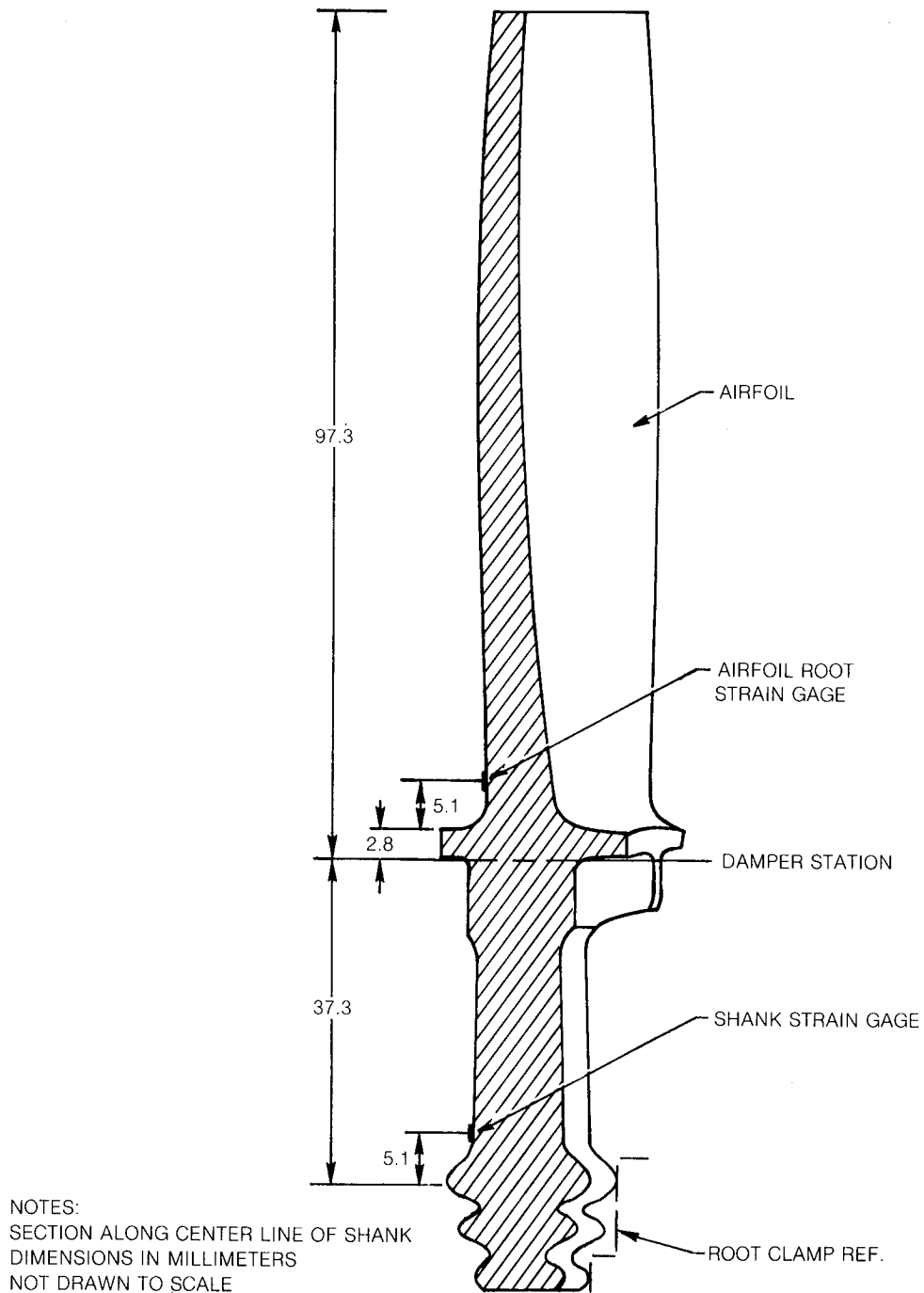


**Figure 59. Turbine Blade Test Piece Geometry**

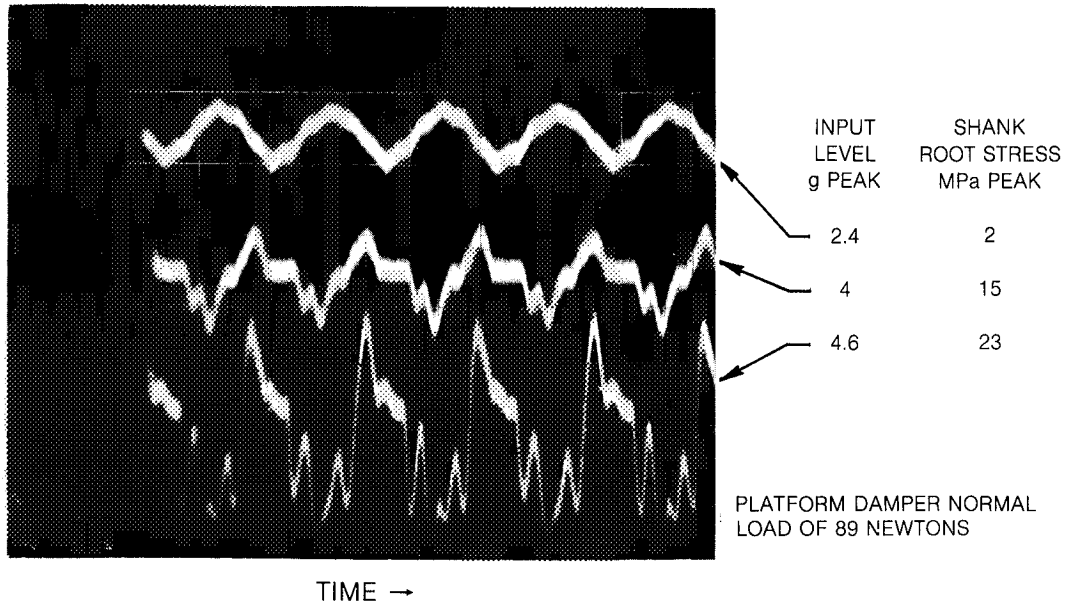


**Figure 60. Damper Stress Response Signals for Varying Input Acceleration Levels**

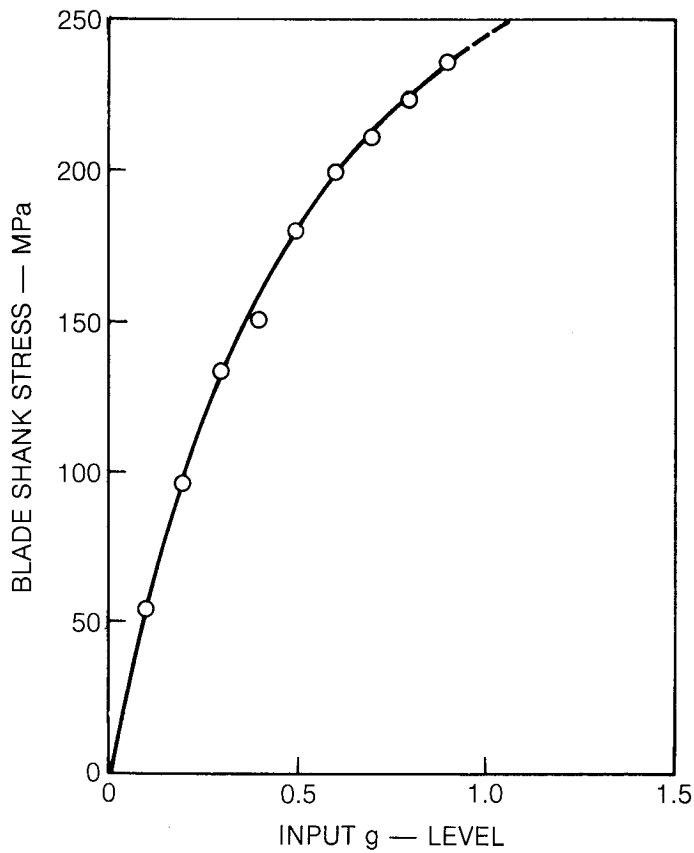


**Figure 61. Baseline Conditions for Turbine Blade**

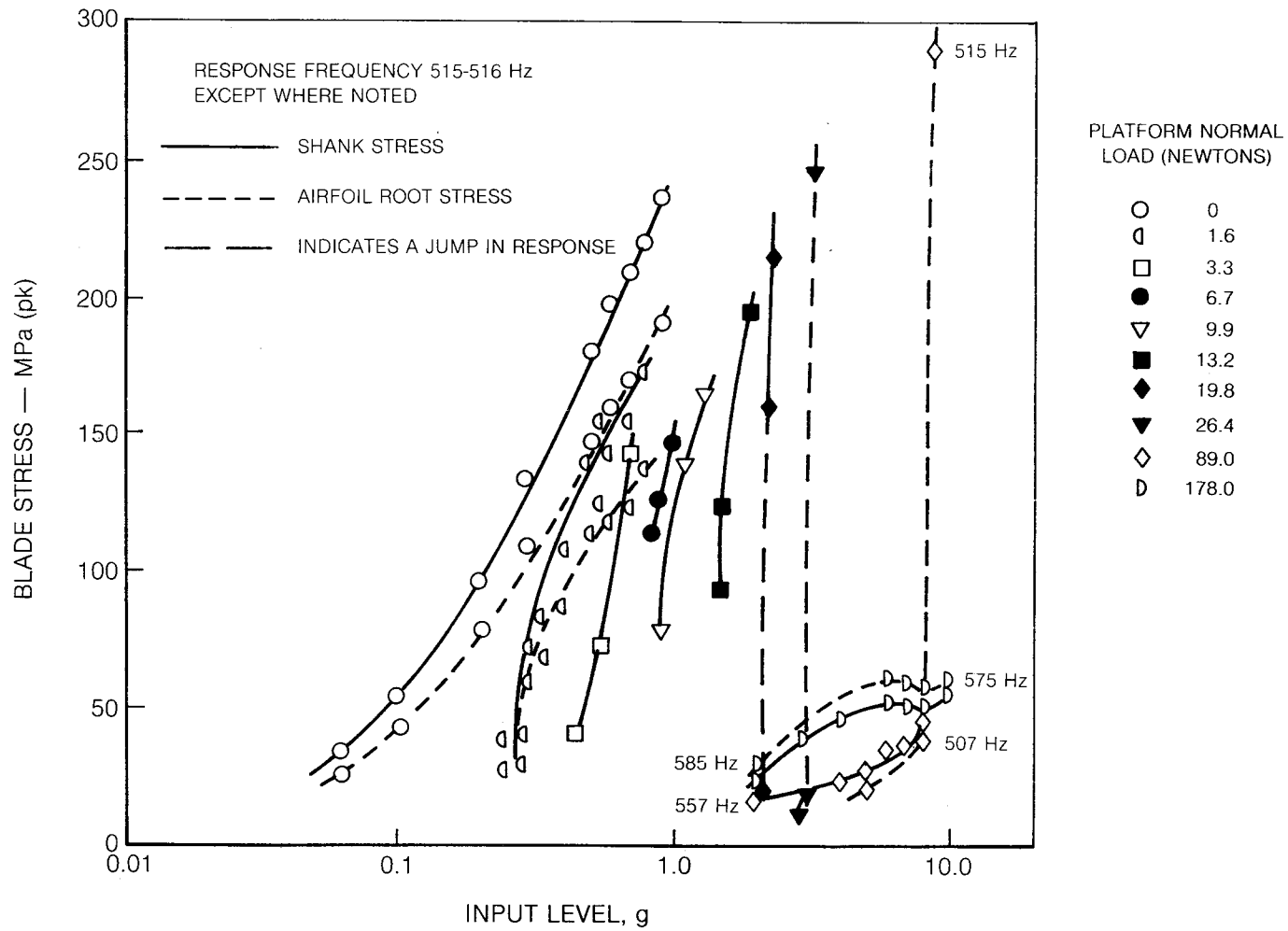


Figure 62. Platform Damping Test Results (Large Damper)

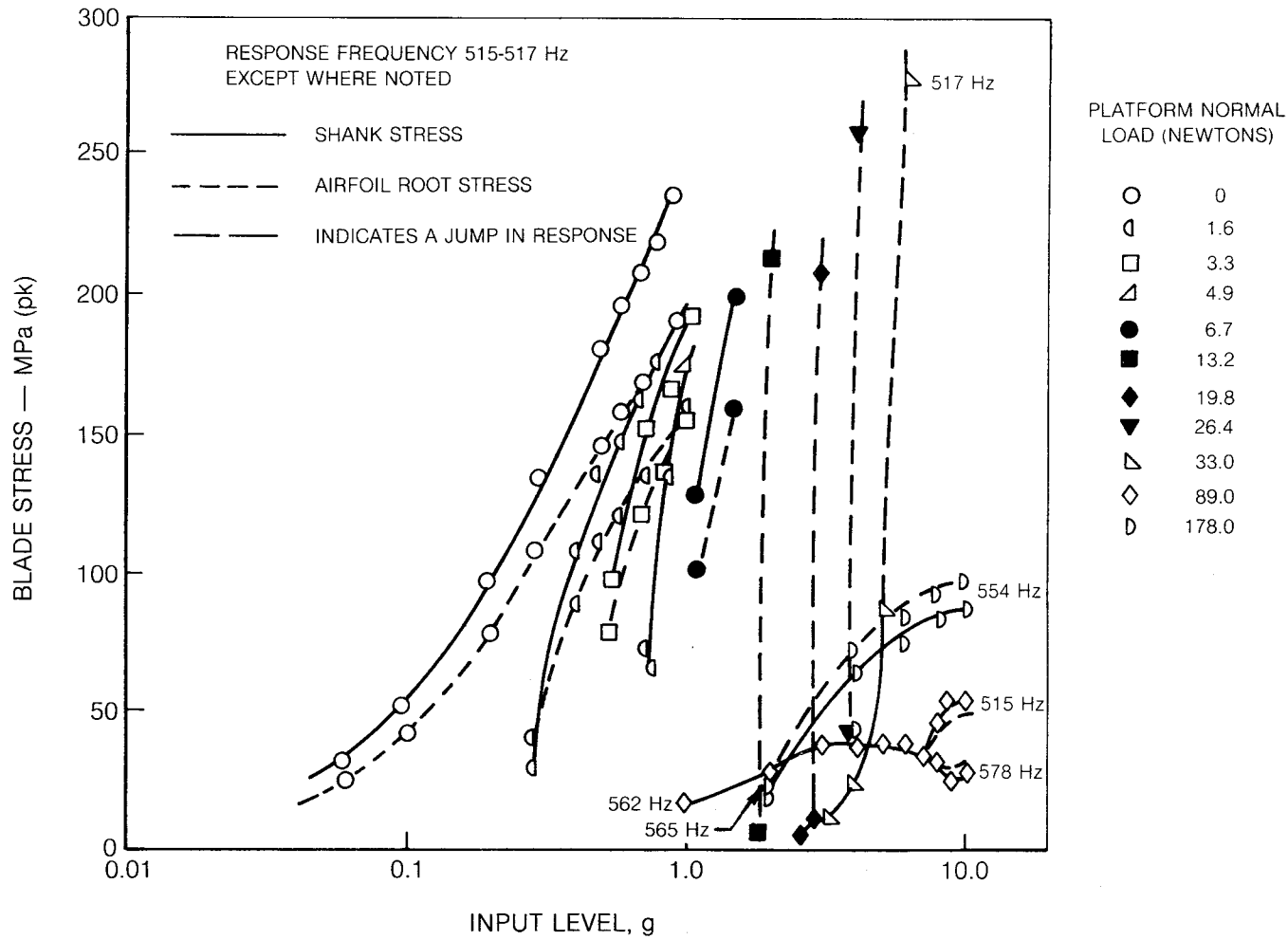


Figure 63. Platform Damping Test Results (Small Damper)

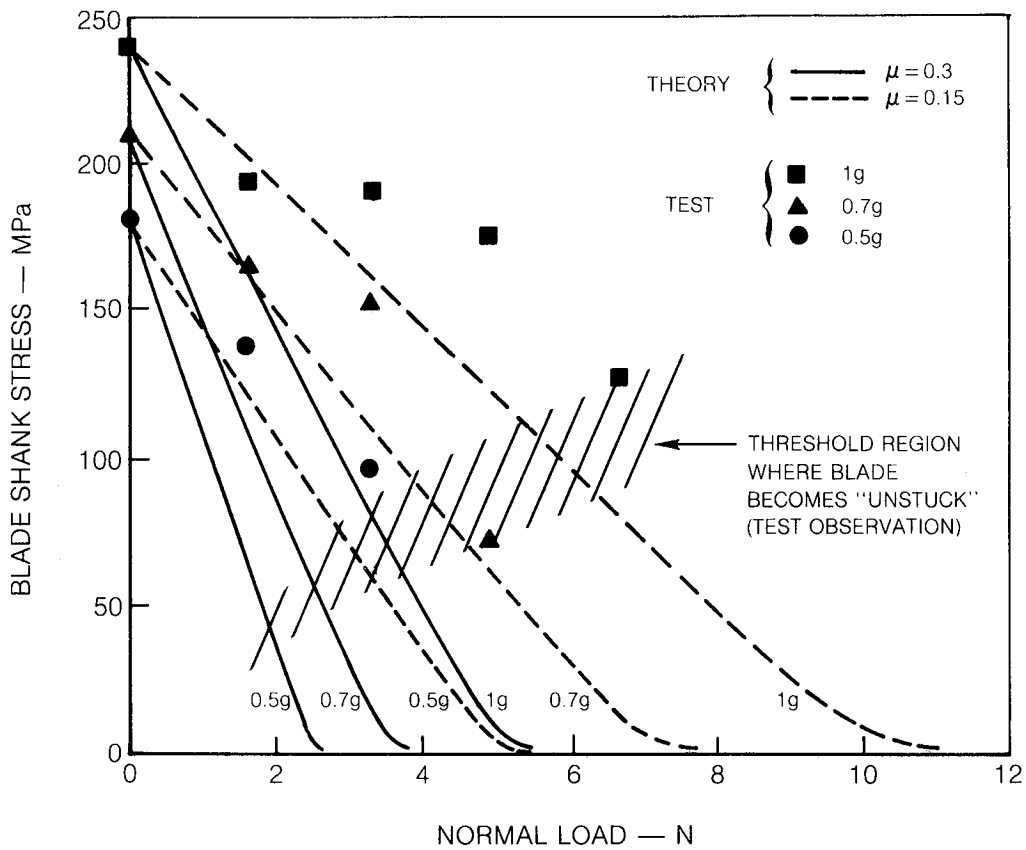


Figure 64. Turbine Blade Platform Damping Characteristics (Small Damper)

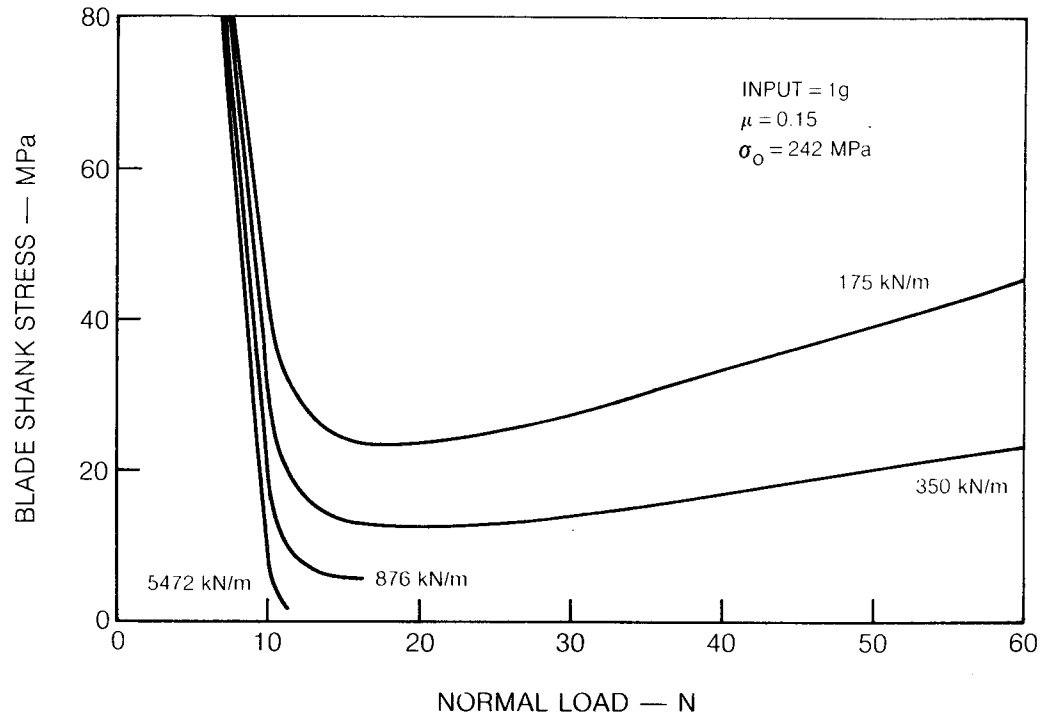


Figure 65 Influence of Damper Stiffness on Platform Damping

1. Report No. CR 165406	2. Government Accession No.	3. Recipient's Catalog No. N 81 29130	
4. Title and Subtitle TURBOJET ENGINE BLADE DAMPING		5. Report Date July 1981	
		6. Performing Organization Code	
7. Author(s) A. V. Srinivasan, D. G. Cutts, S. Sridhar		8. Performing Organization Report No. R81-91441031	
9. Performing Organization Name and Address United Technologies Research Center East Hartford, Connecticut 06108		10. Work Unit No.	
		11. Contract or Grant No.	
12. Sponsoring Agency Name and Address NASA Lewis Research Center 21000 Brookpark Road Cleveland, OH 44135		13. Type of Report and Period Covered	
		14. Sponsoring Agency Code	
15. Supplementary Notes Final Report Project Manager: L. J. Kiraly, Mail Stop 49-6 NASA Lewis Research Center 21000 Brookpark Road Cleveland, OH 44135			
16. Abstract The potentials of various sources of nonaerodynamic damping in engine blading are evaluated through a combination of advanced analysis and testing. The sources studied include material hysteresis, dry friction at shroud and root-disk interfaces as well as at platform type external dampers. A limited series of tests was conducted to evaluate damping capacities of composite materials (B/AL, B/AL/Ti) and thermal barrier coatings. Further, basic experiments were performed on titanium specimens to establish the characteristics of sliding friction and to determine material damping constants J and n.  All the tests were conducted on single blades. Mathematical models were developed to represent the several mechanisms of damping. Procedures to apply this data to predict damping levels in an assembly of blades have also been developed and discussed.			
17. Key Words (Suggested by Author(s)) Gas Turbine Engines, Damping, Blade Vibration, Hysteresis, Friction, Root and Shroud Damping, Platform Dampers		18. Distribution Statement Unclassified, Unlimited	
19. Security Classif. (of this report) Unclassified	20. Security Classif. (of this page) Unclassified	21. No. of Pages 168	22. Price*

